CONTENTS

1 Introduction

1.1 The Memory Effects

Shape Memory is a generic term used to describe a group of alloys that display unique mechanical and thermal responses. These effects manifest themselves either at constant temperature where very large but spontaneously recoverable strains are possible (superelasticity) or upon a change in temperature where an apparently plastic strain can be fully recovered. Both effects involve recovery of the alloys original geometry and it is through this shape change that the alloys 'memory' can be exploited. Duerig[1] divides the methods of harnessing the memory effect into four categories:-

Free Recovery - Where an alloy may be strained apparently beyond its elastic limit and then upon the application of heat will recover its original shape and maintain it during subsequent cooling. The function of the alloy element is therefore to cause motion or strain.

Constrained Recovery - Where the alloy may be prevented from full shape recovery thus generating a stress on the constraint element.

Actuation Recovery - Where the alloy is able to recover its shape but is operating against an applied stress, resulting in work production.

Superelastic Recovery - The only isothermal application of the memory effect, superelastic recovery (also known as pseudoelasticity) involves the storage of potential energy through comparatively large but spontaneously recoverable strains.

In many cases such a separation of the thermal and isothermal applications is not possible. Many of the superelastic applications described later in this dissertation also involve free and constrained recovery and these terms should

not be confined to thermal effects. However, this broad type of categorisation is useful for conceptualising how the shape change phenomena may be applied within mechanical systems.

1.2 The Memory Alloys

Arguably the first shape memory related observations were carried out by Ölander[2] in 1932 in his study of a 'rubber like effect' in the Au-Cd system and Greninger and Mooradian[3], 1938, in their study of Cu-Zn alloys (where they observed irrationality in the crystallography of a Cu-Zn alloy). However, it was many years later that Chang and Read[4] first reported the term 'shape recovery' between the orthorhombic and cubic phase in Au-Cd alloys. It was not until 1963 however, in a study on NiTi alloys, that Buehler et al first introduced the phrase 'shape memory effect' as a material property. Indeed it was the discovery of the effect in these NiTi alloys that really kick started the interest in shape memory applications. During the 1960's the NiTi alloys and their early applications began to move the effect away from fundamental phenomena to useful engineering property and fuelled a great deal of international research.

Despite the ever growing list of alloys that display the memory effect, to this day, the only alloys to have been commercially exploited are Cu-Zn-Al, Cu-Al-Ni and NiTi. The problem with all these alloys is their comparatively high cost. There is great current interest in Fe based alloys such as FeMnSi, FeMnSiCrNi and FeMnSiCoNi and it is hoped that these alloys may eventually yield a low cost alternative to those traditionally employed. The crystallography of the transformation mechanism in these alloys is not the same however, and instead, occurs through the motion of Shockley partial dislocations on alternate close packed planes of the parent f.c.c. phase changing the stacking sequence to hcp. The stress directed reorientation creates the shape recovery.

By far the most important commercial shape memory alloys are those of the NiTi system. It is the very large recoverable strains and excellent corrosion resistance[5] that have really set this alloy apart in terms of commercial application.

1.3 Applications of the Memory Effects

Although there are examples of NiTi SMA applications in all of the four categories described earlier, the greatest number of applications have emerged in the area of superelasticity. Many excellent and unique devices have been constructed out of NiTi for the medical industry and the market is still growing at a considerable pace. It is perhaps, the reported bio-compatability[6,7,8] allied to the less complicated design procedure for superelastic applications that has resulted in the high number of devices utilising this effect.

Guide wires for non-invasive surgery[9], orthodontic arch wires[10,11], highly flexible surgical tools[12] and stents for the re-canalisation of arterial and esophageal strictures[13,14] have all been successfully produced out of NiTi superelastic wires. In addition to the medical market, superelastic components are successfully used in consumer products such as spectacle frames[15], under wired bras[15,16]and mobile phone antennae[17].

The three categories of thermal shape recovery have met with much less commercial success and are limited to just a few niche areas. Of these perhaps the most famous is also one of the first. This is the coupling that was designed by Raychem to employ constrained recovery in joining pipes together in the Grumman F-14 aircraft[18]. A ring of NiTiFe alloy was expanded at very low temperatures and fitted over the coupling area of the pipes. As the ring returned to comparatively higher ambient temperatures it tried to contract to its original diameter and thus exerted high forces on the pipes resulting in a very strong and reliable coupling.

As well as pipe couplings SMA's have also been used in various electrical connectors and fastener type applications, all utilising the constrained recovery effects[19,20].

Unconstrained recovery applications of SMA's are few. Devices that have been produced exploiting only the shape change of the material include fire protection devices and thermal cut out switches[21]. In these applications the alloy element acts as both thermal sensor and cut out actuator and tend to be concerned with flow cut out valves. For instance the Proteus Gas Valve was specifically

designed to cut off gas flow in case of fire[22]. A CuZnAl spring expands at a particular ambient temperature pushing a steel ball through a retaining ring. The valve can only be reset manually and does not have to undergo repeated actuation or operate against constant loads.

The area of thermal application that perhaps has the greatest potential is that of work producing actuation[23,24]. To differentiate this type of actuator from those previously described it can be said that this type of actuator must produce reversible motion between high and low temperatures.

Many patents exist based on the hypothesis of using the SMA element as a thermal actuator that will convert electrical or thermal energy into mechanical work[25]. However, because of the complicated design criteria of matching the desired motion, cycle life and actuation temperatures to an 'off the shelf' material[26,27] the number of successful repeatable actuation devices is limited. The devices that have met commercial success are those that have been designed allied to stringent actuator research and development programmes. A good example of this is the air conditioner actuator developed by Matsushita Electrical Industrial Company Limited and the excellent fundamental research carried out by Todoroki[28]. Through his work a successful actuator was produced specific to the application. However, it is obvious that the cost of this type of research is high and many SMA actuator design ideas do not get any further than a concept stage.

Information on fatigue life when operating against constant loads and the effect of processing and operating conditions on long term memory stability are essential for design engineers and essential for the commercial future of SMA actuator devices.

The following dissertation attempts to examine some of these issues through a series of experimental programmes and in addition considers the commercial future of NiTi shape memory alloys and the market environments where they may be usefully employed.

1.4 Why Not Use Bimetals?

This question is often asked of shape memory researchers and manufacturers and deserves to be answered at the beginning of the dissertation. The displacement of bimetallic strips tends to be much smaller than that achievable with shape memory alloys and varies linearly with temperature rather than showing the switch type change associated with SMA's. In addition SMA's may be configured into many different shapes, i.e. a spring or a tubular cross section and can reverse deformation in any direction. Finally, and particularly important for thermal actuator applications, SMA's can exert recovery forces up to 100 times greater than bimetallic strips!

2 Martensitic Transformations and the Shape Memory Mechanism

Shape memory results from a particular type of phase transformation that produces the structure known as martensite. First observed in steels, martensite results from the solid state process of martensitic transformation. Taking its name from Professor Martens the reaction is displacive in nature and forms through a highly ordered crystallographic shear transformation, which involves no change in chemical composition or atomic diffusion, i.e. no atomic redistribution between phases.

Martensitic reactions normally occur athermally and martensite is formed upon cooling from a higher temperature phase called the parent phase. In steels this parent phase is known as austenite and this is also the term often used to describe the parent phase in shape memory alloys although technically speaking this is incorrect.

Although in his early work Cohen[29] describes the formation of martensite as being free from nucleation and growth, it is now accepted that the fundamental characteristics of martensite type transformations are in fact consistent with the nucleation-growth concept. The martensite reaction in plain carbon steels proceeds from an equilibrium austenite phase to a non-equilibrium (metastable) low temperature martensite phase. Since the martensite is metastable it will only form through very rapid cooling. In fact the rate of growth is so high in these reactions that the volume change associated with the reaction is controlled almost entirely by the nucleation rate.

In many martensitic transformations however, the low temperature phase is itself an equilibrium phase rather than a metastable one. In these cases the phase transformation occurs by the fast growth martensitic mode even with very slow cooling rates. The transformations in these systems occur martensitically but there is no need for a rapid quench to secure the fast growth mode as there is in steel. This is the case with shape memory alloys and many pure elements.

The formation of martensite in shape memory alloys may be explained in terms of both crystallographic structural changes and thermodynamics[30,31,32]. The rest of this chapter considers the reaction from both perspectives.

2.1 A General Crystallographic and Structural Perspective

Structurally, martensite forms through a twinning type process that is very similar in nature to deformation twinning. This is very useful for explaining some of the crystallographic theory.

Deformation twinning must :-

- Involve pure shear
- Preserve the lattice structure (i.e. The unit cell of the parent phase must be the same as the product phase). The only difference will be some kind of rotation.

To satisfy these requirements, twinning must occur through a pure shear transformation that maintains the unit cells vectors and also their mutual angles.

For a pure shear transformation there must be three non-coplanar vectors that :-

1. Retain their mutual lengths upon transformation
2. Retain their mutual angles upon transformation

To meet these requirements planes that are undistorted during transformation must be identified. These planes must retain their lengths upon transformation and keep the same atomic arrangement before and after transformation.

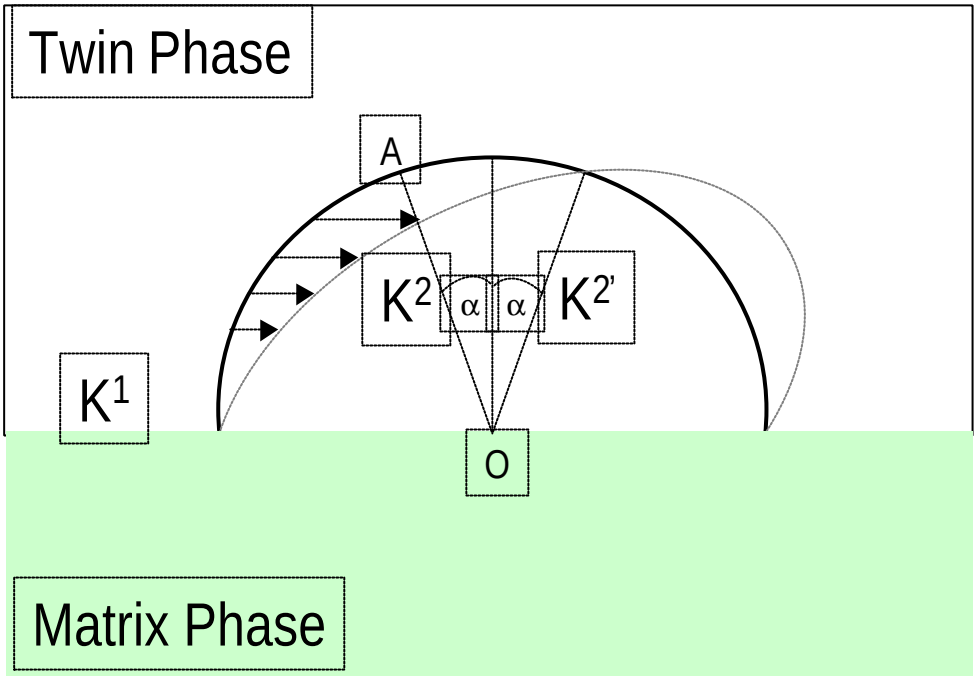

Figure 2-1 Semicircle of material undergoing shear transformation

Figure 2-1 shows untwinned material as a solid semicircle that undergoes pure shear into an ellipse. It can be seen that the only two planes undistorted during the shear process are planes K^1 (known as the twinning plane) and K^2. The only direction above the twinning plane that does not change in length during the transformation is OA. Therefore the non-coplanar vectors that retain their mutual lengths and angles must lie within these planes.

Figure 2-2 shows planes K^1 and K^2 in a material undergoing pure shear transformation so that K^2 is transformed into $K^{2'}$. The three non-coplanar vectors that satisfy the requirements stated previously must lie within these planes. If we let

- η^1 = a vector in K^1 perpendicular to the intersection I
- vectors 1 and 2 = any vector in K^2 making the angle β with η^1

Then it can be shown that during twinning the vector lengths and their mutual angles α, β and γ are all preserved. If these three vectors are also rational then the three requirements for pure shear have been fulfilled.

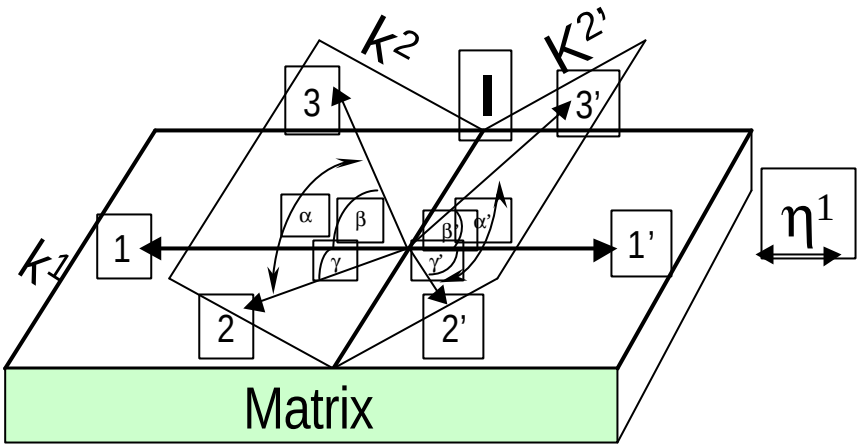

Figure 2-2 pure shear transformation in a 'twin of the second kind'

As vectors 2 and 3 are arbitrary and since they must both be rational then it follows that plane K^2 must also be rational. A twin of this form that requires plane K^2 to be rational and direction η^1 also to be rational is known as a 'twin of the second kind'.

If we now take

- η^2 = a vector in K^2 perpendicular to intersection I
- vectors 1 and 2 = any arbitrary vector in K^1 making an angle β with η^2

This is known as a 'twin of the first kind'. In this case it is required that plane K^1 and direction η^2 be rational.

For the twins in cubic, hexagonal and trigonal metals, K^1, K^2, η^1 and η^2 are all rational and the twins in these systems are called 'compound twins'.

The nature of the atom movement during twinning is illustrated by **Figure 2-3**. On the first plane above the twinning plane the atoms move by vector <t> and on each succeeding plane above this, the atoms shift by an additional vector <t>. Each atom moves relative to its neighbour by the same vector <t>. This is a co-operative motion since all atoms move through the same vector relative to its neighbour. At n planes above the twinning plane the strain is proportional to n<t>, i.e. a large strain is produced by many smaller, co-operative atom movements.

Twins grow predominantly in directions parallel to the K^1 planes with lesser growth in directions normal to the K^1. This type of growth results in the twin having a plate like morphology. Where these plates meet a free surface, a step like surface relief is formed due to a considerable strain in the surrounding

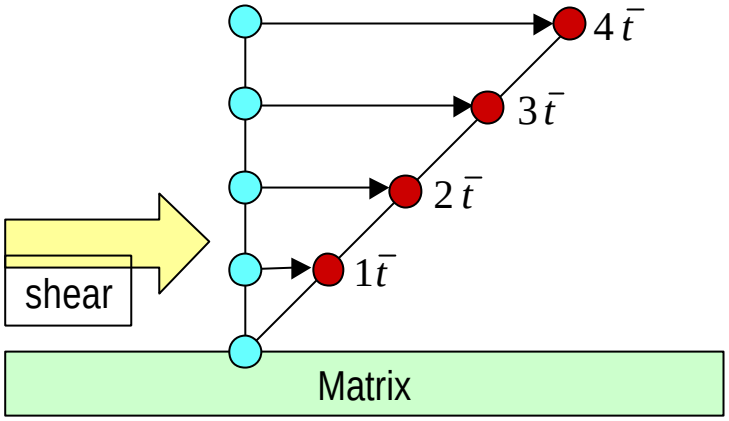

Figure 2-3 Shear strains as a result of atom motion in twinning planes

parent phase. This strain is needed to maintain a coherent twin/matrix interface. As the plate thickens perpendicular to K^1 the free surface of the twin forms a shear type step in relation to its original orientation and the surrounding matrix becomes severely strained.

It is also found that martensite has a plate like morphology that produces the same surface relief as deformation twinning, **Figure 2-4**. This observation implies that the mechanism of martensite formation is similar to deformation twinning. Further experimental work has revealed other observations that also bear similarities to deformation twinning.

2.1.1 Experimental Observations of Martensite Formation

Figure 2-4 shows the surface relief that results from the shape change taking place during martensite plate formation. Several experimenters have shown that if a scratch is inscribed on the surface of the parent material (known as a fiducial line) that then transforms into martensite, the line remains continuous. That is, there is no break in the line where it crosses the matrix/martensite interface. This

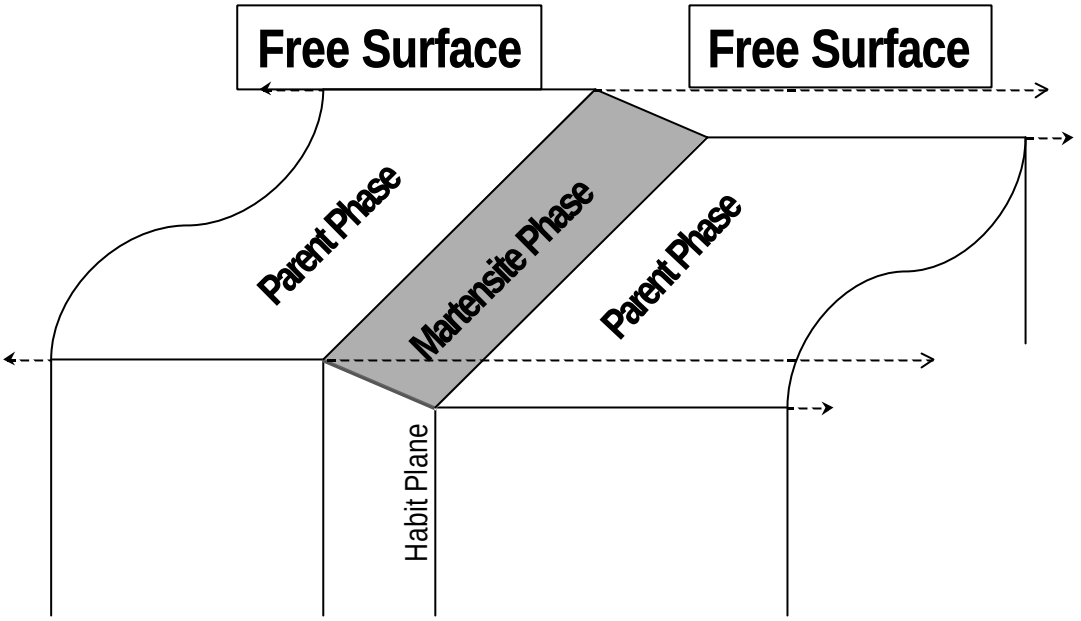

Figure 2-4 Surface relief formed by the martensite plate intersecting a free surface

observation shows that the interface between parent material and martensite plate remains coherent.

It is also observed that fiducial lines remain linear after transformation, that is they do not curve or bend. Therefore the free surface of the martensite plate remains planar and straight lines transform into straight lines and planes transform into planes. This type of transformation is known as **homogeneous**.

The linearity and coherency of the matrix/martensite interface tells us two important facts about the crystallography of martensite transformations:

The habit plane[1] is an invariant plane, i.e. a plane of zero distortion and zero rotation (just as the K^1 plane in deformation twinning).

The strain that produces the transformation is an invariant plane strain, i.e. an homogenous deformation with an invariant habit plane[1] this type of strain results in the displacement of any point being a linear function of its distance from the invariant plane. An example of this is the shear that occurs in the deformation twin of **Figure 2-3**.

In fact martensite involves a slightly more complicated invariant plane strain where the displacement also includes a uniaxial tensile or compressive

[1] The habit plane (or the shear plane of the transformation) is defined as the {hkl} planes of the parent phase that are parallel to the plane of the martensite plate.

component normal to the invariant plane sometimes referred to as the **dilatation** component.

Although the habit plane is frequently quoted as being a rational plane of zero distortion, it has been shown that in fact the habit plane in martensite transformations is irrational. Greninger and Troiano[33] first demonstrated this in the Fe-Ni-C system when considerable scatter was observed in the measured habit planes, **Figure 2-5**. It is thus customary to quote the habit plane as some rational plane around which the scatter lies.

Finally the last observation resulting from experimentation concerns the structure of the martensite. As well as the plate like structure already discussed martensite may be found to have a lath type morphology (long, optically unresolvable thin plates). However, shape memory alloys have the plate like morphology and therefore lath martensite is not of direct relevance to this dissertation.

When observed in an optical microscope, martensite plates appear to be single homogenous crystals. However, electron microscopy reveals that these plates have a sub structure of very fine twins and is another very obvious difference from the deformation twinning described earlier.

This observed substructure and the irrationality of the habit planes, clearly indicates that the martensite habit plane is only an invariant plane on a macroscopic scale and that the shape strain is only homogenous on a macroscopic level.

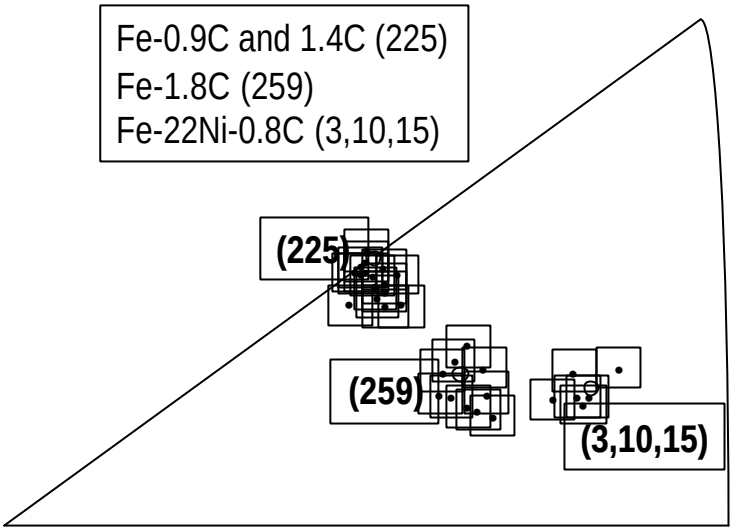

Figure 2-5 Some habit plane determinations in iron alloys. Greninger and Troiano [33] [34]

2.1.2 Crystallographic Theory of Martensite Transformations

So far only the experimental observations of martensite formation have been discussed. This section considers the theory behind these observations with direct reference to some of the classical theories of martensite crystallography.

Essentially the crystallography of martensite transformations must consist of two parts: -

1. That needed to produce the new structure from the old
2. That needed to accommodate the structural change

In 1924 E.C.Bain[35] produced a very simple theory to satisfy part 1 of the two requirements stated above that is still used today. He used iron alloys to show how the FCC unit cell of the parent phase could transform into the BCT unit cell of the martensite phase during transformation.

Figure 2-6 shows two FCC cells of the parent phase sharing a common (010) face. In the middle of the (010) face is an atom which is also the central atom

of a BCT unit cell drawn in heavier lines.

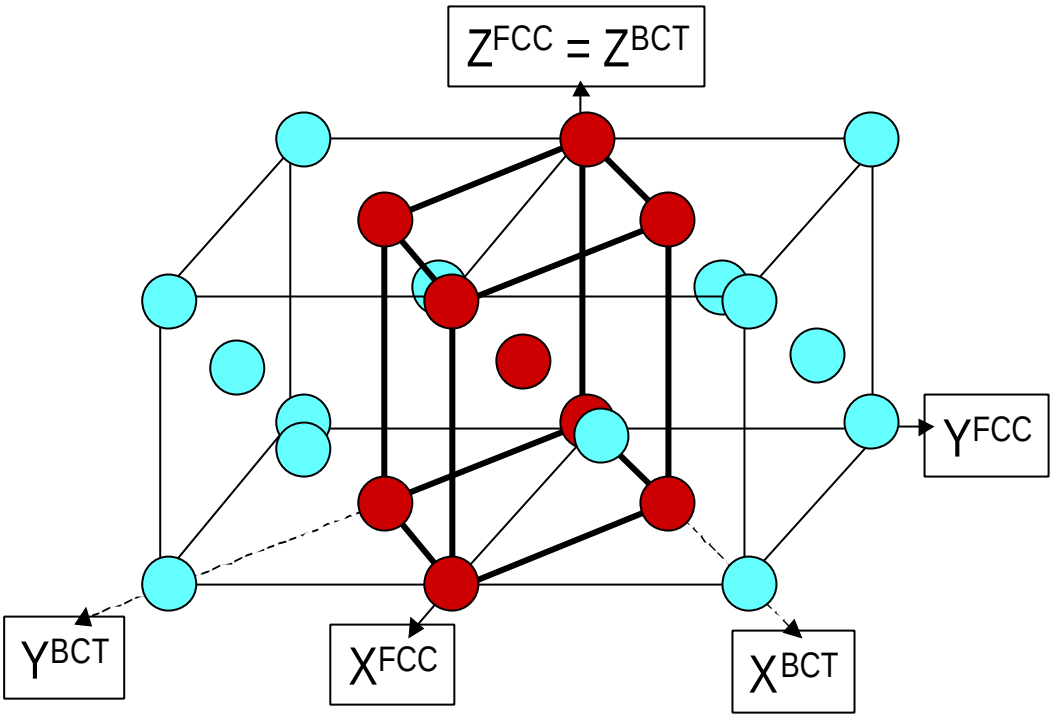

Figure 2-6 Mechanism of the FCC-BCT transformation proposed by Bain

Bain showed that if this BCT cell is contracted along the Z axis by 18% and expanded along the X and Y axes by 12% then the correct BCT unit cell for the martensite formed in Fe-C alloys is formed, **Figure 2-7**. This combination of contraction and expansion to achieve an homogeneous change in unit cell is often called the **Bain distortion** or **Bain Strain**.

Bain's mechanism requires a particular structural unit in the parent cell to become the unit cell of the martensite product phase. The relationship between these structures is often called the **lattice correspondence** and is defined as:

A unique relationship between any lattice point in the initial lattice and the point it becomes in the final lattice

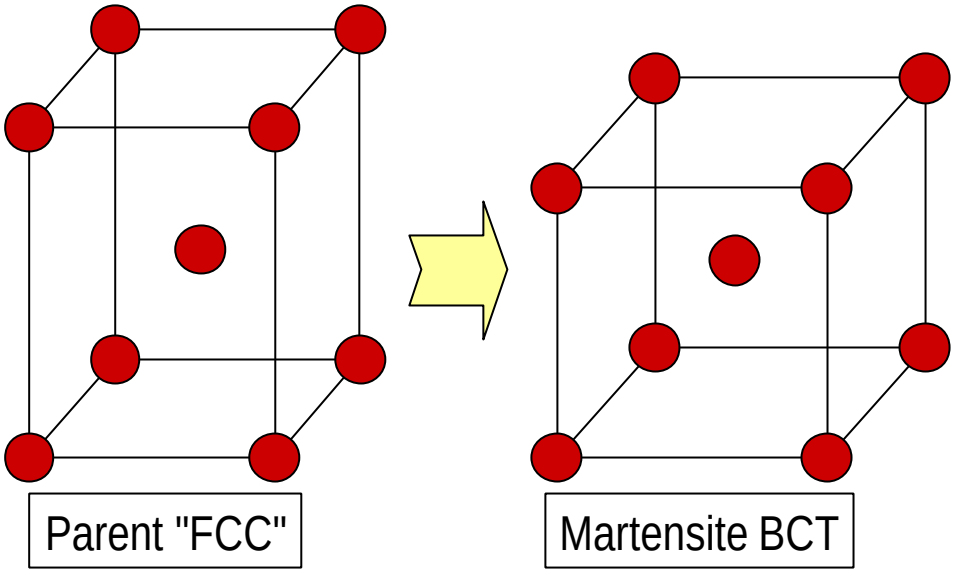

Figure 2-7 Bain distortion of the BCT unit cell

This specifies the structural unit in the parent phase, which is transformed into a unit cell of the product. A given direction in the parent phase will thus correspond to a particular direction in the product phase and can be defined by a correspondence matrix. It can be seen from **Figure 2-6** that the correspondence matrix of the Fe-C, FCC to BCT transformation is: -

$$\begin{pmatrix} x_2 \\ y_2 \\ z_2 \end{pmatrix} = \begin{pmatrix} 1 & -1 & 0 \\ 1 & 1 & 0 \\ 0 & 0 & 1 \end{pmatrix} \begin{pmatrix} x_1 \\ y_1 \\ z_1 \end{pmatrix}$$

Or

$$r_2 = Ar_1$$

(2-1)

Where ***A*** represents the correspondence matrix and r_1 represents any lattice direction transformed by the operator matrix ***A*** into r_2.

$$\text{I.e.} \quad \left[1\bar{1}0\right]^{fcc\ parent} A = \left[100\right]^{bct\ martemsite}$$

$$\text{And} \quad \left[010\right]^{fcc\ parent} A = \left[\bar{1}10\right]^{bct\ martemsite}$$

A similar correspondence exists for the planes in the two lattices.

Whilst Bain's theory very simply explains how the FCC unit cell can be transformed into the BCT unit cell with the minimum of atomic movement, it does not result in a plane of zero distortion necessary for the invariant plane strain associated with the martensitic transformation.

Figure 2-8 shows the initial FCC lattice represented as a unit sphere and an ellipsoid representing the final BCT lattice. The principal distortions follow Bain's theory with x and y undergoing 12% expansions and z an 18% contraction. The

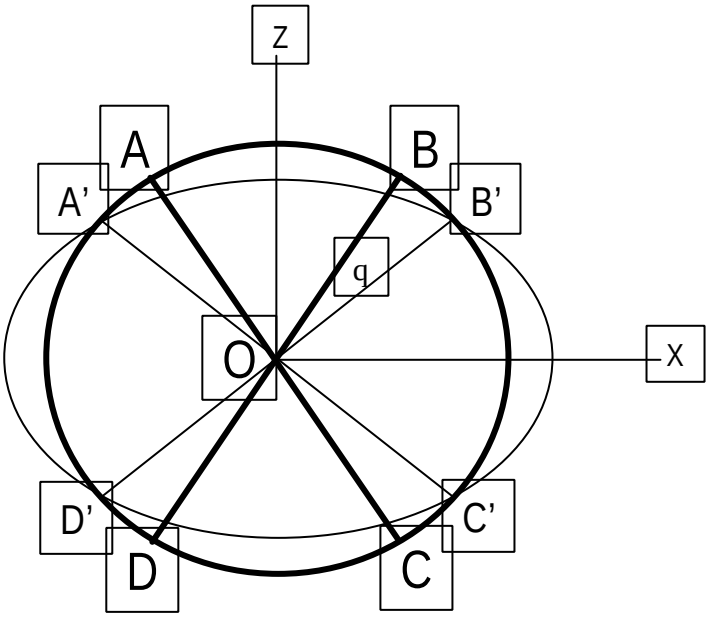

Figure 2-8 Effect of Bain distortion on a sphere

only points on the ellipsoid that remain at the same distance from the origin as

they were before the distortion lie along the circles A'-B' and C'-D' (originally A-B and C-D). Therefore the only invariant vectors associated with the Bain distortion lie along the cones OA'B' and OC'D'. In addition these are only invariant in length, as they have undergone a rotation from OAB and OCD. Hence there is no plane of zero distortion associated with the Bain distortion as it stands and the Bain correspondence cannot apply to the martensitic transformation.

If just one section of the sphere and ellipsoid are considered, as in **Figure 2-9** it is possible to show how a plane of zero distortion can be achieved.

If one of the principal distortions is collapsed back down its axis, such as axis y in **Figure 2-9**, then an undistorted plane of contact will result, A'OB'. The transformation now fits the theory put forward by Bilby and Christian [36]. They stated that for an undistorted plane to exist after homogenous deformation, one of the principal distortions must be greater than unity, one must be less than unity and one must be equal to unity. In general, lattice correspondences that satisfy these conditions along the principal strains do not exist. In addition, although the plane A'OB' is one of zero distortion, it has rotated form its original position, AOB.

Wechsler, Lieberman and Reed[37] and Bowles and Mackenzie[38] both put forward theories on certain restrictions that must be met by the martensite transformation, thereby formulating a theory of how the transformation takes place. Essentially these theories must: -

1. Allow a lattice distortion to generate the new lattice.
2. Obtain a plane of zero distortion i.e. one principle distortion is zero.
3. Rotate the martensite matrix so that the plane of zero distortion has its original position.

Step two must not change the structure generated in step one. Therefore the shear strain required to satisfy step two is termed a **lattice invariant shear**. The lattice invariant shear may be obtained in one of two ways, either by slip along parallel planes or by generating stacks of twins, **Figure 2-10**. Thus, it is necessary with this theory that the martensite phase have an internal substructure of twins or be severely slipped along parallel planes in order to **accommodate**

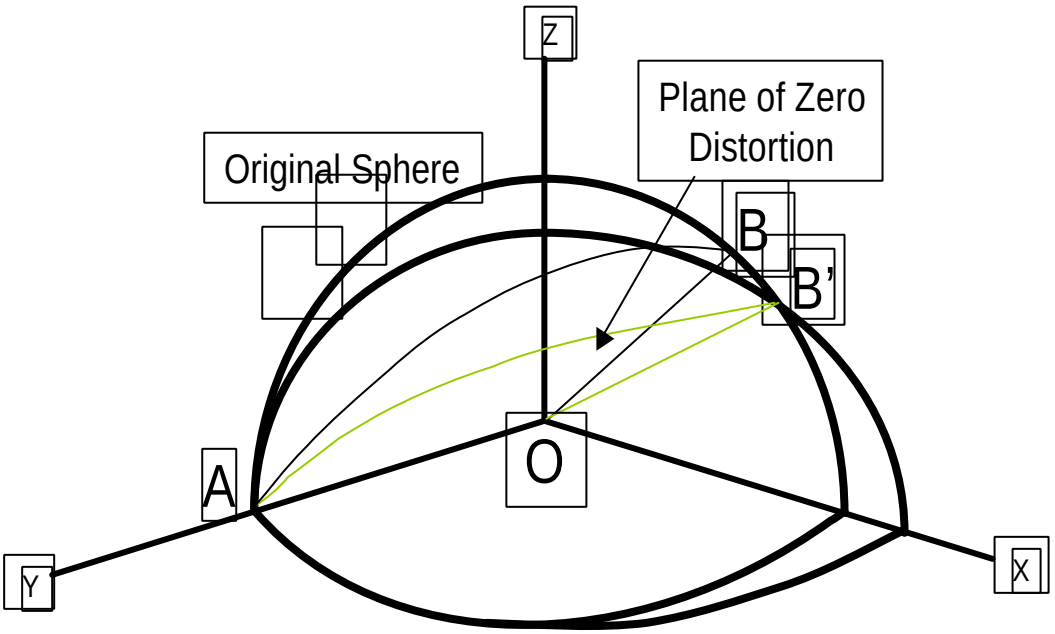

Figure 2-9 Bain distortion with one strain of zero, one greater than zero and one less than zero

the shear strain.

If the following data is put into this theory : -

1. The structure and lattice parameters of the parent and martensite phase.
2. The lattice correspondence.
3. The lattice invariant shear.

Then it possible to predict : -

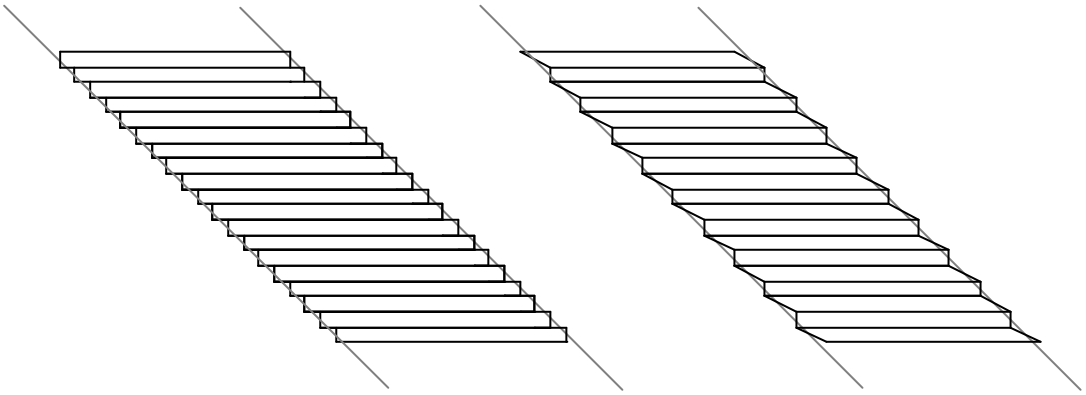

Figure 2-10 lattice invariant shear through slip and internal twinning

1. The martensite habit plane.
2. The shape strain.
3. The crystallographic orientation relationship between the parent and martensite phases.

Agreement between this theory and experimental results has been good, particularly for martensites involving low shape strains (as we will see later these include the shape memory alloys).

In summary, these crystallographic theories generally present a good model of the martensite transformation. They also account for the fine internal substructure of martensite and the irrational habit planes that are observed experimentally.

2.2 A General Thermodynamic Perspective

Martensite forms because it has a lower free energy than the corresponding parent phase. As there is no compositional change associated with the transformation the free energy curves as a function of temperature may be represented as in **Figure 2-11**. In this diagram the temperature, T_E , is the point where the two phases are in thermodynamic equilibrium and the difference in free energy, ΔG, between the martensite and parent phase = 0.

There is a strong nucleation barrier to the formation of martensite and thus significant supercooling is necessary before enough free energy is available to provide the driving force for the nucleation of the M phase. In **Figure 2-11**, the term: $\Delta G^{P \rightarrow M}$, at temperature M_s, represents the amount of free energy difference required to start the martensite transformation. Similarly, a term M_f is used to signify the finish temperatures of martensitic transformations.

The same argument applies to the reverse transformation where considerable superheating is required. In this case, the terms: A_s and A_f are used to signify the parent phase start and finishing temperatures. (The designate letter: A, is a reference to the austenite parent phase found in steels).

It is obvious from **Figure 2-11** that if the free energy for the forward transformation ($\Delta G^{P\rightarrow M}$) is the same as the free energy for the reverse transformation ($\Delta G^{M\rightarrow P}$) then :

$$\mathbf{T_E = \tfrac{1}{2}(M_s + A_s)} \qquad \mathbf{(2\text{-}2)}$$

It will be shown in subsequent sections however, that this statement is not true of

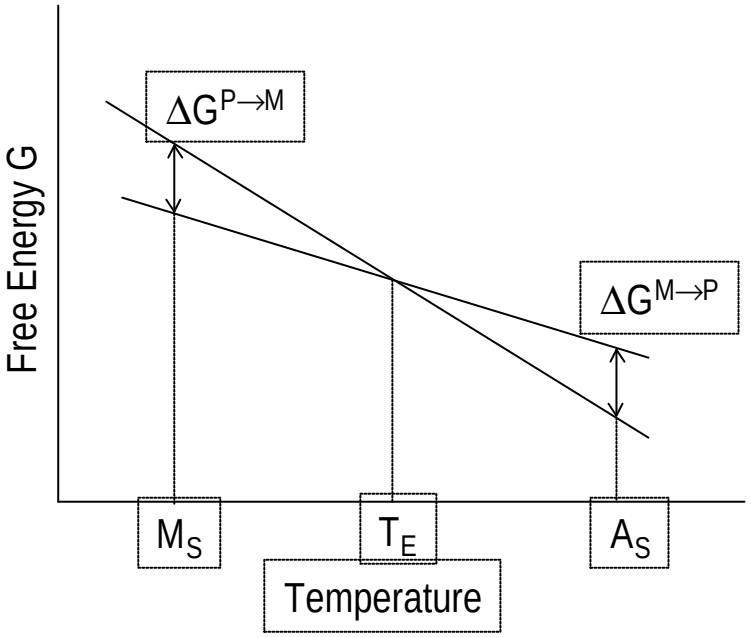

Figure 2-11 Free energy curves for the martensite/parent phase

all martensites[39,40,41].

For a thermodynamic process to occur spontaneously ΔG must be less than zero and depends on the function :

$$\mathrm{D}\mathbf{G} = \mathrm{D}\mathbf{E} - \mathbf{P}\mathrm{D}\mathbf{V} - \mathbf{T}\mathrm{D}\mathbf{S}$$

(2-3)

where **E** is the total energy change, **P** is pressure. **V** is volume, **T** is temperature and **S** is entropy. In most processes involving solids and liquids at atmospheric pressures the term $P\Delta V$ is negligibly small so that equation **(2-3)** becomes :

$$\Delta G = \Delta E - T\Delta S$$

(2-4)

In a reversible proceess at constant pressure the heat energy exchanged between the system and its surroundings equals the enthalpy (Δ**H)** change of the system and equation **(2-4)** may be written as :

$$\Delta G = \Delta H - T\Delta S$$

(2-5)

As stated previously, the change in free energy at T_E is equal to zero so that :

$$\Delta G^{TE} = 0 = \Delta H^{TE} - T_E \Delta S^{TE}$$

(2-6)

And therefore at temperature T_E :

$$\Delta H^{TE} = T_E \Delta S^{TE}$$

(2-7)

In addition, as the terms : Δ**H** and Δ**S** are independent of temperature we can combine equations : **(2-5)** and **(2-6)** to form an equation that can give an approximation of the amount of free energy available for any transformation as a function of supercooling :

$$\Delta \mathbf{G} = \Delta \mathbf{H} \frac{\Delta \mathbf{T}}{\mathbf{T_E}} = \Delta \mathbf{S} \Delta \mathbf{T}$$

(2-8)

As $\Delta \mathbf{H}$, $\mathbf{M_s}$ and $\mathbf{A_S}$ can be measured using differential scanning calorimetry and $\mathbf{T_E}$ can be estimated from equation **(2-2)** it is possible using equation **(2-7)** to calculate $\Delta \mathbf{S}$ and equation **(2-8)** to calculate $\Delta \mathbf{G}$ for any given $\Delta \mathbf{T}$.

It is worth considering the ΔG term for martensitic reactions in greater detail. The ΔG referred to in the above equations is in fact a net free energy resulting from the interplay of various energy terms operating during the transformation[42] :

$$\Delta \mathbf{G_{net}} = \Delta \mathbf{G_c} + \Delta \mathbf{G_s} + \Delta \mathbf{G_e} = \Delta \mathbf{G_c} + \Delta \mathbf{G_{nc}}$$

(2-9)

where $\Delta \mathbf{G_c}$ is a chemical energy term resulting from the structural change from parent to martensite, $\Delta \mathbf{G_s}$ is a surface energy term resulting from the production of internal interfaces during the transformation and $\Delta \mathbf{G_e}$ is an elastic strain energy term stored in the system as the transformation proceeds on cooling. The surface energy term and strain energy term are often combined to define the non-chemical energy $\Delta \mathbf{G_{nc}}$ opposing the transformation[43].

Equation **(2-9)** is useful as it clearly indicates why supercooling and superheating are necessary for the transformation. That is, in most martensites the $\Delta \mathbf{G_{nc}}$ is equally as large as the $\Delta \mathbf{G_c}$ term and considerable supercooling or superheating is required to provide the further free energy required for the transformation to proceed.

The presence of the non-chemical free energy also explains why the transformation finish temperatures are not the same as the start temperatures. As the transfomation proceeds further cooling or heating is required to overcome the concomitant increase in $\Delta \mathbf{G_{nc}}$ resulting from the formation of the new phase.

Similarly, the enthalpy of transformation may also be defined in terms of a net value. Salzbrenner and Cohen[39] showed that as the martensite transformation proceeds, non-chemical strain energy is stored in the system resulting in a decrease of the observed heat evolution ($\Delta H^{P\rightarrow M}_{net}$) compared to the chemical enthalpy change ($\Delta H^{P\rightarrow M}_{ch}$). This results in : $\Delta H^{P\rightarrow M}_{net}$ being less negative[2] than $\Delta H^{P\rightarrow M}_{ch}$. They therefore defined the net enthalpy change accompanying the transformation in the additive form :

$$\Delta \mathbf{H_{net}} = \Delta \mathbf{H_{ch}} + \Delta \mathbf{H_{el}} + \Delta \mathbf{H_{I}} \qquad \textbf{(2-10)}$$

where $\Delta \mathbf{H_{net}}$ is the net enthalpy change measured by differential scanning calorimetry (DSC), $\Delta \mathbf{H_{ch}}$ is the chemical enthalpy, $\Delta \mathbf{H_{el}}$ is the enthalpy change associated with the elastic strain energy of the transformation and $\Delta \mathbf{H_{I}}$ arises from the production of internal interfaces during transformation. Therefore, in a similar way to equation **(2-9)**, the non-chemical enthalpy change of transformation **($\Delta \mathbf{H_{nc}}$)** may be defined as :

$$\Delta \mathbf{H_{nc}} = \Delta \mathbf{H_{el}} + \Delta \mathbf{H_{I}} \qquad \textbf{(2-11)}$$

2.3 Thermoelastic and non-thermoelastic transformations

Martensite transformations may be divided into two categories: thermoelastic and non-thermoelastic. **Figure 2-12** shows how the volume fraction of parent phase varies with cooling and heating of two such transformations.

[2] Convention assigns the heat generated during the exothermic martensite transformation a negative sign, i.e. energy is lost from the system during exothermic reactions.

It is shown that thermoelastic transformations display a comparatively small hysteresis compared to non-thermoelastic transformations. This is because a much smaller driving force is required for thermoelastic transformations due to the greater mobility of the parent/martensite interface.

In non-thermoelastic transformations lowering the temperature below M_s causes the martensite to grow to its limiting size and upon further cooling, additional transformation only occurs by the nucleation of new plates. Old plates will not grow even at lower temperatures.

During thermoelastic transformation, again the plate grows to a limiting size for a specific temperature below M_s. Further cooling however, causes additional transformation by the growth of old plates as well as by the nucleation of new plates. The continued growth of thermoelastic martensite occurs in a jerky motion. The growth rate remains high but occurs over very small distances as more free energy becomes available with the decreasing temperature.

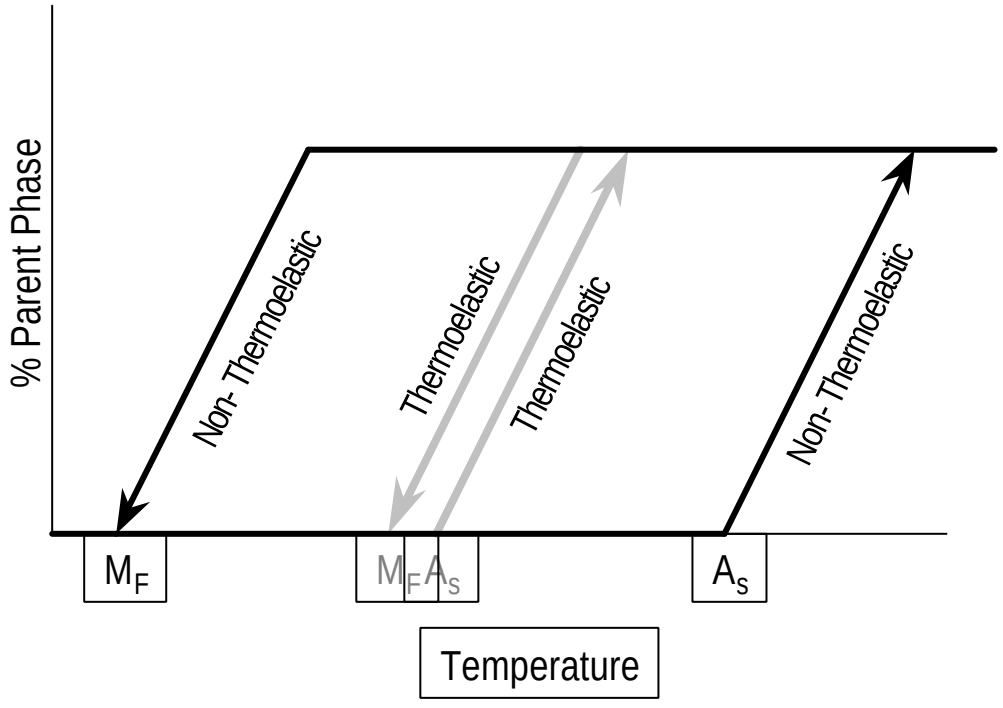

Figure 2-12 transformation curves for thermoelastic and non-thermoelastic martensites

It is obvious from equation **(2-8)**, that greater free energy is required for non-thermoelastic transformations as ΔT is much larger. This is probably a result of the larger shear that is required to form these martensites. It is the thermoelastic type of transformation however, that is at the heart of the memory effect.

Figure 2-13 illustrates how the invariant plane strain of the martensite formation can be resolved onto two components[45], a shear component, m_1^p and a dilatational component, m_1^n. Since shear strain does not involve a volume change, the m_1^n component may be considered as being equivalent to the volume change of the transformation. In thermoelastic transformations the m_1^n component is very small and thus the volume change is very small (eg 0.3%). This results in the transformation being very close to a simple shear.

In thermoelastic transformations growth stops when the free energy available to drive the reaction is counter balanced by the strain energy generated in the parent matrix. Because of the very small volume change, plastic flow does not occur and a balance is achieved between the elastic strain energy made available by the lower free energy state of the martensite phase. It is this balance that defines the term: thermoelastic. As the temperature is lowered, so new equilibria are created. The rate at which the bulk interface moves is governed by how fast the temperature is lowered.

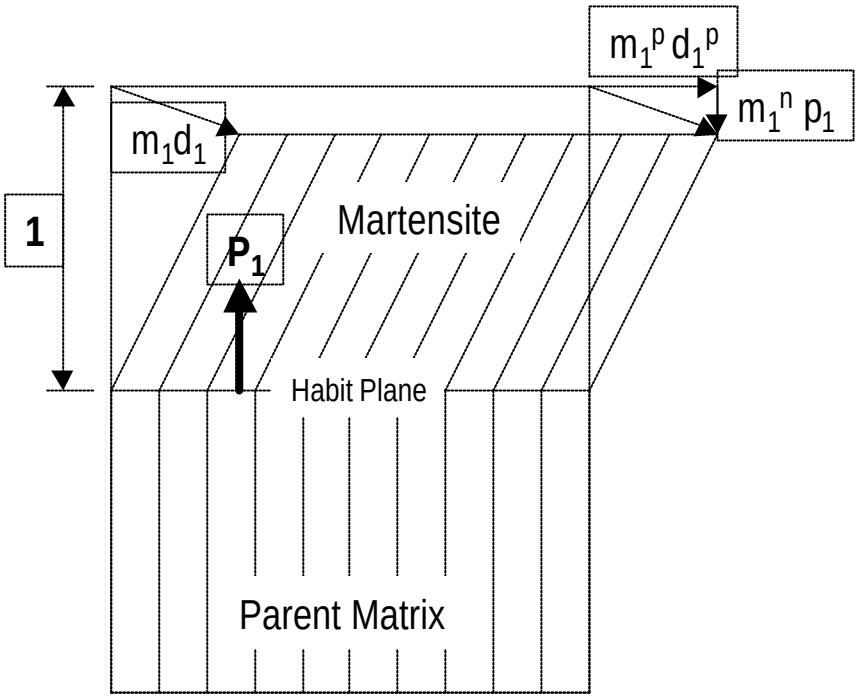

Figure 2-13 Invariant plane strain and its resolution into two components[45]

2.4 Stress Effects on the Formation of Martensite

Another important factor affecting martensite formation is whether or not a stress is applied to the system. Depending upon the form of loading, an applied stress will either have a positive or a negative effect on the amount of chemical free energy required for martensite nucleation. **Figure 2-14** shows how a stress applied to the parent phase at a temperature between $\mathbf{M_s}$ and $\mathbf{T_E}$ will provide an additional mechanical driving force, **U**, which is added to the chemical driving force $\Delta\mathbf{G_c}$. In this case the martensite transformation starts at the critical temperature or applied stress where the net driving force is equal to the $\Delta\mathbf{G_{net}}$ required for the transformation to proceed.

$$\Delta G^{P \to M}_{MS} = \Delta G^{P \to M}_{T1} + U \qquad \textbf{(2-12)}$$

where $D\mathbf{G}^{\mathbf{P}\to\mathbf{M}}_{\mathbf{MS}}$ is the free energy required for transformation when no stress is applied and $D\mathbf{G}^{\mathbf{P}\to\mathbf{M}}_{\mathbf{T1}}$ is the free energy available at a temperature of **T1** in **Figure 2-14**.

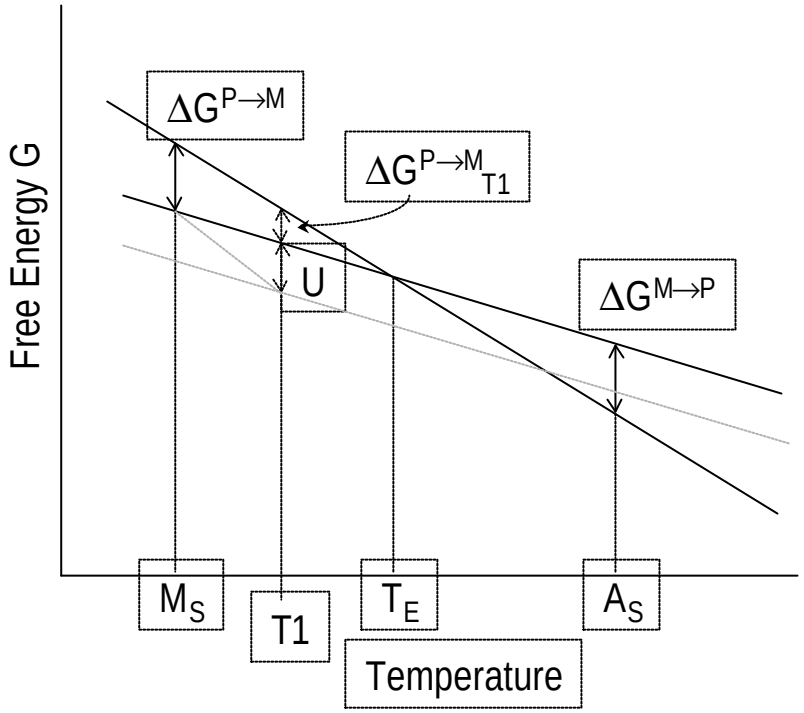

Figure 2-14 the effect of applied stress on the free energy of transformation

Therefore we can say that U is the critical mechanical driving force for transformation to occur at temperature T1.

The driving force, U, was shown by Patel and Cohen[44] to be a function of the applied stress and the orientation of the transforming plate, expressed as :

$$\mathbf{U} = t\,\mathbf{m_1}^{\mathbf{p}} + s\,\mathbf{m_1}^{\mathbf{n}} \qquad \textbf{(2-13)}$$

where : -

τ = the shear stress resolved along the transformation shear direction in the habit plane.

$\mathbf{m_1}^{p}$ = the transformation shear strain along the transformation shear direction in the habit plane.

σ = the normal stress resolved perpendicular to the habit plane. By convention this is positive for a tensile stress and negative for a compressive stress.

$\mathbf{m_1}^{n}$ **=** the dilatational component of the transformation shape strain. In most martensites the dilatation is negative.

If we consider how the τ and σ terms are affected by the applied stress, σ_1 in **Figure 2-15**, where :-

σ_1 = absolute value of applied stress

θ = the angle between σ_1 and the habit plane normal, **N**

α = the angle between the transformation shear direction, **S**, and the maximum shear direction of the applied stress on the habit plane, $\mathbf{S_{max}}$

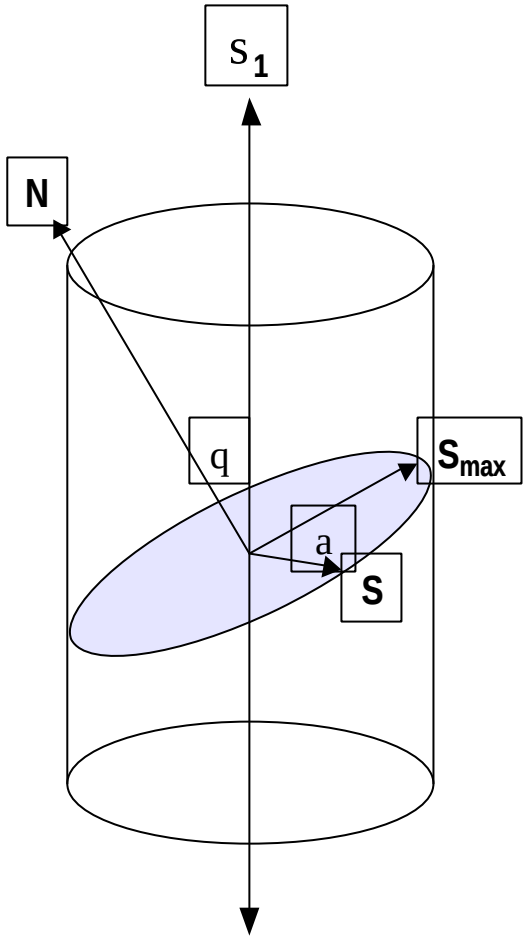

Figure 2-15 the relation between an applied stress and the shear stress and normal stress components of the mechanical driving force, U

For any given orientation of martensite plate[43] : -

$$t = \frac{1}{2} s_1 \sin 2q \cos a \qquad \textbf{(2-14)}$$

and

$$s = \pm \frac{1}{2} s_1 (1 + \cos 2q) \qquad \textbf{(2-15)}$$

so that equation **(2-13)** becomes :

$$\mathbf{U} = \mathbf{1/2}\ \sigma_1 \left| \mathbf{m_1^p \sin 2\theta \cos \alpha} \pm \mathbf{m_1^n (1 + \cos 2\theta)} \right|$$

(2-16)

Since usually m_1^p is much greater than m_1^n the first term on the right hand side of the equation is dominant. Thus U is positive for both uniaxial tension and compression[45], i.e. both uniaxial tension and compression aid the martensite transformation.

When a martensitic reaction starts by stressing a polycrystalline parent phase in which the orientation of each grain is randomly distributed, a martensite plate with an orientation that yields a maximum value of U in equation **(2-16)** will be formed first.

It has been shown in a number of alloys that the critical applied stress for the nucleation of martensite increases linearly with temperature[46,47,48].

Another way of considering the effect of a stress on the martensite reaction is via the Clausius-Clapeyron relationship[46] that describes the monovariant two-phase equilibrium of a one component system:

$$\frac{\mathbf{dP}}{\mathbf{dT}} = \frac{\Delta \mathbf{S}}{\Delta \mathbf{V}} = \frac{\Delta \mathbf{H}}{\mathbf{T}\Delta \mathbf{V}}$$

(2-17)

Where **P** is pressure, **T** is equilibrium temperature, Δ**V** is the volume change associated with the transformation, Δ**S** is the entropy change and Δ**H** is the enthalpy change.

This equation is deduced directly from the fundamental equation relating Gibbs free energy (**dG**) to its natural independent variables - pressure (**P**) and temperature (**T**):

$$\mathbf{dG} = \mathbf{VdP} - \mathbf{SdT}$$

(2-18)

Where **V** is volume and **S** is entropy.

Burkart and Read[49] were the first to realise that the influence of an external load on the martensite transformation start temperature can be described by an equation directly analogous to the Clausius-Clapeyron equation **(2-17)**.

Wollants, Roos and Delaey[46] base their analysis of uniaxially stress-induced martensite and an associated description of elastic work, on the conjugated thermodynamic variables of uniaxial stress s and strain e.

Provided reference is made to the molar volume of the specimen they describe how the following Clapeyron like equation may be formulated to describe the effect of stress on the martensite transformation.

$$\frac{\mathbf{d}s}{\mathbf{d}\mathbf{M_s}} = -\frac{D\mathbf{S}}{De} = -\frac{D\mathbf{H}}{\mathbf{T}De}$$

(2-19)

Where s is uniaxial stress, $\mathbf{M_s}$ is martensite start temperature, e is the strain associated with the transformation, $D\mathbf{S}$ is the entropy change per unit volume and $D\mathbf{H}$ is the enthalpy change per unit volume and **T** is the equilibrium temperature.

The Clausius-Clapeyron equation is usually written without a negative sign. However the negative sign is necessary in this case if the correct sign is assigned to both sides of the equation[48].

The relationship described by **(2-19)** will be referred to again in later sections.

2.5.1 The crystallographic and structural origins of shape memory

If we consider a one dimensional model of the martensite transformation, **Figure 2-16**, then it can be seen that to restore the original geometry of the parent matrix from the twinned martensite matrix requires only two directions of shear. These directions are known as **variants** and are necessary for the full three dimensional **self-accommodation** of the martensite plates. During a thermoelastic transformation an initial parent phase crystal will transform into self accommodating variants of martensite plates known as **plate groups**.

It is also apparent that the parent phase has greater symmetry than does the martensite phase. This means that there are several ways in which the martensite can form from the parent structure but only one possible route that will restore the parent structure. In **Figure 2-16** two shear directions can be applied to the parent squares to produce two different rhombus martensite variants. There are no other possible variants of the parent phase however, and during the reverse transformation the rhombus shapes can only follow one transformation pathway to return to the original square geometry.

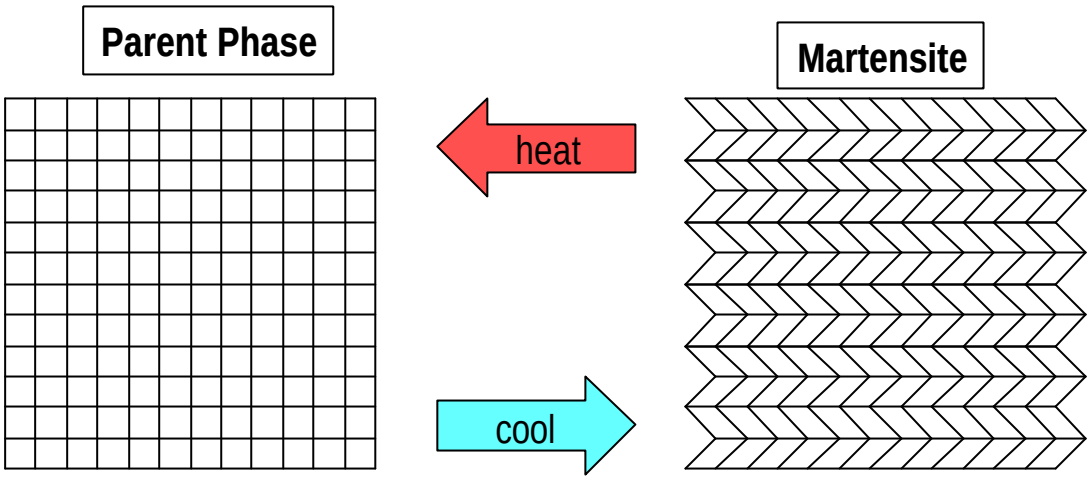

Figure 2-16 two dimensional model of the twinning accommodation mechanism in martensite

The twin boundaries[3] separating the variants in martensite are said to be glissile due to the fact that they are quite mobile. If a stress is applied to the martensite shown in **Figure 2-16** then the balance of variants will change by movement of the twin boundaries. The realigned martensite variants can thus better accommodate the applied stress. The variants that are most favourably orientated to the direction of applied stress dominate the resulting shape strain, **Figure 2-17**. This process is known as **de-twinning**.

The re-orientation and subsequent restoration of the martensite variants during and after de-twinning respectively is at the heart of the shape memory effect.

[3] It is worth stating that the term twin boundary not only refers to the twins within martensite plates but also to the boundaries between the plates themselves. That is, the martensite plates are also twins with respect to adjacent plates.

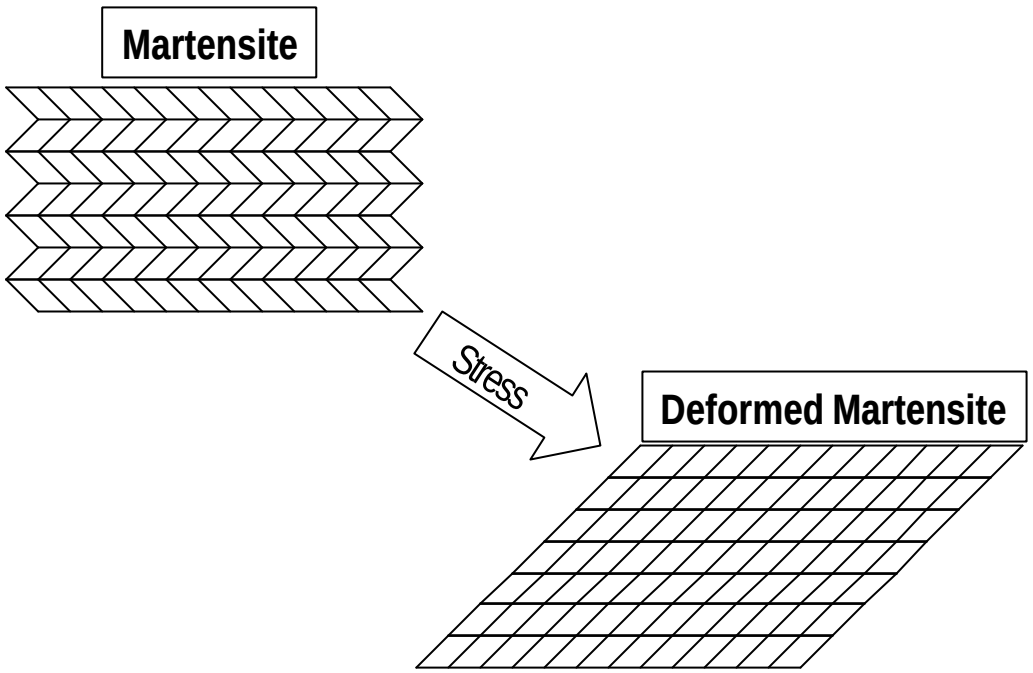

Figure 2-17 the re-orientation of martensite variants wtih applied stress

Figure 2-18 shows how the shape memory effects manifest themselves in terms of shape strain. If an alloy, at a temperature below A_f, is deformed by a tensile stress, **Curve A**, and subsequently unloaded then an apparent plastic strain will remain. If the alloy is now reheated to a temperature above A_f (the red arrow in **Figure 2-18**) then the apparent plastic strain will fully recover and the alloy will be restored to its original shape. This is known as the **one-way shape memory effect**.

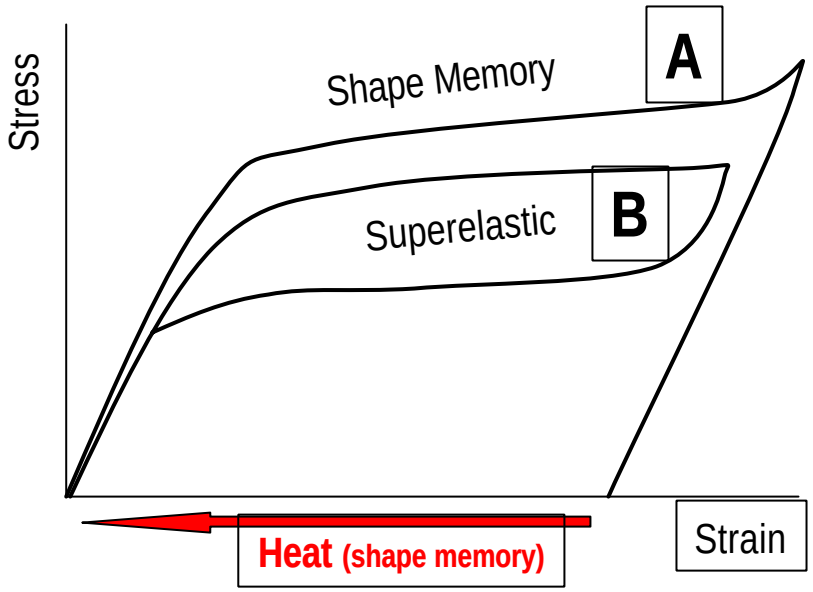

Figure 2-18 Stress/strain curves for the shape memory effects

If the same alloy is deformed in a similar manner at a temperature above A_f, then this time when it is unloaded, the strain is simultaneously recovered, **curve B**. This effect is known as **superelasticity**.

Again, the structural changes that take place during **Figure 2-18** can be thought of in two dimensional terms, **Figure 2-19**. During the deformation of curve A, the alloy starts in the twinned martensite condition, during loading de-twinning occurs and the structure becomes one of deformed martensite resulting in a net macroscopic shape change. When the alloy is unloaded the deformed martensite structure remains resulting in the apparent plastic strain. If the alloy is now reheated to a temperature above A_f then the original parent phase structure and orientation is restored via a thermoelastic type of transformation. No matter what the distribution of the martensite variants, there is only one, possible symmetry of the reverted parent structure. When the alloy is cooled back down to below M_f the twinned martensite structure is restored. It should be noted that the

transformation between parent phase and self-accommodating martensite results in no macroscopic shape change. Thus a **one way shape memory** is achieved.

The total maximum strain that can be recovered i.e. without any real plastic deformation occurring depends upon the shape memory alloy system. Depending upon the alloy system, typically it is in the range of 1-6% for polycrystalline alloys.

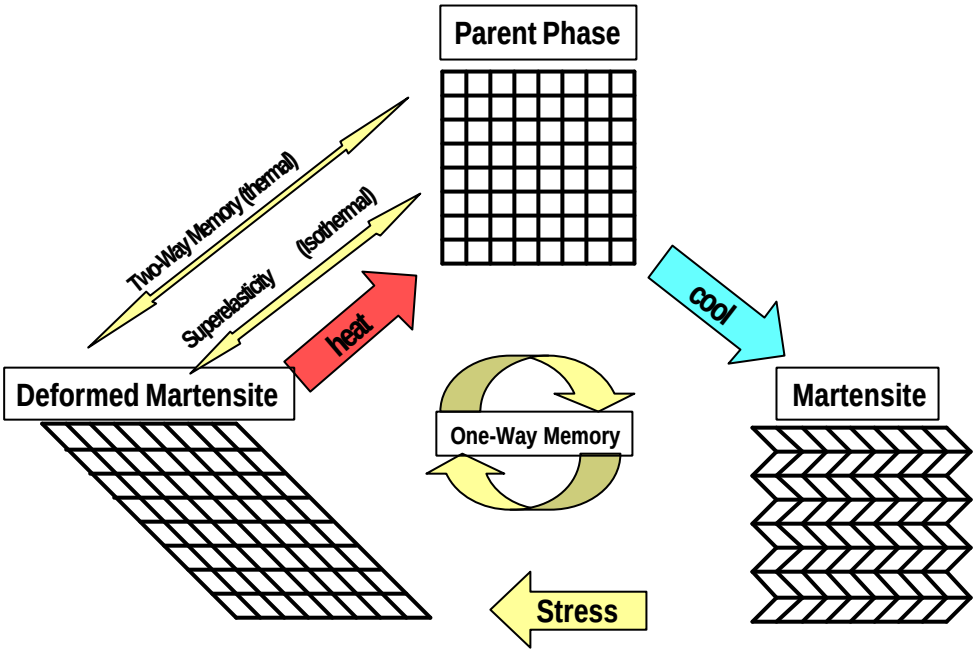

Figure 2-19 two dimensional model of the structural changes involved with shape memory transformations

If the alloy can be trained to remember a hot shape and cold shape (i.e. deformed martensite shape) then a **two-way memory** may be established where the component may be cycled between two different shapes without any external stress being applied.

Figure 2-19 can also explain the origin of the **superelastic effect** displayed by **Curve B** in **Figure 2-18**. In this case, the alloy is deformed at a temperature above A_f and the martensite transformation is entirely stress induced. The symmetrical parent phase is changed into the lower symmetry, deformed

martensite phase directly. Upon unloading, the decreasing stress and surrounding elasticity of the matrix results in the martensite plates shrinking back and the original parent phase structure being restored.

2.5.2 Superelasticity and stress induced martensite

As was demonstrated in section **2.5.1** the superelastic effect is an isothermal martensitic transformation that takes place on the application of stress at a temperature above A_s. The martensite formed in this way is known as stress induced martensite (SIM). The relationship between the applied stress and the temperature is given by the Clausius-Clapeyron equation, **(2-19)**.

Superelastic transformations take place when a thermoelastic shape memory alloy is above A_s but below M_d. Within this temperature range the martensite is made stable by the application of stress and becomes unstable when the stress is removed.

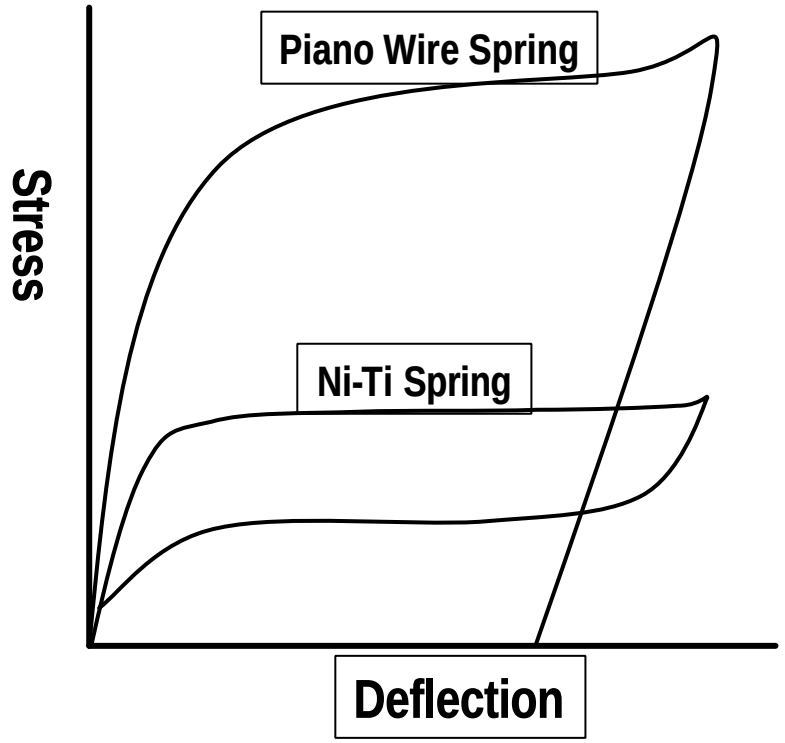

Figure 2-20 Superelastic deformation compared to conventional spring alloy

Figure 2-20 shows how the mechanical behaviour of a superelastic wire compares to that of a conventional spring material such as piano wire.

When the superelastic wire is deformed it fully recovers for strains of up to 6 or 8% in certain alloys. The upper plateau corresponds to the martensite formation under stress while the lower plateau is the reversion stress of the martensite as the applied stress is released. For the same deformation however, the piano wire does not display the lower plateau and the strain is not recovered resulting in permanent plastic deformation. It is both the large recoverable strain and the constant recovery stress plateau that can be utilised in superelastic applications.

2.5.3 One-way shape memory effect

The one-way shape memory effect occurs when a thermoelastic shape memory alloy is deformed at a temperature below A_s resulting in deformed martensite through the crystallographic pathways described in **Figure 2-19**. The deformation may be of any type, i.e. tension, compression or bending as long as the total strain does not induce plastic deformation.

At temperatures $\leq M_f$ the one-way memory mechanism is exactly as that described in **2.5.1**. However at temperatures between M_f and A_s the mechanism may first involve stress inducing the martensite depending upon the condition of the alloy. That is, if the alloy is in the martensitic condition between these two temperatures then the deformation mode is the same as for temperatures $\leq M_f$. If however, the alloy is in the parent phase condition between these temperatures then the martensite must first be stress induced to produce a memory effect upon re-heating to temperatures above A_s.

It is worth noting that the transformation temperatures for the memory effect are affected by an applied stress in the same way as the iso-thermal stress induced transformations. In superelastic transformations the temperature is held constant while the stress is varied. In the case of memory transformations the stress or applied load is held constant while the temperature is varied. The Clausius-Clapeyron equation **(2-19)** applies to both cases and the $d\sigma/dM_s$ slopes are equal. All the transformation temperatures are affected in the same way during

shape memory transformation and the Clausius-Clapeyron relationship can be written in the more generalised form:

$$\frac{ds}{dT} = -\frac{\Delta S}{\varepsilon} = -\frac{\Delta H}{\varepsilon T} \qquad \textbf{(2-20)}$$

This is very important when considering shape memory alloys for actuator applications. If the alloy is to operate against an applied load then $d\sigma/dT$ for that alloy is fundamental to its operating parameters. The value of $d\sigma/dT$ is often referred to as the **stress rate**.

It is possible to plot the temperature/stress conditions for superelasticty and memory effect on one diagram for the same alloy, **Figure 2-21**.

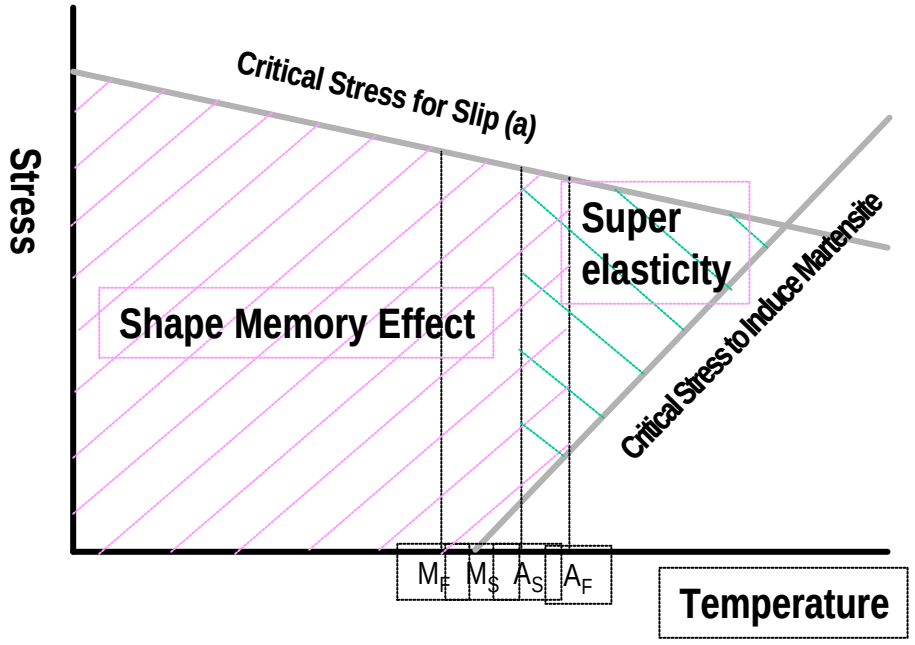

Figure 2-21 Shape memory and superelasticity as a function of stress and temperature coordinates

Depending upon the temperature and stress co-ordinates, the alloy will either display the mechanical superelastic effect or the thermal memory effect. The Clausius-Clapeyron relationship is shown as a positive gradient being

intersected by the negative gradient of the critical stress for slip line. As plastic deformation induced by slip can never be recovered by either heating or unloading, the applied stress must be below the critical stress for slip, for either memory effect to occur.

There is also some cross over of the two effects shown in **Figure 2-21**. Between A_s and A_f both effects partially occur, as described earlier in this section.

2.5.4 Two-way shape memory effect

In the one-way memory effect described in section **2.5.3** only one shape is remembered by the alloy, i.e. the hot parent phase shape. If however the alloy can be trained to remember a specific martensite shape as well as a hot shape then a two-way memory can be achieved. The shape change taking place in the two-way effect is entirely reliant upon the generation of internal forces resulting from internal stresses[50]. In this case the self-accommodation of the martensite variants will be lost on cooling and predominant variants form resulting in a memorised shape change. Subsequent heating results in the inverse transformation to the parent phase and another shape change to the second memorised shape.

As with superelasticity, the martensite transformation takes place under the influence of stress, though in this case the stresses are internal rather than external. These forces may be induced in a number of ways, usually referred to as **training** the alloy. Through training, the nuclei of the internal stress field which control the martensitic transformation upon cooling are created inside the parent phase. These sites must be stable with respect to the transformation and are usually a certain pattern of irreversible defects such as dislocations caused by deformation[51,52] or second phase particles or precipitates[53] created through stress ageing[54]. The most common methods of training are : -

- By deforming an alloy below its M_f temperature to a strain above its critical value for producing true plastic deformation, dislocations are formed which in turn produce the characteristic stress field. The specimen is then unloaded and

heated to above A_f before once more cooling to below M_f. The alloy is cycled through this process a number of times. As the number of cycles increases the re-orientation of the martensite variants becomes easier.

- By repeatedly straining the alloy specimen above A_f to produce stress-induced martensite. This cycling builds up dislocation debris within the alloy and after training the martensite variants are re-orientated as a result of the applied stress selecting a predominant variant[55].

In addition to dislocations being the source of the nuclei there are other methods. The most common of these is ageing the alloy under constant constraint. The effect differs from system to system and can result in either the stabilisation of martensite from the deformation, or the decomposition during aging producing orientated second phases within associated strain fields.
The presence of these nuclei result in stress/strain fields that cause the growth of non self-accommodating variants during 'stress free' thermal cycling. It is noted that some permanent plastic deformation is essential for the two-way shape memory effect and that complete shape recovery does not occur either by heating or cooling of the alloy. In this respect it may be argued that shape recovery does not fully occur[56]

2.5.5 Alloys that display the Shape Memory Effects

The first memory effect was observed in the Au-Cd system by Chang and Read[57] in 1951. However, it was the discovery of the memory effects in the near equi-atomic NiTi alloys by Buelher et al[58] in 1963 that resulted in renewed interest.
The thermoelastic alloys that display the memory effect all have an ordered structure. An ordered structure results in good reversibility and avoidance of slip. Ordered alloys can only have one transformation pathway for retransformation into the parent phase without destroying the original ordered structure. The wrong path of transformation actually increases the energy of the system and

changes the structure of the alloy. Reversibility is therefore guaranteed in an ordered alloy.

Certain disordered alloys do demonstrate a memory effect, i.e. Fe based alloys such as Fe-Mn-Si and Fe-Mn-Si-Co-Ni. The actual mechanism is different from that described and will not be discussed further in this dissertation. However more information can be found on these alloys in the literature.[59,60,61]

Although a large number of ordered alloys have now been found that demonstrate the shape memory effect, the only ones that have met with any commercial success are : -

- **Cu-Zn-Al**
- **Cu-Al-Ni**
- **Ni-Ti**

The response behaviour of these alloys can be altered and controlled through particular processing and alloying procedures. Varying composition allows control of many properties such as actuation temperatures (phase transformation temperatures), strength and work output during transformation. Cold work and heat treatment temperatures can also be employed to control these properties.

The copper based alloys tend to be the only practical choice for high temperature applications, (i.e. >100°C), although they can suffer from low ductility which can cause the alloy to fracture before the maximum recoverable strain is achieved. The practical recoverable strain of these alloys in the polycrystalline form ranges from approximately 3% in Cu-Al-Ni alloys to 4% in Cu-Zn-Al alloys. Copper based alloys tend to suffer from low strength and poor corrosion resistance.

The Ni-Ti alloys exhibit by far the greatest recoverable strains of commercially available polycrystalline shape memory alloys, but have lower actuation temperatures. Fully recoverable strains of 6% are easily achievable with these alloys and their comparatively high strength and excellent corrosion resistance has resulted in many unique shape memory applications. Their corrosion

resistance has resulted in a number of specialised medical applications particularly in the superelastic form.

Another advantage these alloys have over the copper based systems is their comparatively poor electrical conductivity. This presents the interesting possibility of using the alloys in solid state actuator applications where the alloy is heated by electrical current. For this reason the recent growth of research and commercial interest in **smart structures** incorporating solid state actuators, has also resulted in concurrent research into NiTi alloys.

By appropriate alloying and processing the NiTi alloys can be tuned to have M_s temperatures of –200°C to +110°C again, presenting many interesting medical opportunities.

In the next chapter the NiTi alloys will be considered in greater detail.

3 Nickel Titanium Shape Memory Alloys

3.1 History

Soon after its discovery by Buehler et al[62,63] at the Naval Ordnance Laboratory in California, U.S.A., the memory effect in NiTi alloys received considerable attention from the National Aeronautics and Space Administration, culminating in an extensive report by Jackson et al[64] on its physical and mechanical properties. Although the NASA report is undoubtedly useful in its overview of the alloy it does have a number of shortfalls that have since received much attention. This has lead to relatively consistent theories concerning the memory effect in NiTi.

3.2 Physical and Mechanical Properties

3.2.1 Phase Diagram

Many investigations have been carried out on the NiTi phase diagram, some of which were carried out before the discovery of the shape memory effect in near equiatomic alloys. One of the main discrepencies between authors concerns the boundaries of the single phase, TiNi β region about the equiatomic composition; particularly below about 800°C. Based on minimal data points, Margolin et al[65] suggested that the NiTi phase, was homogenous over a comparatively wide range of composition and stable down to room temperature. Various other authors, however, have disagreed about the extent of the stable NiTi region[66,67], identifying a low temperature eutectoid decomposition from NiTi into Ni_3Ti and $NiTi_2$. Poole and Hume-Rothery[68] found a much more pronounced narrowing of the solubility range as temperature decreased than Margolin et al[65] and experimentally confirmed the decomposition into Ni_3Ti and $NiTi_2$ found by Duwez and Taylor[67] by low temperature annealing.

Discrepancies arising from the phase diagrams may be due to variations in the processing of the alloys being investigated. For instance, titanium is very reactive in the molten state and some oxygen is invariably present in the alloy. It

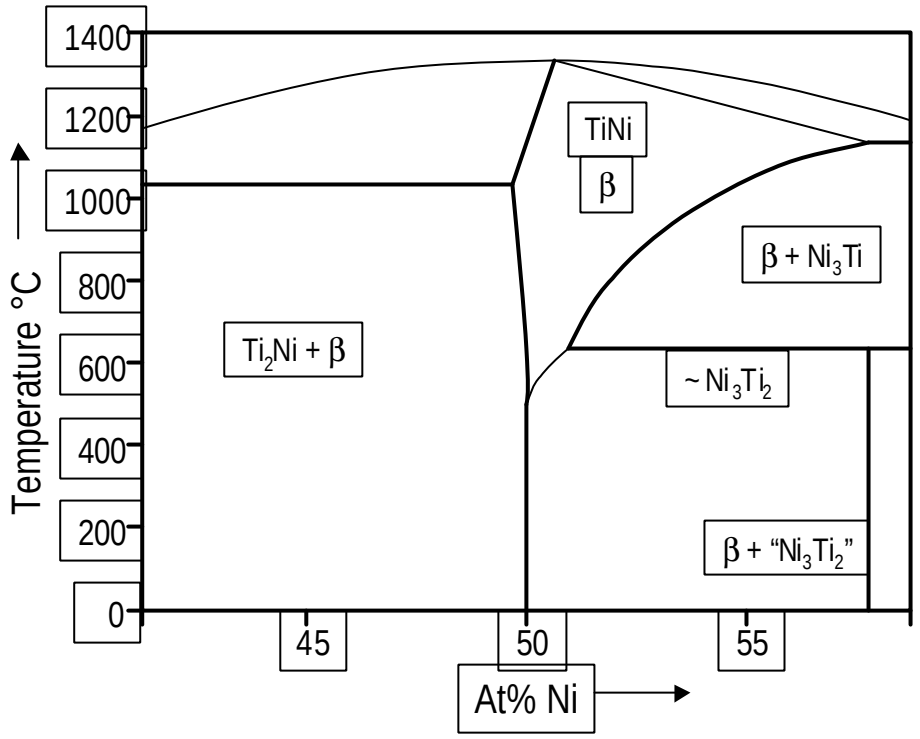

Figure 3-1 Schematic Phase Diagram of the NiTi System Around the Equiatomic Composition

has been shown that oxygen will greatly decrease the stoichiometric range of the NiTi [69] and may also result in the formation of second phase particles[70].

An extensive investigation of the phase diagram close to the equiatomic composition[71,72,73], revealed that NiTi exists as the stable compound down to room temperature although the range of homogeneity is very limited. These findings are in agreement with those of Purdy and Parr[74] and it is now generally accepted in the literature[75,76] that the NiTi β phase exists as a stable phase down to room temperature in a very narrow region between 50.0 and 50.5 at% Ni. Because of the narrow range however, the alloys may often contain precipitates of a second intermetallic phase[70]. A schematic version of a generally accepted phase diagram is shown in **Figure 3-1**.

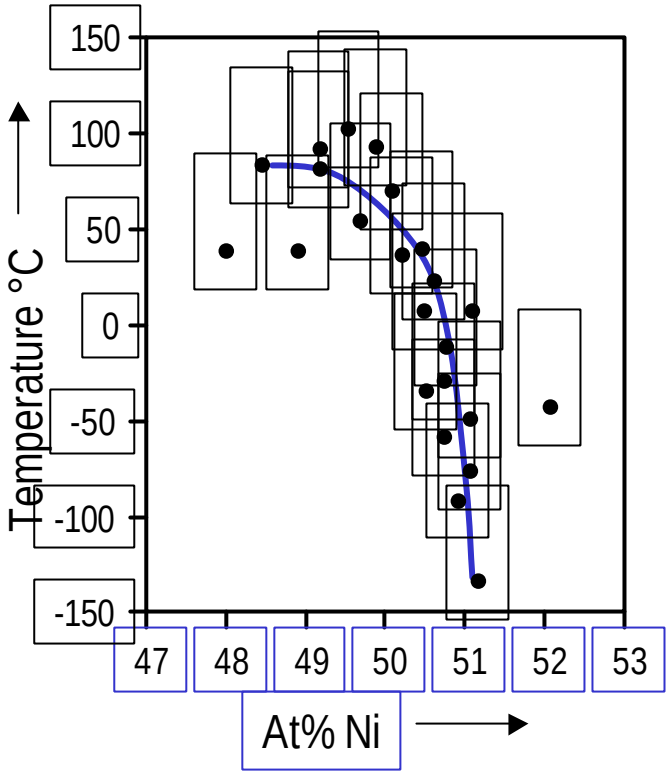

Figure 3-2 Transformation Temperature Ms Variation With Composition

Within the compositional range where the NiTi phase is stable, the transformation temperatures associated with the structural formation of thermo-elastic martensite can differ considerably. **Figure 3-2**, adapted from Melton[70], shows how the M_s temperature is particularly sensitive to composition on the Ni rich side of the NiTi phase.

Figure 3-2 is over simplified by Melton as it does not indicate the percentage of cold work in the alloys measured or the nature of heat treatment procedure. Both of these variables greatly influence the transformation temperatures but are often ignored by authors when characterising their alloys.

The sensitivity of the transformation temperatures also emphasises the need for extremely strict control when melting the alloys. Between 0.1% and 0.01% is needed to produce an alloy for a predetermined transformation temperature.

Nickel rich alloys are also susceptible to aging effects. An Ni rich alloy that has been quenched and aged at temperatures of between 200°C and 300°C decomposes into a more Ti rich matrix with higher transformation temperatures together with Ni rich second phase particles dispersed within it.

3.2.2 The Martensite Transformation in NiTi Alloys

The parent phase of NiTi equiatomic alloys has a highly ordered B2 CsCl structure that upon transformation produces a monoclinic unit cell martensite phase. The monoclinic martensite has been found to have either a P12/*c*1 a $P112_1/m$ [77] or a $P2_1/m$ [78] type unit cell. Golestaneh and Carpenter[79] found by time of flight neutron diffraction techniques that the structure could consist of either a P12/*c*1 or a $P112_1/m$ monoclinic structure. In addition they give good arguments as to why some of the work that found only a $P2_1/m$ type unit cell was flawed, including the misinterpretation of one of the intensity peaks and the possibility of errors arising from the researchers fitting process.

Whichever space group the martensite belongs to, its monoclinic structure is not in doubt. It is usually referred to as the B19' structure or the strained B19 orthorhombic structure[80] (B19 being the orthorhombic + shuffle martensite found in AuCd).

In terms of the Bain strain associated with the transformation, the monoclinic structure may be thought of as a BCC lattice in its equivalent FCT orientation that has undergone a Bain distortion to the base centered orthorhombic unit cell, B19. In addition, it has shuffled to produce the monoclinic martensite arrangement, B19'.

The successive steps in a NiTi martensite which is deformed and then recovered are shown in **Figure 3-3a**.

The volume change associated with the Bain distortion is extremely small in NiTi alloys when compared to the volume change associated with martensite transformation in steels. In the FCC to BCT transformation in steels an expansion of approximately 4% occurs whilst in the NiTi martensite transformation a volume change of just 0.34% occurs. It is this very small volume change that allows the NiTi martensite to be thermoelastic.

Depending upon alloy composition and thermomechanical processing, an intermediate phase can sometimes occur before the martensite transformation,

Figure 3-3b. This is the R-phase transformation so called because it has a rhombohedral unit cell.

Essentially the R-phase is in competition with the martensite reaction. Methods of suppressing the M_s will thus allow the R-phase to form. These include :-

- Lattice dislocations[81,82]
- The formation of precipitates in Ni rich alloys[83,84]
- Ternary elements[85,86]

In Ti rich NiTi phases the M_s temperature may be high enough to suppress the R-

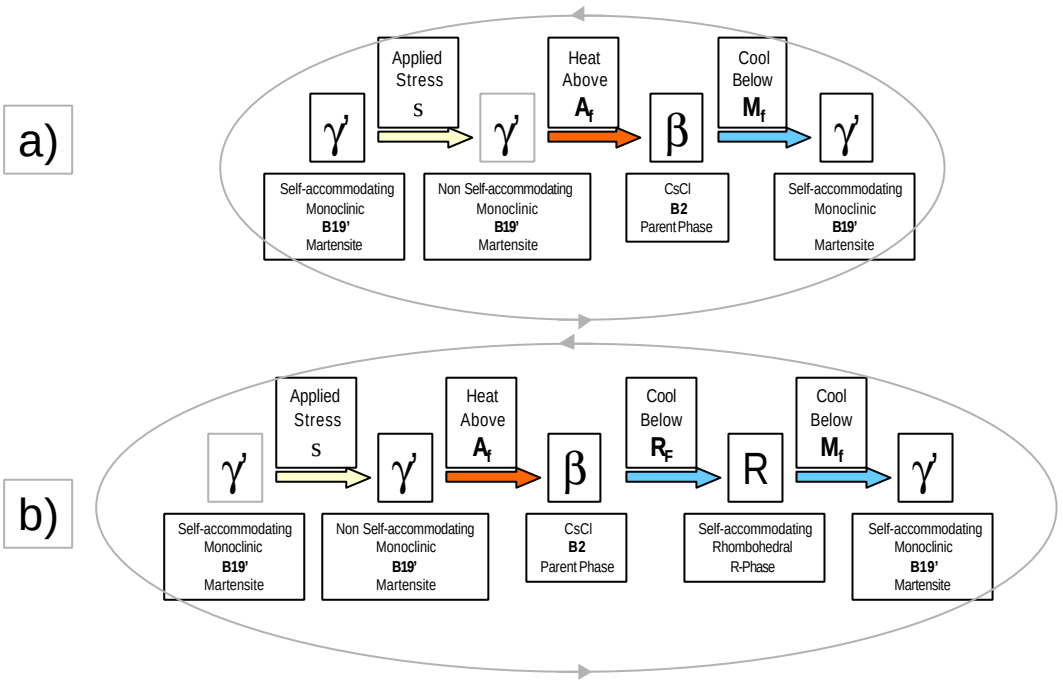

Figure 3-3 Crystallographic cycle in One Memory Cycle in NiTi

phase even if dislocations are introduced into the lattice.

The memory properties of the R-phase transition have met with great interest as it is characterised by a very small hysteresis (typically 2-5°C) and excellent

fatigue properties[81]. Unfortunately the memory strain associated with the transformation is only in the order of 0.5 – 0.8%.

3.2.3 Mechanical Properties

The ambient temperature deformation behaviour of NiTi alloys is very dependant upon the phase of the alloy and its transformation temperatures. This is shown below in **Figure 3-4**. Labelling of the different deformation regions is in accordance with that used by Liu et al[87] and other authors.

Curve 1 represents an alloy in the parent phase where the M_d temperature (i.e. the temperature above which martensite cannot be stress induced) is below ambient. The curve shows a conventional elastic limit followed by plastic deformation. In general, as the Ni content of the alloy decreases, the yield strength of the parent phase decreases[70].

Curve 2 shows an alloy tested above A_f but below M_d. Stage 1 shows some initial elastic loading of the parent phase. At a particular stress, martensite is induced and further strain results in the stress orientated variant growth plateau represented by stage 2. If the alloy is unloaded at this point then superelastic shape recovery will take place and the curve will follow the path represented by the broken line.

If the alloy is not unloaded however, the further strain results in elastic deformation of the stress induced martensite, stage 3, until eventually the yield stress is exceeded and plastic deformation takes place, stage 4. Ultimately ductile fracture takes place via void coalescence around second phase particles.

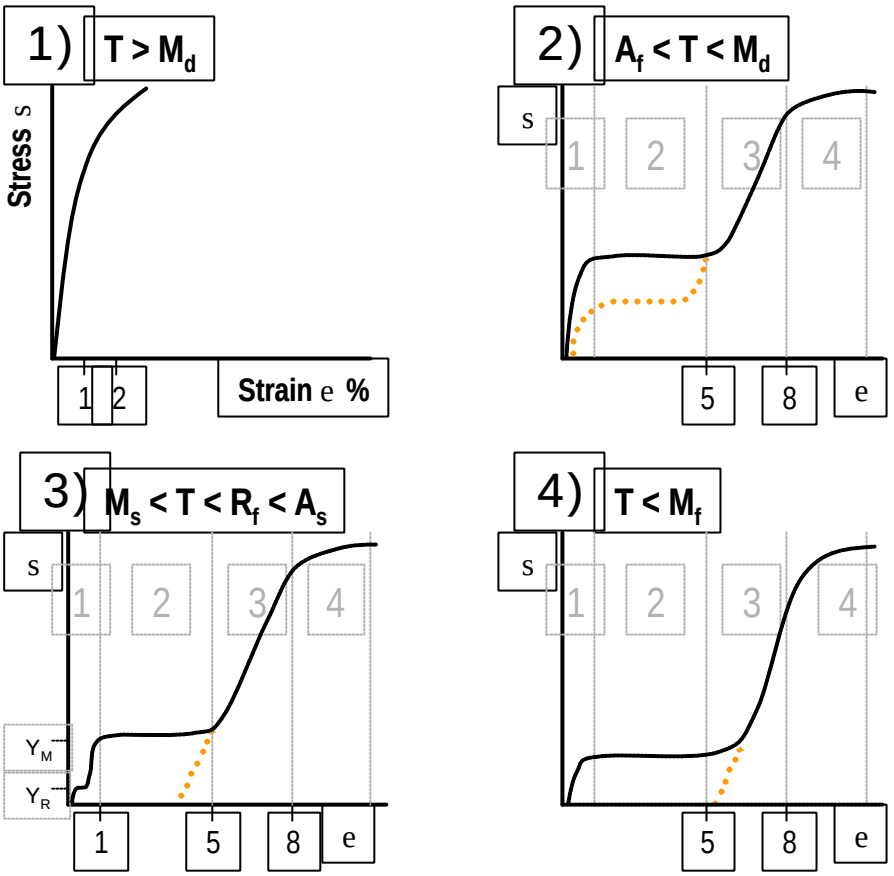

Figure 3-4 Stress Strain Behavour of NiTi

Curve 3 shows an alloy that has been cooled from the parent phase and the ambient testing temperature is between A_S and M_S but below R_f. During stage 1 deformation an initial yielding takes place at Y_R due to the rearrangement of the R-phase variants over a strain range of approximately 0.8%.

A stress induced martensite plateau (stage 2) is formed at $Y_{M.}$ This is a lower stress than the equivalent in Curve 2 and is complete after a total strain of approximately 5%. If the alloy is unloaded after re-orientation of the martensite variants is complete, then the strain formed by the elongation is left in the alloy, this is represented by the broken line. This strain can be recovered via the one-way memory effect by heating above A_f.

If the stress is not released after stage 2 then subsequent loading results in elastic deformation of the re-orientated martensite variants (stage 3). Eventually

the stress required for slip to take place is exceeded and permanent deformation takes place (stage 4) leading to eventual ductile failure. If the same alloy was tested below A_s but above R_s then Y_R would not occur during stage 1.

Curve 4 is an alloy tested below its M_f temperature in the fully self accommodating, martensitic condition. At a very bw stress after the stage 1 elastic deformation of the martensite, the plate variants begin to realign at a constant stress until reorientation is complete (stage 2). Subsequent loading results in elastic deformation of the martensite variants (stage 3) and eventual plastic deformation (stage 4) and failure.

The yield point due to reorientation of the R-phase is absent from stage 1 in this alloy as the structure is fully martensitic before the test, therefore no R-phase can exist.

This simple description of stage 3 deformation as : the elastic strain of the detwinned, fully reorientated martensite variants, is favoured by many authors[88,89]. However, Melton and Mercier[90] showed with an excellent TEM study on the deformation behaviour of NiTi that the stage 3 type deformation shown in **Figure 3-4** is in fact due to a combination of effects. They found that in some colonies of martensite, further recoverable strain in the direction of applied stress is possible by the nucleation of new martensite orientations which intersect those already present. For unfavourably orientated colonies however, the stress to nucleate these new variants is large and consequently this process does not occur. Stress concentrations resulting from strain incompatibilities between adjacent colonies can lead to local stresses exceeding the yield point and some localised slip occurring.

The work carried out by Melton and Mercier[90] was on an alloy almost fully martensitic prior to testing. They also propose a similar deformation mechanism wherever the test takes place in relation to its transformation temperatures. They state that the slopes of the stage 3 deformation shown in **Figure 3-4** are similar whether the alloy is martensitic prior to testing or whether the martensite is stress induced during stage 2. However, It is possible that during stage 3 deformation after stress induced martensite is formed, a smaller proportion of colonies are unfavourably orientated with respect to the applied stress and the creation of

new intersecting variants. This is because during deformation in superelastic alloys, the variants are selected and grown in relation to the applied stress[90]. This results in fewer localised stress concentrations and less dislocations being generated during stage 3. By this reasoning, one might expect the gradient of stage 3 deformation in an alloy deformed above its A_f temperature to be less than that of the same alloy in the martensitic condition prior to testing.

It is also believed that the new orientations of martensite formed during stage 3 deformation provide additional heat recoverable strain[90]. The total recoverable strain therefore becomes the reorientation strain produced during stage 2 (typically 5-6%) plus the reorientation strain produced during stage 3 (typically 2-3%) resulting in an often quoted figure of 7-8% recoverable strain for NiTi alloys. It is obvious that the maximum recoverable strain depends heavily upon the stage 2 plateau strain. This can vary greatly with alloy composition, testing orientation, deformation mode and prior thermo-mechanical testing[70]. Therefore the 8% figure should be considered an ideal rather than a norm.

3.2.4 The Effect of Prior Processing on Mechanical Properties

The processing history and microstructure of NiTi alloys also has a marked effect on mechanical properties[91,92]. The shape of the stage 2 stress-strain curve shown in **Figure 3-4** changes greatly with prior thermo-mechanical processing and testing temperature and can vary between a continuous curve with an inflection point to a horizontal plateau with a very well defined start and finish point[93].

The combination of heat treatment temperature and prior cold work is fundamental in establishing an alloy with good mechanical properties and a stable memory effect. It is regrettable that so many authors neglect this fact when carrying out experiments on the alloys. It is not enough to quote only the alloying content; prior cold work and the heat treatment temperature are often of equal importance when attempting to interpret results.

A NiTi alloy that is in the as received condition will usually have an amount of residual cold work resulting from the wire drawing process. If no anneal is carried out, then the mechanical yield strength will be high but the memory properties are poor and only low recoverable strains are possible. If an annealing step is carried out however, then the dislocation structure introduced by the cold work becomes rearranged which results in improved memory characteristics but lower values of internal stress. The lower internal stress results in less resistance to applied stresses and lower yield strengths. A minimum stress for slip in the parent phase, reorientation of the martensite variants and stress induced martensite, occurs at the recrystallisation temperature of the alloy[93], approximately 600°C.

Concurrent with the decrease of internal stress in the structure is an increase in the transformation temperatures. It is difficult to find a full explanation of this effect. It has been found that aging alloys of relatively high Ni content (>50.6 at%) results in the precipitation of a Ni rich second phase resulting in a titanium rich matrix and higher transformation temperatures. For lower Ni contents however, the process is less clear. It is likely that the redistribution of the dislocations and internal stress fields somehow assist the martensite transformation in a manner similar to the Clausius-Clapeyron effect when an external stress is applied. It will be shown later that the transformation enthalpies also increase with the annealing and transformation temperatures.

Often, high cold work is given as a way of forming a superelastic alloy. It should be remembered that cold work, heat treatment temperature, resistance to slip, reorientation stress of the martensite and transformation temperatures are all interrelated. Increasing cold work does not produce superelasticity in its own right, rather it increases the resistance to slip and lowers the transformation temperatures which may result in superelasticity for a given ambient temperature. **Figure 3-5** shows a series of stress-strain curves for a Ti-50.2at%Ni alloy annealed at 400°C for 1Hr given varying degrees of prior cold work[76]. The amount of cold work is indicated above each curve. The tests were

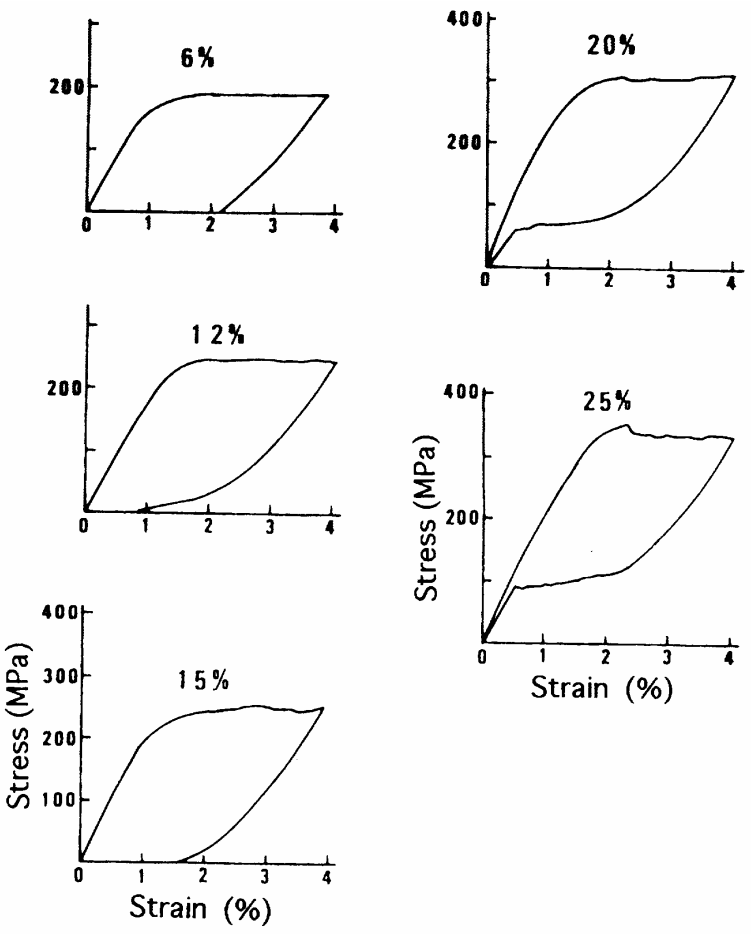

Figure 3-5 The variation of stress-strain behaviour with cold work[76]

carried out at 50°C. It is shown that the strain recovered on unloading increases with prior cold work. Above 20% cold work the alloy shows complete superelasticity.

Similar curves are obtained if the annealing temperatures are varied while the prior cold work is kept constant. Again, this emphasises the close interplay of the various processing variables and how they affect the memory characteristics and mechanical properties.

3.2.5 Corrosion Characteristics

One of the differentiating benefits of NiTi over other commercial shape memory alloys is its excellent corrosion resistance. In fact the Naval Ordnance Laboratory that discovered the shape memory effect in this alloy were initially researching its corrosion resistance. In the galvanic series it has a nobility greater than that of 316 stainless steel thanks to the passivity of the naturally formed and very thin titanium oxide (TiO_2) film which forms on the surface. The formation of this film is exactly the same as that for pure titanium. The film is very stable and resistant to many forms of potentially corrosive attack. Breaks in the surface however, can be slow to recover.

The corrosion resistant behaviour has led to studies on the biocompatibility of NiTi and a number of medical applications. It has been found through clinical tests that the biocompatibility is excellent with no metallic contamination of the organs. The titanium rich oxide surface prevents the nickel content of the alloy reaching the tissue. This has resulted in great activity in the medical market and has been one of the catalysts driving shape memory research.

3.2.6 Summary of Mechanical and Physical Properties

NiTi alloys offer many unique memory properties. In addition, their high recoverable strains and excellent corrosion resistance differentiates them from the copper based memory alloys. Unfortunately, their comparatively high cost and poor workability is often a factor in determining whether an application has commercial feasibility. For reference and comparison, **Table 3-1** summarises the physical, mechanical and commercial properties of NiTi and copper based shape memory alloys.

Table 3-1 Summary of the Physical, Mechanical, Memory and Economic Properties of Binary NiTi and the Copper Based Alloys. Compiled From[94,95,96,97]

Physical Properties	NiTi	Cu Based Alloys
Density	6.4-6.5 gcc^{-1}	7.1-8.0 gcc^{-1}
Melting Point	1250ºC	950-1050ºC
Thermal Conductivity		
Martensite	8.6-10.0 W $mºC^{-1}$	- W $mºC^{-1}$
Parent Phase	18.0 W $mºC^{-1}$	75-120 W $mºC^{-1}$
Electrical Resistivity		
Martensite	0.5-0.6 $\times10^{-6}\Omega m$	0.14 $\times10^{-6}\Omega m$
Parent Phase	0.82-1.1 $\times10^{-6}\Omega m$	0.07 $\times10^{-6}\Omega m$
Coeff' of Thermal Expansion		
Martensite	6.6 $\times10^{-6}ºC^{-1}$	16.0-18.0$\times10^{-6}ºC^{-1}$
Parent Phase	10.0-11.0 $\times10^{-6}ºC^{-1}$	- $\times10^{-6}ºC^{-1}$
Specific Heat Capacity	470-620 J Kg $ºC^{-1}$	390-440 J Kg $ºC^{-1}$
Enthalpy of Transformation	19.0-28.0 JKg^{-1}	7.0-9.0 JKg^{-1}
Transformation Temperature Range	-200-120ºC	-200-+200ºC
Corrosion Performance	Excellent	Poor
Bio-compatibility	Excellent	Assumed Poor

Mechanical Properties	NiTi	Cu Based Alloys
Young's Modulus		
Martensite	28-41 GPa	70GPa
Parent Phase	70-97 GPa	70-100GPa
Yield Strength		
Martensite	70-140 MPa	80-300 MPa
Parent Phase	195-690 MPa	150-350 MPa
Ultimate Tensile Strength		
Fully Annealed	895 MPa	400 MPa
Work Hardened	1900 MPa	1000 MPa
Elongation at Failure		
Fully Annealed	25-50%	8-15%
Work Hardened	5-10%	8-15%
Hot Workability	Poor-Fair	Very Good
Cold Workability	Poor	Good
Machinability	Poor	Very Good
Poisson's Ratio	0.33	-
Wear Resistance	Good	-

Memory Properties	NiTi	Cu Based Alloys
Transformation Temperature Range	-200-+120ºC	-200-+200ºC
Hysteresis	20-50ºC	15-20ºC

One-way Memory Max.	8%	4-6%
Two-way Memory Max.	3-5%	1-4%
Superelastic Strain	8-10%	2%
Work Output	1-4 Jg^{-1}	1 Jg^{-1}

Economic Properties	NiTi	Cu Based Alloys
Composition Control	Very Strict	Fair
Unit Cost	High	Fair
Forming Cost	High	Fair

4 Strategic Research Requirements and Market Issues For The commercial Future of NiTi Shape Memory Alloys

4.1 Overview

Soon after Buehler first discovered the shape memory effect in NiTi alloys the commercial world began to try and assimilate the unique characteristics of the alloy with product applications. It is perhaps, because of the fact that NiTi shape memory effects first became realised in the 1960's that so much initial effort went into finding applications. During this decade and the one before it, new materials were heralded as the key to economic growth and commercial success throughout many industrial sectors. The impact of thermoplastics, semiconductors and new metallic alloys resulted in this period being referred to as the materials revolution and the discovery of a metal that would change its shape was seen as yet another material that would 'shape' the future of industry. Of course the effect had already been found in the copper based systems but had so far only been viewed as a physical curiosity that may be used to learn more about martensitic transformations.

In addition to the NiTi alloy being discovered at the height of the new materials revolution it was also the geographical location of the discovery that resulted in such commercial interest. During the 1960's California was the innovation centre of the world, as from music to hi-technology the state was booming in every way. Undoubtedly, the NiTi alloys rode this wave of industrial optimism in the 1960's and innovative engineers from many industrial sectors struggled to find applications for it.

The Raychem Corporation, an American materials technology company, grew out of California at this time and in 1971 were the first to bring out a large scale product based on the NiTi shape memory alloy system. This was the cryogenic coupling device used to connect titanium hydraulic tubing in the Grumman F-14 aircraft[98]. The idea of the shape changing alloy had a commercial fit with the heat shrinkable polymeric tubing known as Thermofit® tubing already produced by Raychem. The new range of NiTi couplings that shrunk on removal from liquid

nitrogen became registered as Cryofit® couplings and the future appeared to be bright for shape memory application.

In a recent publication K.N.Melton referred to the pipe couplings developed by the Raychem Corporation as being a classic case of technology adapting to a real market need. While it is true that Grumman were experiencing difficulty in finding a reliable coupling system for their titanium hydraulics it is difficult to say what really came first the problem or the solution. Melton is correct in saying however, that the 15 years proceeding the Cryofit® couplings were spent looking for an additional market for NiTi technology, a classic case of technology push.

During the 1950's and through to the end of the 1960's it was generally assumed that industrial technological innovation was more or less a linear process, beginning with scientific discovery, passing through industrial research and development and finishing with a marketable new product. During this period the marketplace was a passive end point for thrusting R&D. This process epitomises the so called 'technology push' model of industrial innovation and was a strategy that continued up until the late 1960's and into the early 1970's.

By 1971, the time the Grumman couplings finally came to market, the strategy of innovation was changing. A new model began to take shape placing much more emphasis on the role of the market place in innovation. Empirical results based on real innovations[99] began to establish a new 'market pull' strategy sometimes referred to as 'need pull'. It began to be realised that the most successful innovations tended to result from either perceived or clearly defined customer needs, resulting in closely focused research and development. However, shape memory alloy manufacturers continued with the technology push strategy well into the 1980's leaving behind them a trail of failed products such as the thermally activated greenhouse latch[100] and the VEASE® [101] electrical actuator for automobile fog lamp louvres.

In the early 1980's, at last a genuine market pull began to develop in the shape memory industry. Slowly it became apparent that the number of papers being presented on potential medical applications began to increase. Shape memory manufacturers and medical device companies who recognised the potential value in this market began to file strategic patents and develop products that

provided unique solutions to medical problems. The market pull on shape memory applications gradually intensified during the 1980's until in 1994 the first international conference on shape memory and superelastic technologies took place concentrating on practical applications. The influence of the medical market pull was obvious from the number of papers presented on biocompatibility and medical applications. This conference has now become a regular event and a European version took place in Belgium in September 1999. Around the beginning of the 1990's a new market for shape memory alloys began to emerge, that of 'Smart Materials' and 'Smart Structures'. Whilst not being a specific, tangible market segment like that of the medical industry, the recent interest in smart structures has resulted in considerable market pull on shape memory alloy research and development.

It is beyond the scope of this thesis to argue too deeply about the correct definition of what constitutes a smart material or structure, there being already numerous publications that do just this. The following definition however, based on reports resulting from the DTI OSTEM (Overseas Science and Technology Expert Mission) to Japan in 1993, does summarise the important issues concerning the nature of the field and the materials that can be used within it :-

- ***Smart Structures*** – Systems with added functionality imparted by the integration of physical elements such as sensors and actuators with non active materials.
- ***Smart Materials*** – Materials with inherent functionality designed at a molecular level.

Again, it is beyond the scope of this thesis to define which of these categories shape memory alloys fall into, some researchers saying neither and some saying both. It is sufficient to say, that the proactive research surrounding this area, has produced its own specific journals and conferences and has resulted in a resurgence of interest in using shape memory alloys in actuator applications. For this reason it has become an important strategic segment for shape memory

alloy manufacturers and a major driver of current shape memory research and development.

It is interesting that the two markets exerting a pull on shape memory alloys are essentially concerned with utilising different memory effects. That is, the major applications and patents within the medical sector are concerned with superelasticity, whilst the smart structures researchers' concern is that of repeatable shape change in actuator applications.

Strategically it is important for the shape memory alloy manufacturer and engineer to understand how the alloys' unique characteristics offer potential competitive advantage over other systems in the same application. The following section considers how and why the NiTi alloys offer such advantages.

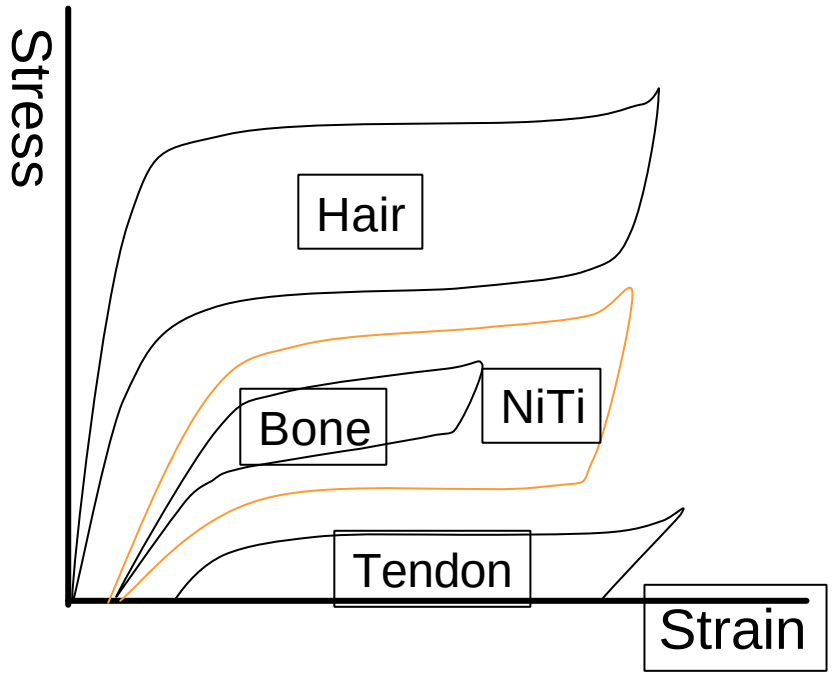

Figure 4-1 The Stress-Strain Bio-Mechanical Compliance of Nitinol

4.2 the shape memory effect for competitive advantage

4.2.1 Shape Memory Alloys as Superelastic Medical Materials

During ICOMAT 98 held in Argentina, Tom Duerig, the chief executive officer of Nitinol Devices and Components in the U.S.A., gave a keynote lecture on the state of the NiTi medical device industry. In it he stated that during live stenting operations relayed by CCTV to medical conferences, over half of the American surgeons now ask their colleagues :

"Shall I use a Nitinol Stent?"

This demonstrates the extent to which NiTi (Nitinol) alloys have entered the medical market. Their success and continued development is thanks to their unique combination of properties that offer the following benefits within medical applications :-

- Nitinol stents can be self expanding within the host. This allows the stent to adapt to complex shapes both in situ and during insertion. Stainless steel stents tend to be of the ballooning type where the stent is expanded to a pre-determined shape after insertion and does not easily follow complicated insertion paths.
- Nitinol devices can be deployed elastically or thermally using chilled saline to maintain the martensite phase.
- Due to its high recoverable strains, Nitinol can provide kink resistance in micro instruments and guide wires that are passsed through blood vessels for directing catheters. The use of stainless steel or titanium alloys under the same strains results in permanent deformation.
- The biocompatability of Nitinol has been shown to be excellent.
- The stress-strain behaviour of Nitinol results in a unique bio-mechanical compliance within the patient**, Figure 4-1**.
- Nitinol stents can be tuned to have a very low chronic outward force. That is, the force with which the stent expands to its operating shape can be tuned to a very low plateau. Equally the radial resistance force of the stent can be

tuned to a high value thus resisting deformation during service. These forces are demonstrated in **Figure 4-2**.

- Nitinol stents and instruments are compatible with magnetic resonance imaging. Stainless steel components black out the whole screen.
- Unlike stainless steel, Nitinol devices can be expanded uniformly under a

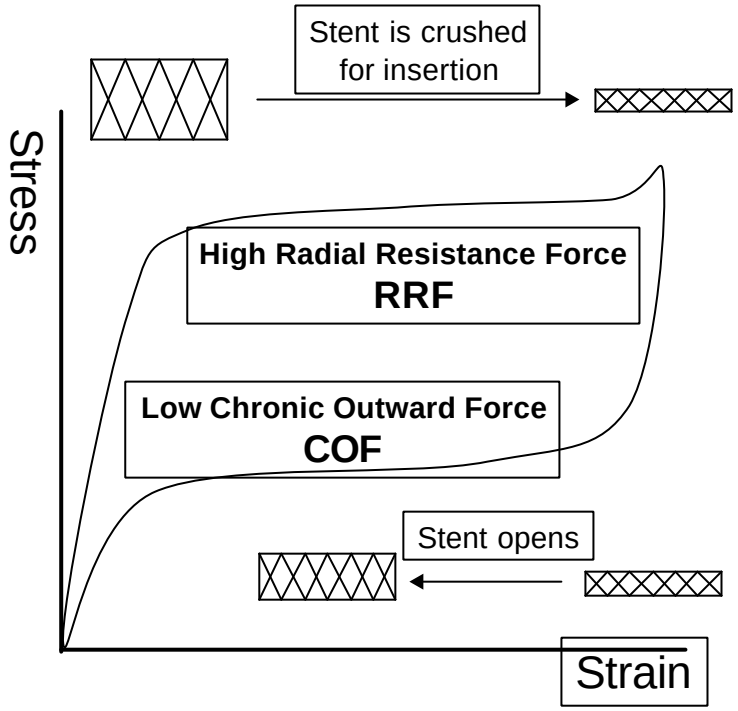

Figure 4-2 The Low Chronic Outward Force and High Radial Resistance Force of Nitinol Stents

constant deployment stress via the growth of the martensite variants.

4.2.2 Shape Memory Alloys as Actuators

Actuation is the controlled production of work output or energy release. It is likely that the main use of shape memory alloys within smart structures will be as

actuators operating through the conversion of thermal energy into kinetic energy and work output.

The use of these alloys as solid state actuators offers many benefits[102]:-

- High recovery forces
- Large recoverable output strains
- Different actuation modes (linear, bending, torsion)
- High work output per unit volume or mass

It is perhaps the large strains and high work output that offer most opportunities for innovative design with SMA's. Graphically we can consider how the **material function** of the shape memory effect differentiates them from other actuating materials such as piezoelectrics and magnetostrictives, **Figure 4-3a**.

When considering the differentiating benefits of SMA actuators some disadvantages should also be considered. **Figure 4-3b** shows how compared to other possible actuators SMAs suffer from low efficiency (i.e. high loss actuation) and very poor response times or actuation frequencies. Successful applications will build on SMA strengths whilst taking into account its weaknesses.

The properties so far described emphasise how shape memory alloys may offer great opportunities for innovation when used within structures or as stand alone components. To successfully promote and encourage the commercial acceptance of SMA's within the markets that are exerting the greatest pull on R&D, strategies for assimilating the unique properties with applications must be considered.

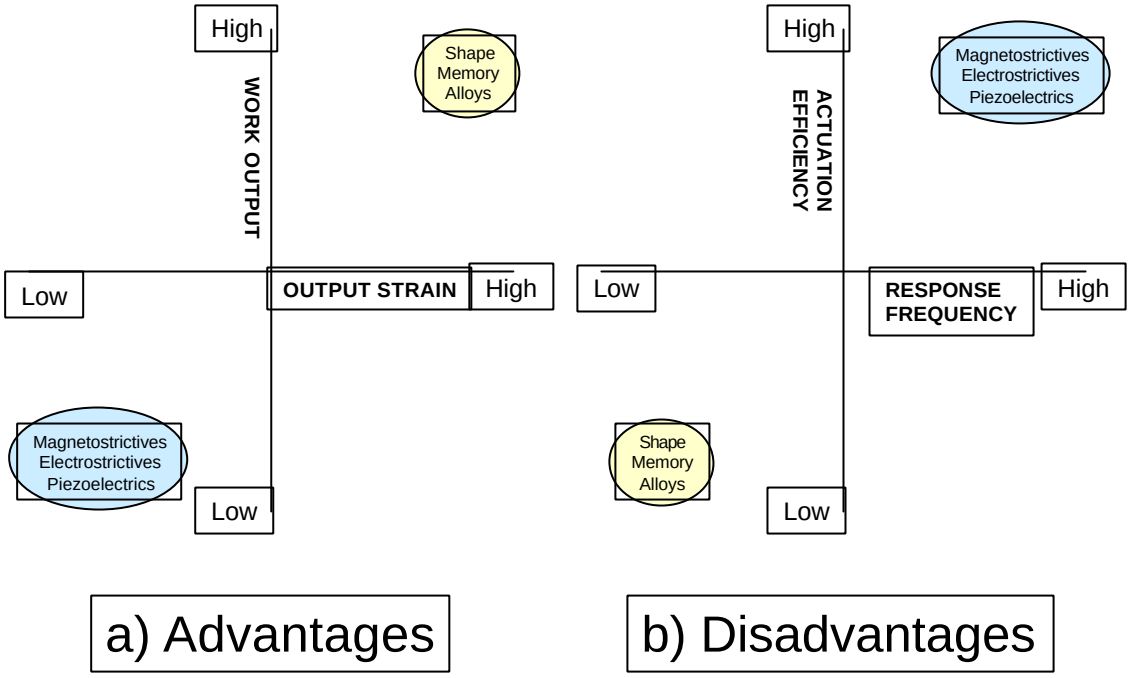

Figure 4-3 Differentiating material function of shape memory alloys

4.3 the shape memory alloy awareness and assimilation strategy

The role that new products play in gaining and maintaining competitive advantage within high technology industries is widely recognised and understood[103]. The unique property of shape memory has often attracted innovative design engineers from many major industries, including the aerospace and automotive sectors. The designers see shape memory as a way of differentiating their product from their competitors and adding value to produce a component more attractive to their customers. A good example of this was the automatic choke system developed by Mercedes Benz and the VEASE®[101] actuator previously referred to. However, the high costs involved in producing new shape memory alloy products and the many application barriers that also exist, often prevent SMA applications coming to fruition.

Figure 4-4 graphically describes how these barriers stand between the memory effect in NiTi alloys and the final commercial exploitation.

4.3.1 Primary Barriers

It is shown that the primary barrier to SMA applications is that of awareness. Few engineers and designers are aware of SMA's and their potential as an engineering material. In order to increase this awareness, shape memory alloys and the unique advantages that may be gained through their use should be promoted to those engineers and designers seen as innovators in their

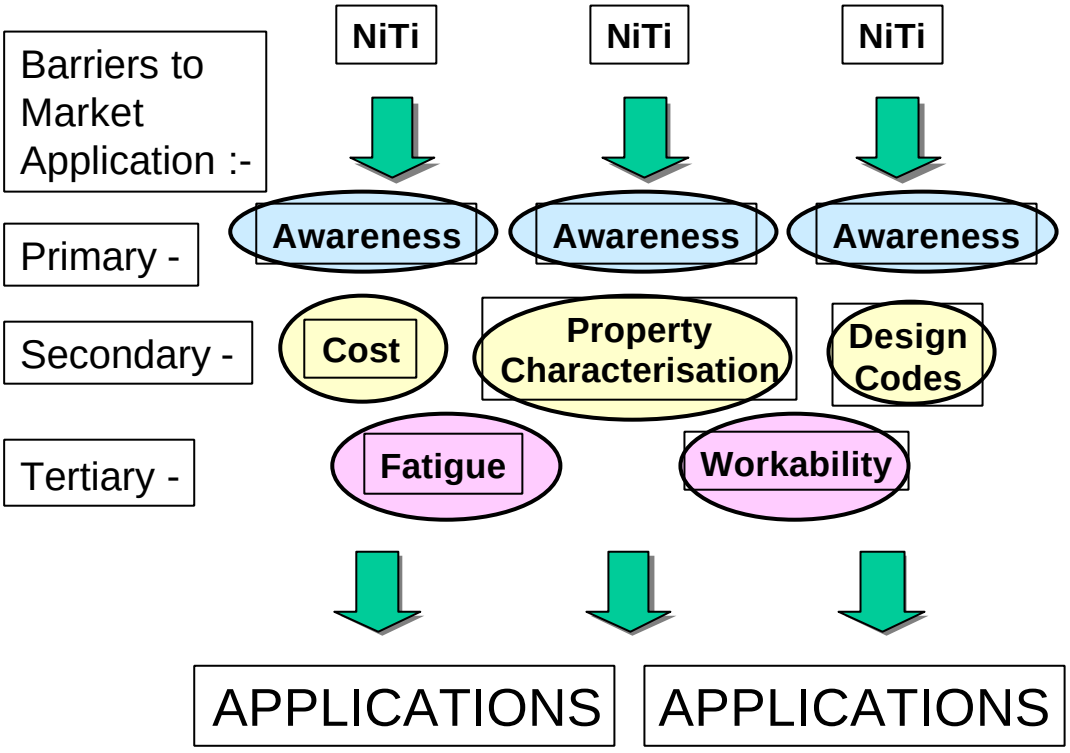

Figure 4-4 The awareness and assimilation barriers to shape memory alloy applications

particular industries. For instance, it is more likely that a medical device manufacturer with a reputation for innovation will pursue a shape memory product than a manufacturer who only tends to develop products based on recognised designs and off the shelf materials.

However for these engineers and designers to then assimilate the idea of shape memory properties with real applications there are a number of secondary barriers that must also be overcome.

4.3.2 Secondary Barriers

The secondary barriers emphasise the need for accurate property characterisation and design codes with the comparatively high cost of shape memory alloys compared to more conventional materials.

Many products will fail at the secondary barrier stage. The greenhouse actuator for instance was never able to match wax actuators on price and was never taken up by nurseries already operating in a market where profit margins were tight. A nursery produces its own product and a plant grown in a greenhouse using shape memory actuated windows will have no more value than a plant grown with wax operated windows.

In some markets however, the secondary barriers may not prevent application on their own. An example is in markets that are not strictly driven by price or in markets where the value added through the use of shape memory may be passed on to the end user.

Shape change characterisation can still only be usefully obtained from shape memory alloy manufacturers. Shape change properties such as transformation temperatures and recovery strains are not easily accessible which is mainly due to their heavy dependence upon thermomechanical processing. Tables giving NiTi transformation temperature ranges of between : -200ºC and +110ºC with recovery strains of 8%, are misleading and do not help engineers in establishing which material to use. This leads to telephone calls from engineers with good intentions asking for alloys that will change from one shape to another over a temperature range of 5ºC with a recoverable strain of 7%. From the table the engineer will think this is easily achievable, but upon contacting a supplier they will be disappointed to find that in fact an alloy which is able to match these requirements does not exist. They will be told that to operate over 5ºC they must put up with a maximum recoverable strain of 0.7% or to achieve a higher strain

they must operate over a temperature range of 50ºC. The engineer then loses interest and goes away thinking that indeed the shape memory effect is only an interesting phenomena and will never find large scale application.

Closely linked to characterisation needs is the design codes barrier. Due to the fact that the shape recovery characteristics are so dependent upon applied stresses, it is very difficult to design shape memory products using anything like conventional design paradigms. For instance, in the example described previously; if the engineer did find an alloy suitable for the application but then decided it was going to have to operate against an applied stress of 300MPa; then due to the Clausius Clapeyron relationship, the transformation temperatures and transformation strains would be greatly affected. This barrier is particularly prominent when attempting to design an actuator product that is required to do work.

If the secondary barriers can be overcome, i.e. a design has been formulated using an acceptable alloy within specified cost constraints then a final set of tertiary barriers must be addressed. These are shown in **Figure 4-4** as workability and thermomechanical fatigue.

4.3.3 Tertiary Barriers

NiTi alloys in particular, suffer from poor workability and, until very recently, have only been available in wire form. However, the major shape memory manufactures are now able to supply NiTi in tube, strip and even plate form. The availability of NiTi in these forms and continued research in areas such as workability and powder forming is gradually addressing the shape limitation problem of NiTi applications.

So, finally, if a design has been formulated using an acceptable alloy within specified cost constraints and it can easily be formed into the required net shape an extensive thermomechanical fatigue programme may need to be carried out if it is to undergo repeated phase transformation during service.

Unlike conventional alloys, the functional properties of shape memory alloys necessitate an extension of the usual definition of fatigue[104]. That is, in addition

to failure by cyclic stress or strain at constant temperatures, changes in physical properties and degradation of the memory effect due to cycling through the transformation region are also possible. These changes may take place at constant temperature (superelastic transformation) or through pure thermal cycling (one and two-way transformations). The reliability of a shape memory application depends on its lifetime performance. If the component is required to carry out repeatable transformation cycles, then the thermomechanical behaviour of the alloy in the application operating conditions is of paramount importance. Little systematic research has been carried out on thermomechanical fatigue. As will be shown in the next chapter, what work has been carried out, appears to yield often contradictory results. Systematic research could avoid these apparent contradictions and more reliable predictions of the long term behaviour of shape memory alloys could be assessed[104]. This would also provide the decision making arguments in the choice of alloy composition and design, which will in turn lead to more shape memory applications.

It is easy to see from the model described in **Figure 4-4** how NiTi alloys main commercial application has become non-actuating products. Exact property characterisation is not so important as long as the alloy is superelastic and will undergo the required strain without breaking. More conventional paradigms may be followed for the product design and may often follow designs already established in alternative materials. In addition, cost is not always of overriding importance since medical devices do not tend to be cost driven but rather they are value driven. If the superelastic effect adds value to the product, which is passed on to the patient in terms of the function it performs, then the added cost of using the alloy is not a priority. Most of the products are easily formed from the shapes readily available, i.e. : wire, tubing etc. Fatigue is not believed to be a problem by most NiTi manufacturers; certainly thermomechanical fatigue is not a problem in isothermal superelastic applications. However, even purely stress induced superelastic transformations involve the martensite plates and interfaces constantly moving through the matrix and many researchers believe much more fatigue data are required on all memory effects before medical applications are widely accepted.

Strategies that are focused on achieving certain market objectives through appropriate R&D and promotion could increase the market opportunities for shape memory alloys whilst making the whole product development process much more efficient. By following an awareness and assimilation strategy that concentrates on application barriers, a simultaneous increase in SMA applications may occur leading to shape memory alloy market growth. For instance, the need for systematic thermomechanical fatigue data is of paramount importance in actuator type applications. Shape memory alloys will never see wide spread use within smart type structures without it.

4.4 shape memory product life cycles and the diffusion of applications

The stage of product development within an industry or market segment is an important consideration for any commercial development strategy[105]. The Product Life Cycle (PLC), concept is a simple but useful tool when considering

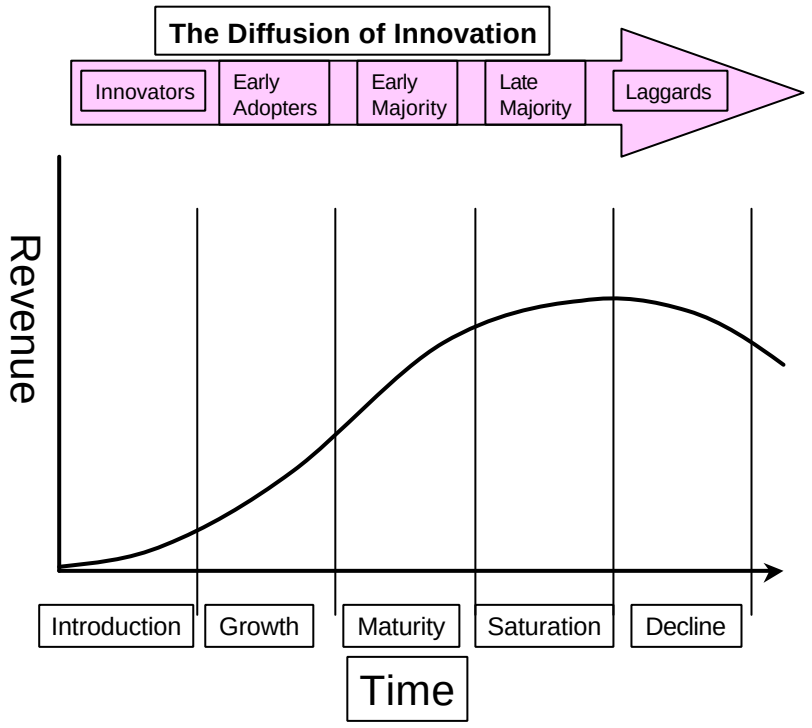

Figure 4-5 The diffusion of innovation within the product life cycle

technological and market strategies for shape memory alloys. The PLC, **Figure**

4-5 describes how any product exhibits a time dependent sales pattern. It suggests that different application strategies may be required at different times and that future research and development can be planned around historic and present sales trend. In reality, a product's life cycle may not be the simple curve shown here, but essentially it will show the same type of trends with time.

The early part of the curve denotes a struggle to get the product known; sales are hard to come by and a lot of time and energy is likely to go into developing awareness and acceptance, this is known as the ***introduction*** phase. Next there comes a time when the product 'takes off', this is called the ***growth*** phase. After this, the rate of growth slows and the product enters the ***maturity*** phase. Eventually there comes a ***saturation*** stage when the product loses its appeal and demand begins to level out and steadily begins to ***decline***.

Although shape memory alloys have been in existence for some years, in many potentially lucrative markets, as will be shown in section **4.4.2** , they are still in the introduction phase. It is these markets where manufacturers and small to medium business units should focus their strategic efforts. Equally, manufacturers of products where sales are showing a decline also need to make important strategic decisions on the future of their product.

In addition to the life cycle, **Figure 4-5** also shows how the diffusion of a product into the market place takes place. Identifying innovators and early adopters within identified market segments may correspond to sales growth. During the introduction phase, profits are likely to be low or even negative and product strategies should aim to diffuse shape memory alloys into the target market through those customers or manufacturers considered to be innovative. Careful thought and investigation will identify who the market innovators and early adopters are likely to be and promotion and advertising should aim to build awareness and encourage trial amongst them. The user and commercial value that may be added to their products through the use of shape memory alloys should thus become apparent.

It is interesting to analyse the product life cycle both in terms of the NiTi alloy as a core product and in terms of the core products resulting from the use of NiTi.

4.4.1 The PLC of NiTi as a core product

Figure 4-6 describes, qualitatively, how NiTi sales have varied with their time in market. From 1965 to 1970 sales were low as a major product had yet to be found. Then, in 1971, the Raychem Cryofit® couplings resulted in the NiTi alloys entering a growth stage. By the beginning of the 1980's, however, the couplings market had reached maturity and was beginning to go into decline. At this stage a new market segment began to develop; the medical market. It is difficult to say how far into its own life cycle the NiTi medical market has gone. However, what is certain is that it has contributed greatly to the overall market for NiTi shape memory alloys[98]. The total value of the worldwide market for NiTi alloys and components is estimated at about $50 million, with the retail value of products that rely largely on the unique properties of NiTi being several times that amount[106].

During the late 1980's the Japanese also started to become successful in developing niche commercial applications of NiTi alloys. This was partly thanks to a MITI initiative in the early part of the decade and several products such as air conditioning vents[107], mobile phone antenna[108] and underwire brassiere wires[109] came onto the market. These were all examples of market pull and resulted from the breadth of shape memory awareness amongst the Japanese engineering community.

Also during this time, superelastic elements for eye glass frames came into production. These are steadily increasing their market share within the eyeglass market but they remain a niche application. Again, the higher cost of the product containing shape memory, balanced with the benefits it passes on to the consumer (flexibility and comfort) may ultimately result in failure of this product. Does a consumer in the market for a new pair of eyeglasses, assumming the optics are the same, buy on cost or on comfort? The memory glasses product is currently receiving considerable attention due to a marketing campaign in the U.K.

In addition to the growth of NiTi alloys started by the medical industry, during the early 1990's the interest in smart structures also started to contribute significantly to NiTi sales. While these sales are so far exclusively for the smart structures research market, if a large scale application can be found for NiTi as an actuator within an adaptive structure then the smart market may be the next segment to extend the NiTi life cycle. If not, then the early part of the next century may see NiTi

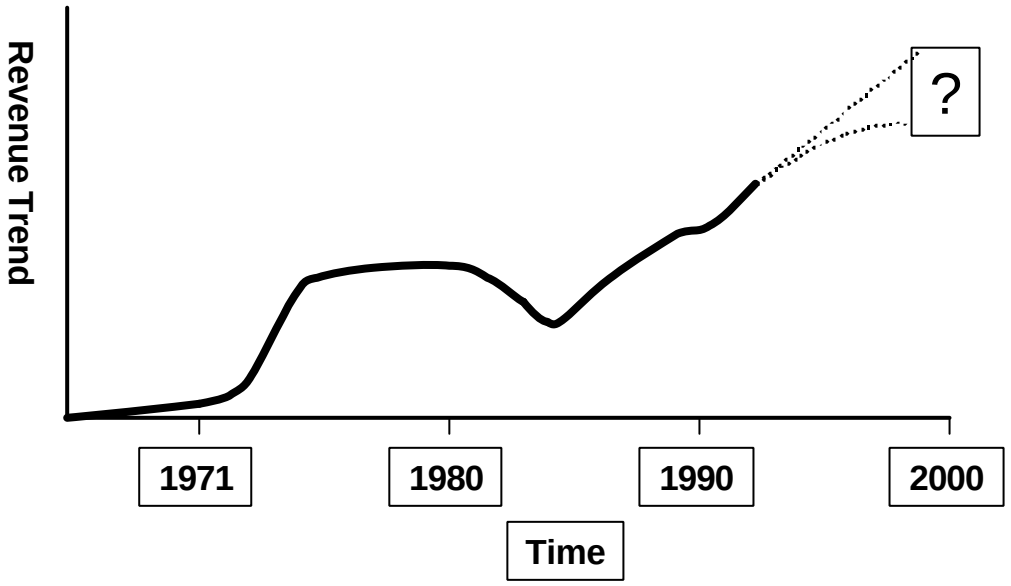

Figure 4-6 The Product Life Cycle of the NiTi Shape Memory Alloy

sales begin to decline once more.

4.4.2 The PLC's of Products Using NiTi Shape Memory Alloys

Because the PLC is an important consideration for product strategies it is also worth analysing some of the individual products arising from the use of NiTi, **Figure 4-7**.

4.4.2.1 Couplings

For some years, the coupling product shape memory business has been in decline. Shrewdly, the Raychem Corporation sold their shape memory alloy coupling business to the Memry Corporation in June 1996. Raychem's only memory alloy involvement is now a marketing agreement between the two

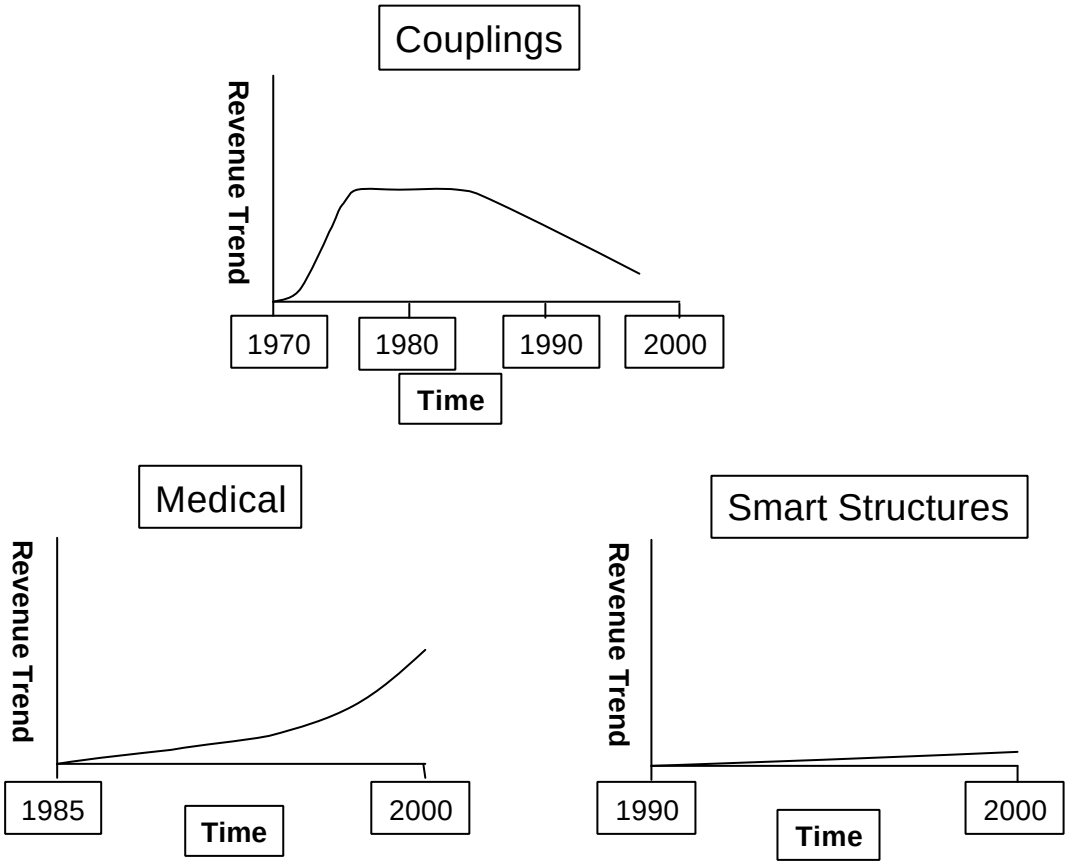

Figure 4-7 Individual PLC's of Three NiTi Based Product Groups

corporations. The Memry Corporation's main business however, is in NiTi medical products and this is entirely separate from the Raychem marketing and sales agreement, all medical products being sold under the Memry brand name.

4.4.2.2 Medical

The NiTi medical market is very much in the growth stage. It is likely that growth will continue for some years. Products that have for some years been awaiting clinical approval are beginning to diffuse into mainstream surgical use. These include the Symphony Stent originally developed by Nitinol Medical Technologies and now licensed to the Boston Scientific Corporation[106], and the Simon Nitinol Vena Cava Filter also developed by Nitinol Medical Technologies and distributed by C.R. Bard [110]. A number of large companies are now showing interest in NiTi medical technologies and are looking to acquire expertise and patents. Nitinol Devices and Components were acquired by Cordis, a Johnson & Johnson company in February 1997. The newly formed group is using NDC's expertise in shape memory technology for product development, particularly for crush-recoverable devices[106]. In addition, United States Surgical Corporation entered into an agreement with EndoTex Interventional Sytems, Inc. to acquire its NiTi based technology for aneurysm repair[106].

If the medical market is to carry on growing, definitive information is required on biocompatibility and fatigue. A worse case scenario for the NiTi business would be if the alloys began to show incompatibility with biological systems and poor fatigue characteristics in repeated phase transformation applications.

Eventually the rate of growth in the medical NiTi market will slow, particularly if many major manufacturers enter the market. This could result in price competition and some firms dropping out of the market. Growth may drop off as demand begins to level out.

As demonstrated by the high number of biomedical applications presented at the Shape Memory and Superelastic Technologies Conference 1997, there is already a proactive focus from SMA manufacturers and researchers onto the medical market. In recent years surgical techniques and biomedical materials have shown significant growth and medical engineering is now a highly

opportunist market segment where NiTi (Nitinol) may make a real contribution to improving medical treatments.

Political, economic, social and technological forces will lead to a number of key factors which will influence the medical market and may ultimately dictate whether SMA's prove to be successful in creating innovation and competitive advantage within the industry. This is shown below in **Figure 4-8**.

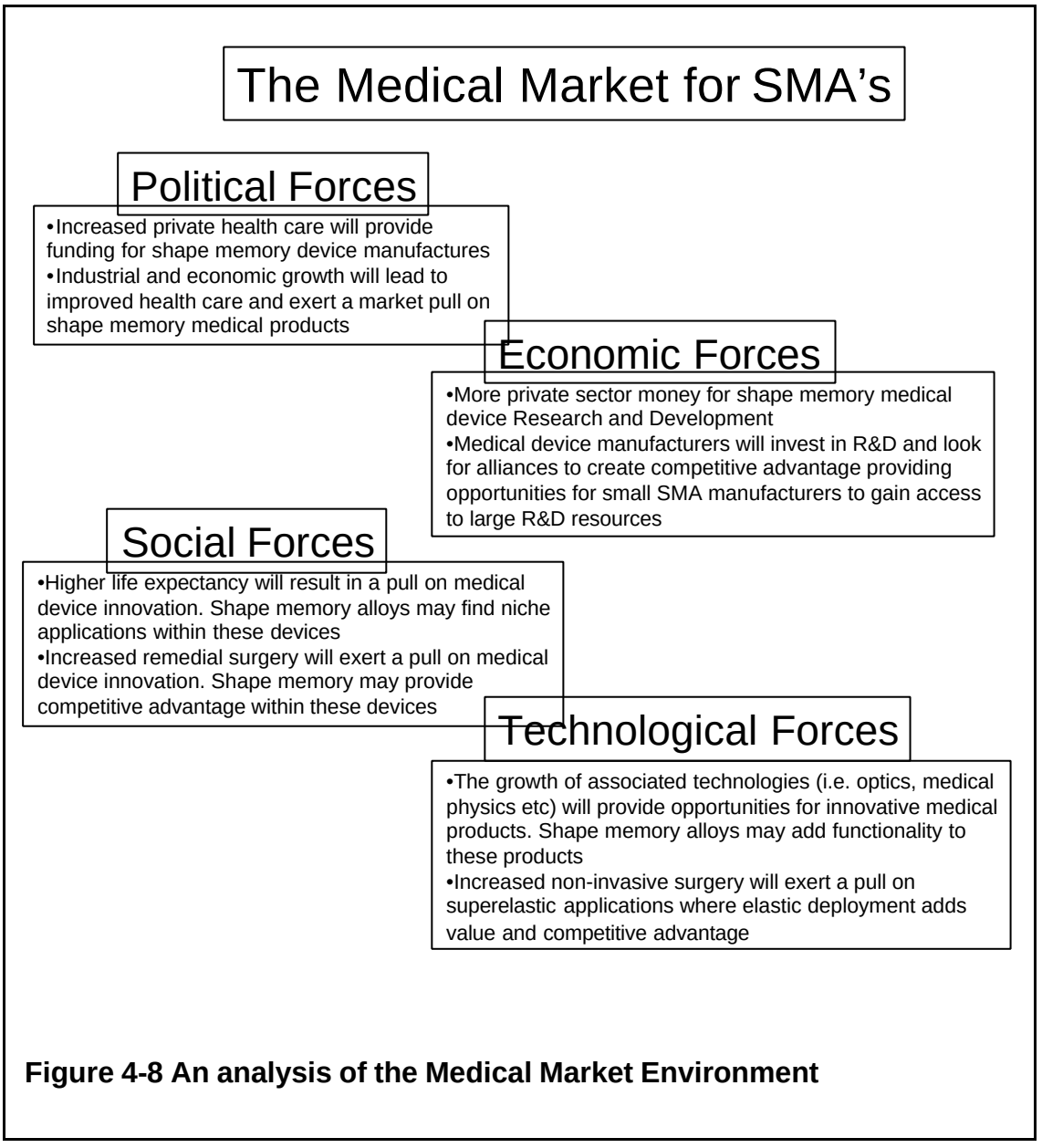

Figure 4-8 An analysis of the Medical Market Environment

4.4.2.3 Smart Structures

The use of NiTi alloys in smart structures is very much in the introduction stage. Whilst many researchers are working on applying NiTi to actuator applications in smart structures, fundamental problems for their use remain. These include

control paradigms and thermomechanical fatigue effects. However, some major players are looking into their use, including British Aerospace PLC and DERA in the UK. If a new high volume application can be found then growth in this sector will follow.

Much is said about the potential of the smart materials/structures market. For instace, Thompson and Gandhi[111] predict :

"Smart materials and structures technologies will revolutionise a broad segment of the international market place for products in the defence, aerospace, automotive and commercial-products industries…The total market

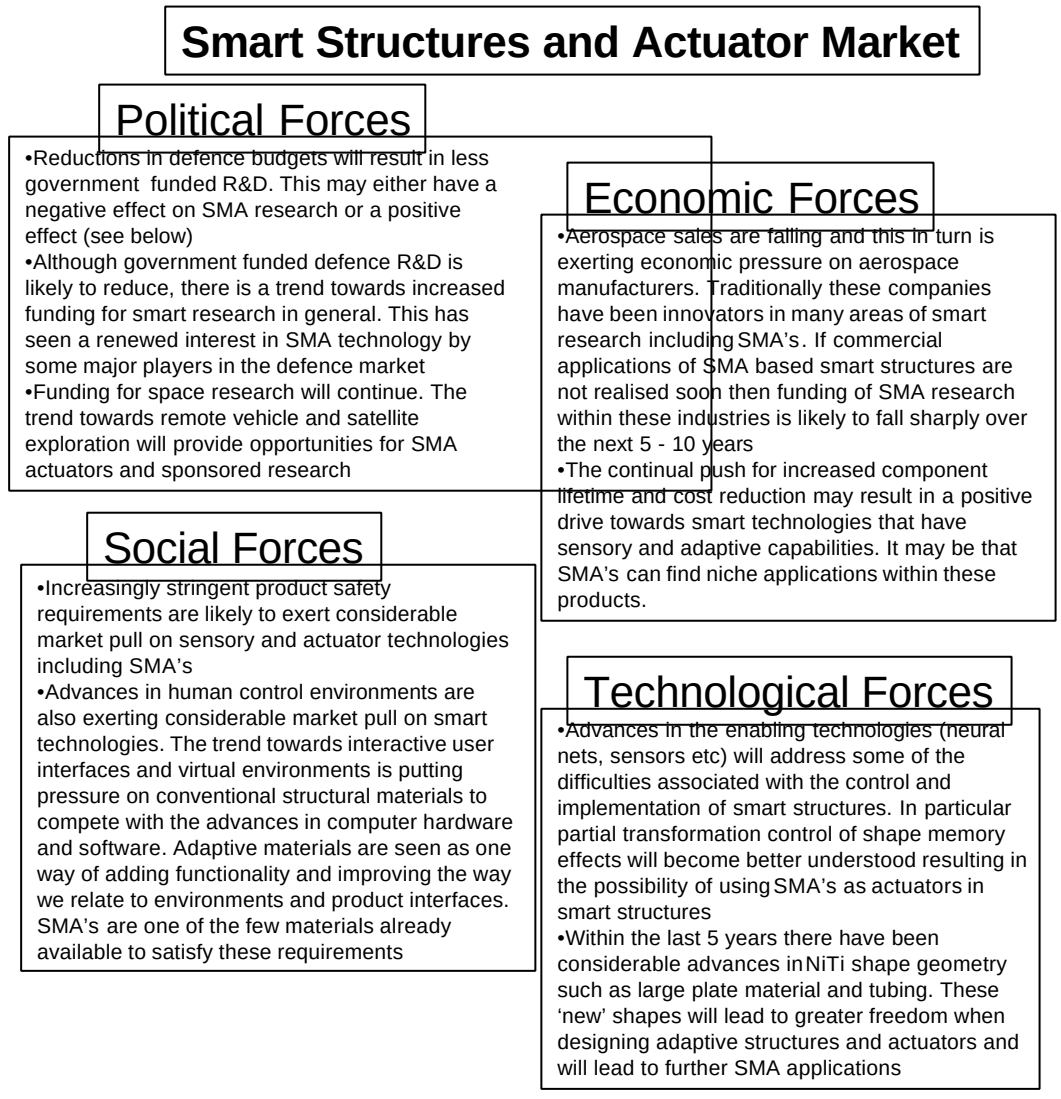

Figure 4-9 Analysis of the Smart Structures Market Environment[112,113,114]

share of smart materials and structures is projected to exceed $65 000 000 by the year 2010."

No basis is given for this optimistic figure however and it is not broken down into the respective enabling technologies. **Figure 4-9** presents some of the key issues for the future of NiTi alloys in smart structures.

4.5 interactive strategies for assimilation and application diffusion

For shape memory alloys to diffuse into real applications and markets, systematic R&D on all design and product relevant properties must be carried out. Failure to do this will prevent the full potential of shape memory alloys from being realised. Shape memory alloys still face barriers to the type of diffusion process described because of the lack of knowledge on relevant properties (e.g. cyclic stability under load) and the many technical difficulties and processing constraints. Properties and phenomena that are inherent to the SMA, such as transformation temperature, hysteresis profiles, cyclic stability etc. need to be properly and reliably evaluated so as to provide the type of data essential for the design of high technology SMA products and their subsequent commercial acceptance.

To achieve cost effective and accurate property evaluation, backward and forward integration from universities and manufacturers is necessary. Increasing alliances between universities and SMA manufacturers could reduce the cost of research while increasing its commercial value and focus on the secondary and tertiary barriers to application[115]. In addition, many products will require collaboration with the end user, or those who have particular expert knowledge within the market segment. This type of collaboration would help create an **R&D/Market interface** focusing the research onto the market diffusion of commercially available shape memory alloys. SMA manufacturers should not be afraid of losing profits or intellectual property through this type of technology

transfer but rather they should regard it as an opportunity for growth and as an investment for future commercial success.

This idea of the need for technology transfer, was first presented at ESOMAT

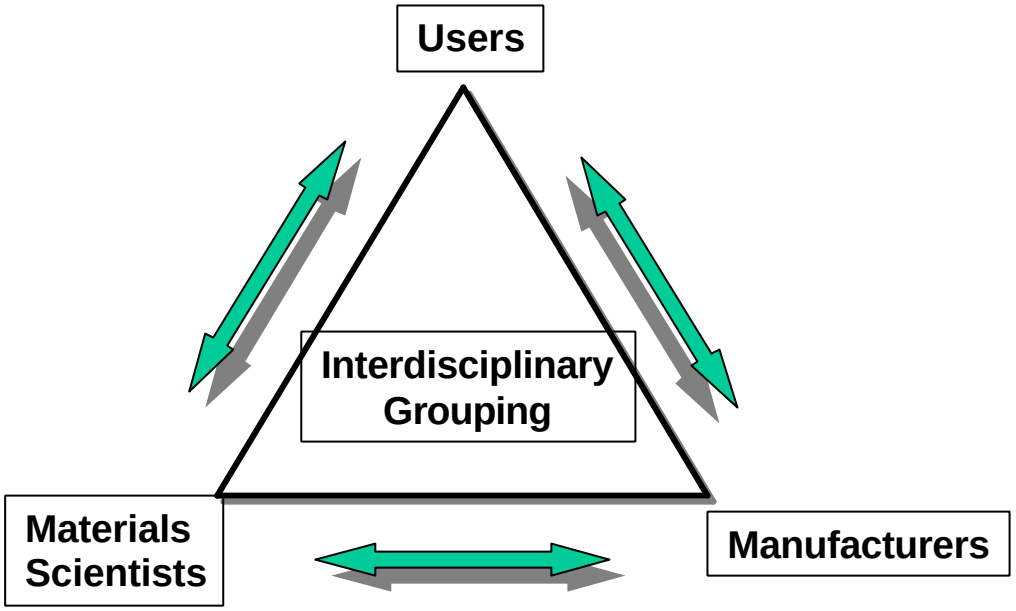

Figure 4-10 Interdisciplinary Grouping Model (after Miyazaki ICOMAT 98)

97[116], subsequently, at ICOMAT 98, Professor Miyazaki took the idea one step further to describe an interdisciplinary grouping for technology transfer within the medical and engineering NiTi fields. This is graphically shown in **Figure 4-10 .**

Allied to this commercial interface and inter-disciplinary information flow is the increasing need for expert networks. A solid international network in the area of shape memory alloys would not only facilitate the exchange of information, but may also attract investment from industrial innovators keen to exploit the product potential of the shape memory effect. The closest shape memory alloys come to this, are the unofficial networks built up between delegates at various shape memory related conferences. The exchange of ideas and research findings at these events is invaluable for the shape memory alloy industry. If however, more end users could be brought into the network, such as surgeons and design

engineers, then the assimilation of shape memory effects with commercial applications may be greatly increased. A step towards this was the Medical Applications For Shape Memory Alloys day organised by the Institute of Mechanical Engineers in September 1999. Here, potential end users were invited to find out more about the shape memory alloy effects. Lunch time discussions resulted in many potential application ideas coming from the delegates.

4.6 conclusions

This chapter has sought to examine some of the issues associated with the application of shape memory alloys within commercial markets. The differentiating benefits of certain shape memory properties offer real opportunities for product innovation. If this potential is ever going to be realised however, consideration should be given to how these market opportunities can be best exploited.

To date, shape memory alloy based products have tended to result from SMA product strategies driven by the inherent shape memory effects. Conventional materials are more likely to have their properties dictated by the product design and in this respect the design may be thought of as the property driver. This is a more reactive strategy which concentrates on market needs and highlights the need for application relevant research.

Both reactive market opportunities and proactive technological opportunities need to be present for successful innovation through shape memory alloys. By careful market analysis and segmentation it may be possible to combine both a reactive strategy responding to market requests for innovation and proactive market segmentation resulting from technological initiative. However for this type of interactive strategy to work, the SMA manufacturer and supplier must be responsive to the product design criteria and equally, the design engineer must be aware of the shape memory alloy as an engineering material and be able to have confidence in its reliability.

It must also be stressed to designers, that although the use of shape memory alloys may increase the unit cost of the product, cost reduction is not always of overriding importance in gaining competitive advantage. High value added products arising from the use of shape memory alloys may command high profit margins within a particular market segment as long as the product differentiation is of genuine value to the user/customer. If this strategy is to be employed successfully, then it is likely that the product is aimed at a particular niche in a market segment and will therefore require a very focused approach when considering potential markets. Equally, it may be that a reduction in manufacturing costs through innovative design and the use of shape memory alloys will actually result in no change of price or even a reduction in price. Again for this strategy to work the customer must be identified. Those known to be innovative within the chosen market segments should be targeted to diffuse the alloy into mainstream use.

The medical device manufacturers and smart structure researchers are requiring higher performance, more functional materials and devices. The relevant developments in these areas are already exerting a pull on shape memory alloy development and this is likely to intensify as we enter the next century. For shape memory alloys and SMA products to diffuse into markets successfully, R&D must be carried out on relevant properties for product application. Increasing alliances between universities and SMA manufacturers may facilitate this type of research concentrating on the key areas of fatigue and transformation stability.

5 A Review of Fatigue Effects and Memory Stability With Transformation Cycling

As described in **Chapter** 4, shape memory fatigue effects are a major barrier to NiTi applications. In particular, fatigue and stability data on the one-way memory effect is essential for repeatable actuator type applications. However, due to the close relationship of the memory effects and superelastic effect many stability characteristics should be common to both. This is often overlooked by authors but will be demonstrated within this chapter.

'Fatigue', when used to describe the stability of shape memory alloys requires an extension of the usual definition. The following definition is a modified version of that given by Van Humbeeck[117] where the fatigue of shape memory alloys is characterised in the following three ways :-

1. Failure by fracture - *Stress or strain cycling at constant temperature*. Three different situations are possible:-

- The alloy is martensitic during cycling
- The alloy is in the parent phase during cycling
- The martensite is stress induced during cycling

2. Changes in physical, mechanical and memory properties - Due to pure thermal cycling through the transformation region.

3. Changes in physical, mechanical and memory properties – Due to a combination of thermal cycling through the transformation region with constant stress or strain loading.

Van Humbeeck[117] therefore defines the main parameters to be considered when studying the global lifetime of a shape memory alloy as : temperature, stress and macroscopic shape strain during deformation. However, it should be kept in mind that these are all macroscopic parameters that merely control the

microstructural phase transformation within the alloy. Therefore, an understanding of the microstructural and thermodynamic changes associated with the observed cycling effects is the key to defining how temperature, stress and strain relate to the stability of shape memory alloys. It will be shown that cycling results are often contradictory, if more emphasis was placed on relating the microstructural and thermodynamic effects with the macroscopic parameters a better understanding of shape memory stability may result.

Van Humbeeck's[117] three parameters should therefore be extended to :-

- Temperature
- Stress
- Strain
- Microstructure

Interestingly, because the microstructure of the alloy controls the thermodynamic behaviour, the importance of these four factors and their inter-relationship is emphasised by the Clausius-Clapeyron equation in the form:

$$\frac{\mathbf{d}s}{\mathbf{dT}} = -\frac{D\mathbf{S}}{e} \qquad \textbf{(5-1)}$$

where s is a uniaxial stress, **T** is transformation temperature, e is the strain associated with the transformation and $D\mathbf{S}$ is the entropy change per unit volume.

Perhaps the most important aspect of this relationship is the stress/temperature, $d\sigma/dT$ profile of the memory effect and how it varies with repeated phase transformation depending upon the type of application :-

Superelastic applications are likely to operate at an applied temperature (often ambient) over a particular stress envelope defined by the stress required

for inducing the martensite transformation. It is likely that the stability of the transformation stresses and their associated strains will be of primary importance when considering the lifetime of the alloy.

Actuator applications are likely to operate against an applied stress over a particular temperature envelope defined by the M_f - A_f range required for martensite transformation. It is likely that the stability of the transformation temperatures and the strains at various temperatures will be of primary importance when considering the lifetime of the alloy.

The close relationship between the possible superelastic cycling effects and one-way memory cycling effects are thus apparent. A study of cycling effects should not be polarised into one or other of them. For instance, an increase of transformation temperatures during memory cycles, may be caused by the same microstructural changes that result in a change of transformation stresses during superelastic cycles.

This chapter will consider the fatigue and stability of shape memory alloys with respect to the memory and superelastic effects. The conventional fatigue properties of individual phases during stress or strain cycling will not be fully reviewed.

5.1 Superelastic Stability

5.1.1 The effect of cycling on transformation stresses

This is perhaps one of the few areas where previous work is in great agreement. All authors have found that the tensile uniaxial stress required for the forward martensite transformation, σ_M, decrease with number of cycles[118,119,120,121,122,123124]. Associated with this decrease in stress, tends to be a change in the gradient of the stress induced martensite plateau, (i.e. the gradient becomes steeper) and a decrease of the stress hysteresis. Both these effects are clearly shown in **Figure 5-1** taken from Miyazaki et al[122].

Miyazaki suggests that the decrease in transformation stresses is due to internal stresses created by permanent slip deformation mechanisms taking place during cycling. His hypothesis is that the internal stresses created by the slip actually assists the formation of martensite; thus reducing the critical applied stress : σ_M.

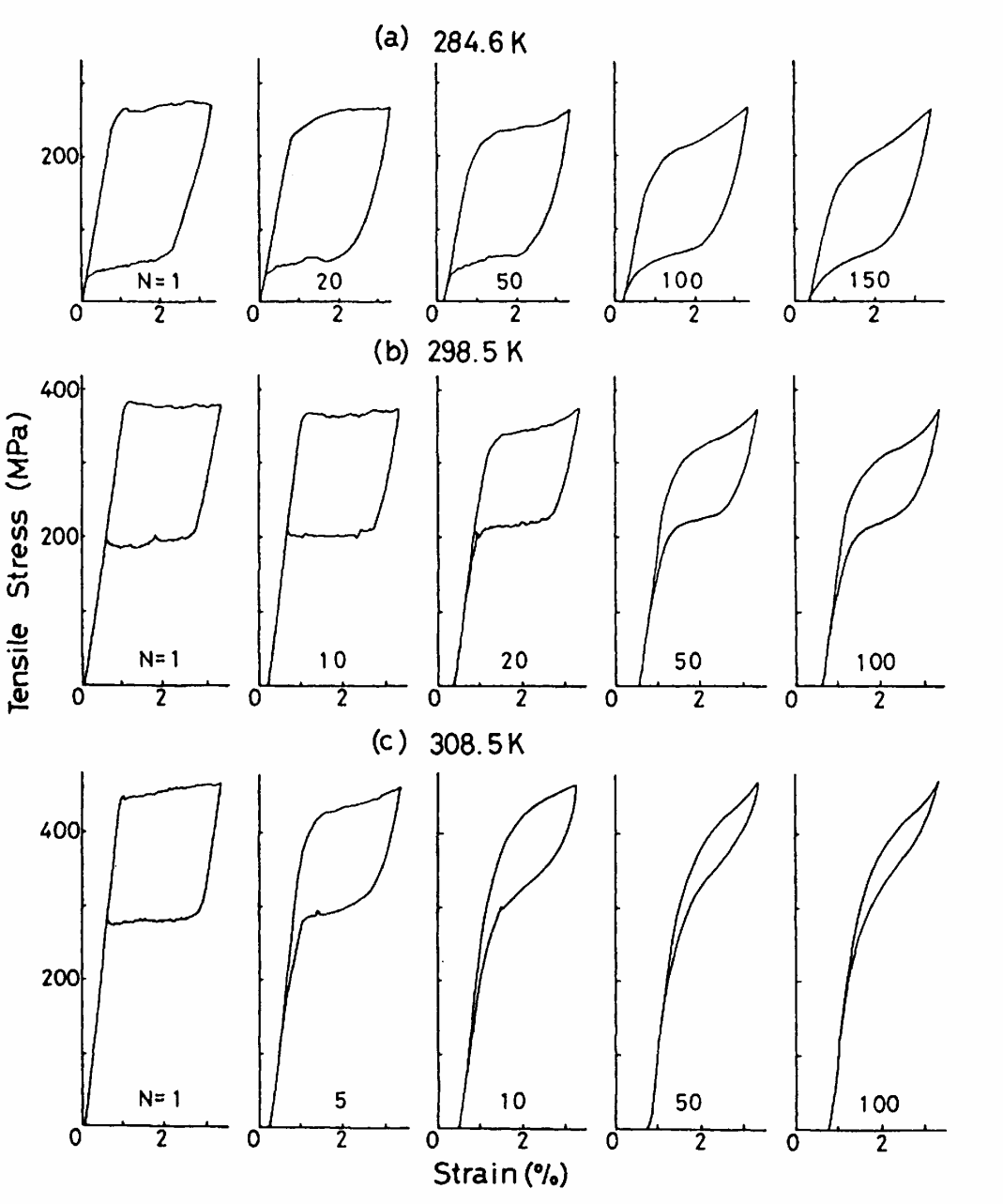

Figure 5-1 The effect of cyclic deformation on stress-strain curves at various temperatures for the Ti-50.5at%Ni alloy which was annealed at 1000°C for 1hr followed by furnace cooling[122].

It has been shown that the stress induced transformation occurs by Lüders like, inhomogeneous deformation[125] where a stress concentration moves through the alloy resulting in the stage 2 plateau shown in the stress-strain curves of **Figure 3-4**. However, after cycling, Miyazaki[122] states that the internal stress field resulting from the slip deformation will have a 'gradient in its strength'. Therefore, the applied stress for inducing martensite increases with increasing strain during stage 2 and an increase in the stress-strain gradient is observed.

A more formal way of analysing the change in stress gradients observed by Miyazaki[122] is to consider the origin of the hysteresis profile associated with shape memory. The progress of transformation is not solely controlled by the chemical free energy resulting from the change in temperature. There are also microstructural dependent factors that will influence the width and gradient of the hysteresis[126].

The elastic strain energy stored in the alloy during the forward martensite transformation and its release during the reverse transformation and the frictional force due to the movement of interfaces and creation of defects are both controlling factors in the profile of the observed hysteresis. The effect of these factors during a temperature controlled transformation is shown below in **Figure 5-2**.

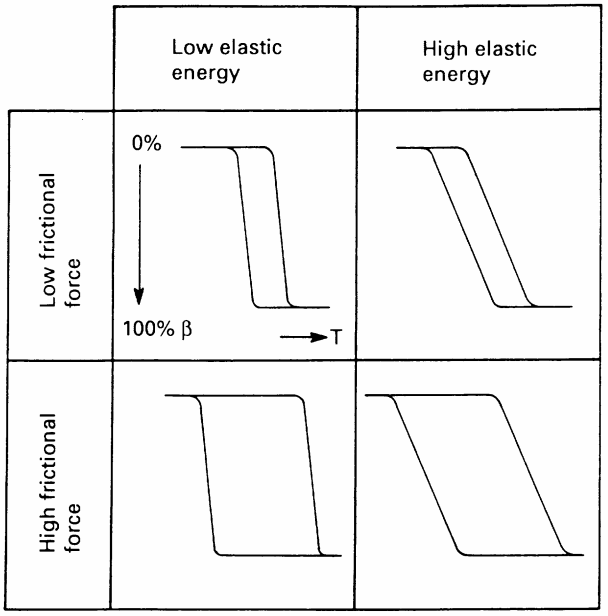

Figure 5-2 The influence of the elastic strain energy and the frictional force on the hysteresis curve of a thermoelastic martensite transformation[126]

The frictional energy is associated with an energy loss, the greater the frictional energy, the greater the hysteresis width. The frictional energy dissipation is mainly caused by friction of the interface movement within the matrix and will therefore depend upon the alloy's defect volume and distribution. This term will oppose the chemical free energy created during the temperature change and will result in a greater degree of under-cooling or overheating being required for the transformation to proceed.

Van Humbeeck et al[126] state that the elastic energy stored or released during transformation will hinder the forward transformation but assist the reverse transformation. Another way to consider this, is that the alloy becomes 'more thermoelastic' when the stored elastic strain energy is increased. In other words the elastic term opposing the forward transformation increases. The same increase in stored elastic energy will assist the reverse transformation when the temperature is raised.

Van Humbeeck et al[126] do not explicitly describe the change in slope of the hysteresis as the elastic strain energy increases. It is likely, that as the elastic energy within the alloy increases, the temperature range of the thermoelastic balance increases and accordingly the M_s-M_f and A_s-A_f range increase. This results in a less square hysteresis profile.

If the same theory of frictional and elastic strain energies is related to the results of Miyazaki et al[122] shown in **Figure 5-1** then a fuller explanation of the change in the observed hysteresis profiles may be postulated. In the case of superelastic transformations, the temperature axis of **Figure 5-2** may be substituted for an applied stress axis. The gradual decrease in hysteresis between the forward and reverse transformation stress with superelastic cycling found by Miyazaki[119,122,125] and other authors[120,121,123,127] can therefore be described by a gradual decrease of internal friction energy. It is likely that this decrease of internal friction is associated with the creation of new defects and possibly the rearrangement of existing ones. The creation and redistribution of defects in this

way will also result in the creation of localised stress fields that may assist the forward transformation thus reducing σ_M. It is not clear however, how these same internal stress distributions will affect the reverse transformation.

In **Figure 5-1** the σ_P stress increases with cycling, which is not explained by Miyazaki et al[122]. Other authors, who have also found decreases in the stress hysteresis and values of σ_M, have found that the σ_P stress actually decreases with cycling[123] or remains constant[121]. If the microstructure of the Miyazaki et al[122] alloy was to be examined before cycling then it is likely that a relatively low dislocation density and large grain size would be found. This is because the alloy was fully annealed well above the re-crystallisation temperature thus removing any traces of prior cold work. In this condition, the alloy is very sensitive to permanent slip mechanisms. The accumulation of slip is likely to increase the accommodation elastic strain energy of the alloy leading to an increase in the stage 2 superelastic gradient, both for the forward and reverse transformation. This is confirmed by **Figure 5-1**. If the alloy is annealed below the re-crystallisation temperature as that in Tobushi et al[118], then the dislocations resulting from prior cold work will become rearranged but will remain in the matrix to provide some resistance to internal slip and the introduction of internal elastic energy. This may explain why the curves shown in **Figure 5-3** taken from Tobushi et al[118] maintain a flat Lüders like deformation appearance even after 100 stress induced cycles.

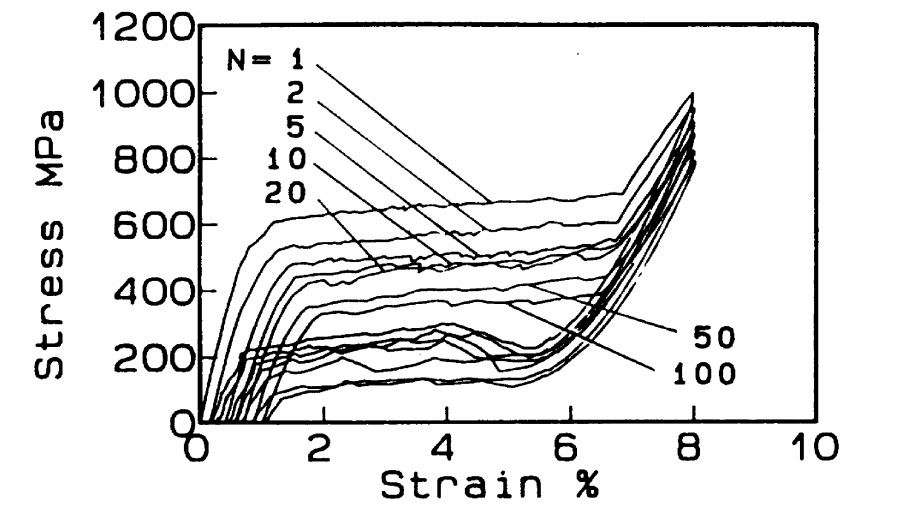

Figure 5-3 The effect of cyclic deformation on stress-strain curves at various temperatures for a Ti-50.2at%Ni alloy which was annealed at 400°C for 20min followed by furnace cooling[118]

Enough dislocations remain in the **Figure 5-3** alloy after heat treatment to resist an increase in elastic energy resulting from the stress induced cycling.

As previously mentioned, **Figure 5-1** displays an increase of σ_P with cycling and **Figure 5-3** a decrease in σ_P, it is therefore possible that this is also connected to a build up of slip deformation and stored elastic energy. An increase in elastic energy opposing the forward martensite growth would assist the reverse transformation. In the case of superelasticity, this may result in the parent phase having enough free energy for transformation at a higher observed σ_P.

Equally, if there is no appreciable increase of stored elastic energy during cycling, then the reverse transformation will not be assisted and may actually occur at a lower value of σ_P. The same reductions of internal frictional energy that lead to the narrowing of the hysteresis profiles and reductions of σ_M, may also result in the martensite plates remaining thermodynamically stable at lower applied stresses.

These results therefore, imply that the reverse transformation stress, σ_P, depends on the opposing effects of decreasing frictional energy and increasing elastic energy. The energy term, which has the greatest effect on σ_P, depends on the microstructure of the alloy.

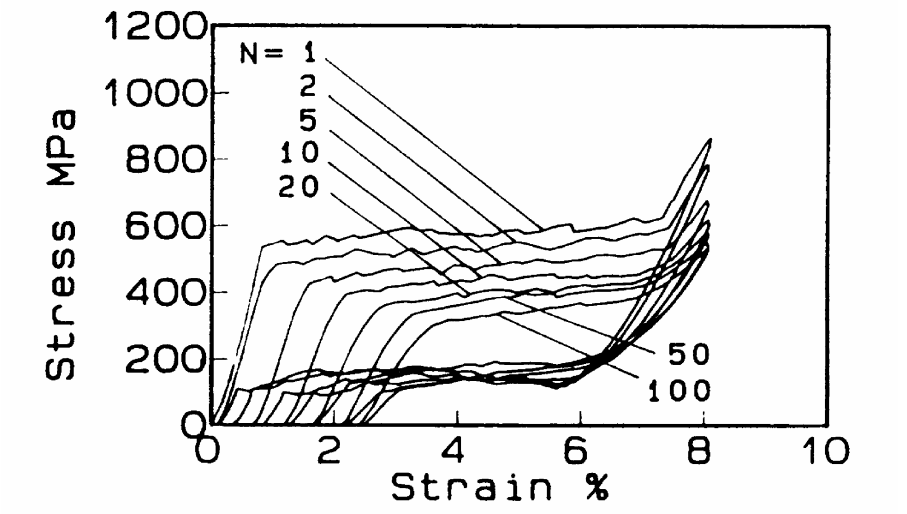

Figure 5-4 The effect of cyclic deformation on stress-strain curves at various temperatures for a Ti-50.2at%Ni alloy which was annealed at 500°C for 20min followed by furnace cooling[118]

Figure 5-4 shows the same alloy and testing conditions as that of **Figure 5-3**. However, this time the heat treatment temperature has increased to 500°C. A higher heat treatment temperature may lead to some elastic strain energy being introduced to the alloy with cycling. If the above hypothesis is true then the introduction of elastic energy should, in turn, reduce the observed internal friction effects on σ_P that are seen in **Figure 5-3**.

The reverse transformation plateau and σ_P remain virtually constant in **Figure 5-4** supporting the hypothesis proposed here. In addition, the gradient of the forward transformation plateau increases more than that observed in **Figure 5-3** with cycling. This implies that some elastic energy is definitely introduced due to the higher heat treatment temperature. The overall hysteresis width also decreases implying a reduction in the overall internal friction energy.

5.1.2 The effect of transformation cycling on permanent strains

Another feature of the results presented in this chapter is the permanent strains produced as a result of stress induced transformation cycling. This may be defined as the deviation of the starting points of the stress-strain curves from the original starting point.

Miyazaki et al[122] state that the cause of this residual strain is probably the occurrence of slip deformation during the preceding deformation as pointed out by Melton and Mercier[128]. The internal stress formed by the slip deformation also assists the formation of the stress-induced martensites, thus the critical applied stress σ_M, decreases. In other words the same deformation that causes changes of internal friction and elastic energy also results in permanent macroscopic shape strain. Therefore, the permanent strain must also be linked to the microstructure of the alloy. Comparing **Figure 5-3** and **Figure 5-4** reveals that the higher heat treatment temperature results in greater permanent strains.

Again this confirms the importance of prior cold work and heat treatment temperature on shape memory degradation mechanisms.

Microstructural observations of the alloy surface before and during superelastic cycling[122] reveals residual martensite plates that do not revert back to parent phase even when the applied stress is completely removed. These retained plates are probably due to the stress field formed by slip deformation. The plates tend to be located at grain boundaries where the dislocation density and associated stress fields are likely to be highest.

Miyazaki et al[122] consider the slip deformation and retained martensite plates to be the cause of permanent strains after cycling. Interestingly, the variants of martensite which are retained are the same as those stress induced indicating that the stress fields formed around them are of the same sense as the applied stress. Thus, the stress field assists the applied stress, causing the decrease in σ_M.

5.1.3 Processing for stable superelastic loops

The hypothesis taken from the previous sections suggests that the most stable alloys are those that will resist slip during cycling and those where changes of internal friction due to the interaction of defects with the interface are minimised.

Again, taking data from Miyazaki et al[122], **Figure 5-5** may be used to test this hypothesis. Two mechanisms are available to raise the critical stress for slip in NiTi shape memory alloys :

- Precipitation Hardening
- High dislocation densities rearranged by low temperature heat treatment

Precipitiation hardening may be achieved by solution treating Ni rich alloys at 1000°C followed by aging at 400°C for 1hr.

Rearranged dislocation hardening may be achieved by annealing any near equiatomic NiTi shape memory alloy at 400°C for 1hr after prior cold work usually produced during cold drawing the NiTi to a wire.

In **Figure 5-5** (a) and (b) are alloys that have been precipitation hardened, (c) is a titanium rich alloy that has been cold worked and annealed, (d) is a Ni rich alloy that has been cold worked and annealed.

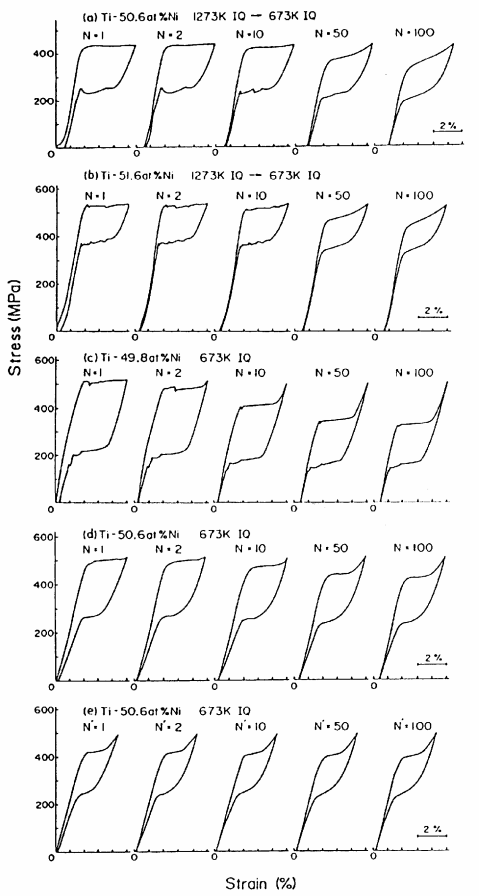

Figure 5-5 Effect of cyclic deformation on the stress-strain curves of NiTi alloys subjected to various thermomechanical treatments[122]

In curves (a) and (b) the stage 2 plateau gradually changes to an increasing slope with cyclic deformation. However, the stage 2 plateau is retained in (c) and (d) even after 100 cycles. Miyazaki recognises this effect but does not try to explain it. If the elastic strain energy hypothesis is correct then these results suggest that alloys which rely solely on precipitation hardening for stability, are more susceptible to increases of elastic energy than those which are cold worked. Looking at it in a different way; cold work prior to low temperature annealing reduces the elastic energy effects of stress induced phase

transformation cycling. Therefore cold work is effective in reducing cycling effects.

It is also interesting that the reduction in hysteresis associated with superelastic cycling (possibly as a result of internal friction decreasing) is greatest in curve (c) and that this curve also has the widest initial hysteresis at cycle N=1. Again, It is possible using internal friction effects to explain these results.

Internal friction is greatest at N=1 in alloys that have been hardened by cold work. This is due to dislocation arrays within the microstructure interfering with the movement of martensite interfaces and results in the greatest hysteresis widths. With stress induced cycling however, these dislocations become rearranged and form stress fields which not only result in lower internal friction but also causes the stress for martensite formation, σ_M, to decrease.

Sample (d) in **Figure 5-5** appears to be the most stable of the alloys tested from N=1. As the ageing temperature and annealing temperatures are the same for these alloys then it seems likely that a combination of the two hardening effects occur in Ni rich alloys that are cold worked and subsequently annealed. **Figure 5-5** (d) confirms this.

Finally, the most stable alloy is that shown in **Figure 5-5** (e). This is a Ni rich alloy that has undergone a heat treatment at 400°C after prior cold work and subsequently been cycled 100 times. Therefore, the labelling of the first curve as N=1 by Miyazaki et al[122] is perhaps a little misleading, N=101 more accurately describes the starting point. Curve (e) however, does emphasise that the major changes in hysteresis profiles and strains take place in the early cycles, and that to achieve a really stable superelastic shape memory effect in NiTi, some prior training, via deformation cycling is required.

5.2 The Stability of Shape Memory Effects with Thermal Cycling

Unfortunately the published literature on thermal cycling effects is much more contradictory than that on superelastic effects. Again, if authors were more

specific as to the composition of the alloys and their physical condition then perhaps the degradation mechanisms that occur would become clearer.
The following list, summarises some of the main effects that have been found to result from the thermal cycling of NiTi alloys :-

- Increase of M_s temperature [118,129,130,131,132,133,134,135,136,137,138,139]
- Increase of M_f temperature [118,129,130,131,132,133,135,136,137,138,]
- Increase of A_s temperature [118,121,129,131,132,133,136,137,140]
- Increase of Af temperature [118, 121,129,131,132,133,135,136,137,140]
- Decrease of M_s temperature [133,141,142,143,144,152]
- Decrease of Mf temperature [133,137, 141,145,152,]
- Decrease of A_s temperature [133,136,137,138,141.145]
- Decrease of Af temperature [131,133, 138,141,144]
- Constant M_s temperature[133,137,138]
- Constant M_f temperature[133,138]
- Constant A_s temperature [130,135,138]
- Constant Af temperature [130,135,138]
- Increase of Thermal Hysteresis [121,133,139]
- Decrease of Thermal Hysteresis [118,121,131,132,135,136,137,138]
- Increase of Recoverable Strain [118,121, 129,136,138,139,146,148]
- Decrease of Recoverable Strain [118,129,130,131,132,135,136, 138,146,147,148]
- Permanent Strain [118,129,131,132,134,135,136,137, 138,139,140,143,146,148,149,150,151,152]
- Accumulation of Residual Two-Way Memory Strain [121,129,138,143,146,148,151,152]
- Changes in the heat of transformation [139,153]

Similar effects and contradictions are also found in copper based shape memory alloys[154,155,156,157,158] and iron based shape memory alloys[159].

It is obvious from this list how a design engineer may become confused when attempting to gather information on the stability of shape memory effects. The discrepancies in these results are not down to experimental error. Rather, they emphasise how different degradation effects occur within shape memory

systems depending upon alloy type, thermo-mechanical processing and loading stresses. Very careful analysis of the above references is therefore required to establish any kind of coherent working hypothesis on the exact degradation mechanisms that are taking place.

5.2.1 The Effect of Thermal Cycling on Transformation Temperatures

The discrepancies in transformation temperature are perhaps one of the most interesting parameters to consider first as they are highly dependant upon the microstructure and internal stress state of the alloy. Again, Miyazaki has carried out some interesting work in this area[133]. He states that there are several irreversible processes that affect the transformation temperatures :-

1. A change in the degree of order[160,161,162]
2. Introduction of dislocations[163,164]
3. Ageing effects[165,166]

By cycling several alloys against zero stress Miyazaki concludes that dislocation build up is responsible for shifts in transformation temperatures with repeated transformation. He found that in microstructures where no shift in transformation temperature was observed there was very little dislocation generation. He found that the most stable alloys were those that were either aged nickel rich alloys or alloys that were annealed at a temperature below that of re-crystallisation after substantial cold work.

One of the most interesting findings of Miyazaki is that of the pre-strain effect on transformation temperatures. Generally Miyazaki found that where changes in transformation temperatures were observed they were associated with a decrease in both the forward and reverse transformation temperatures. By pre-straining the alloys that were most susceptible to dislocation generation (i.e. a solution treated Ti-49.8at.%Ni alloy with no previous cold work) so that a residual

plastic strain is measured after unloading, he found that pre-straining the alloys resulted in a lower martensite transformation temperature. However, by repeated thermal cycling of the alloys, M_s increases with pre-strains of 4.6% and 11.8% and is almost constant when the pre-strain is as high as 22.8%. When no pre-strain is induced a decrease in M_s is observed. These results are shown in **Figure 5-6** where the change in M_s is shown as a function of the number of thermal cycles. It is shown that the degree of change in M_s is dependant upon the amount of pre-strain and that therefore the effect of thermal cycling against zero stress is suppressed by work hardening. If the pre-strain is small, then new dislocations may be generated or the existing dislocations may be rearranged. This will lead to a change in the internal stress field resulting in a shift of M_s. In a strongly work hardened condition, dislocations will find it very difficult to move during thermal cycling and thus M_s will change very little.

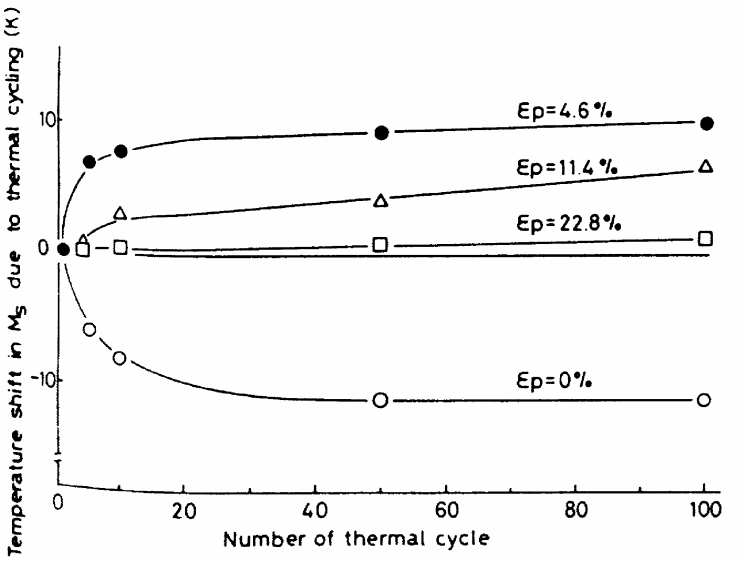

Figure 5-6 Temperature shift in M_s due to thermal cycling for specimens with various pre-strains[133]

Figure 5-7 shows the individual temperature shifts of M_s with thermal cycling used by Miyazaki to create **Figure 5-6**. It is interesting that although the M_s is generally depressed from the non pre-strained cycle N=1, M_s of approximately 290K, the amount of reduction in M_s decreases with increasing pre-strain! This is

shown in **Figure 5-7**, the N=1 M_s of the 22.8% pre-strain alloy is approximately 275K, a reduction of 15K from the non pre-strained alloy, whilst the N=1 M_s of the 4.6% pre-strain alloy is approximately 265K, a reduction of 25K from the non pre-strained alloy. This result is not stated by Miyazaki in his paper but deserves to be referenced here. It seems to suggest that the greater pre-strain somehow assists the martensite transformation and that the M_s increases of the lower pre-strained alloys is related to their degree of pre-strain. That is, in the lower pre-strained alloys the shift in M_s is greatest and tends towards the M_s of the 22.8% pre-strain sample. This suggests that some kind of dislocation/stress field saturation takes place with thermal cycling that follows the Clausius-Clapeyron relationship and increases the M_s temperature. This is supported by the fact that with thermal cycling, the M_s of the 11.4% pre-strain alloy increases to the temperature of the 22.8% pre-strain M_s of approximately 275K.

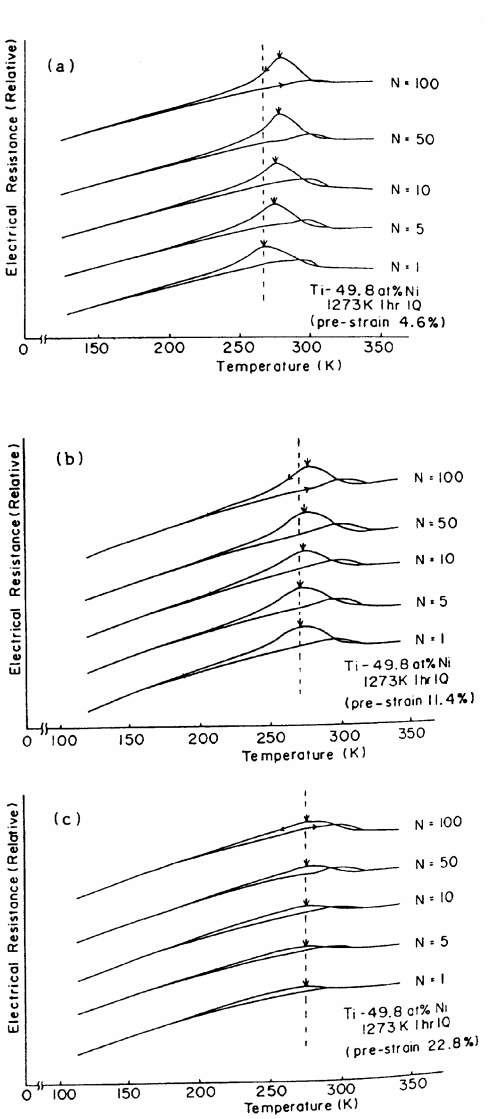

Figure 5-7 Effect of thermal cycling on the electrical resistance vs temperature curve of the pre-strained Ti-49.8at%Ni specimens which were solution treated at 1273K for 1hr prior to pre-straining. The arrows indicate the M_s temperature[133]

It is also interesting that the decrease in M_s of the non pre-strained alloy saturates at a similar temperature to that of the increasing M_s of the pre-strained alloys, i.e. approximately 275-280K.

Miyazaki also states that the temperature difference ($M_s - M_f$) can be explained by internal stress. He attributes this to the effective transformation temperature being different from place to place in the specimen because the internal stress decreases with increasing distance from the dislocations. However this

broadening of (M_s – M_f) is the same as that described in **5.1.1** and **Figure 5-2**, where the effect is ascribed to increasing stored elastic energy resulting from the build up of dislocations. The latter hypothesis is more consistent with thermoelastic behaviour and ties in well with the superelastic results of **Figure 5-1** where similar changes in hysteresis profiles were attributed to the build up of dislocations resulting in a 'gradient in strength' [119]. This same dislocation build up that is responsible for an increasing applied stress being needed to induce further martensite growth in superelastic alloys, would also account for a greater range of under-cooling being required for martensite growth in the thermal memory alloys. This is interesting as it demonstrates the similarities between superelastic and thermal memory cycling effects.

There is also another interesting connection between the superelastic and thermal memory effect work of Miyazaki et al[119,133]. It appears that if stress is applied to the system, (as it is with superelastic cycling and as it is in the pre-straining of the alloys shown in **Figure 5-6**), the resulting deformation assists the martensite transformation. This manifests itself as a decrease in σ_M for superelastic cycling and an increase of M_s with thermal memory cycling. Again, this emphasises the importance of stress on all the shape memory effects.

5.2.2 The Effect of Thermal Cycling on Transformation Temperatures at Constant Load

It is obvious that actuator applications of shape memory will in some way involve some form of applied stress and as shown in the previous section, this may have important implications for temperature stability. Despite this fact little systematic research has been carried out on actuating NiTi elements against applied loads. Of the work that has been carried out on constant load cycling contradictions again make easy understanding of the degradation processes difficult. However some agreement can be found in certain areas. For instance where authors do observe changes in M_s transformation temperatures it always tends to be an increase. This is not the case for A_s temperatures where both increases and decreases can be observed.

A good example of the effect of constant stress cycling on M_s and hysteresis characteristics is shown in **Figure 5-8** taken from the work of Stachowiak and McCormick[135] .

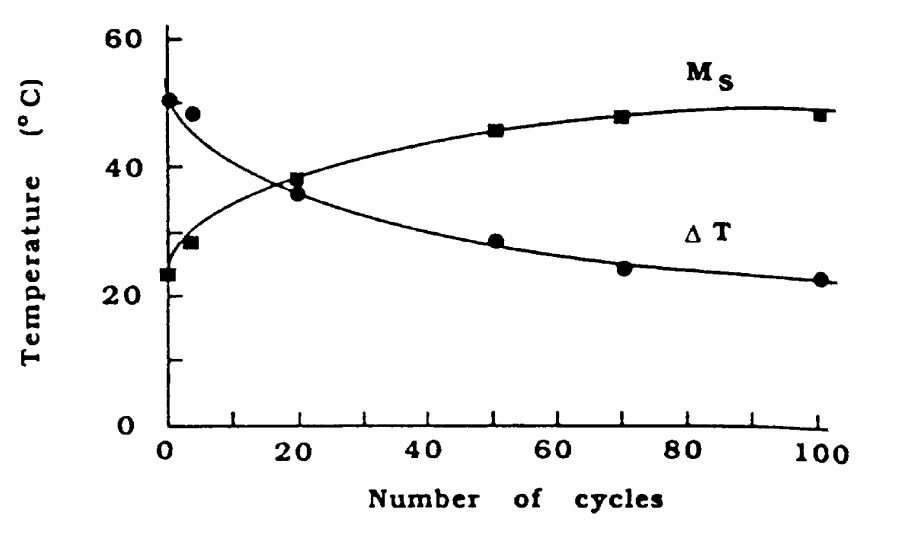

Figure 5-8 The Effect of Thermal Cycling on M_s and DT

They found that in a Ti-50.2at%Ni alloy heat treated at 500°C for 15 minutes, thermally cycled against an applied load of 200MPa, the M_s rises whilst the A_s stays constant. This results in the hysteresis, ΔT, decreasing with the number of cycles. From **Figure 5-2** the decrease of ΔT observed by Stachowiak and McCormick[135] implies that the internal friction associated with the transformation gradually decreases with cycling. Similar results were observed by Thoma et al[131] in a titanium rich alloy.

In another paper where the same alloy, only heat treated at 400°C for 20 minutes, was again cycled against an applied load, an increase in M_s and A_s was observed[118]. Unfortunately there is no reference as to the level of applied stress and an effects comparison is thus made very difficult. Even in this alloy however, the hysteresis, ΔT, was found to decrease due to M_s increasing at a greater rate than the A_s.

A slightly more systematic analysis, again on the same Ti-50.2at%Ni alloy heat treated at 520°C for 60 minutes, was carried out by Todoroki et al[138]. In his work he found that the direction and amount of transformation temperature drift was

related to the level of applied load. At an applied load of just 18MPa the M_s decreased and the ΔT increased, at 81MPa they remained virtually constant, at 145MPa the M_s increased, the A_s decreased and the ΔT decreased. However the experiments were only carried out over three thermal cycles.

In all these results the hysteresis gradients, ($M_s - M_f$ and $A_s - A_f$), were found to remain approximately constant. Again, referring to Humbeeck et al[126] and **Figure 5-2**, this implies that there was little change in stored elastic energy during transformation as a result of thermal cycling against applied stresses.

It is common for the results described here to be attributed to dislocation generation, defect redistribution, or both. It is reasonable to associate physical changes during cyclic deformation against applied stress with defect generation. However very little confirming evidence is ever provided.

Miyazaki has shown with transmission electron microscopy that dislocations are generated during stress free transformation cycling[133]. It is obvious how dislocation generation may interfere with the transformation mechanism thus reducing the M_s temperature. It is less clear how the generation of dislocations either prior to thermal cycling (by pre-straining the alloy), or during thermal cycling (via a constant applied load) may actually assist the transformation, raising M_s.

If dislocation generation is responsible for the observed increase in M_s temperatures, then the mechanism by which this occurs must be similar to that which causes two-way memory, i.e. distributed stress fields which assist the transformation[135].

5.2.3 The Effect of Thermal Cycling on Permanent Strain and Shape Recovery

Discrepancies also arise when considering the generation of permanent strains. Some alloys display permanent shape deformation, some show no permanent deformation and some show greater deformation at low stresses than high stresses.

A good example of the confusion that can arise may be found in Todoroki et al[138]. Whilst the alloy cycled at 145MPa shows greater permanent length deformation than that cycled at 81MPa, both in hot and cold length, the alloy cycled at 18MPa appears to show the greatest increase of all in cold shape length. Concurrent with these changes, the recoverable strain decreases in the alloys cycled at 81 and 145MPa whilst it increases in the 18MPa alloy. The paper is mainly concerned with the generation of the two-way effect and little reference is made to changes in permanent strain.

However, Todoroki et al[138] do conclude that the alloys which display the R-phase prior to martensite transformation are more dimensionally stable than those which do not. Unfortunately there is a fundamental flaw in their experiment. That is, to achieve a transformation from parent phase to martensite phase with no intermediate R-phase, they simply heat treated an alloy which does display the R-phase to a greater temperature. The higher temperature heat treatment has the effect of raising the M_s to a point where the R-phase transformation is completely suppressed. The temperature employed by Todoroki, 660°C is well above the re-crystallisation temperature of the Ti-50.2at%Ni alloy used in their experiments. To compare an alloy heat treated at 660°C to one heat treated below the re-crystallisation temperature at 520°C and assign stability differences to the presence of R-phase, ignores the important role that dislocations are thought to play in transformation stability.

Thoma et al[131] also found that dimensional stability decreased with increasing heat treatment temperatures. Thoma defined hot and cold increases in alloy length as hot and cold creep. They found that the degree of creep was dependant upon the heat treatment and the level of applied stress. They found that the greatest dimensional stability (least amount of creep) occurs at low heat treatment temperatures and low applied stresses.

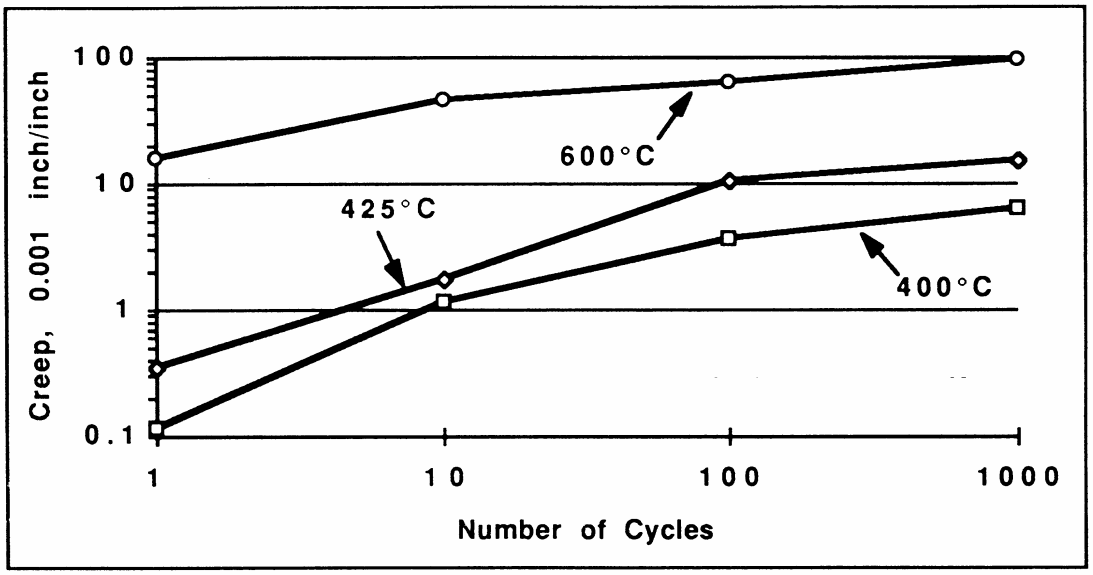

Figure 5-9 Effect of Heat Treatment Temperature on Creep at 69MPa

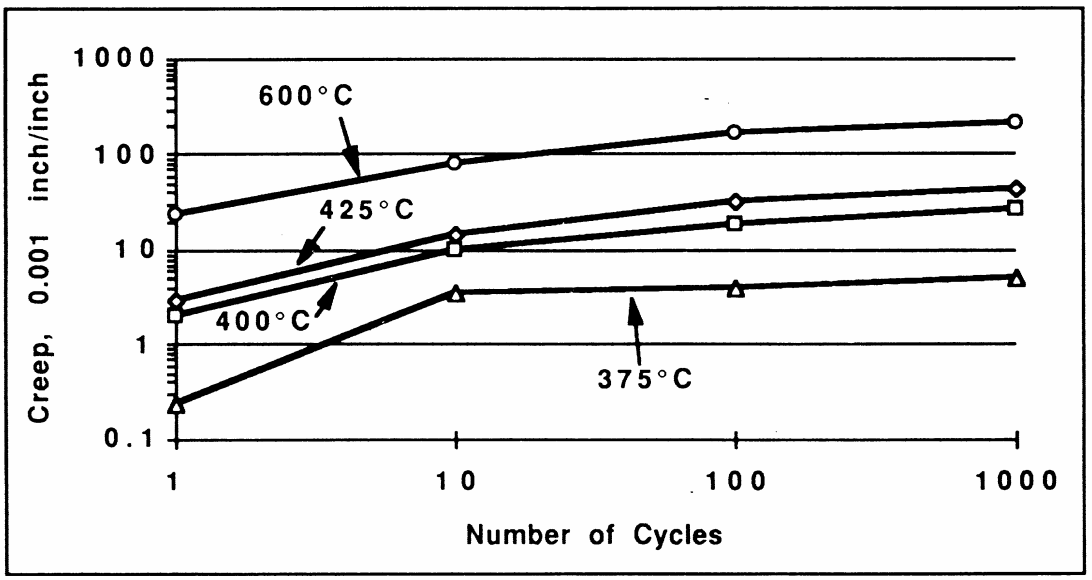

Figure 5-10 Effect of Heat Treatment Temperature on Creep at 207MPa

Thoma's results are shown in **Figure 5-9** and **Figure 5-10**. This strongly implies that dislocations are responsible for dimensional stability in NiTi shape memory alloys. The material used by Thoma et al was a titanium rich alloy that had been cold worked by die drawing to between 35-40%.

Thoma postulates that with no applied stress, high heat treatment temperatures result in the generation of dislocation defects during thermal cycling. At low heat

treatment temperatures, Thoma attributes defect redistribution to the cycling effects. If a stress is applied to the alloy during cycling he postulates that both mechanisms occur and that therefore dimensional instability must be a result of defect generation and redistribution. No direct evidence is given to support this.

All references where thermal cycling against appreciable applied loads is carried out show some signs of permanent deformation. Often the greatest degree of permanent deformation appears in the parent phase shape. This is demonstrated in **Figure 5-11** where the change in strain of the high temperature shape is more significant than that of the change in strain of the low temperature shape.

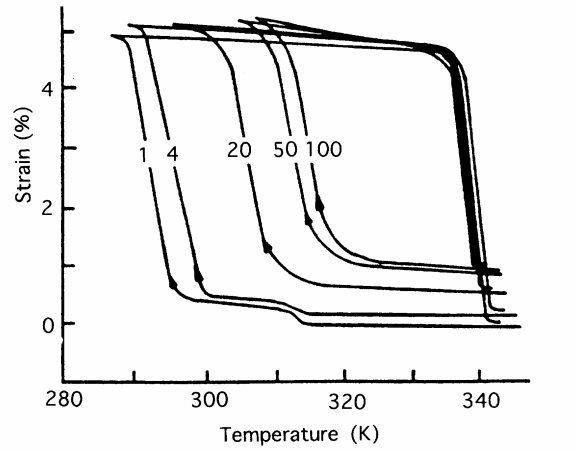

Figure 5-11 Influence of repeated thermal cycling on the transformation behaviour of a Ti-50.2at% Ni wire annealed at 500°C for 15 minutes after cold drawing. Applied Stress = 200MPa

It is also found that as the permanent strain in the alloy increases, so the recovery strain or stroke of the memory effect decreases. These effects are of course very closely linked. It is likely that the same structural changes induced by martensitic transformation are responsible for the decrease in recoverable strain and increase of permanent strains[135].

5.2.4 The Stability of R-Phase Transformations

Thermal cycling an alloy which displays the R-phase under an applied load, in a temperature range such that only the R-phase transformation is induced, i.e. the B19' martensite is not, has been shown to produce very stable actuation. **Figure 5-12** shows an example of such a transformation taken up to 500 000 cycles. It appears, therefore, that the B2-R transformation cycle induces little structural change.

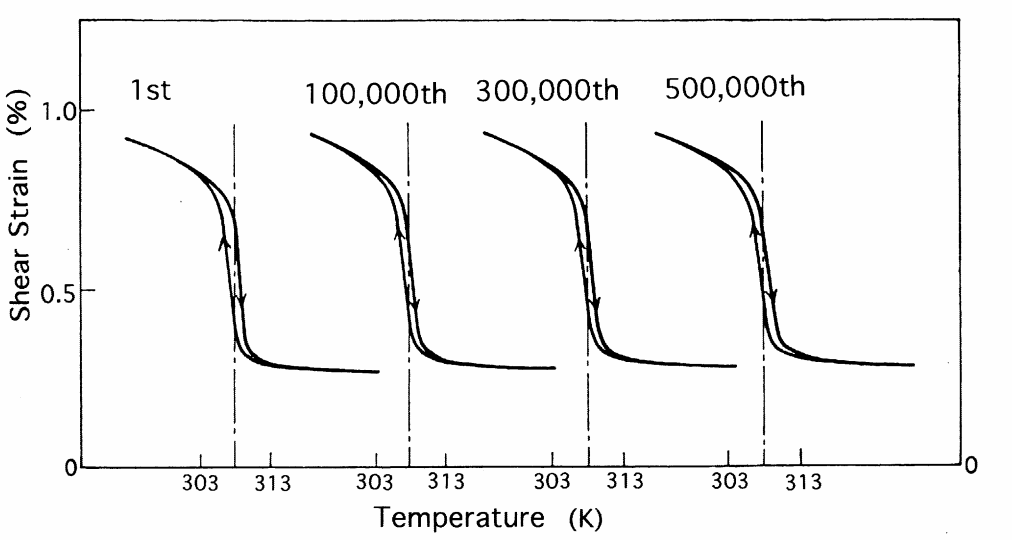

Figure 5-12 R-Phase Cycling at Constant Load of a Ti-49.8%Ni Spring Annealed at 475° C after Cold-drawing[167]

5.2.5 Summary Of Thermal Cycling Effects

It is clear from this chapter that multiple phase transformations do have a marked effect on shape memory parameters. It is also clear that processing parameters and operating conditions greatly influence the stability of the alloys. However, it is very difficult to formulate firm conclusions on the processing and operating conditions required to optimise shape memory fatigue life.

Much of the published literature concentrates on stress free cycling. It appears that the cycling effects observed during stress free cycling are quite different to those observed when transforming against an applied stress. For instance, M_s temperatures tend to decrease during stress free cycling but increase for certain applied stress conditions. Equally, permanent deformations and changes in

recoverable stresses occur when a stress is applied to the system. These differences emphasise the problem of applying published fatigue data to real NiTi applications. Although many applications utilising the superelastic effect have been produced, actuator applications are continually held back by a lack of clear data on actuating fatigue effects and how to design against them. Obviously stress free data is of limited value to designers of actuator systems. In most potential actuator applications the applied load is an inherent part of the application. It should also be noted that many similarities between superelastic cycling and thermal memory cycling effects have been observed. As such, work on thermal cycling against applied loads may also have important implications for superelastic medical applications.

Reviewing the literature in this way does indicate however which parameters may be most important for long term fatigue life when operating against applied loads. The literature implies that cold work, applied stress, alloy type and heat treatment temperature need to be carefully balanced to obtain a stable actuating element. Despite these implications, little research has been carried out on these parameters and in particular their interactions. Many respected researchers such as Humbeeck[117], and Miyazaki[133] have also identified the importance of a systematic programme of work when researching this area. The difficulty of adopting such an approach is often down to the time required for long term testing and the problem of designing experiments that will identify the relevant importance of the processing and operating parameters.

Based on the findings of this literature review, the following sections of this dissertation will attempt to address the need for systematic cycling data. Using an established method of experimental design such that a number of factors and their relative interactions may be analysed concurrently, a series of experimental results will then be presented.

Further analysis of the changes in hysteresis characteristics will be related to the findings of this factorial analysis. Thermodynamic measurements will be presented as a method for analysing the associated structural changes and variations of internal stress.

6 Experimental Programme

6.1 Gaps in Theory and Application Specific Knowledge

It is clear from the previous section that gaps exist in the understanding of NiTi fatigue behaviour. Specifically, the individual and combined effects of operating and processing conditions are not well understood. The following experimental programme attempts to close some of these gaps and relate the macro effects of thermal cycling, such as permanent strains, to the microstructure and kinetics of transformation.

The literature demonstrates that a complex relationship between: cold work, applied stress, heat treatment temperature and alloy composition exists. It is these parameters that the experimental programme will address. In addition, it is believed that work on cycling rate effects has never been carried out and this will be added as an extra operating parameter into the experimental design.

6.2 Factorial Experimental Design

6.2.1 Introduction

The design of experiments has received a lot of exposure in recent years particularly in industry. The area is often coupled with the name of Genichi Taguchi, as in the 'Taguchi Method'. Taguchi is one high profile methodology in the technique of defining and investigating all possible conditions in an experiment involving multiple factors. In the literature this technique is often referred to as **Factorial Design**. Numerous applications of this type of approach, especially in the chemical and pharmaceutical industries have been carried out.

When a large number of factors are to be analysed the number of experimental runs required for a full factorial analysis becomes extremely large. It is here where Taguchi made his main contribution. He simplified and standardised the factorial designs in such a manner that two engineers conducting tests

thousands of miles apart will always use similar designs and obtain similar results.

To perform a general factorial design, an investigator selects a fixed number of levels for each of a number of variables (factors) and then runs experiments with all possible combinations. If there are l_1 levels for the first variable, l_2 for the second,….and l_n for the n^{th}, the complete arrangement of $l_1 \times l_2 \times \ldots \times l_n$ experimental runs is called an $l_1 \times l_2 \times \ldots \times l_n$ factorial design. For example, a $2 \times 3 \times 6$ factorial design requires $2 \times 3 \times 6 = 36$ runs, and a $2 \times 2 \times 2 = 2^3$ factorial design, 8 runs. The two level type of factorial design is of particular importance for a number of reasons:-

1. They require relatively few runs per factor studied. Although they are unable to fully explore a wide region in the factor space, they can give a good indication of major trends and thus determine a promising direction for further experimentation.
2. The interpretation of the observations produced from these designs can proceed largely by using common sense and basic arithmetic.
3. They can be used to form the basis of fractional factorial designs where very large numbers of experimental runs would otherwise be required, i.e. Taguchi Methods.
4. Interactions between factor variables can be easily analysed using a standard methodology.

It is unnecessary and beyond the scope of this thesis to fully describe factorial experimental design and all its variations. However, the following simple example is given to describe the principles upon which the experimental method used in this thesis is based. The example is based on the notes taken from a course run by the School of Industrial and Manufacturing Science, Cranfield University, Bedfordshire, England.

Example

Suppose that the effect of two input variables (control factors) at two different values (levels) on one or more output (response) variables is to be investigated. Factor **A** will take one value called level 1 and a second value called level 2; similarly for the other factor **B**. **A** might be a temperature for instance where its levels are 350°C and 370°C or the levels may be qualitative, i.e. 'present or absent'.

Table 6-1 shows the experimental combinations of the levels of control factors **A** and **B**. The low level is assigned a – sign and the higher level a + sign. The y values represent the observed response for each experimental treatment combination. There are 4 possible combinations and each occurs the same number of times; once.

Experimental Programme	**A**	**B**	Observed Response- may be more than one
1	-	-	Y_1
2	+	-	Y_2
3	-	+	Y_3
4	+	+	Y_4

Table 6-1 The Experimental Matrix of Factors A and B

For any one characteristic, the four observed responses can be combined to estimate the so-called 'effect' of each factor.

A was at level 1 for responses 1 and 3 and at level 2 for responses 2 and 4. Comparison of the averages of these two sets of responses indicates the effect of changing **A** from level 1 to level 2. Note that **B** was at both of its levels within each set.

$$\text{Effect of } \mathbf{A} = \tfrac{1}{2}(y_2 + y_4) - \tfrac{1}{2}(y_1 + y_3)$$

Apart from the factor of ½, this algebraic expression can be obtained by applying the signs of **Table 6-1** to the observed responses, thus:

$$- y_1 + y_2 - y_3 + y_4 = (y_2 + y_4) - (y_1 + y_3)$$

Similarly the effect of changing **B** from its level 1 to level 2 can be estimated from the signs as one half of:

$$- y_1 - y_2 + y_3 + y_4 = (y_3 + y_4) - (y_1 + y_2)$$

leading to:

$$\text{Effect of } \mathbf{B} = ½ (y_3 + y_4) - ½ (y_1 + y_2)$$

These two comparisons of the four responses are known as ‘contrasts’. In fact there are three independent contrasts that can be made from the four responses. The third is:

$$y_1 - y_2 - y_3 + y_4 = (y_4 + y_1) - (y_2 + y_3)$$

leading to:

$$\text{Effect of } \mathbf{AB} = ½ (y_1 + y_4) - ½ (y_2 + y_3)$$

This is know as the interaction effect and is where factorial designs of this type are so powerful.

Table 6-1 can be extended to show the signs needed to calculate the interaction term (**AB**). This is done by simply multiplying, row by row, the signs of **A** and **B**. Like signs become ‘plus’ and unlike signs become ‘minus’. This is shown in **Table 6-2** with example responses.

Experimental Programme	**A**	**B**	**AB**	Response
1	-	-	+	16
2	+	-	-	12
3	-	+	-	24
4	+	+	+	20
Σ_+	32	44	36	72
Σ_-	40	28	36	0
$\Sigma_+ - \Sigma_-$	-8	16	0	72
Divisor	2	2	2	4
Effect	-4	8	0	18

Table 6-2 Experimental Matrix of Factors A and B Including the Interaction AB

The calculations performed to obtain the various effects are characterised by the table of signs. Division by two (because the means of two responses are being compared) lead to numerical estimates of the effects, i.e. the **A** main effect is calculated thus:

$$\frac{-\mathbf{16} + \mathbf{12} - \mathbf{24} + \mathbf{20}}{\mathbf{2}} = -\mathbf{4}$$

Inspection of **Table 6-2** leads to the following conclusions:-

1. There is no interaction between **A** and **B**, i.e. 0 effect.

2. Changing **A** from low to high level will reduce the response by 4 units, whichever level of **B** is used.
3. Changing **B** from low to high level will increase the response by 8 units, whichever level of **A** is used.

Arranging the table for analysis in this way is known as a *Table of Contrast Coefficients*.

Although the example described here is very simple and the results idealised, it does show how factorial experimental design and tables of coefficient contrast can be used to analyse individual and interactive variable effects.

6.2.2 The Design of a Factorial Experiment on the Processing and Operating Variables of NiTi Shape Memory Alloys

6.2.2.1 Ascribing the Factors Upper and Lower Levels

As described in 6.1 five variables have been identified as being of particular relevance to the thermo-mechanical fatigue of NiTi shape memory alloys. These are specifically:-

1. Heat Treatment Temperature
2. Cold Work
3. Alloy System
4. Applied Load
5. Heat/Cooling Rate

To employ a two level factorial experiment for their analysis, upper and lower values must be chosen for each variable. The values used are shown below in **Table 6-3**.

Level	Heat Treatment Temperature °C	Cycling Rate s/Cycle	Applied Stress MPa	Prior Cold Work %	Alloy Type at% Ti

+	500	70	165	30	50.12
-	400	170	85	6	49.74

Table 6-3 Factorial Level Values of the Processing and Operating Variables

These levels were chosen after careful analysis of the literature and consideration of how to vary the factors such that their effect on cyclic stability is easily observed.

Heat treatment temperatures used by other workers tend to be in the range of 400°C to 500°C. Therefore the upper and lower limit of this range was chosen for the factor levels.

Cycling rates were chosen as the fastest rate achievable using the rig described in the next section and a rate significantly slower. The + sign is assigned to the fast rate, i.e. 70 seconds per thermal cycle.

The applied stress levels were chosen such that the lower level was close to the onset of stress induced martensite in these alloys and the upper level was significantly higher than the stress induced plateau. The plateau stresses were measured from tensile tests performed on the alloys and stresses of 165MPa and 85MPa were chosen to represent the upper and lower levels respectively.

Other workers have found that cold work significantly affects cyclic stability in NiTi alloys, particularly at levels greater than 25-30%. Therefore an upper level of 30% was chosen for the factorial experiment and a lower level of 6%. The significance of the cold work level could then be assessed.

Finally, two alloys were chosen, one on either side of the equi-atomic composition. This corresponded to a 49.88at%Ni - 50.12at% Ti alloy and a 50.26at%Ni – 49.74at% Ti alloy. The titanium rich alloy was designated the + sign for the factorial analysis.

6.2.2.2 Choosing the Responses for Measuring Factor Effects

The responses chosen for measuring factor effects were based on shape stability and recovery strains. Specifically these are:-

- Parent phase strain (increasing 'permanent' strain in the hot length)
- Martensite phase strain (increasing 'permanent' strain in the cold length)
- Recovery strain (decreasing recovery strain i.e. Hot length – cold length)

Hysteresis strain-temperature profiles were also collected. A simple way of fitting the analysis of transformation temperatures and hysteresis profiles into a table of contrasts could not be established. Thus, the effect of factor levels on thermal hysteresis was assessed by inspection not calculation.

6.2.2.3 Designing the Table of Contrast Coefficients

To carry out a full factorial analysis of the 5 factors described above, set at two different levels requires 32 experimental runs, i.e 2^5 experiments. The full table of contrast coefficients is shown in **Appendix A**.

7 Experimental Procedure

7.1 Cycling Rig Design

The design of the rig for cycling the shape memory alloys was essentially carried out by applying the following steps:-

7.1.1 Problem

Design and build a test rig that will allow the NiTi alloys to be thermally cycled against applied loads.

7.1.2 Objectives

The rig must :-
Hold a NiTi wire fixed at one end whilst applying a load to the other free end.
Allow cycling between approximately 20°C and 120°C.
Collect strain and temperature information automatically during high cycle number tests.
Allow for relatively fast cycle rates to reduce the time required for each experimental run.

7.1.3 Design Conception

It was found from the literature that the most popular methods of thermally cycling NiTi alloys were:-

- Oil baths
- Hot air blowers
- Furnace element heating
- Electrical Resistance Heating

The method of heating appeared to have a large bearing on both the cost of the rig and the cycling speed at which it could operate.

One of the short comings of many previous workers data on cyclic stability is the low number of cycles employed for the experiment. For instance, the effects analysed by Todoroki[138] were carried out over just three cycles. His machine used an inert liquid which was heated and cooled to thermally cycle the alloy. Although no figure is given, it is likely that each cycle required relatively long time periods. Stachowiak and McCormick[135] used a similar oil bath method for carrying out 100 thermal cycles.

Tobushi[129] used quite a complex experimental set up combining a tensile testing machine with a hot air blower to achieve 100 thermal cycles. Thoma[131] does not implicitly state his method of thermal cycles, but does imply it is some type of environmental cabinet. However, he does give a cycling rate of 5°C per minute both during heating and cooling. This would result in one 100°C temperature cycle requiring approximately 40 minutes!

Tamura et al[137] described thermal cycles of 2 minutes where the whole test apparatus is immersed into hot and cold water baths to achieve a complete forward and reverse transformation. This is a relatively fast cycle but does have the added complication of finding a method for automatic immersion of the whole fixing apparatus.

Previous successful experiments were carried out by Friend and Morgan on resistively heating NiTi wires embedded in composite beams[168,169]. It was found that the parent phase transformation was easily achievable by applying just 2.0 A to a 0.3mm diameter wire. In addition, relatively high cycle rates were thought to be achievable with this method.

A site visit to the shape memory testing facility at the University of Leuven, Belgium allowed close examination of both an oil bath testing machine and a direct resistance heating machine. During discussions at this meeting it became clear that to achieve high cycle rates and automatic response measurements within a reasonable budget, electrical resistance heating was the most feasible method of testing.

7.1.4 Preliminary Designs

A number of preliminary designs were sketched and compared. The critical considerations for the design were broken down into the following requirements:-

- A method of gripping the wires.
- A method of automatically applying electrical current increases and decreases.
- A method of automatically measuring the length strain and recovery strain in the wire.
- A method of applying the fixed loads to the wire.
- A method of saving the recorded data into a spread sheet
- A method of recording the wire temperature for strain-temperature plots.

Finally a design was formulated that could achieve all of the above requirements apart from automatic hysteresis recording which would require the operator manually switching on a chart recorder. This was deemed acceptable.

7.1.5 Final Automated Test Rig Design

Figure 7-1 shows a diagram of the experimental set up. Essentially, the rig consists of:-

- A Thornley TSB 3510P programmable power supply
- A Hewlett Packard HP 3457A multimeter
- An Opto non-contact optical displacement measuring laser
- A 486DX 8Mb computer with Labview® software
- A rigid structure for holding the wires, weights and displacement measurer
- An X-Y recorder for displacement-temperature recording

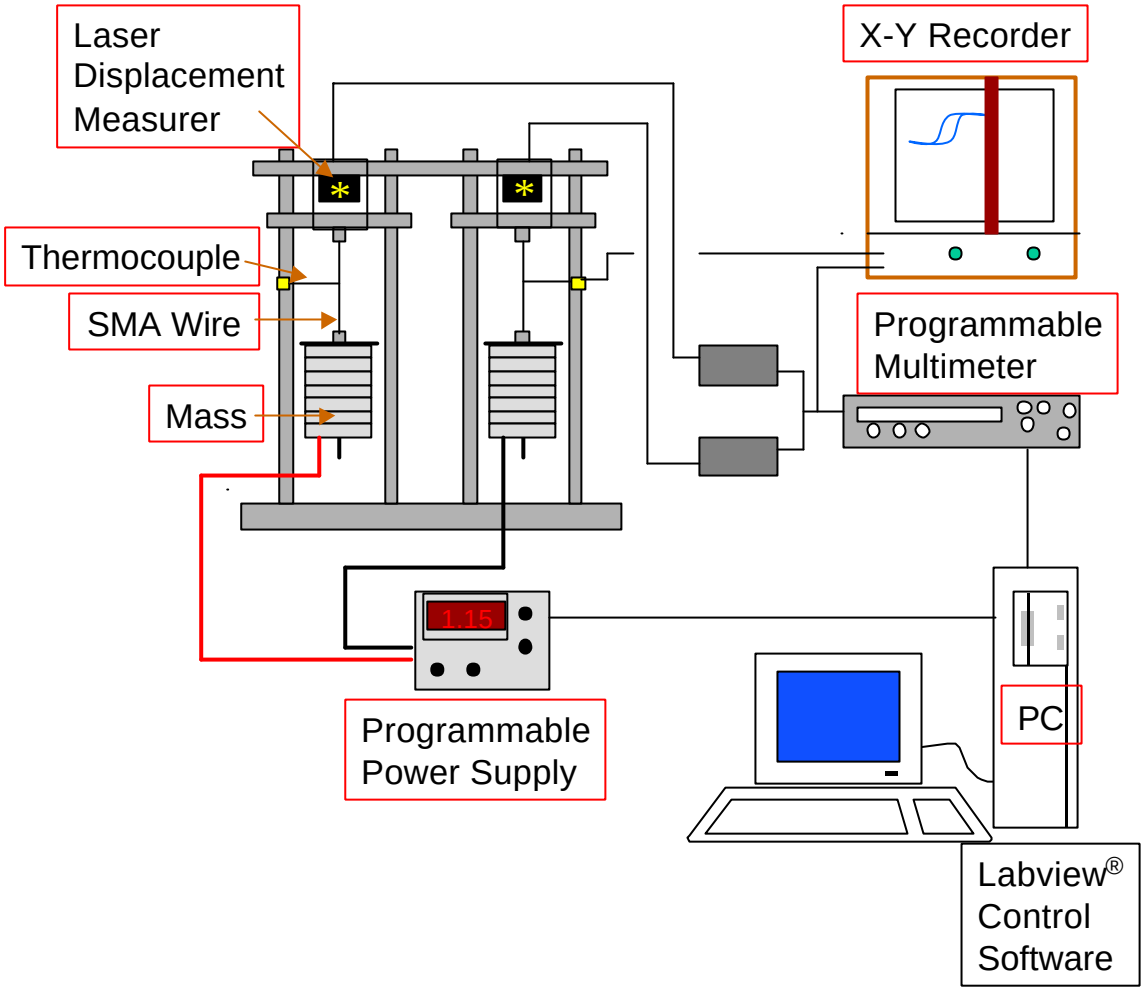

Figure 7-1 Diagram of Test Rig Design and Experimental Set-up

The rig was designed such that it incorporated four test cells. Only two cells were used during testing due to the expense of the laser measurement device. However, it was felt that incorporating four cells would allow future expansion of the testing facility. It was felt that having at least two operational cells would greatly speed up the testing of the alloys and would be particularly useful for long cycle runs.

A full drawing of the rig design is shown in **Appendix B**. The cycling rig operates thus:

The wire is attached to the upper plate by a drill chuck capable of holding very small diameters (<0.5mm). The free end of the wire has a series of weights

attached to it, again via a small diameter drill chuck. The drill chuck clamped to the free end has a 300mm threaded bar attached to it. Weights can be threaded onto the bar and fixed by a nut. Altering the number of weights thus alters the stress on the wire.

Current is fed to the wire through the upper plate and the lower weight assembly. The current is applied by a programmable power supply controlled by the PC. In this manner the current can be gradually stepped up for wire heating and stepped down for wire cooling

During cycling the length of the wire increases and decreases as the martensite and parent phase are cycled respectively. Attached to the lower weight assembly is a white, perspex® target, that the laser displacement sensor can reflect off. The laser is attached to the top of the rig on a runway above the upper plate. Being on a sliding rail it allows accurate alignment of the laser in the horizontal plane.

The laser based measuring device operates via a non-contact triangular measuring principle. A point of light is projected onto the target. The position of the object is determined by the distance of the scattered light on the target from the detector. The system works with light pulses, so the dependence on constant ambient light is very low. The output of the laser device is a linear analogue +/- voltage of 10.0V corresponding to the displacement range of the sensor and the back scattered light focused onto a position sensitive detector in the laser assembly. A voltage change of 1.0V corresponds to a change in distance of 5mm, i.e. +/- 10.0V = +/- 50.00mm.

A great advantage of this laser based measuring device is the fact that it is non-contact. This avoids the complicated counterbalanced LVDT design which is employed on the cycling rig at the shape memory testing facility, University of Leuven, Belgium.

When setting up the rig for a cycling run, the vertical position of the top plate is set such that the voltage output of the laser is 0.0V. This means that any changes in length can be calculated directly from the voltage reading. If the voltage changes from 0.0V to 1.2V during cycling, this corresponds to an increase in wire length of 6.0mm. Measuring the change of length in this way results in a displacement resolution of 0.03mm.

Voltage changes are fed directly to the programmable multimeter each time the current is changed, i.e. each time the temperature in the wire is changed. The multimeter is also interfaced to the PC via a GPIB serial board. The voltage changes are read by the PC and converted by the control programme into millimetres.

In addition to the computer controlled measurements, temperature readings are taken directly from the NiTi wire and recorded on the X channel of an X-Y recorder. Strain measurements are passed to the Y channel of the X-Y recorder. In this way hysteresis profiles can be recorded. Unfortunately the X-Y recorder cannot be controlled automatically, therefore the recorder must be switched on manually whenever a hysteresis plot is required.

Temperature measurements are taken using a thin foil (0.002mm), butt bonded, K-type thermocouple attached directly to the actuating gauge length of the NiTi wire. This type of thermocouple is extremely sensitive to temperature changes and provides fast, accurate measurements of the wire temperature.

The whole rig is controlled by LabView® software installed on 486DX *Mb PC.

LabView® software is a control programme that can be used to create 'virtual instruments'. Using a graphics based programming language created by National Instruments®, sophisticated control instruments can be created for the operation of remote devices and the recording of measured data.

7.2 The Cycling Rig Control and Record Programme

LabView® utilises a graphical programming language to create programs in block diagram form. It has extensive libraries of functions and subroutines for many programming tasks, thus speeding up programme development.

LabView® uses modular programming to divide an application into a series of tasks, which can then be divided again until a complicated application becomes a series of simple subtasks. Each task is performed by a series of LabView® programmes known as *virtual instruments or VI's.*

The programmer builds a VI to accomplish each subtask and then combines those VI's on another block diagram to accomplish the larger task. Therefore, the final top-level VI contains a collection of sub VI's that represent application functions.

The exact details of the programme constructed for the cycling rig is shown in **Appendix C**. The basic sequence of the programme however, is described in **Figure 7-2** and in the text below.

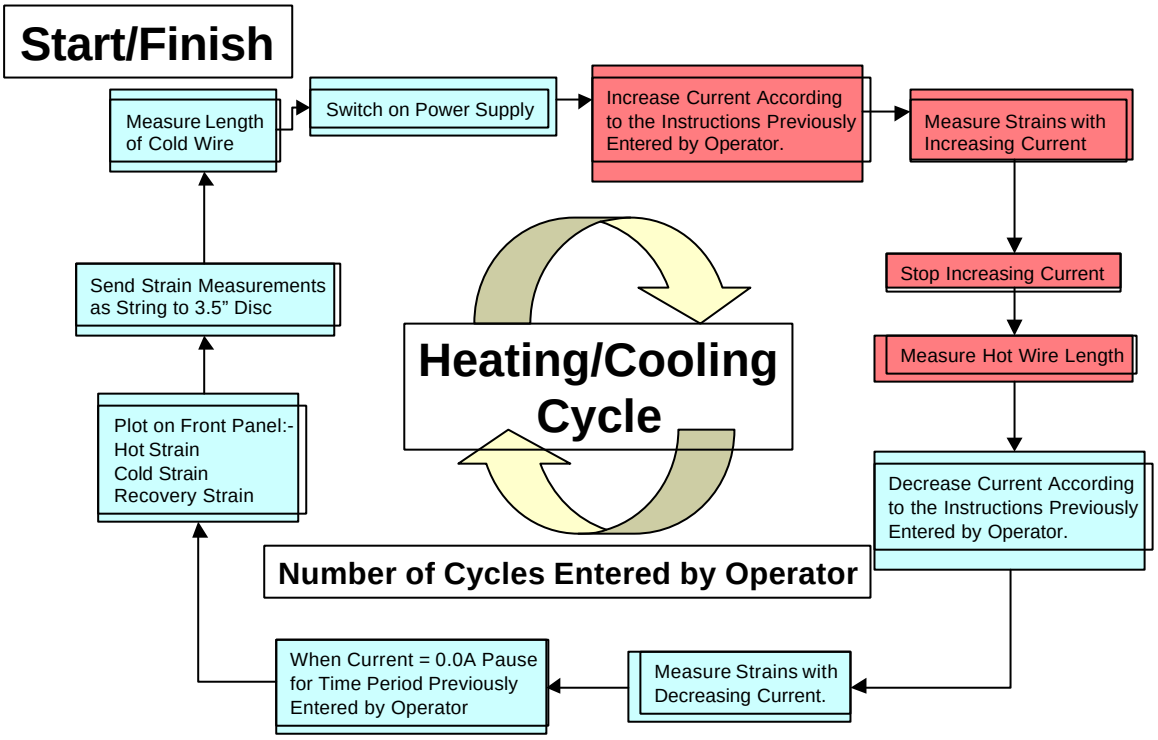

Figure 7-2 Block Diagram of the Rig Control Programme

Step 1

Measure the length of wire in cell 1 and cell 2 with no applied current, i.e. measure the cold length.

Step 2

Switch on power supply and begin to increase the current in predetermined steps to a set limit.

Step 3

Carry on increasing the current whilst measuring the strains in the NiTi wire of cell 1 and cell 2 with each stepped increase.

Step 4

Stop increasing current and measure strain of NiTi wire in cell 1 and cell 2, i.e. measure the hot length.

Step 5

Begin to decrease current in equal steps to those used for heating.
Measure strains of NiTi wire in cell 1 and cell 2 with each stepped decrease.

Step 6

When applied current is 0.0A stop cycle and pause for predetermined time period.
Plot: Strains on Heating and Cooling, Hot Length, Cold Length and Recovery strain of wire for both cell 1 and cell 2 on the front panel of the user interface shown on monitor.
Send strain measurements as a data string to 3.5” disc.
Return to Step 1.

As referred to in Step 6, the whole control programme is controlled by a front panel, which is displayed on the monitor. The rig control programme is written such that the: number of cycles, number of current steps, value of current steps and time delay between current steps can all be controlled via this panel. It is this type of user interface that leads to the term: virtual instrument, which is often used to describe LabView® programmes.
In addition, the rig control programme has been constructed such that the strain data is displayed graphically on the screen during successive experimental runs.

The data is updated during step 6 above, i.e. at the end of each thermal cycle. The front panel is automatically sent to print at the end of the test to provide a hard copy of the test run. Data is sent to 3.5” disc to facilitate analysis through standard spread sheet packages such as Sigma Plot® and Excel®.

8 Results of the Factorial Design Experiment on NiTi Wires

Factorial Analysis of Processing and Operating Variables over 500 Thermal Cycles With Constant Load

8.1 Alloy Characterisation

The first stage of the factorial experiment was to characterise the alloys both mechanically with tensile tests and thermodynamically with differential scanning calorimetry (DSC) tests. The two alloys were designated the following codes for easy reference:-

SMA 6 **49.88at% Ni – 50.12at%Ti cold worked by 6%**

SMA 30 **49.88at% Ni – 50.12at%Ti cold worked by 30%**

SMC 6 **50.26at%Ni – 49.74at%Ti cold worked by 6%**

SMC 30 **50.26at%Ni – 49.74at%Ti cold worked by 30%**

The factorial analysis was carried out such that each experiment was run over 500 thermal cycles, i.e. 32 runs of 500 thermal cycles each. The strain data was then fed into the contrast coefficient matrix shown in **Appendix A** and the main effects of the factor levels were calculated. Calculations and effects analyses were carried out in specially constructed spread sheets. This meant that the measured responses could simply be fed into the computer, speeding up the whole analysis process. Due to the space required, the full analysis of individual and interactive effects is not included in this thesis.

Tensile and DSC tests were carried out to fully characterise the alloys and establish the effect of heat treatment temperature on the phase transformation. These results are presented in graphical form.

8.1.1 Tensile Tests

Tensile tests were performed on a Houndsfield H25 tensometer machine at a cross head speed of 5mm min^{-1}. Three stresses were measured from each curve: Stress 1, Plateau Stress and Stress 2, these are defined in **Figure 8-1**.

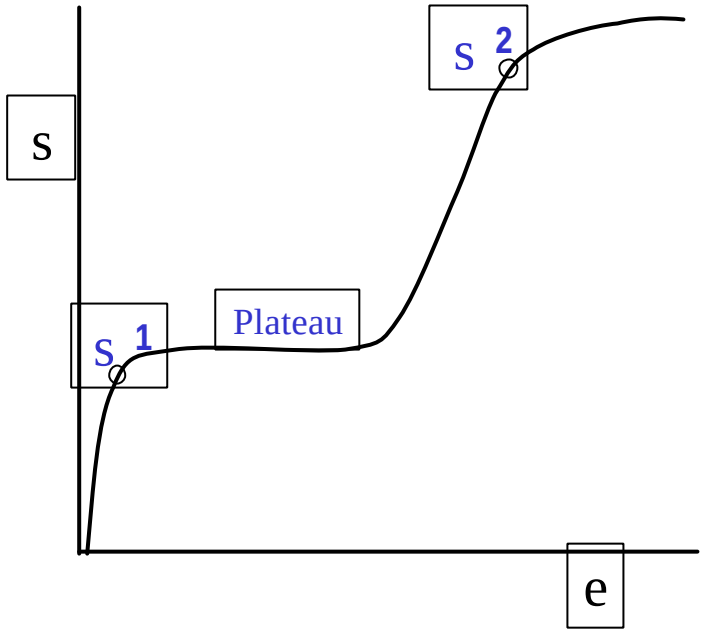

Figure 8-1 Stresses measured from tensile curves

Stress 1 corresponds to the stress required for inducing martensite or re-orientating existing martensite variants depending upon the transformation temperatures of the alloy under test. The plateau stress corresponds to the stress require to grow preferentially orientated variants at the expense of others. Stress 2 is the stress where the elastic limit of the re-orientated martensite is exceeded and real plastic deformation begins.

Graph 8-1 and **Graph 8-2** show these stresses plotted for the two cold work levels in each of the two alloys at various heat treatment temperatures. That is, **Graph 8-1** shows stresses: 1,2 and plateau after various heat treatment temperatures for the Ti rich alloy (**SMA**), with either 6% prior cold work (**SMA6**), or 30% prior cold work (**SMA30**). Likewise, **Graph 8-2** shows stresses: 1,2 and plateau after the same heat treatments, for the Ni rich alloy (**SMC**), with either 6% prior cold work (**SMC6**), or 30% prior cold work (**SMC30**).

The higher heat treatment temperatures tend to result in a decrease of the stress 1 and stress 2 values. In particular, the stress 2 of both the 30% cold work alloys decreases markedly between 450°C and 550°C. This decrease is likely to be associated with the start of recovery in the significantly deformed microstructure of the alloys with 30% cold work, followed by the start of recrystallisation.

The decrease of stress 2 is greatest in the SMA30 (Ti rich) alloy, implying greater recovery in these samples than the SMC30 (Ni rich) equivalents. This may be due to the lower recrystallisation temperature in the Ti rich alloy (previously measured as approximately 500°C) compared to the Ni rich alloys (approximately 575°C).

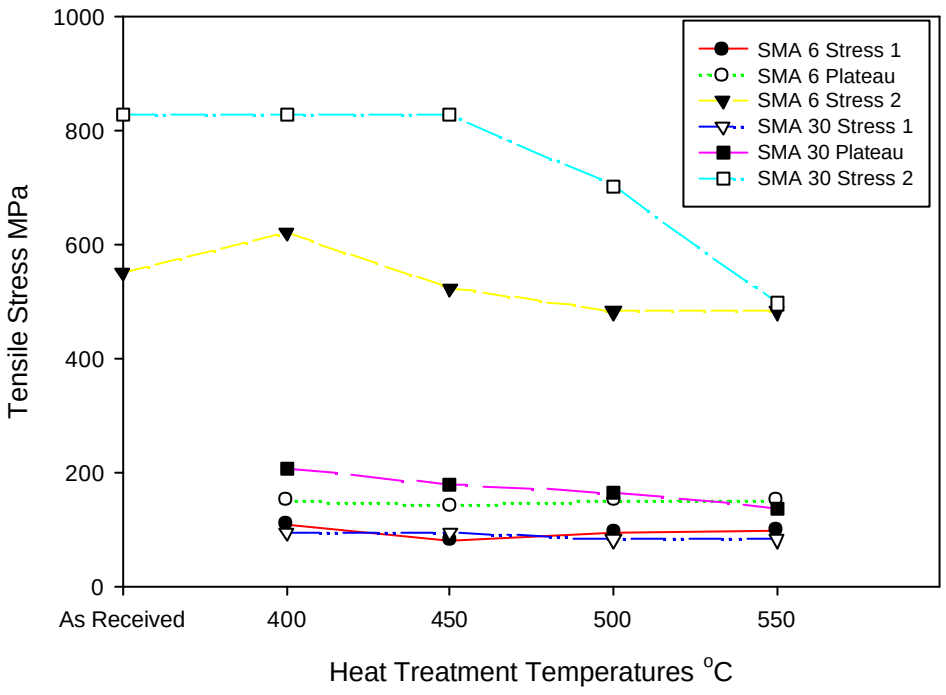

Graph 8-1 SMA6 and SMA30 Tensile Stresses Vs. Heat Treatment Temperatures

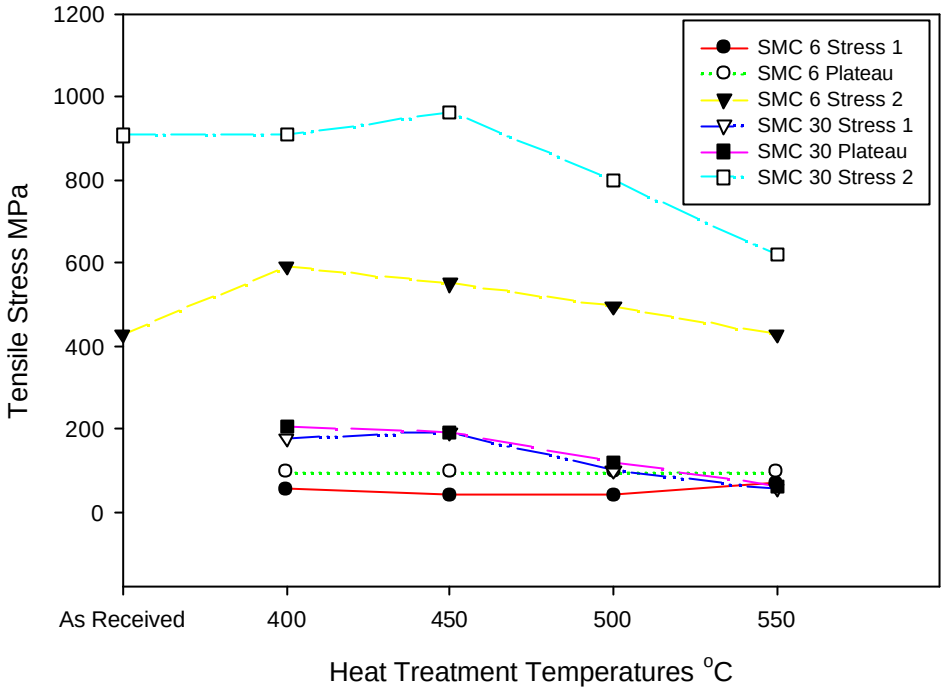

Graph 8-2 SMC6 and SMC30 Tensile Stresses Vs Heat Treatment Temperature

8.1.2 Transformation Temperatures

Several different methods exist to determine shape memory transformation temperatures. The most common are: differential scanning calorimetry, constant load measurement and active A_f measurement[170]. The latter two methods utilise the alloys' movement during heating and cooling and requires accurate measurement of both temperature and the associated deflection. The most precise method of determining the transformation temperatures at zero load is that of differential scanning calorimetry (DSC). By measuring the amount of heat absorbed or given off during the phase transformation, plots are obtained similar to those shown in **Figure 8-2**. Although the DSC method yields accurate and repeatable data, it can sometimes be inconclusive if there is a large amount of residual cold work within the alloy.

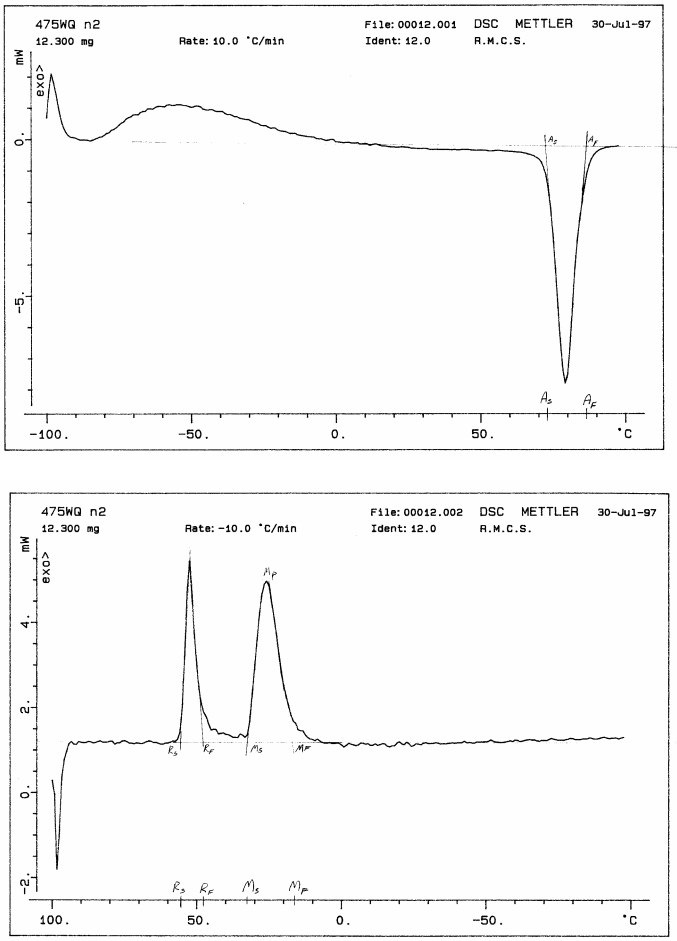

Figure 8-2 Typical DSC Heating and Cooling Traces for NiTi Alloy. The lower cooling curve trace displays two peaks corresponding to the R-Phase and Martensite phase.

The start and finish temperatures of the respective phase changes are measured from a tangent line drawn against the peak, as demonstrated in **Figure 8-2**. In practice this is performed automatically by the DSC machine.

All tests were carried out on the METLER® DSC machine at Cranfield University, Shrivenham. One heating run and one cooling run were performed on samples taken from each heat treated wire subsequent to the tensile tests described in the previous section. The measured transformation temperatures are plotted below in **Graph 8-3** to **Graph 8-6**. R-phase temperatures are not included, these remaining very constant with increasing heat treatment temperature.

Again, the sample coding is such that SMA and SMC correspond to the Ti rich and Ni rich alloys respectively while the additional suffix of 6 and 30 corresponds to 6% and 30% cold work.

It can be seen that the transformation temperatures tend to increase with heat treatment temperature. Just as with the tensile tests, this corresponds to recovery of the microstructure. Again, the 30% cold worked alloys show the greatest increases of transformation temperatures and in particular the SMA30 samples.

As previously described, the transformation temperatures tend to increase with annealing temperature because of the redistribution of the dislocations and internal stress. Somehow, this assists the martensite transformation in a manner similar to the Clausius-Clapeyron effect when an external stress is applied. Of particular interest is the decrease of the temperature difference between M_s and M_f as heat treatment temperature increases. This confirms the previous reference of Humbeeck[126], that a decrease of elastic strain energy is concurrent with a decrease of temperature change between the start and finish of transformation.

Commonly the hysteresis width is defined as $A_s - M_s$. Humbeeck states that a decrease in $A_s - M_s$ is concurrent with a decrease of internal friction. In **Graph 8-3** to **Graph 8-6** the higher heat treatment temperature tends to result in an in crease of $A_s - M_s$ thereby implying an increase of internal friction.

Higher heat treatment temperatures result in increasing microstructure recovery and recrystallisation. If internal friction is due to the movement of interfaces and creation of defects then a microstructure that is relatively defect free (i.e. recrystallised) may result in greater internal friction as new defects are formed. This is because movement of the interfaces is easier as they are less impinged by dislocation networks and defects can be generated in the relatively defect free lattice. This results in an energy loss and increase of hysteresis width.

Therefore, in summary it can be said that the higher heat treatment temperature results in higher transformation temperatures, lower elastic strain energy and greater internal friction.

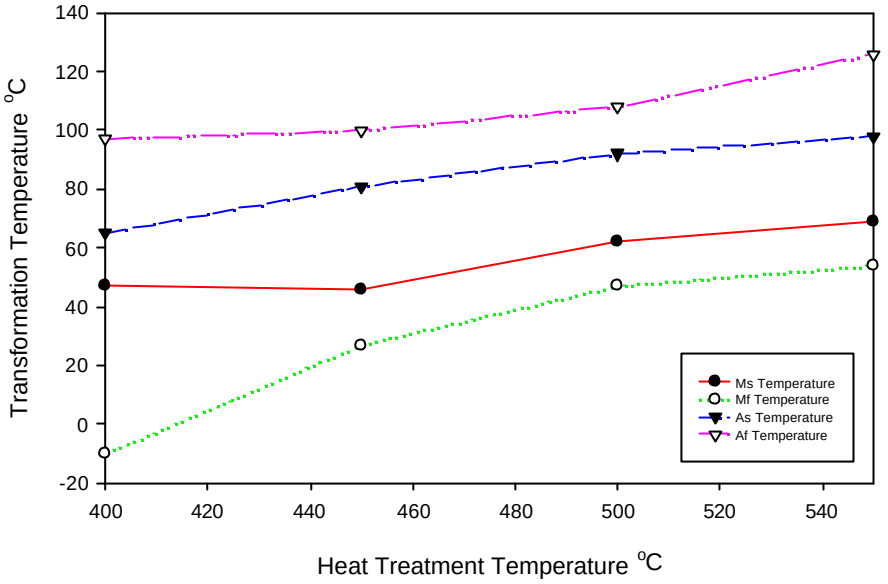

Graph 8-3 SMA30 Transformation Temperatures After Heat Treatment

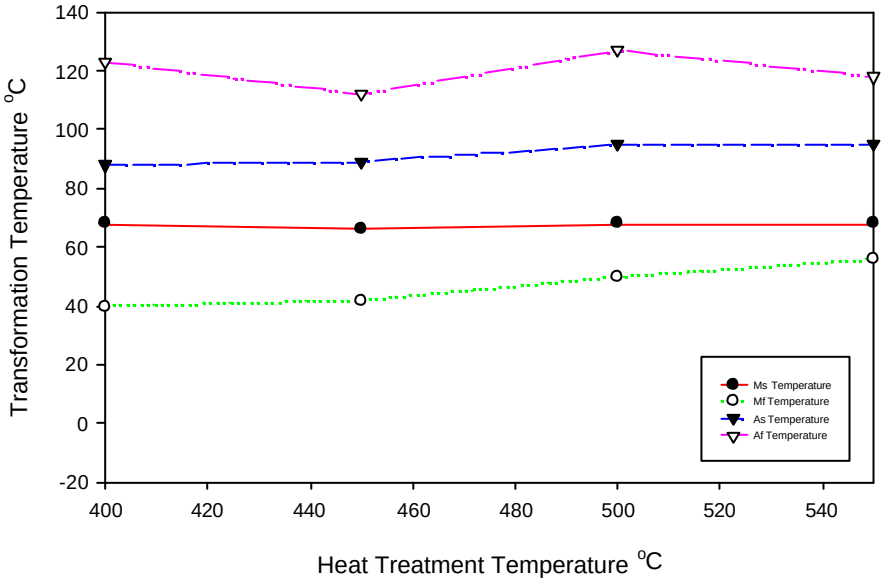

Graph 8-4 SMA6 Transformation Temperatures After Heat Treatment

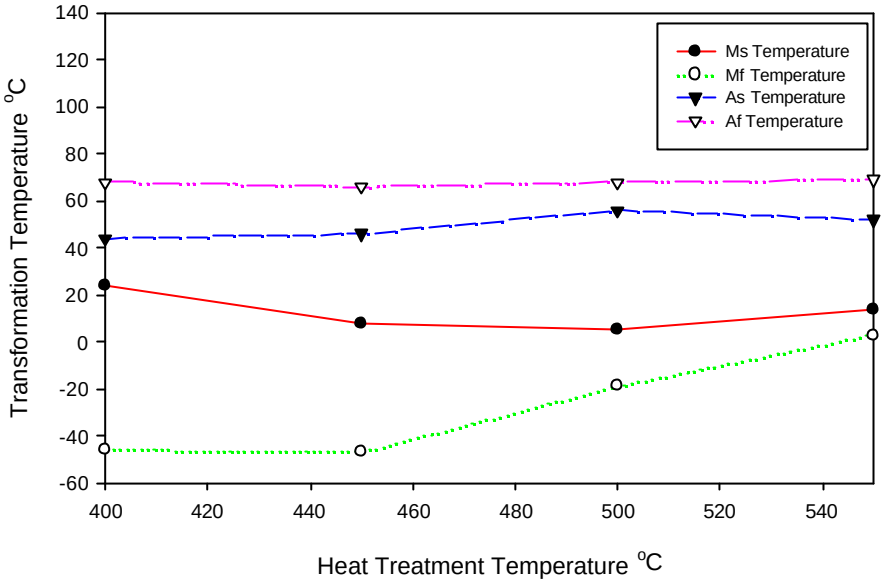

Graph 8-5 SMC30 Transformation Temperatures After Heat Treatment

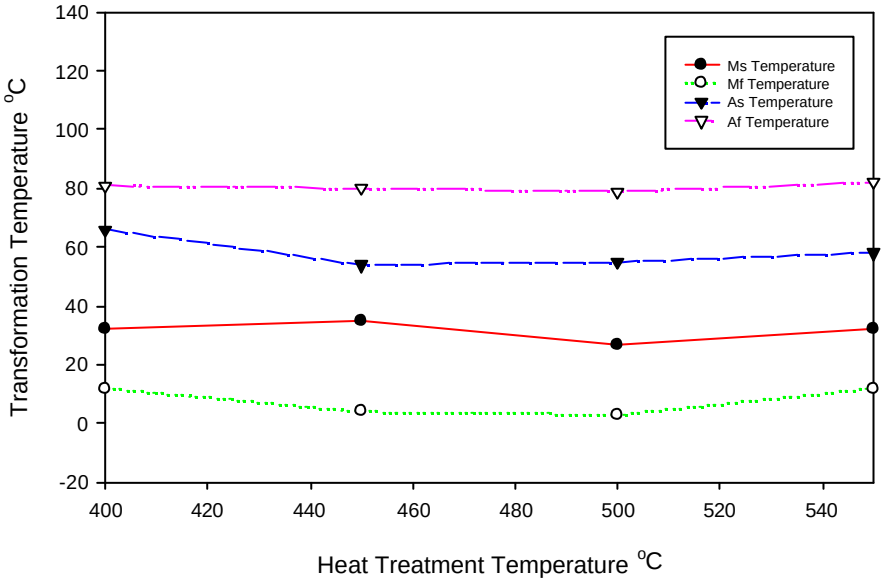

Graph 8-6 SMC6 Transformation Temperatures After Heat Treatment

8.1.3 Heats of Transformation

The heats of transformation during heating and cooling may also be measured from the DSC traces. The total area under the respective peaks is integrated by computer and related to the total mass of the sample under test, thus quantifying the total heat released (exothermic) or absorbed (endothermic) during transformation.

The heat of transformation measured by standard DSC, is often referred to by workers as the enthalpy of transformation, ΔH. This term should be used carefully as in fact the enthalpy of transformation measured by DSC is a resultant heat of transformation dependant upon **equation (2-10)**, repeated below:

$$\Delta \mathbf{H_{net}} = \Delta \mathbf{H_{ch}} + \Delta \mathbf{H_{el}} + \Delta \mathbf{H_{I}}$$

(8-1)

where $\Delta \mathbf{H_{net}}$ is the net enthalpy change measured by differential scanning calorimetry (DSC), $\Delta \mathbf{H_{ch}}$ is the chemical enthalpy, $\Delta \mathbf{H_{el}}$ is the enthalpy change associated with the elastic energy of the transformation and $\Delta \mathbf{H_{I}}$ arises from the production of internal interfaces during transformation.

Salzbrenner and Cohen[39] showed that as the martensite transformation proceeds, the non-chemical strain energy is stored in the system resulting in a decrease of the observed heat evolution ($\Delta H^{P\rightarrow M}_{net}$) compared to the chemical enthalpy change ($\Delta H^{P\rightarrow M}_{ch}$). This results in: $\Delta H^{P\rightarrow M}_{net}$ being less negative than $\Delta H^{P\rightarrow M}_{ch}$.

The net enthalpy changes, $\Delta \mathbf{H_{net}}$, or heats of transformation, are shown in **Graph 8-7** to **Graph 8-10**, (an experimental error derived from repeat tests was estimated at $5.0 Jg^{-1}$) . These show the effect of prior cold work and heat treatment on the transformation enthalpies of each alloy. Again the most significant changes tend to be associated with the 30% cold work alloys. In both the SMA30 (Ti rich with 30% cold work) and SMC30 alloys (Ni rich with 30% cold work), the heat of transformation during the martensite transformation increases with heat treatment temperature. The heat of transformation associated with the R-phase and parent phase does not appear to change significantly with heat treatment temperature. The increase of the

DSC measured, martensite ΔH_{net}, implies a decrease in the non-chemical free energy opposing the transformation. If the value of ΔH_I , i.e. the energy associated with the production of interfaces is considered to be very small, the reduction of non-chemical free energy must be associated with a reduction in the elastic energy, ΔH_{el} , stored during transformation. Again, this is consistent with the tensile and transformation temperature results already presented.

The greater the reduction in elastic energy (non-chemical) opposing the martensite transformation, the closer the values of ΔH_{net} between the forward and reverse transformation. This also implies that the difference in heats of transformation between the forward and reverse reaction indicates the amount of non-chemical free energy opposing the martensite formation.

Following these arguments, the 6% cold work alloys should have very similar heats of transformation for both the forward and reverse transformation at all heat treatment temperatures. This is indeed the case for the SMC6 samples, but is not the case for the SMA6 samples, i.e. **Graph 8-10** and **Graph 8-8** respectively. The very low values of the martensite heats of transformation for the SMA6 samples can only be explained by experimental error.

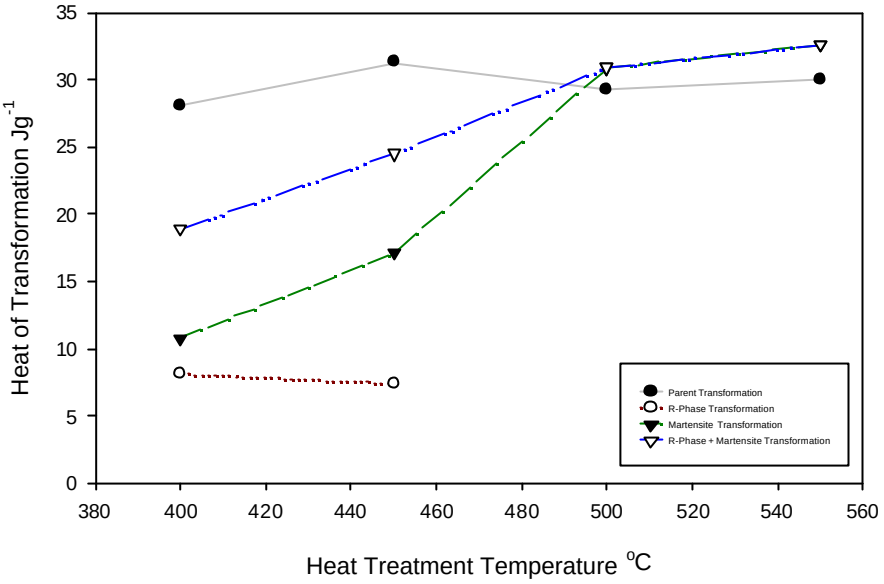

Graph 8-7 SMA30 Heats of Transformation After Heat Treatment

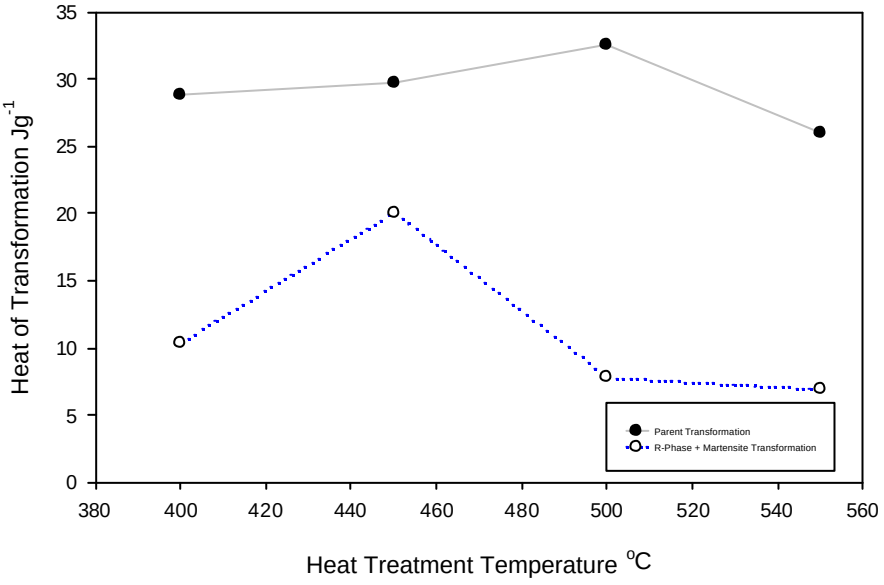

Graph 8-8 SMA6 Heats of Transformation After Heat Treatment

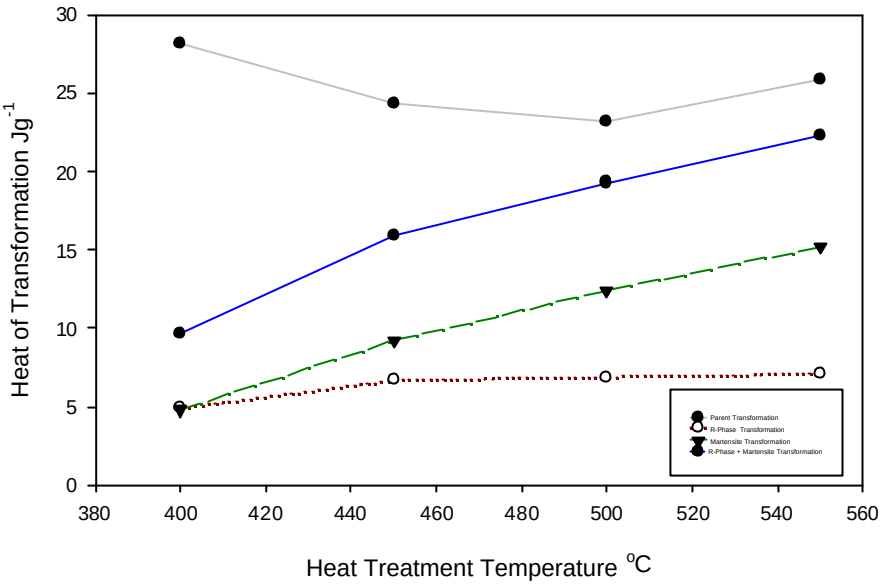

Graph 8-9 SMC30 Heats of Transformation After Heat Treatment

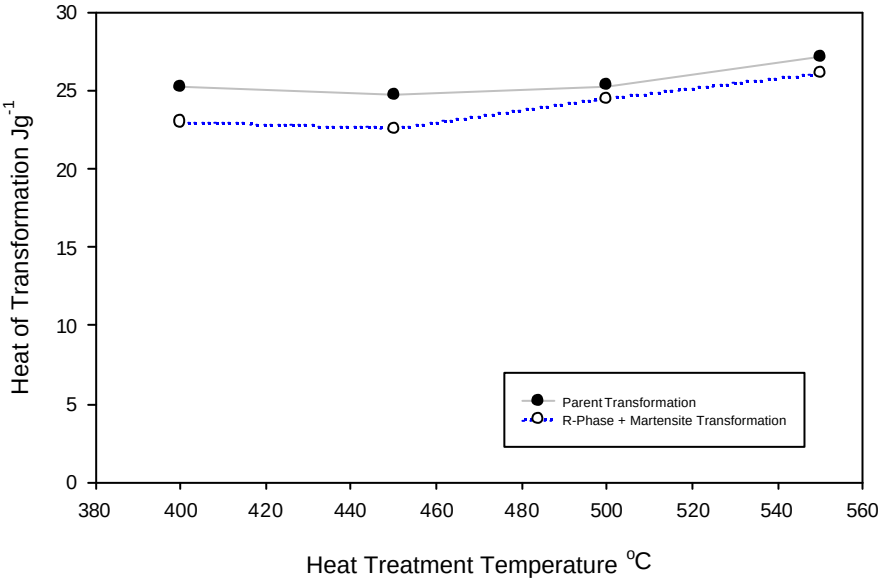

Graph 8-10 SMC6 Heats of Transformation After Heat Treatment

8.2 Factorial Experimental Results

The results of the factorial analysis are such that the relative significance of each factor can be identified. The relative significance of individual factors and their interactive effects will be presented in this section.

8.2.1 % Strain Recovery (%e)

The % strain recovery of each actuating element was measured as the difference between the parent phase strain and martensite phase strain for each successive cycle. The strain recovery was analysed after cycles: 1, 100 and 500. Due to large residual deformation in wire length, the recovery strain at cycle 500 could not be measured in all the alloys under test. Therefore, the analysis of the factors described here and their significance is taken from the % recovery strain at cycle 1 and cycle 100 only. The unit of strain recovery used throughout this analysis is designated the symbol: **%e**.

The **mean average** of all the recovery strains for all 32 tests, on an initial actuating wire length of 100mm at **cycle 1** was: **3.3%e**

The **mean average** of all the recovery strains for all 32 tests, on an initial actuating wire length of 100mm at **cycle 100** was also: **3.3%e.**

The identical average recovery strains at cycle 1 and 100, are due to some recovery strains increasing during cycling and some decreasing. This has the effect of producing the same average even after 100 cycles. The graphs and factorial analysis that follows; shows which recovery strains and factorial effects change with cycling.

The individual recovery strains are plotted in sets of eight on **Graph 8-11** to **Graph 8-14**. These graphs are plotted for different cold work levels and alloy types. The curve colours correspond to the same heat treatment, applied stress and cycling rate.

The graphs show that recovery strain may either increase, decrease or remain essentially constant during 500 thermal cycles. The individual and interactive, factorial analysis that follows after the graphs, is used to help explain the origin of these cycling effects.

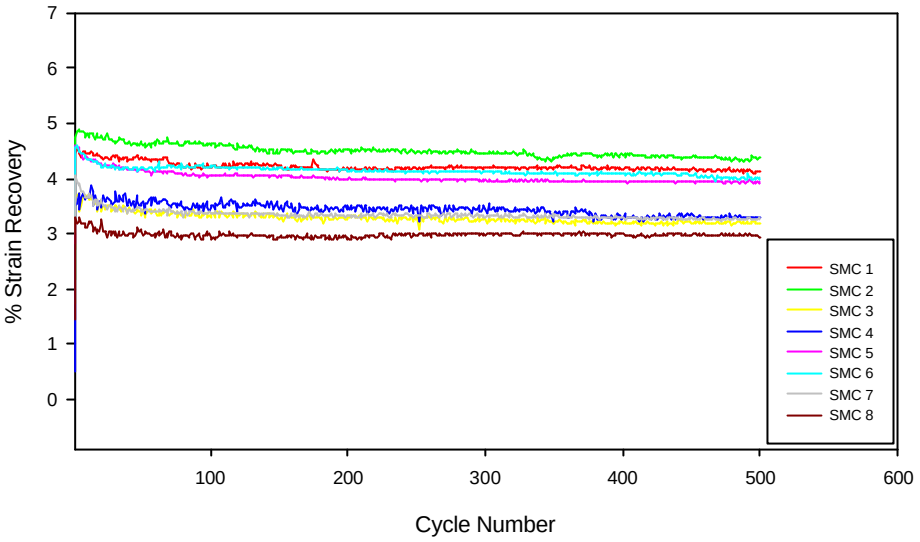

Graph 8-11 Recovery Strain in the SMC6 (Ti-50.26at%Ni, 6% Cold Work) Alloy During 500 Thermal Cycles

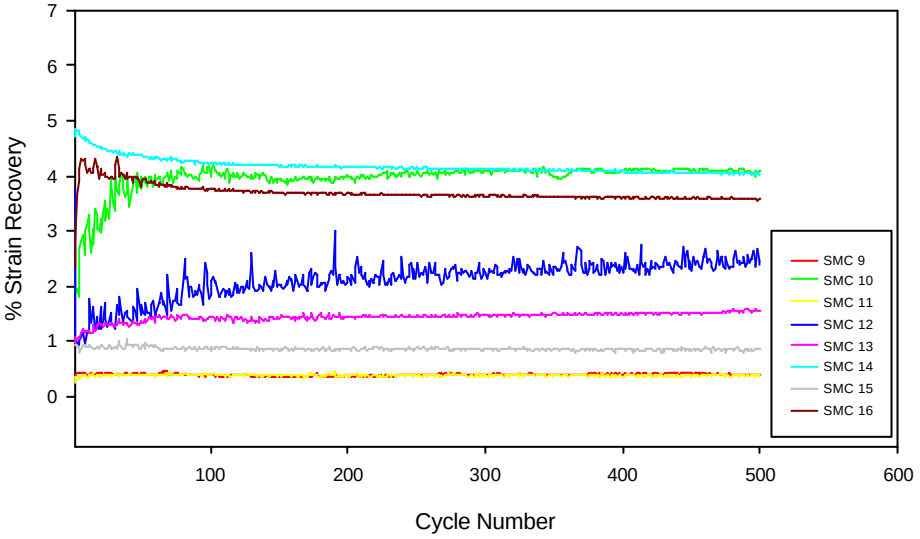

Graph 8-12 Recovery Strain in the SMC30 (Ti-50.26at%Ni, 30% Cold Work) Alloy During 500 Thermal Cycles

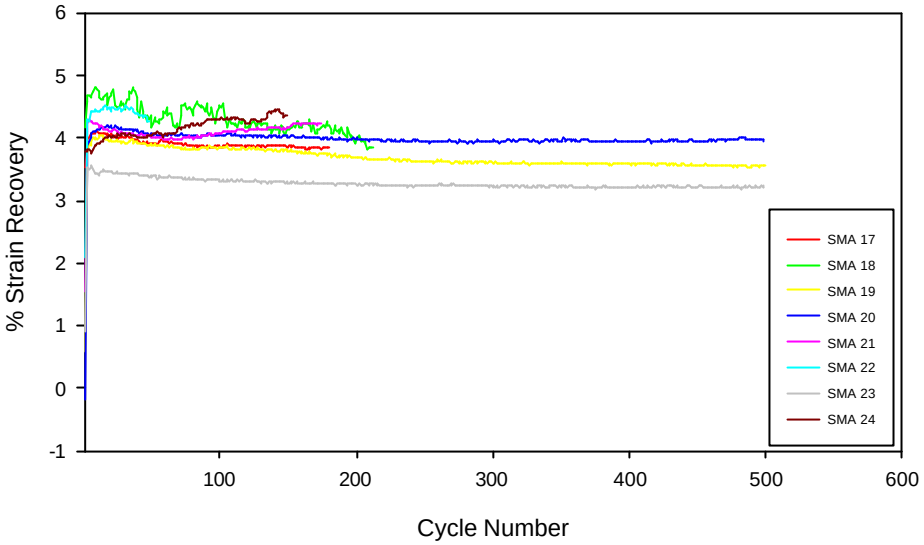

Graph 8-13 Recovery Strain in the SMA6 (Ti-49.88at%Ni, 6% Cold Work) Alloy During 500 Thermal Cycles

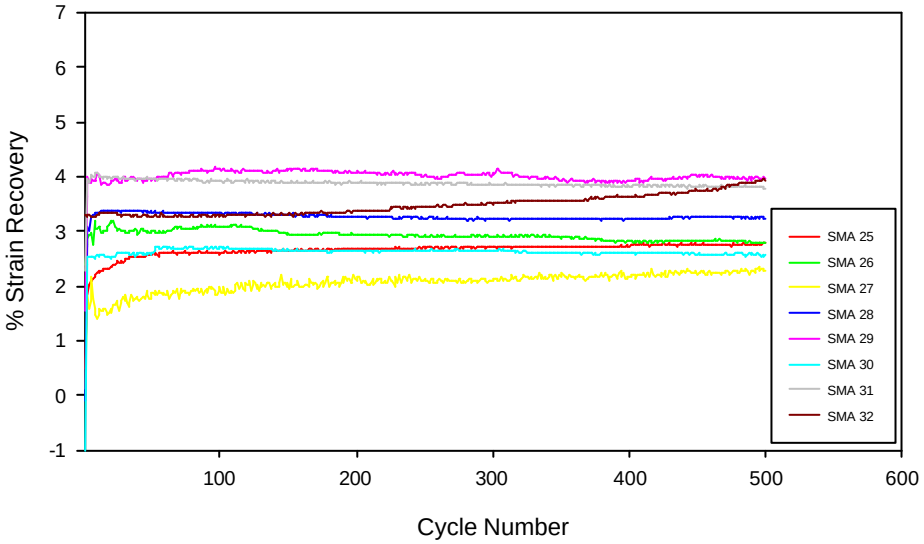

Graph 8-14 Recovery Strain in the SMA30 (Ti-49.88at%Ni, 30% Cold Work) Alloy During 500 Thermal Cycles

The tables of contrast coefficients, **Table 8-1** and **Table 8-2** show the sample factor levels and main effect calculations of recovery strain at cycle 1 and cycle 100. Whilst all the individual main effects are included in these tables, for ease of comprehension and conciseness, only the most significant interaction effects are shown. A divisor of 16 is used to calculate the main effects because the means of two responses are being compared over a total of 32 tests.

The significance of the main effects was calculated by comparison with an estimated standard error in strain recovery of 0.25%ε. This error was calculated from higher order interaction effects where four and five factor interactions are supposed negligible. If this is the case, then differences arising from these higher order interactions will measure differences arising principally from experimental error.

If any calculated main effect was less than, or very close to the experimental error value of 0.25%ε, it is not included in the table or used for analysis. The main effects that were deemed most significant are those with the greatest variation from the experimental error value.

For instance, if a main effect is calculated from a factor column to be 1.90%ε±0.25%ε then this is deemed to be significant compared to the overall recovery strain of 3.3%ε. If however, a main effect is calculated to be 0.30%ε±0.25%ε then it is not deemed to be significant compared to the overall recovery strain of 3.3%ε. In this way only the most significant main effects are analysed.

For individual factor analysis the sign of the calculated main effect will also indicate how the factor affects the overall calculated average. A negative main effect indicates that the factor corresponding to that column will increase the average recovery strain if set to the low level (i.e. –ve). A positive main effect will indicate that if the factor is at the high level (i.e. +ve) then the recovery strain will increase. The main effects are described with respect to their sign and in order of significance.

Table 8-1 Main Effects Table of the Recovery Strain at Cycle 1

	Individual Effects						Two-Way Interactions				3-Way
Sample Code	Output Strains e%	HT Heat Treatment	RATE Cycling Rate	s Stress	CW Cold Work	Ti% Alloy Comp.	CW x Ti%	s x CW	HT x Ti%	HT x CW%	HT x CW x Ti
1	4.58	-4.58	-4.58	-4.58	-4.58	-4.58	4.58	4.58	4.58	4.58	-4.58
2	5.01	5.01	-5.01	-5.01	-5.01	-5.01	5.01	5.01	-5.01	-5.01	5.01
3	3.71	-3.71	3.71	-3.71	-3.71	-3.71	3.71	3.71	3.71	3.71	-3.71
4	3.71	3.71	3.71	-3.71	-3.71	-3.71	3.71	3.71	-3.71	-3.71	3.71
5	4.79	-4.79	-4.79	4.79	-4.79	-4.79	4.79	-4.79	4.79	4.79	-4.79
6	4.93	4.93	-4.93	4.93	-4.93	-4.93	4.93	-4.93	-4.93	-4.93	4.93
7	4.26	-4.26	4.26	4.26	-4.26	-4.26	4.26	-4.26	4.26	4.26	-4.26
8	3.53	3.53	3.53	3.53	-3.53	-3.53	3.53	-3.53	-3.53	-3.53	3.53
9	0.41	-0.41	-0.41	-0.41	0.41	-0.41	-0.41	-0.41	0.41	-0.41	0.41
10	1.92	1.92	-1.92	-1.92	1.92	-1.92	-1.92	-1.92	-1.92	1.92	-1.92
11	0.37	-0.37	0.37	-0.37	0.37	-0.37	-0.37	-0.37	0.37	-0.37	0.37
12	1.05	1.05	1.05	-1.05	1.05	-1.05	-1.05	-1.05	-1.05	1.05	-1.05
13	0.98	-0.98	-0.98	0.98	0.98	-0.98	-0.98	0.98	0.98	-0.98	0.98
14	5.22	5.22	-5.22	5.22	5.22	-5.22	-5.22	5.22	-5.22	5.22	-5.22
15	0.94	-0.94	0.94	0.94	0.94	-0.94	-0.94	0.94	0.94	-0.94	0.94
16	3.01	3.01	3.01	3.01	3.01	-3.01	-3.01	3.01	-3.01	3.01	-3.01
17	4.06	-4.06	-4.06	-4.06	-4.06	4.06	-4.06	4.06	-4.06	4.06	4.06
18	4.84	4.84	-4.84	-4.84	-4.84	4.84	-4.84	4.84	4.84	-4.84	-4.84
19	3.66	-3.66	3.66	-3.66	-3.66	3.66	-3.66	3.66	-3.66	3.66	3.66
20	3.67	3.67	3.67	-3.67	-3.67	3.67	-3.67	3.67	3.67	-3.67	-3.67
21	4.49	-4.49	-4.49	4.49	-4.49	4.49	-4.49	-4.49	-4.49	4.49	4.49
22	4.44	4.44	-4.44	4.44	-4.44	4.44	-4.44	-4.44	4.44	-4.44	-4.44
23	3.62	-3.62	3.62	3.62	-3.62	3.62	-3.62	-3.62	-3.62	3.62	3.62
24	4.16	4.16	4.16	4.16	-4.16	4.16	-4.16	-4.16	4.16	-4.16	-4.16
25	2.04	-2.04	-2.04	-2.04	2.04	2.04	2.04	-2.04	-2.04	-2.04	-2.04
26	2.85	2.85	-2.85	-2.85	2.85	2.85	2.85	-2.85	2.85	2.85	2.85
27	1.75	-1.75	1.75	-1.75	1.75	1.75	1.75	-1.75	-1.75	-1.75	-1.75
28	2.83	2.83	2.83	-2.83	2.83	2.83	2.83	-2.83	2.83	2.83	2.83
29	3.83	-3.83	-3.83	3.83	3.83	3.83	3.83	3.83	-3.83	-3.83	-3.83
30	2.53	2.53	-2.53	2.53	2.53	2.53	2.53	2.53	2.53	2.53	2.53
31	4.07	-4.07	4.07	4.07	4.07	4.07	4.07	4.07	-4.07	-4.07	-4.07
32	3.55	3.55	3.55	3.55	3.55	3.55	3.55	3.55	3.55	3.55	3.55
MEAN =	3.28ε%										
	Main Effect:	**0.61**	**-0.56**	**0.74**	**-1.88**	**0.50**	**0.70**	**0.62**	**0.47**	**-0.44**	**-0.62**

Table 8-2 Main Effects Table of the Recovery Strain at Cycle 100

	Individual Effects						Two-Way Interactions				3-Way
Sample Code	Output Strain e%	HT Heat Treatment	RATE Cycling Rate	s Stress	CW Cold Work	Ti% Alloy Comp.	CW x Ti% Interaction	s x CW	HT x Ti%	HT x CW%	HT x CW x Ti
1	4.21	-4.21	-4.21	-4.21	-4.21	-4.21	4.21	4.21	4.21	4.21	-4.21
2	4.59	4.59	-4.59	-4.59	-4.59	-4.59	4.59	4.59	-4.59	-4.59	4.59
3	3.28	-3.28	3.28	-3.28	-3.28	-3.28	3.28	3.28	3.28	3.28	-3.28
4	3.48	3.48	3.48	-3.48	-3.48	-3.48	3.48	3.48	-3.48	-3.48	3.48
5	4.06	-4.06	-4.06	4.06	-4.06	-4.06	4.06	-4.06	4.06	4.06	-4.06
6	4.23	4.23	-4.23	4.23	-4.23	-4.23	4.23	-4.23	-4.23	-4.23	4.23
7	3.36	-3.36	3.36	3.36	-3.36	-3.36	3.36	-3.36	3.36	3.36	-3.36
8	2.93	2.93	2.93	2.93	-2.93	-2.93	2.93	-2.93	-2.93	-2.93	2.93
9	0.39	-0.39	-0.39	-0.39	0.39	-0.39	-0.39	-0.39	0.39	-0.39	0.39
10	3.99	3.99	-3.99	-3.99	3.99	-3.99	-3.99	-3.99	-3.99	3.99	-3.99
11	0.40	-0.40	0.40	-0.40	0.40	-0.40	-0.40	-0.40	0.40	-0.40	0.40
12	1.83	1.83	1.83	-1.83	1.83	-1.83	-1.83	-1.83	-1.83	1.83	-1.83
13	1.43	-1.43	-1.43	1.43	1.43	-1.43	-1.43	1.43	1.43	-1.43	1.43
14	4.24	4.24	-4.24	4.24	4.24	-4.24	-4.24	4.24	-4.24	4.24	-4.24
15	0.84	-0.84	0.84	0.84	0.84	-0.84	-0.84	0.84	0.84	-0.84	0.84
16	3.76	3.76	3.76	3.76	3.76	-3.76	-3.76	3.76	-3.76	3.76	-3.76
17	3.86	-3.86	-3.86	-3.86	-3.86	3.86	-3.86	3.86	-3.86	3.86	3.86
18	4.52	4.52	-4.52	-4.52	-4.52	4.52	-4.52	4.52	4.52	-4.52	-4.52
19	3.85	-3.85	3.85	-3.85	-3.85	3.85	-3.85	3.85	-3.85	3.85	3.85
20	4.06	4.06	4.06	-4.06	-4.06	4.06	-4.06	4.06	4.06	-4.06	-4.06
21	4.09	-4.09	-4.09	4.09	-4.09	4.09	-4.09	-4.09	-4.09	4.09	4.09
22	5.20	5.20	-5.20	5.20	-5.20	5.20	-5.20	-5.20	5.20	-5.20	-5.20
23	3.32	-3.32	3.32	3.32	-3.32	3.32	-3.32	-3.32	-3.32	3.32	3.32
24	4.31	4.31	4.31	4.31	-4.31	4.31	-4.31	-4.31	4.31	-4.31	-4.31
25	2.58	-2.58	-2.58	-2.58	2.58	2.58	2.58	-2.58	-2.58	-2.58	-2.58
26	3.09	3.09	-3.09	-3.09	3.09	3.09	3.09	-3.09	3.09	3.09	3.09
27	1.97	-1.97	1.97	-1.97	1.97	1.97	1.97	-1.97	-1.97	-1.97	-1.97
28	3.33	3.33	3.33	-3.33	3.33	3.33	3.33	-3.33	3.33	3.33	3.33
29	4.14	-4.14	-4.14	4.14	4.14	4.14	4.14	4.14	-4.14	-4.14	-4.14
30	2.70	2.70	-2.70	2.70	2.70	2.70	2.70	2.70	2.70	2.70	2.70
31	3.91	-3.91	3.91	3.91	3.91	3.91	3.91	3.91	-3.91	-3.91	-3.91
32	3.27	3.27	3.27	3.27	3.27	3.27	3.27	3.27	3.27	3.27	3.27
MEAN =	**3.29**										
	Main Effect:	**0.87**	**-0.59**	**0.40**	**-1.34**	**0.70**	**0.32**	**0.44**	**-0.52**	**-0.45**	**-0.85**

8.2.1.1 Recovery Strain at Cycle 1

8.2.1.1.1 Individual Effects

Cold Work Effect – Main Effect **1.88%** e

It was found that cold work was the most significant factor affecting strain recovery in these alloys. The main effect of low cold work was to increase recoverable strain.

Applied Stress – Main Effect **0.74%** e .

High stresses (160MPa) increased recovery strain.

Heat Treatment – Main Effect **0.61%** e

The high heat treatment temperature (500°C) increased recovery strain.

Cycling Rate – Main Effect **0.56%** e

Low cycling rates increased strain recovery

Alloy Composition – Main Effect **0.50%** e

The Ti-49.88at%Ni (i.e. titanium rich) alloys resulted in greater recoverable strain than the nickel rich alloys.

8.2.1.1.2 Factorial Interaction Effects

Often, because of interactions between factors, the individual effects should not be interpreted separately. Factorial experimental design allows interaction effects between variables to be analysed as well as their solo effects. Indeed to only consider the individual effects may result in the wrong conclusions being drawn from the data and really misses the whole purpose of this experimental design. A very useful way of representing variable interactions is to represent the

factor contrasts in a 2x2 matrix. The following interactions are described using this technique.

Two Factor Interactions : -

Percentage Cold Work and Alloy Composition – Main Effect **0.70%**e

The recovery strain in the high cold work alloys was more sensitive to alloy composition, **Table 8-3**, i.e. the Ti rich alloy resulted in 1.19%ε more recoverable strain in the 30% cold worked alloys than the Ni rich alloys.

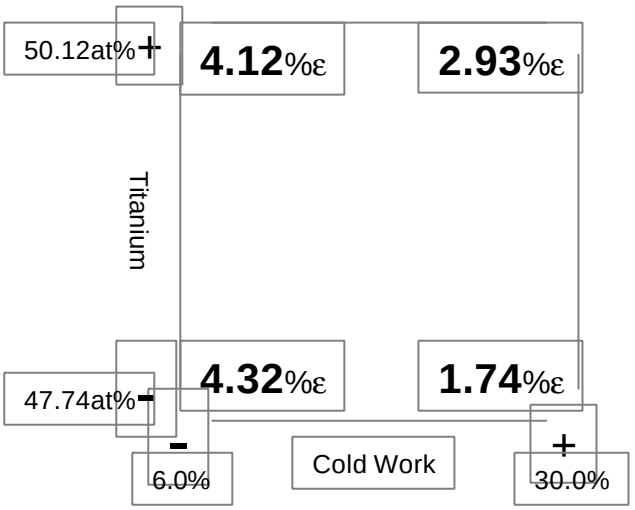

Table 8-3 The Cold Work - Alloy Composition Interaction on Strain Recovery at Cycle 1

Percentage Cold Work and Applied Stress – Main Effect **0.62%**e

The recovery strain in the high cold work alloys was more sensitive to applied stress, **Table 8-4**. The 165MPa applied stress resulted in a greater increase of recoverable strain in the 30% cold worked alloys than those cycled at 85MPa.

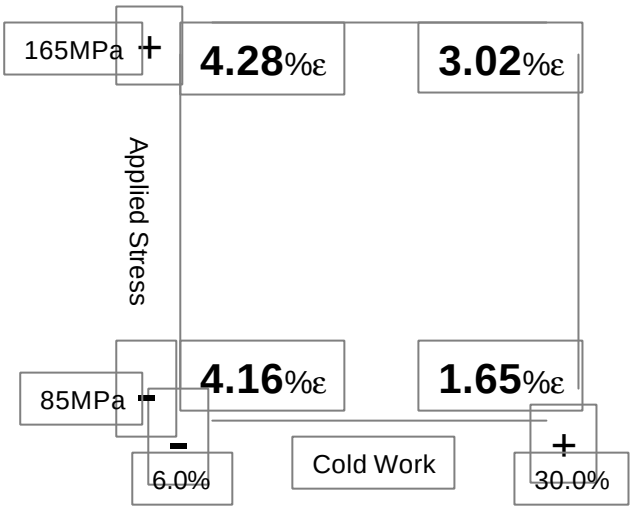

Table 8-4 The Percentage Cold Work - Applied Stress Interaction on Strain Recovery at Cycle 1

Heat Treatment and Percentage Cold Work – Main Effect **0.62%** e

The alloys with high cold work appeared to be more sensitive to heat treatment temperature than the alloys with low cold work, **Table 8-5**.

Heat treating the 30% cold work alloys at 500°C rather than 400°C resulted in an increase of average recovery strain. Heat treating the 6% cold work alloys at the higher temperature resulted in no significant increase of average recovery strain.

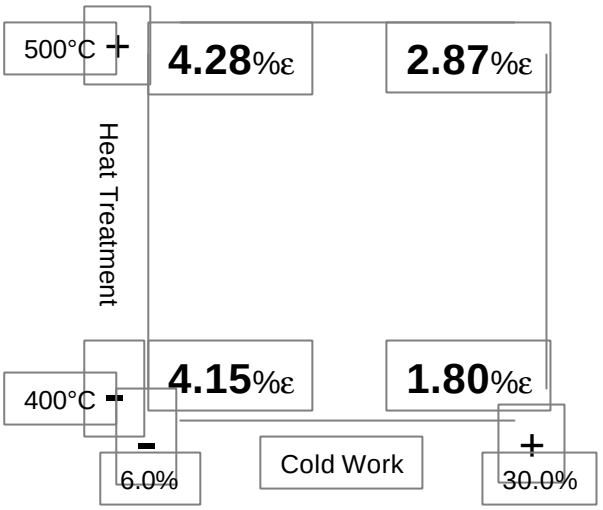

Table 8-5 The Heat Treatment - Percentage Cold Work Interaction on Strain Recovery at Cycle 1

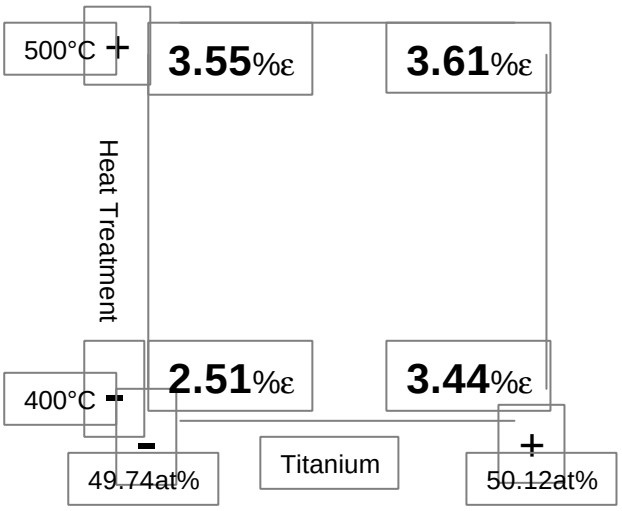

Table 8-6 The Heat Treatment - Alloy Composition Interaction on Strain Recovery at Cycle 1

Heat Treatment and Alloy Composition – Main Effect **0.44%** e

The recovery strain of the low titanium content alloy (SMC) was more sensitive to the heat treatment temperature than the recovery strain of the high titanium alloy (SMA), **Table 8-6.**

Three Factor Interactions

Percentage Cold Work – Heat Treatment – Alloy Composition

Main Effect - **0.62%**ε

Three factor interactions can be illustrated by the use of a 2x2x2 matrix. **Table 8-7** shows how the Ni rich, alloys with 30% cold work, heat treated at 400°C resulted in an average recovery strain of just 0.68%ε. However the Ti rich alloys with 6% cold work, heat treated at 500°C resulted in a recovery strain of 4.28%ε.

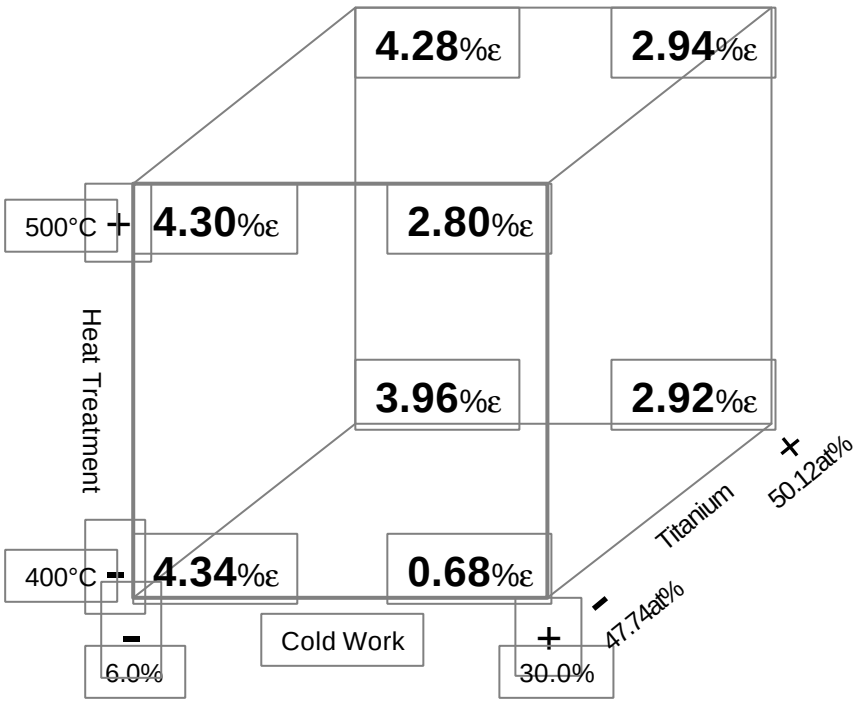

Table 8-7 The Applied Stress - Percentage Cold Work - Alloy Composition Interaction on Strain Recovery at Cycle 1

8.2.1.2 Strain Recovery at Cycle 100

8.2.1.2.1 Individual Factor Effects at Cycle 100

Cold Work Effect - It was found that cold work was the most significant factor affecting strain recovery in these alloys. The effect of low cold work was to increase the average recoverable strain by **1.3%**ε. This is considerably lower than the main effect at cycle 1, i.e. 1.88%ε.

Heat Treatment - The high heat treatment temperature (500°C) resulted in a main effect of increasing the recovery strain by **0.87%**ε, This is an increase from the cycle 1 main effect, 0.61%ε.

Alloy Composition - The Ti-49.88at%Ni (i.e. titanium rich) alloys resulted in a main effect of **0.70%**ε more recoverable strain than the nickel rich alloys. This is an increase from the cycle 1 main effect, 0.50%ε.

Cycling Rate - Low cycling rates were found to have a main effect of increasing recovery strain by **0.59%**ε. This is very similar to the main effect at cycle 1, 0.56%ε.

Applied Stress - High stresses (160MPa) produced a main effect of increasing recovery strain by **0.40%**ε. This is a decrease from the cycle 1 main effect, 0.74%ε.

8.2.1.2.2 Factorial Interaction Effects at Cycle 100

Two Factor Interactions : -

Heat Treatment and Alloy Composition – Main Effect **0.52%**ε

This is very similar to that calculated at cycle 1, i.e. 0.44%ε. Analysing the data in the geometric **Table 8-8,** it can be said that, just as at cycle 1, the recovery strain of the low titanium content alloy (SMC) was more sensitive to the heat treatment temperature than the recovery strain of the high titanium alloy (SMA).

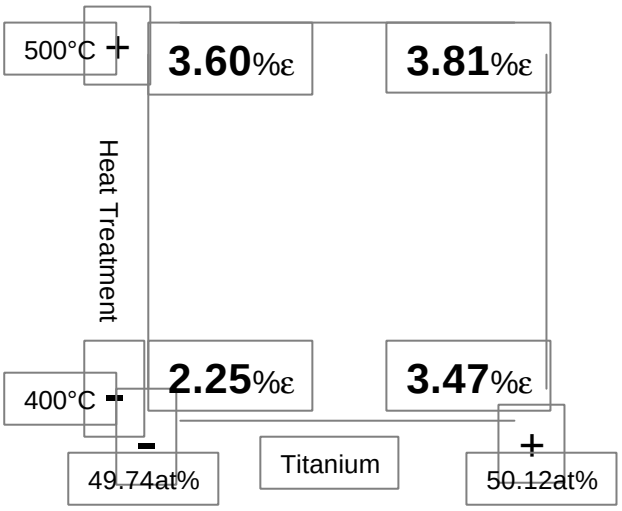

Table 8-8 The Heat Treatment – Alloy Composition Interaction on Strain Recovery at Cycle 100

Heat Treatment and Percentage Cold Work – Main Effect **0.45%**ε

This is shown in **Table 8-9**. Again this is very similar to that found at cycle 1, i.e. 0.47%ε.

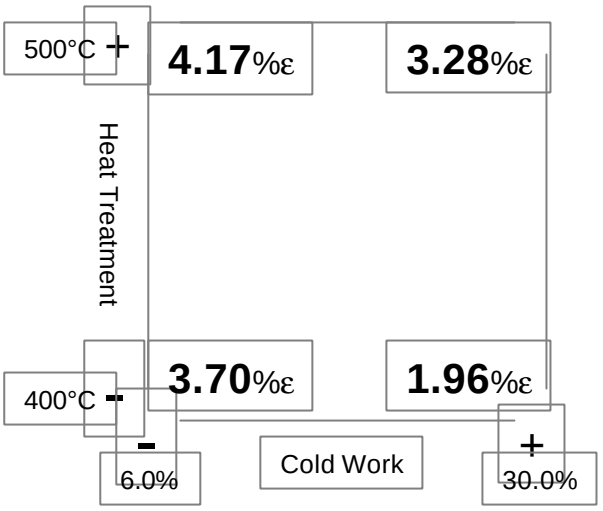

Table 8-9 The Heat Treatment - Percentage Cold Work Interaction on Strain Recovery at Cycle 100

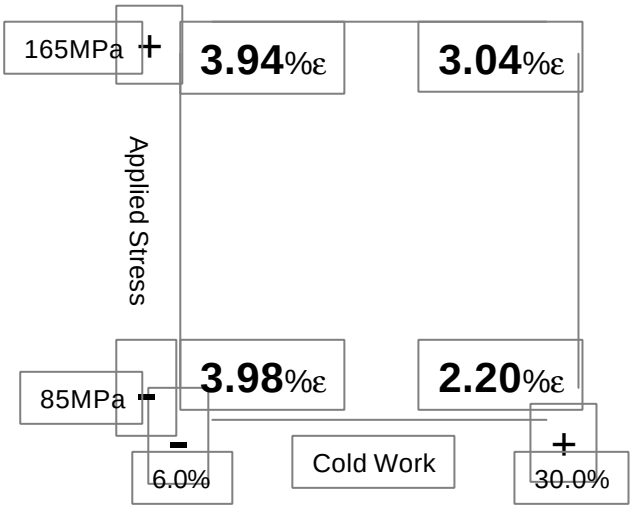

Table 8-10 The Percentage Cold Work - Applied Stress Interaction on Strain Recovery at Cycle 100

Percentage Cold Work and Applied Stress - Main Effect **0.44%**e

The main effect compares to 0.62%ε at cycle 1. Again, the recovery strain in the high cold work alloys was more sensitive to applied stress, **Table 8-10**.

Percentage Cold Work and Alloy Composition – Main Effect **0.32%**e

At cycle 1, this interaction was the most significant (0.70%ε), at cycle 100 it is now one of the least significant. This is explained by comparing **Table 8-3** with **Table 8-11**. The recovery strains in **Table 8-11** are less dependant upon the cold work level and composition. Both the high cold worked alloys have tended to increase recoverable strain whilst the low cold work, Ni rich alloy, has tended to decrease recoverable strain. These effects have tended towards an equalisation of the recoverable strains across the table and reduced the

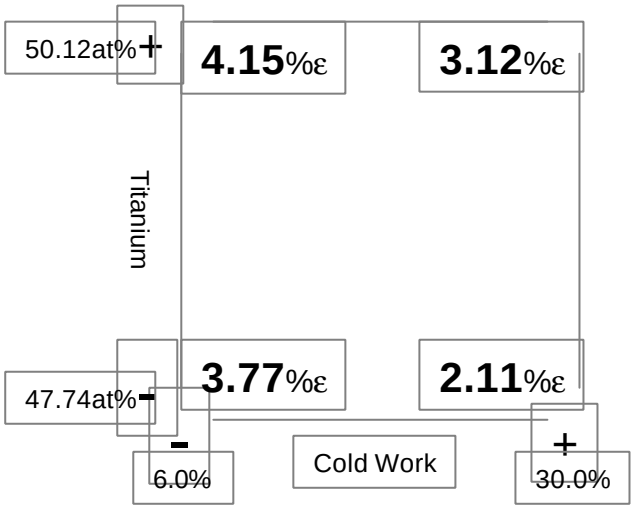

Table 8-11 The Cold Work - Alloy Composition Interaction on Strain Recovery at Cycle 100

interaction effect.

Three Factor Interactions

Percentage Cold Work – Heat Treatment – Alloy Composition

Main Effect **0.85%**e

This compares to a main effect of **0.62%**ε at cycle 1.

Table 8-12 shows how the Ni rich, alloys with 30% cold work, heat treated at 400°C resulted in an average recovery strain of just 0.77%ε. However the Ti rich alloys with 6% cold work, heat treated at 500°C resulted in a recovery strain of 4.52%ε.

It is interesting to compare this three factor interaction shown in **Table 8-12** with the same interaction at cycle 1, shown in **Table 8-7**. Comparing cold work levels in the two tables, it can be seen that over 100 thermal cycles, the recovery strain tended to increase in the high cold work alloys. However, in the low cold work alloys, the strain recovery tended to decrease over 100 cycles.

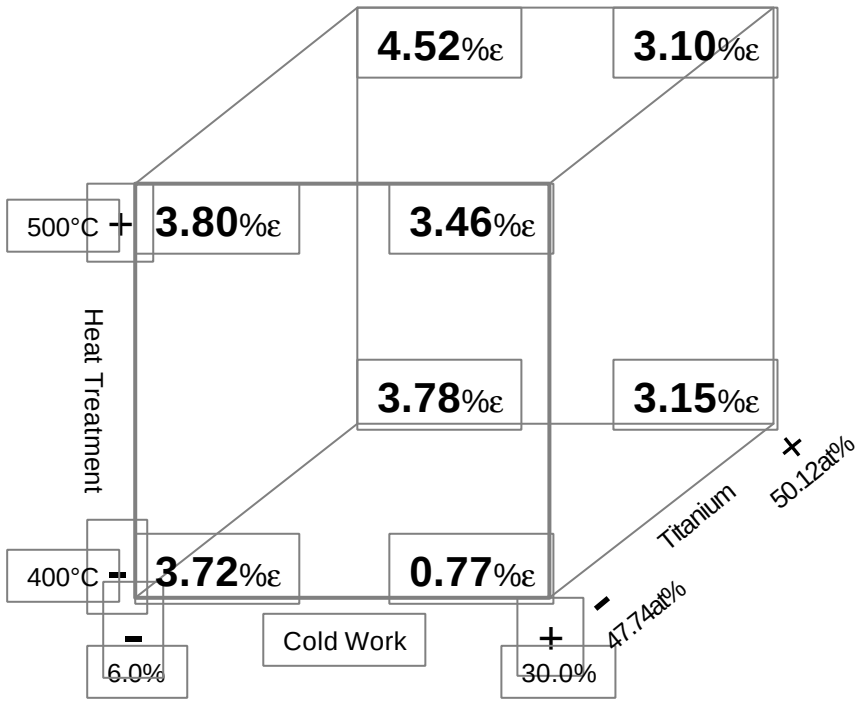

Table 8-12 The Applied Stress - Percentage Cold Work - Alloy Composition Interaction on Strain Recovery at Cycle 100

8.2.1.3 Summary of Variables Effect on Recovery Strain and Recovery Strain Degradation

Strain recovery was found to be particularly dependent upon percentage cold work. Lower cold work resulted in greater strain recovery. However during thermal cycling, the main effect of cold work reduced considerably. This was due to the average recoverable strain over 100 cycles, gradually increasing in the 30% cold work alloys and gradually decreasing in the 6% cold work alloys.

Similarly, although applied stress level was the second most important individual main effect at cycle 1, (the higher stress resulting in considerably greater recovery strain), by cycle 100 it was the least important. This is best explained by the cold work/applied stress, interaction effect. Comparing **Table 8-4** and **Table 8-10** it can be seen that over 100 cycles the recovery strain increases considerably in the 30% cold worked alloys operating against the 85MPa applied stress. Therefore, the differential between the average recovery strain of the 165MPa samples and the average recovery strain of the 85MPa samples is reduced.

By cycle 100 the main effect of heat treatment increases such that it is the second most important variable affecting strain recovery. That is, the average recovery strain in the alloys heat treated at 500°C gradually increased with the number of cycles whilst that of the alloys heat treated at 400°C gradually decreased. Again, this can be more fully explained by considering one of the interaction main effects. Comparing the cold work/heat treatment interaction at cycle 1 and 100, shown by **Table 8-5** and **Table 8-9** respectively, it can be seen that the 6% cold work samples heat treated at 400°C, significantly decreased recovery strain. The 30% cold work alloys heat treated at 500°C however, significantly increased recovery strain.

The main effect of alloy composition also increased with thermal cycling. The average recovery strain of the high titanium alloys increased with thermal cycles whilst that of the Ni rich alloys decreased. It is interesting to analyse the cold work/alloy composition when considering this effect. Comparing **Table 8-3** and **Table 8-11** it can be seen how the recovery strain changed with thermal cycling for these sample groups.

The most significant changes to strain recovery occurred in the Ni rich alloys. There are two contradictory effects occurring in the Ni rich alloys, i.e. the 6% cold work samples gradually decreased recovery strain whilst the 30% cold work alloys gradually increased. In the Ti rich alloys the recovery strain of the 6% samples stayed constant with cycling whilst the 30% cold work alloys increased.
The main effect of cycling rate was not found to change with cycling. This suggests that although the slower rate resulted in greater strain recovery, the cycling rate had no effect on cyclic stability.
Although these results indicate how it may be possible to achieve the greatest recovery strains and most stable recovery strains there is another part to the story which is, the parent phase and martensite phase shape stability. The next section analyses the main effects of the same variables on the residual permanent strains in both phases after 500 thermal cycles.

8.2.2 Residual Permanent Strains

8.2.3 Martensite Residual Permanent Strain

The residual strain in the martensite shape was measured over 500 thermal cycles. Due to large residual strains in some alloys, the length at cycle 500 could not be measured, i.e. the length of the wire had extended so much that it was out of the range of the laser sensor. For an alloy wire to extend beyond the range of the laser a residual strain of 50%ε is necessary. Therefore to facilitate factorial analysis at cycle 500, the alloys that had extended beyond this were designated with a residual strain of 50%ε.
The martensite and parent phase residual strains are defined in **Figure 8-3**.

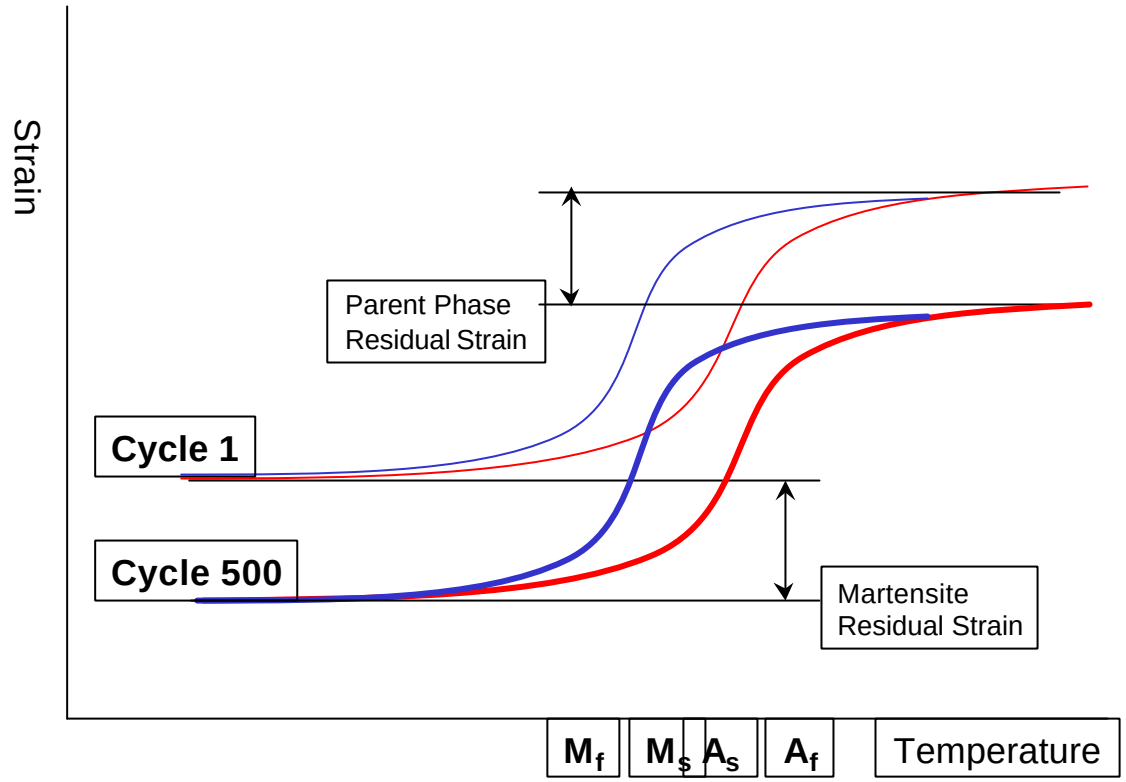

Figure 8-3 Residual Permanent Martensite and Residual Permanent Parent Phase Strains

Martensite residual strain was calculated from:

$$\frac{\textbf{permanent change in length of wire in martensite phase}}{\textbf{starting length of wire in martensite phase}} \times \textbf{100}$$

The mean average of all the residual permanent martensite strains at cycle 500 was: **10.71%** e

The individual residual strains in the martensite phase are plotted in sets of eight on **Graph 8-15** to **Graph 8-18**. As before, these graphs are plotted for different cold work levels and alloy types. The curve colours correspond to the same heat treatment, applied stress and cycling rate.

The graphs show that generally, the residual permanent strain of the martensite shape tended to increase with the number of thermal cycles. The rate of permanent strain degradation tended to be greatest during the early cycles.

The amount of residual strain was greatest in the Ti rich alloys shown in **Graph 8-17** to **Graph 8-18**. Samples: 18, 21, 22, 24 and 32 in particular, showed residual permanent strains so great, that they drift beyond the measuring range of the laser.

The Ni rich alloys of **Graph 8-15** to **Graph 8-16**, show that some of the samples were in fact very stable. Samples: 9, 11 and 15 resulted in very little permanent strain.

The individual and interactive factorial analysis that follows, may be used to help explain the origin of the residual strain effects shown in these graphs.

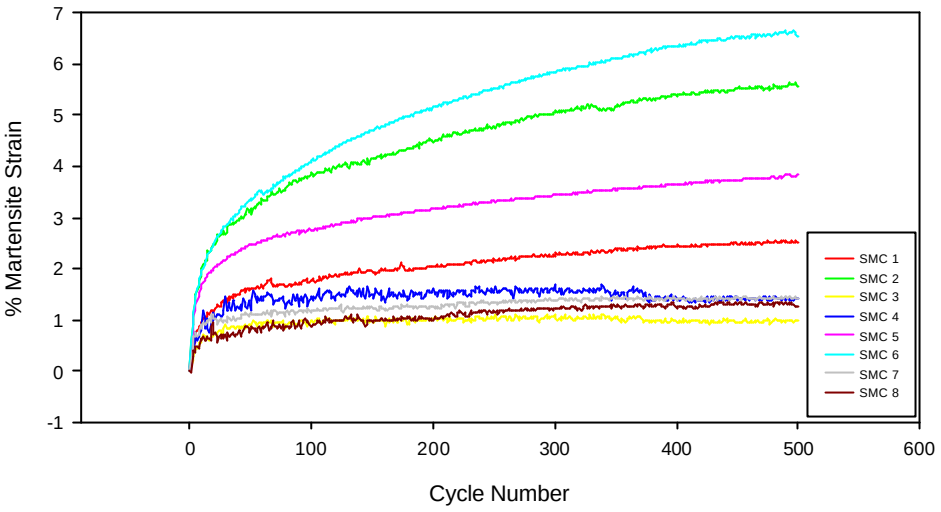

Graph 8-15 Residual Strain in the Martensite Phase in the SMC6 (Ti-50.26at%Ni, 6% Cold Work) Alloy During 500 Thermal Cycles

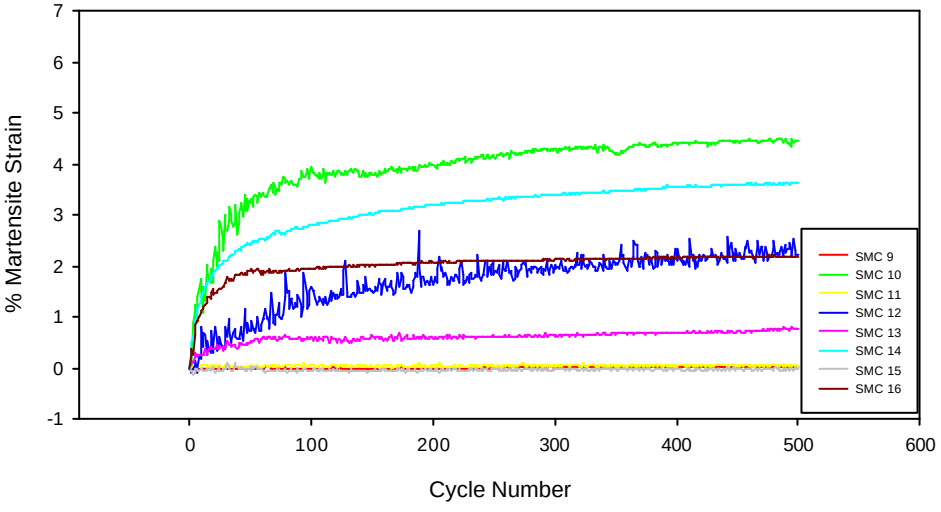

Graph 8-16 Residual Strain in the Martensite Phase in the SMC30 (Ti-50.26at%Ni, 30% Cold Work) Alloy During 500 Thermal Cycles

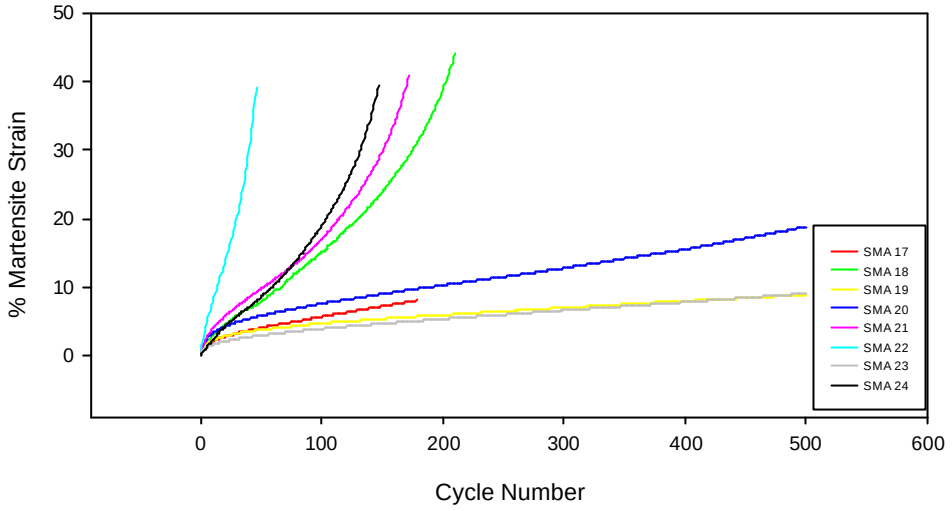

Graph 8-17 Residual Strain in the Martensite Phase in the SMA6 (Ti-49.88at%Ni, 6% Cold Work) Alloy During 500 Thermal Cycles

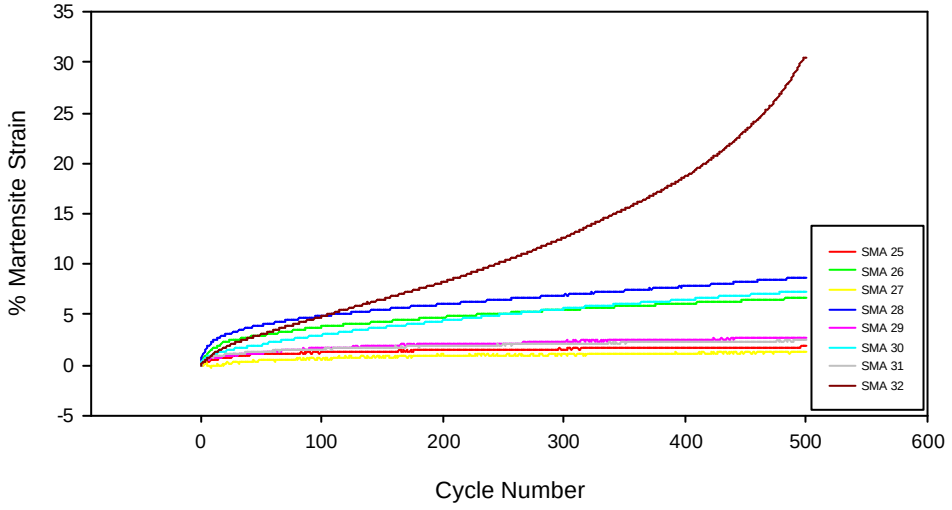

Graph 8-18 Residual Strain in the Martensite Phase in the SMA30 (Ti-49.88at%Ni, 30% Cold Work) Alloy During 500 Thermal Cycles

The factorial analysis was carried out in the same way as that for the recovery strains in the previous section.

Table 8-13 shows the factor levels and main effect calculations of the residual permanent martensite strain at cycle 500. Again, for ease of comprehension and conciseness, only the most significant interaction effects are included in the tables.

The significance of the main effects was calculated by comparison with an estimated standard error of ±3.25%ε. As before, the error was calculated from higher order interaction effects.

If any calculated main effect was less than, or very close to the experimental error value of ±3.25%ε, then it was not included in the table or used for analysis.

Again, the main effects are described in order of this significance.

Table 8-13 Main Effects Table of Residual Strain in the Martensite Phase

	Individual Effects						Two-Way Interactions				Three-Way	
Sample Code	**Residual Strain e%**	**HT Heat Treatment**	**RATE Cycling Rate**	**s Stress**	**CW Cold Work**	**Ti% Alloy Comp'**	**CW x Ti%**	**HT x Ti%**	**CW x Rate**	**s x Ti%**	**HT x s x Rate**	**Rate x CW x Ti%**
1	2.53	-2.53	-2.53	-2.53	-2.53	-2.53	2.53	2.53	2.53	2.53	-2.53	-2.53
2	5.57	5.57	-5.57	-5.57	-5.57	-5.57	5.57	-5.57	5.57	5.57	5.57	-5.57
3	0.98	-0.98	0.98	-0.98	-0.98	-0.98	0.98	0.98	-0.98	0.98	0.98	0.98
4	1.43	1.43	1.43	-1.43	-1.43	-1.43	1.43	-1.43	-1.43	1.43	-1.43	1.43
5	3.83	-3.83	-3.83	3.83	-3.83	-3.83	3.83	3.83	3.83	-3.83	-3.83	-3.83
6	6.56	6.56	-6.56	6.56	-6.56	-6.56	6.56	-6.56	6.56	-6.56	6.56	-6.56
7	1.41	-1.41	1.41	1.41	-1.41	-1.41	1.41	1.41	-1.41	-1.41	1.41	1.41
8	1.27	1.27	1.27	1.27	-1.27	-1.27	1.27	-1.27	-1.27	-1.27	-1.27	1.27
9	0.02	-0.02	-0.02	-0.02	0.02	-0.02	-0.02	0.02	-0.02	0.02	0.02	0.02
10	4.46	4.46	-4.46	-4.46	4.46	-4.46	-4.46	-4.46	-4.46	4.46	-4.46	4.46
11	0.03	-0.03	0.03	-0.03	0.03	-0.03	-0.03	0.03	0.03	0.03	-0.03	-0.03
12	2.22	2.22	2.22	-2.22	2.22	-2.22	-2.22	-2.22	2.22	2.22	2.22	-2.22
13	0.76	-0.76	-0.76	0.76	0.76	-0.76	-0.76	0.76	-0.76	-0.76	0.76	0.76
14	3.63	3.63	-3.63	3.63	3.63	-3.63	-3.63	-3.63	-3.63	-3.63	-3.63	3.63
15	-0.03	0.03	-0.03	-0.03	-0.03	0.03	0.03	-0.03	-0.03	0.03	0.03	0.03
16	2.17	2.17	2.17	2.17	2.17	-2.17	-2.17	-2.17	2.17	-2.17	2.17	-2.17
17	8.07	-8.07	-8.07	-8.07	-8.07	8.07	-8.07	-8.07	8.07	-8.07	-8.07	8.07
18	50.00	50.00	-50.00	-50.00	-50.00	50.00	-50.00	50.00	50.00	-50.00	50.00	50.00
19	8.86	-8.86	8.86	-8.86	-8.86	8.86	-8.86	-8.86	-8.86	-8.86	8.86	-8.86
20	18.75	18.75	18.75	-18.75	-18.75	18.75	-18.75	18.75	-18.75	-18.75	-18.75	-18.75
21	50.00	-50.00	-50.00	50.00	-50.00	50.00	-50.00	-50.00	50.00	50.00	-50.00	50.00
22	50.00	50.00	-50.00	50.00	-50.00	50.00	-50.00	50.00	50.00	50.00	50.00	50.00
23	9.07	-9.07	9.07	9.07	-9.07	9.07	-9.07	-9.07	-9.07	9.07	9.07	-9.07
24	50.00	50.00	50.00	50.00	-50.00	50.00	-50.00	50.00	-50.00	50.00	-50.00	-50.00
25	1.81	-1.81	-1.81	-1.81	1.81	1.81	1.81	-1.81	-1.81	-1.81	1.81	-1.81
26	6.62	6.62	-6.62	-6.62	6.62	6.62	6.62	6.62	-6.62	-6.62	-6.62	-6.62
27	1.26	-1.26	1.26	-1.26	1.26	1.26	1.26	-1.26	1.26	-1.26	-1.26	1.26
28	8.63	8.63	8.63	-8.63	8.63	8.63	8.63	8.63	8.63	-8.63	8.63	8.63
29	2.69	-2.69	-2.69	2.69	2.69	2.69	2.69	-2.69	-2.69	2.69	2.69	-2.69
30	7.30	7.30	-7.30	7.30	7.30	7.30	7.30	7.30	-7.30	7.30	-7.30	-7.30
31	2.39	-2.39	2.39	2.39	2.39	2.39	2.39	-2.39	2.39	2.39	-2.39	2.39
32	30.40	30.40	30.40	30.40	30.40	30.40	30.40	30.40	30.40	30.40	30.40	30.40
MEAN =	**10.71**											
	Main Effect:	**9.71**	**-4.06**	**6.26**	**-12.12**	**16.81**	**-10.83**	**7.49**	**6.54**	**5.97**	**5.94**	**5.42**

8.2.3.1 Individual Factor Effects

Alloy Composition Effect – Main Effect **16.81%**e

The main effect of a titanium rich alloy was to increase permanent martensite strain. Alloy composition was found to be the most significant main effect for permanent strain in the martensite phase. This is confirmed by the much greater strains observed in the Ti rich alloys of **Graph 8-17** to **Graph 8-18**.

Cold Work – Main Effect **12.12%**e

Low prior cold work (6.0%) increased permanent martensite strain.

Heat Treatment – Main Effect **9.71%**e

High heat treatment temperatures increased permanent martensite strain.

Applied Stress – Main Effect **6.26%**e

The high stress (165MPa) increased the permanent strain in the martensite phase.

Cycling Rate – Main Effect **4.06%**e

Low cycling rates increased the permanent strain in the martensite phase.

8.2.3.2 Factorial Interaction Effects

Only interactions of significance will be discussed. Interaction effects less than, or very close to the estimated error of 3.25%ε are not presented.

Two Factor Interactions :-

Cold Work and Alloy Composition – Main Effect **10.83%**e

Analysing the data in **Table 8-14** shows how the effect of this interaction occurred. It can be said that the residual strain in the martensite phase is very much more

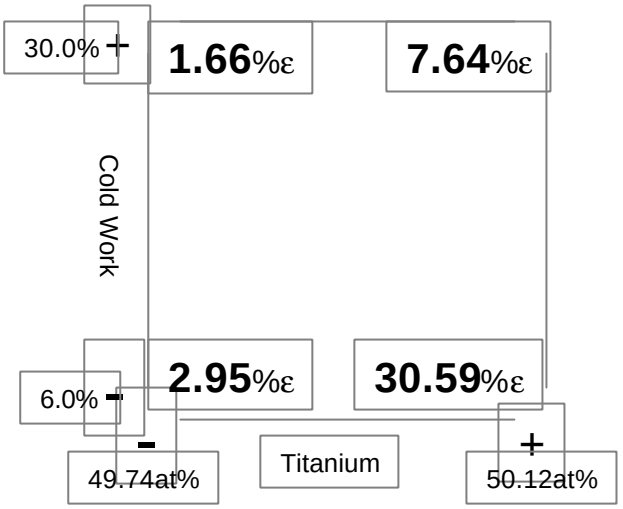

Table 8-14 The Cold Work - Alloy Composition Interaction at Cycle 500

sensitive to alloy composition in the low cold work (6%) condition.

Heat Treatment and Alloy Composition - Main Effect **7.49%** e

Table 8-15 shows how the residual permanent strain of the martensite phase in the Ti rich alloys, heat treated at 500°C, was approximately 23 times that of the high Ni content alloys heat treated at 400°C.

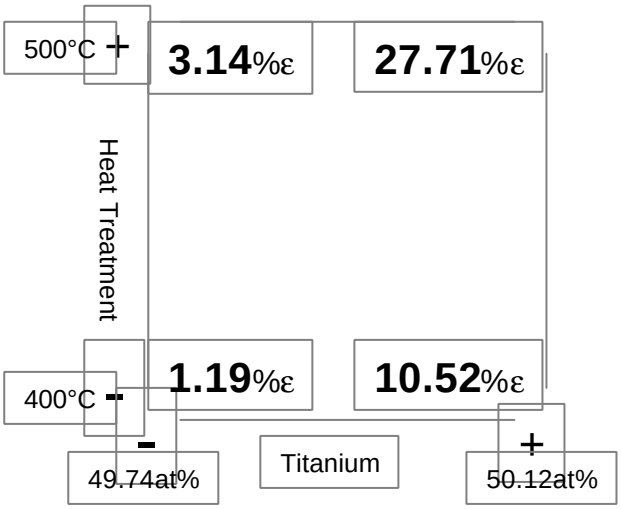

Table 8-15 The Heat Treatment – Alloy Composition Interaction at Cycle 500

Cold Work and Cycling Rate Interaction – Main Effect **6.54%**e

At low cycling rates (170 s/Cycle) the alloys were more sensitive to the degree of prior cold work, this is shown in **Table 8-16**.

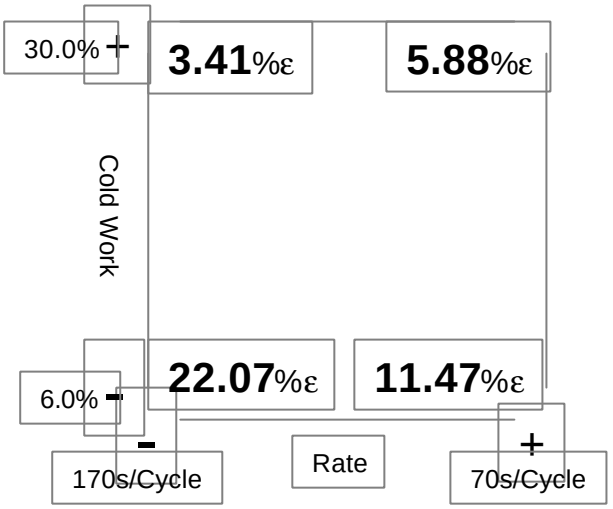

Table 8-16 The Cold Work - Cycling Rate Interaction at Cycle 500

Alloy Composition and Applied Stress – Main Effect **5.97%**e

It is seen from **Table 8-17** that the Ti rich alloys were particularly sensitive to the level of applied stress.

It can also be said that the residual strain in the martensite phase of the Ni rich alloys was not significantly sensitive to applied stress levels.

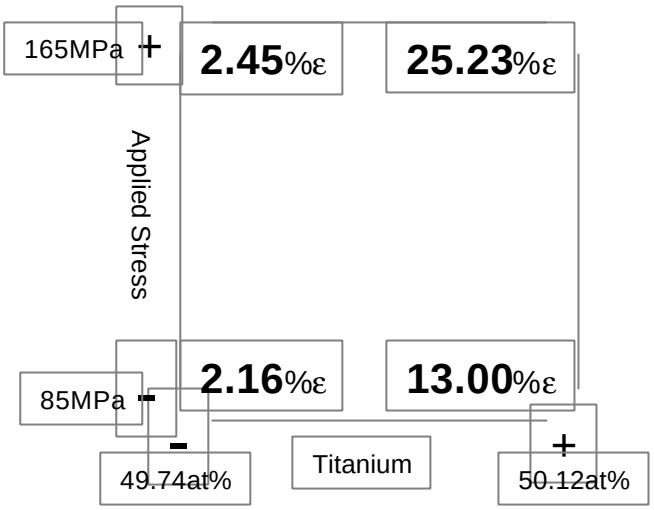

Table 8-17 The Applied Stress - Alloy Composition Interaction at Cycle 500

Three Factor Interactions

Heat Treatment – Applied Stress – Cycling Rate

Main Effect **5.94%**ε

This is illustrated by the 2x2x2 matrix shown in **Table 8-18**.

Perhaps the most interesting effect observed in **Table 8-18** is the amount of residual strain in the martensite phase of the alloys heat treated at the low temperature (400°C) and cycled at a slow rate against 165MPa. The difference between this strain (14.32%ε) and any of the others in the low heat treatment condition was considerable.

Similarly, in the high heat treatment condition (500°), the residual strain in the martensite phase of the alloys cycled at a high rate against an applied stress of 85MPa was considerably lower than any of the other alloys in the high heat treatment condition.

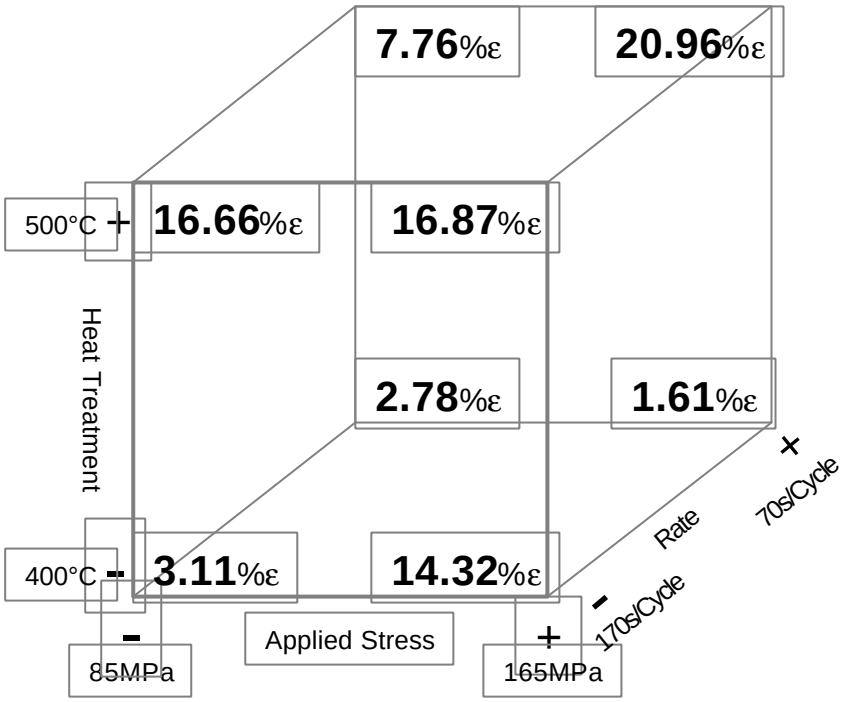

Table 8-18 The Heat Treatment - Applied Stress - Cycling Rate Interaction on Residual Permanent Strain in the Martensite Phase at Cycle 500

Alloy Composition – Cold Work – Cycling Rate

Main Effect **5.42%** e

Table 8-19 shows this graphically. Generally it can be seen that the high cold worked alloys were most resistant to martensite residual strain as were the Ni rich alloys.

In addition the cycling rate was also shown to have an effect. The higher cycling rate appeared to result in less residual martensite strain. The only anomaly to this finding was the Ti rich, high cold work alloy. In this alloy the higher cycling rate appeared to result in more residual strain.

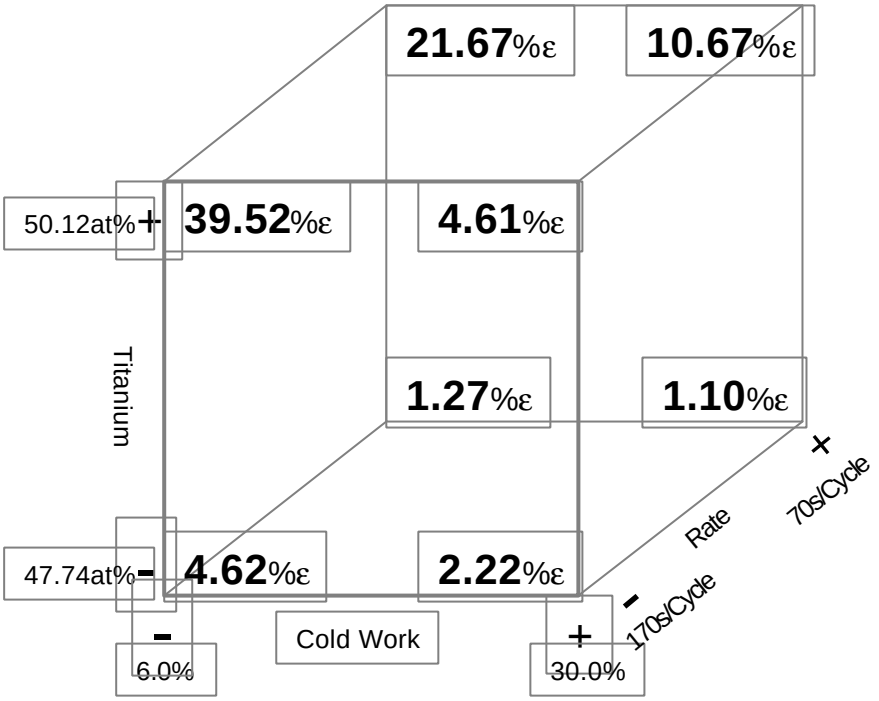

Table 8-19 The Alloy Composition - Cold Work - Cycling Rate Interaction on % Residual Strain in the Martensite Phase at Cycle 500

8.2.3.3 Summary of Variables Effect on Residual Permanent Strain in the Martensite Phase

The results and main effects analysis showed that residual permanent strain in the martensite phase was particularly sensitive to alloy composition and cold work percentage. The titanium rich alloys with just 6% cold work and heat treated at high temperatures resulted in the greatest permanent strains.

Higher stresses also resulted in greater permanent strains although this effect was shown to be particularly sensitive to alloy composition. **Table 8-17** showed that the permanent strain of the martensite phase in the Ti rich alloys was considerably greater at 165MPa than at 85MPa. The Ni rich alloys did not appear to be particularly sensitive to applied stress level.

Slower cycling rates appeared to result in increased permanent martensite strain. This was particularly so in the 6% cold worked alloys as shown in **Table 8-16**.

According to these results, the alloys most resistant to residual permanent strains in the martensite phase were those that were Ni rich, had high cold work and were heat treated at low temperatures. In these alloys, the level of applied stress and cycling rate were not so important in achieving an actuator resistant to permanent strains.

8.2.4 Parent Phase Residual Permanent Strain

The residual strain in the parent phase shape was measured over 500 thermal cycles. As in the previous section, due to large residual strains in some alloys, the length at cycle 500 could not be measured. To facilitate factorial analysis at cycle 500, the alloys which had extended out of range were designated a residual strain of 50%ε.

Parent phase residual permanent strain was calculated from:

$$\frac{\textbf{permanent change in length of wire in parent phase}}{\textbf{starting length of wire in parent phase}} \times \textbf{100}$$

The parent phase residual strain was defined graphically in **Figure 8-3**. The overall mean average of the residual permanent strain in the parent phase at cycle 500 was: **10.69%e.**

It was found that the results were generally very similar to those of the martensite residual strain. This is shown by **Graph 8-19** to **Graph 8-22**. The same observations as those made for the martensite strain may be made.

The graphs show that generally, the residual permanent strain of the martensite shape increased with the number of thermal cycles. The rate of permanent strain degradation tended to be greatest during the early cycles.

The amount of residual strain was greatest in the Ti rich alloys shown in **Graph 8-21** to **Graph 8-22**. Samples: 18, 21, 22, 24 and 32 in particular showed residual permanent strains so great, that they drifted beyond the measuring range of the laser. The Ni rich alloys shown in **Graph 8-19** to **Graph 8-20** showed that some of the samples are in fact very stable. Samples: 9, 11 and 15 showed very little permanent strain.

Although the results and main effects of the martensite and parent phase permanent strains were very similar, there are some notable exceptions and the parent phase analysis is worth presenting separately.

The individual and interactive factorial analysis that follows after the graphs, is used to help explain the origin of the residual strain effects.

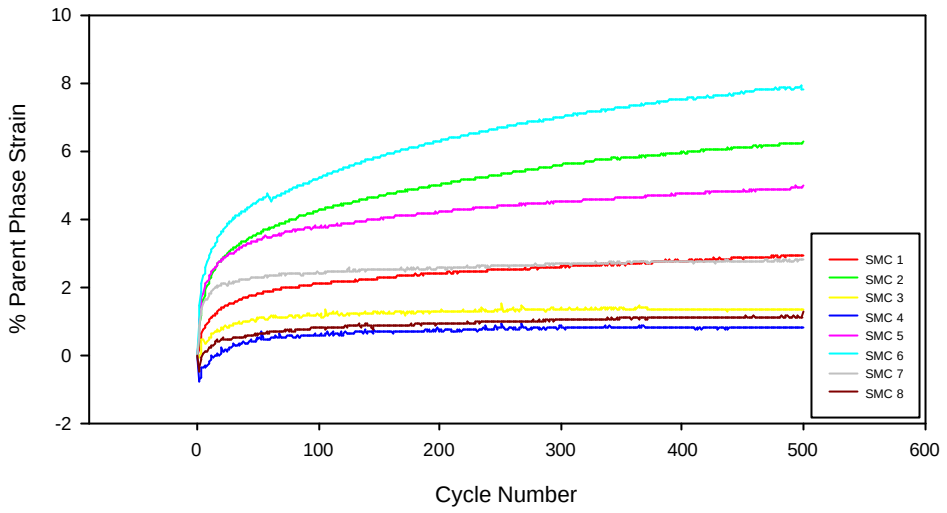

Graph 8-19 Residual Strain of the Parent Phase in the SMC6 (Ti-50.26at%Ni, 6% Cold Work) Alloy During 500 Thermal Cycles

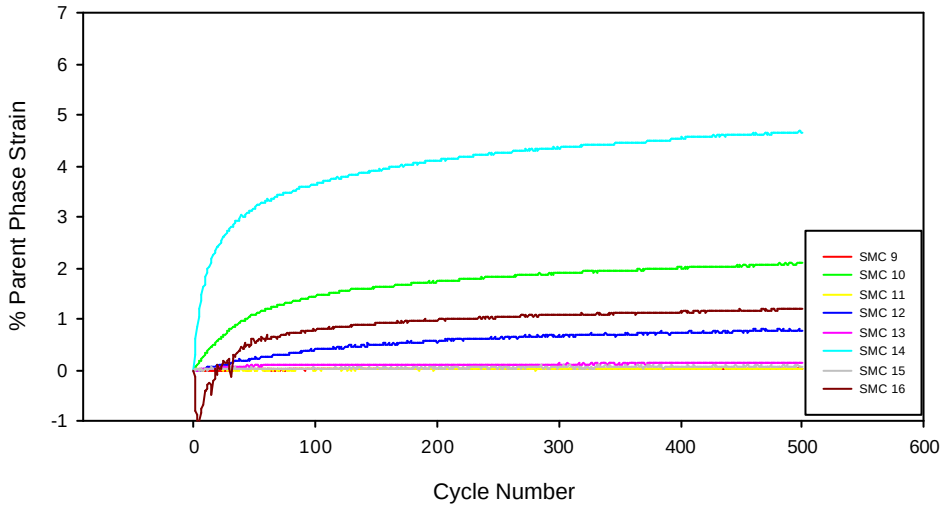

Graph 8-20 Residual Strain of the Parent Phase in the SMC30 (Ti-50.26at%Ni, 30% Cold Work) Alloy During 500 Thermal Cycles

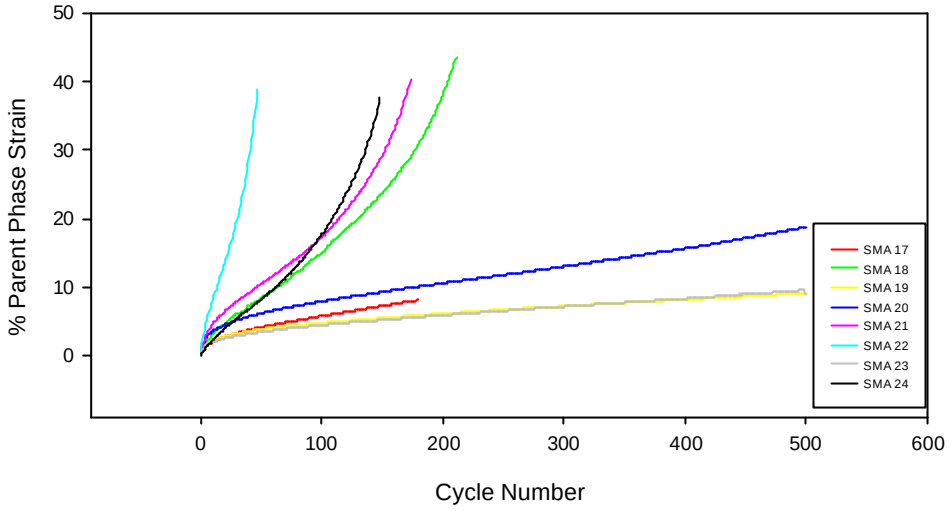

Graph 8-21 Residual Strain of the Parent Phase in the SMA6 (Ti-49.88at%Ni, 6% Cold Work) Alloy During 500 Thermal Cycles

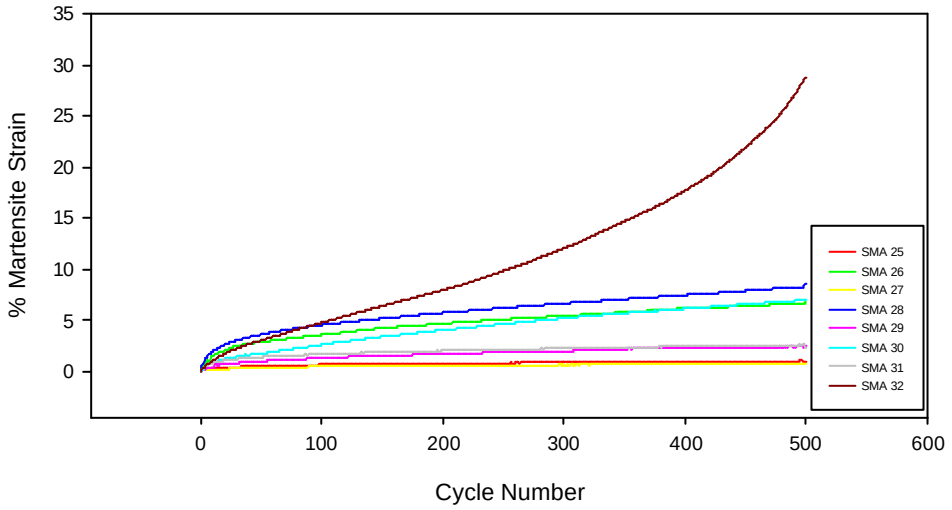

Graph 8-22 Residual Strain of the Parent Phase in the SMA30 (Ti-49.88at%Ni, 30% Cold Work) Alloy During 500 Thermal Cycles

The factorial analysis was carried out in the same way as that for the martensite permanent strains

Table 8-20 shows the factor levels and main effect calculations of the residual permanent parent phase strain at cycle 500. Again, for ease of comprehension and conciseness, only the most significant interaction effects are included in the tables.

The significance of the main effects was calculated by comparison with an estimated standard error of ±3.60%ε. As before, the error was calculated from higher order interaction effects.

If any calculated main effect was less than or very close to the experimental error value of ±3.60%ε, then it was not included in the table or used for analysis. Again, the main effects are described in order of this significance.

Table 8-20 Main Effects Table of Residual Strain in the Parent Phase

	Individual Effects						Two-Way Interactions				Three-Way	
Sample Code	Residual Strain %	HT Heat Treatment	RATE Cycling Rate	s Stress	CW Cold Work	Ti% Alloy Comp'	CW x Ti%	HT x Ti%	CW x Rate	s x Ti%	HT x s x Rate	Rate x CW x Ti%
1	2.69	-2.69	-2.69	-2.69	-2.69	-2.69	2.69	2.69	2.69	2.69	-2.69	-2.69
2	6.28	6.28	-6.28	-6.28	-6.28	-6.28	6.28	-6.28	6.28	6.28	6.28	-6.28
3	1.36	-1.36	1.36	-1.36	-1.36	-1.36	1.36	1.36	-1.36	1.36	1.36	1.36
4	0.82	0.82	0.82	-0.82	-0.82	-0.82	0.82	-0.82	-0.82	0.82	-0.82	0.82
5	4.98	-4.98	-4.98	4.98	-4.98	-4.98	4.98	4.98	4.98	-4.98	4.98	-4.98
6	7.82	7.82	-7.82	7.82	-7.82	-7.82	7.82	-7.82	7.82	-7.82	-7.82	-7.82
7	2.80	-2.80	2.80	2.80	-2.80	-2.80	2.80	2.80	-2.80	-2.80	-2.80	2.80
8	1.15	1.15	1.15	1.15	-1.15	-1.15	1.15	-1.15	-1.15	-1.15	1.15	1.15
9	0.04	-0.04	-0.04	-0.04	0.04	-0.04	-0.04	0.04	-0.04	-0.04	-0.04	0.04
10	2.08	2.08	-2.08	-2.08	2.08	-2.08	-2.08	-2.08	-2.08	-2.08	2.08	2.08
11	0.03	-0.03	0.03	-0.03	0.03	-0.03	-0.03	0.03	0.03	-0.03	0.03	-0.03
12	2.22	2.22	2.22	-2.22	2.22	-2.22	-2.22	-2.22	2.22	-2.22	-2.22	-2.22
13	0.77	-0.77	-0.77	0.77	0.77	-0.77	-0.77	0.77	-0.77	0.77	0.77	0.77
14	4.66	4.66	-4.66	4.66	4.66	-4.66	-4.66	-4.66	-4.66	4.66	-4.66	4.66
15	0.07	-0.07	0.07	0.07	0.07	-0.07	-0.07	0.07	0.07	0.07	-0.07	-0.07
16	1.18	1.18	1.18	1.18	1.18	-1.18	-1.18	-1.18	1.18	1.18	1.18	-1.18
17	8.12	-8.12	-8.12	-8.12	-8.12	8.12	-8.12	-8.12	8.12	8.12	-8.12	8.12
18	50.00	50.00	-50.00	-50.00	-50.00	50.00	-50.00	50.00	50.00	50.00	50.00	50.00
19	9.11	-9.11	9.11	-9.11	-9.11	9.11	-9.11	-9.11	-9.11	9.11	9.11	-9.11
20	18.75	18.75	18.75	-18.75	-18.75	18.75	-18.75	18.75	-18.75	18.75	-18.75	-18.75
21	50.00	-50.00	-50.00	50.00	-50.00	50.00	-50.00	-50.00	50.00	-50.00	50.00	50.00
22	50.00	50.00	-50.00	50.00	-50.00	50.00	-50.00	50.00	50.00	-50.00	-50.00	50.00
23	9.55	-9.55	9.55	9.55	-9.55	9.55	-9.55	-9.55	-9.55	-9.55	-9.55	-9.55
24	50.00	50.00	50.00	50.00	-50.00	50.00	-50.00	50.00	-50.00	-50.00	50.00	-50.00
25	1.03	-1.03	-1.03	-1.03	1.03	1.03	1.03	-1.03	-1.03	-1.03	-1.03	-1.03
26	6.72	6.72	-6.72	-6.72	6.72	6.72	6.72	6.72	-6.72	-6.72	6.72	-6.72
27	0.73	-0.73	0.73	-0.73	0.73	0.73	0.73	-0.73	0.73	-0.73	0.73	0.73
28	8.30	8.30	8.30	-8.30	8.30	8.30	8.30	8.30	8.30	-8.30	-8.30	8.30
29	2.43	-2.43	-2.43	2.43	2.43	2.43	2.43	-2.43	-2.43	2.43	2.43	-2.43
30	6.98	6.98	-6.98	6.98	6.98	6.98	6.98	6.98	-6.98	6.98	-6.98	-6.98
31	2.60	-2.60	2.60	2.60	2.60	2.60	2.60	-2.60	2.60	2.60	-2.60	2.60
32	28.66	28.66	28.66	28.66	28.66	28.66	28.66	28.66	28.66	28.66	28.66	28.66
MEAN =	**10.69**											
	Main Effect:	**9.32**	**-4.22**	**6.57**	**-12.83**	**16.49**	**-10.69**	**7.67**	**6.61**	**5.61**	**5.55**	**5.12**

8.2.4.1 Individual Factor Effects

Alloy Composition Effect - Main Effect **16.49%** e

Composition was the most significant factor affecting the amount of permanent strain in the parent phase. The effect of a titanium rich alloy (SMA) was to increase the average permanent residual strain.

Cold Work - Main Effect **12.83%** e

Low cold work increased the residual strain in the parent phase.

Heat Treatment - Main Effect **9.32%** e

The high heat treatment temperature (500°C) increased the average residual strain in the parent phase.

Applied Stress - Main Effect **6.57%** e

The high stress level of 165MPa increased the average residual strain in the parent phase.

Cycling Rate - Main Effect **3.60%** e

Low cycling rates increased the residual strain in the parent phase.

8.2.4.2 Factorial Interaction Effects

Two Factor Interactions :-

Cold Work and Alloy Composition – Main Effect **10.69%** e

Analysing the data in the geometric **Table 8-21** showed how this interaction occurred. It shows that the residual strain in the parent phase was more sensitive to alloy composition in the low cold work (6%) condition.

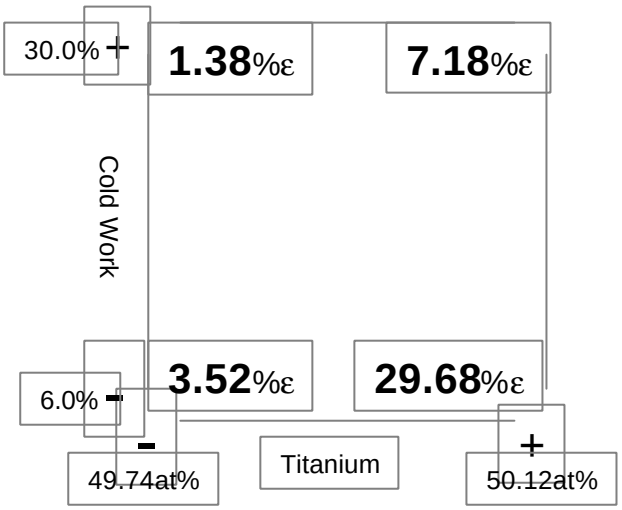

Table 8-21 The Cold Work - Alloy Composition Interaction at Cycle 500

Heat Treatment and Alloy Composition – Main Effect **7.97%** e

Table 8-22 shows that the residual permanent strain of the parent phase in the titanium rich SMA alloys, heat treated at 500°C was 17 times that of the permanent strain in the Ni rich alloy heat treated at 400°C.

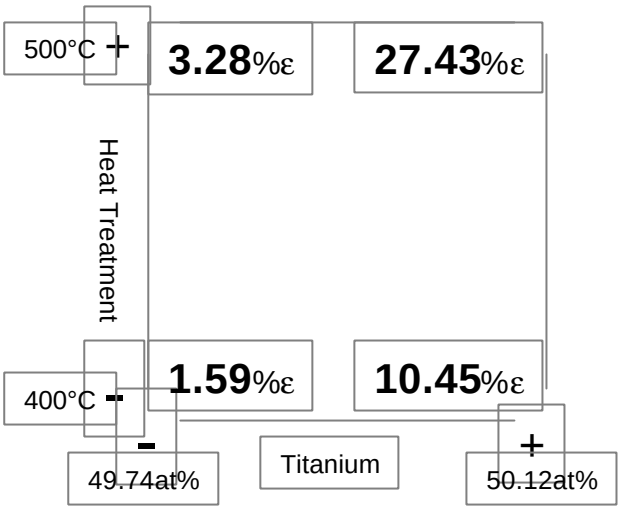

Table 8-22 The Heat Treatment -Alloy Composition Interaction at Cycle 500

Cold Work and Cycling Rate Interaction – Main Effect **6.61%** e

At low cycling rates (170 seconds per cycle) the permanent strain in the alloys was more sensitive to the degree of prior cold work, this is shown in **Table 8-23.**

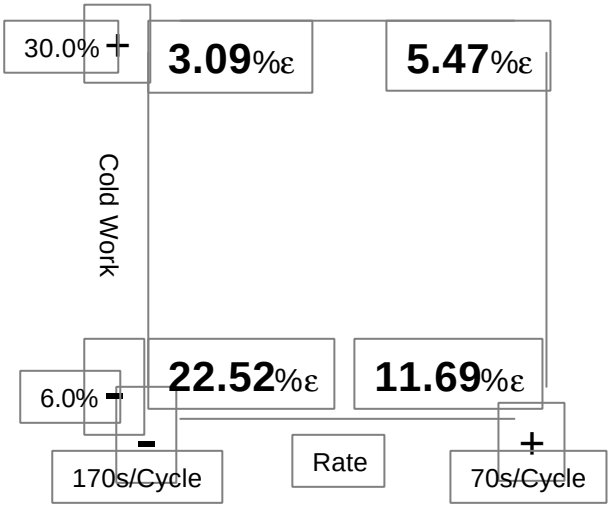

Table 8-23 The Cold Work - Cycling Rate Interaction at Cycle 500

Alloy Composition and Applied Stress Interaction – Main Effect **5.61%**e

It is seen from **Table 8-24** that the Ti rich alloys were particularly sensitive to the level of applied stress.

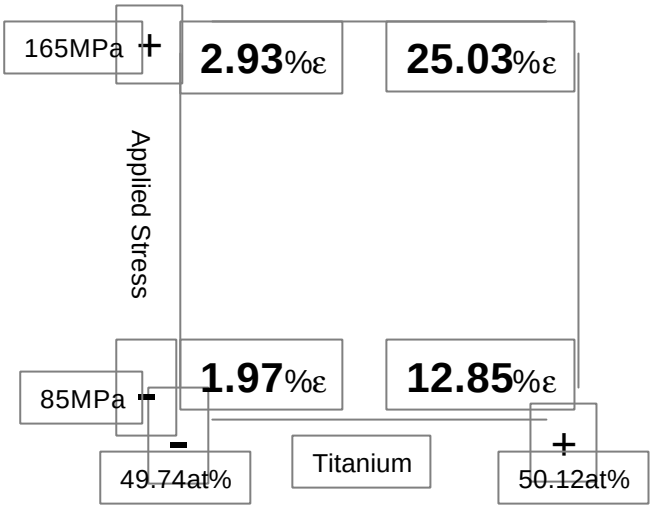

Table 8-24 The Applied Stress - Alloy Composition Interaction at Cycle 500

Three Factor Interactions

Heat Treatment – Applied Stress – Cycling Rate

Main Effect **5.55%**e

This is illustrated by the cubic contrast table shown in **Table 8-25**.

As with the residual strain in the martensite phase, perhaps the most interesting effect observed in **Table 8-25** is the amount of residual strain in the alloys heat treated at the low temperature (400°C) and cycled at a slow rate against 165MPa. The difference between this strain (14.55%ε) and any of the others in the low heat treatment condition was considerable.

Similarly, in the high heat treatment condition (500°), the residual strain in the parent phase of the alloys cycled at a high rate against an applied stress of

85MPa was considerably lower than any of the other alloys in the high heat treatment condition.

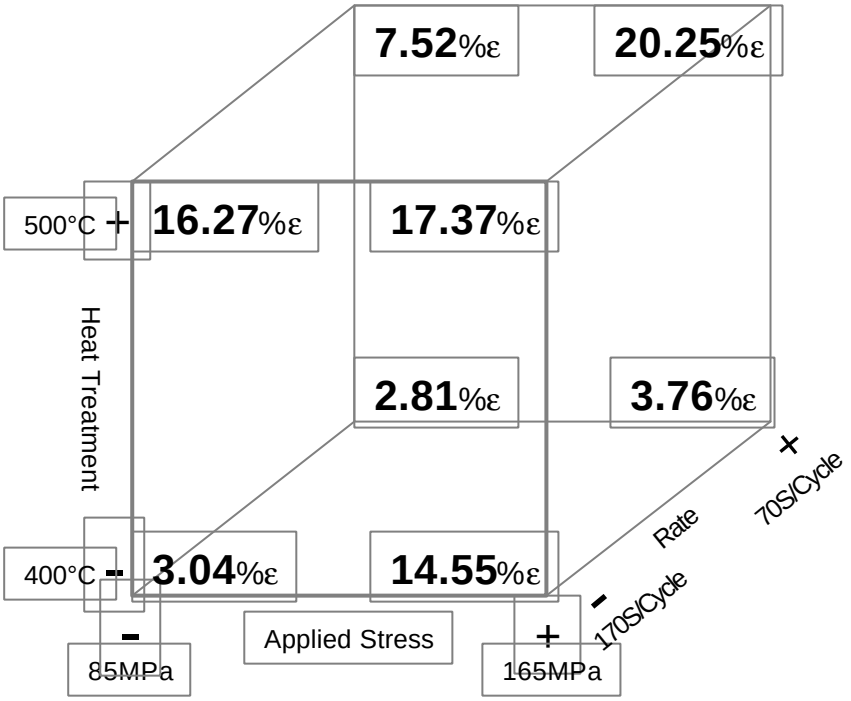

Table 8-25 The Heat Treatment - Applied Stress - Cycling Rate Interaction on Residual Strain Permanent Strain of the Parent Phase at Cycle 500

Alloy Composition – Cold Work – Cycling Rate

Main Effect **5.12%**e

Table 8-26 shows this effect graphically. Generally it can be seen that the high cold worked alloys were most resistant to parent phase residual strain, as were the Ni rich alloys.

In addition the cycling rate was also shown to have an effect. The higher cycling rate appears to result in less residual parent phase strain. As with the martensite phase strain, the only anomaly to this finding was the Ti rich, high cold work alloy. In this alloy the higher cycling rate appeared to result in more residual strain.

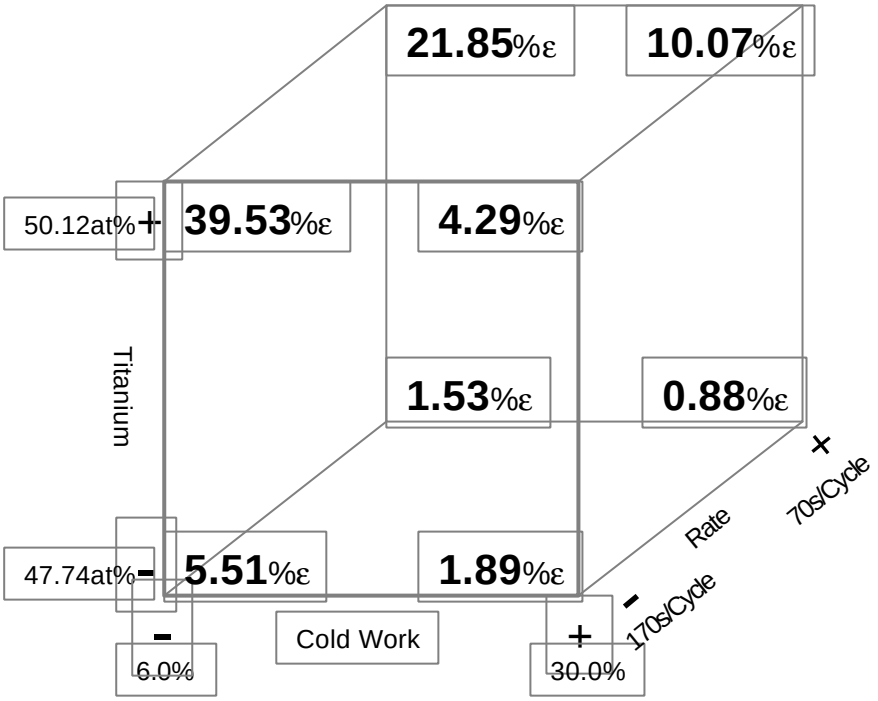

Table 8-26 The Alloy Composition – Cold Work – Cycling Rate Interaction on Residual Permanent Strain in the Parent Phase at Cycle 500

8.2.4.3 Summary of Variables Effect on Residual Permanent Strain in the Parent Phase

Just as was found in the martensite phase, the results and main effects analysis show that residual permanent strain in the parent phase was particularly sensitive to alloy composition and cold work percentage. The titanium rich alloys with just 6% cold work and heat treated at high temperatures resulted in the greatest permanent strains.

Higher stresses also resulted in greater permanent strains. Again, this was shown to be particularly sensitive to alloy composition, **Table 8-24**.

Slower cycling rates also appeared to result in increased permanent martensite strain. As with the martensite strain, this was particularly so in the 6% cold worked alloys as shown in **Table 8-23**.

Just as was found with the permanent strains in the martensite phase, the alloys most resistant to residual permanent strains in the parent phase were those that were Ni rich, had high cold work and were heat treated at low temperatures. In these alloys, the level of applied stress and cycling rate were not so important in achieving an actuator resistant to permanent strains.

9 Transformation Temperatures

Transformation temperatures were measured directly from strain-temperature hysteresis plots taken from an X-Y recorder. Tangential lines were drawn against the hysteresis profile to obtain the M_f , M_s , A_s and A_f temperatures. This method is defined in **Figure 9-1**.

Unfortunately the X-Y recorder was unable to record the fast cycle tests and therefore the results presented in this section are taken solely from the 170 second-cycles.

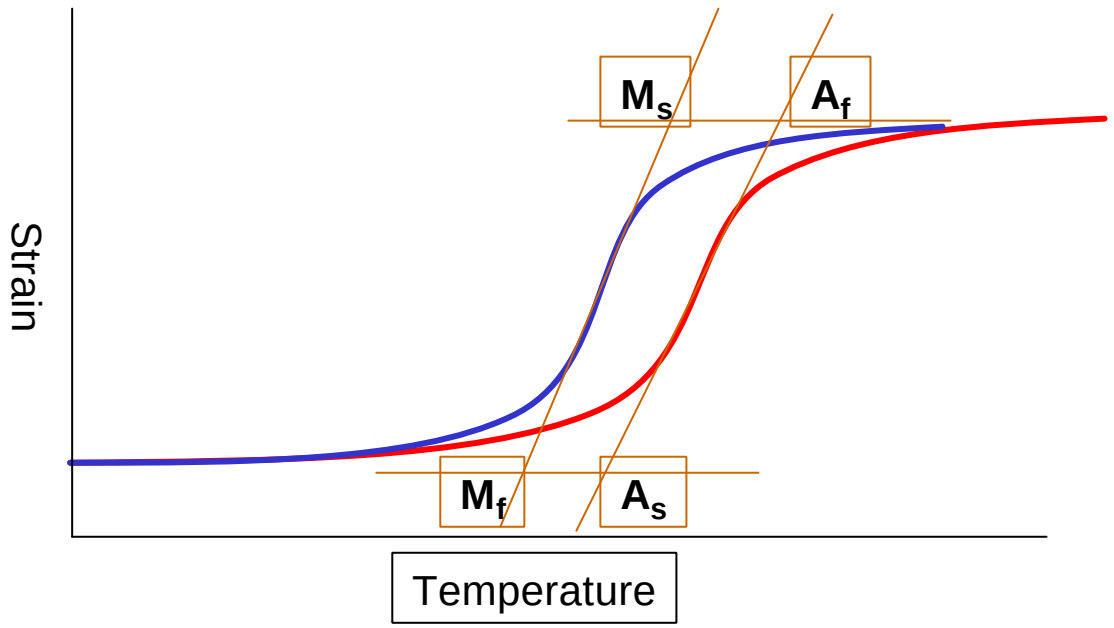

Figure 9-1 The Tangential Method of Measuring Transformation Temperatures from Strain - Temperature Hysteresis Plots

The transformation temperatures are plotted against the applied stress, in addition the temperatures at zero stress taken from the DSC tests are also

plotted. Although this results in only three points per curve, it does indicate the trends in transformation temperature drift.

The temperature window of the cycling experiments are also shown on the stress/temperature graphs. To prevent overheating of the different alloy types, the upper temperature achieved during cycling was controlled to ensure it did not exceed 20°C – 30°C more than the measured A_f at zero stress.

The transformation temperatures at cycle 1, cycle 100 and cycle 500 are plotted. The curve at cycle 1, where the alloy has the same internal structure whatever the level of applied stress, indicates the Clausius-Clapeyron relationship first referred to in **equation (2-19)** :

$$\frac{\mathbf{d}\,s}{\mathbf{d}M_s} = -\frac{\Delta \mathbf{S}}{e} = -\frac{\Delta \mathbf{H}}{e\mathbf{T}} \qquad \textbf{(9-1)}$$

where s is a uniaxial stress, $\mathbf{M_s}$ is the martensite transformation start temperature, e is the strain associated with the transformation, $\Delta\mathbf{S}$ is the entropy change per unit volume, $\Delta\mathbf{H}$ is the enthalpy change per unit volume and **T** is the temperature.

Thus the gradient relationship of:

$$\frac{\mathbf{d}\,s}{\mathbf{d}M_s}$$

can be measured directly from applied stress-temperature graphs.

The curves plotted at cycle 10 and cycle 500 do not strictly show the Clausius-Clapeyron gradient because the alloys are cycled at different stresses and therefore their internal structures are likely to differ.

Cycling at zero stress was not carried out and therefore the transformation temperatures after thermal cycling are only plotted for the 85MPa and 165MPa tests.

The results are plotted such that each graph represents a particular alloy (Ni rich or Ti rich), with a fixed amount of prior cold work (6% or 30%) and a fixed heat

treatment temperature (400°C or 500°C). As stated previously, the cycling rate is fixed at 170 seconds per thermal cycle.

Where appropriate, the R-phase peak temperature (that is, the temperature of the DSC peak), is also shown as a curve labelled R. The R-phase transformation temperatures were found to be very stable with cycling. Therefore, the R phase temperatures are only shown for cycle 1.

9.1 SMC (50.26at%Ni-Ti), 30% Cold Work, 500°C Heat Treatment

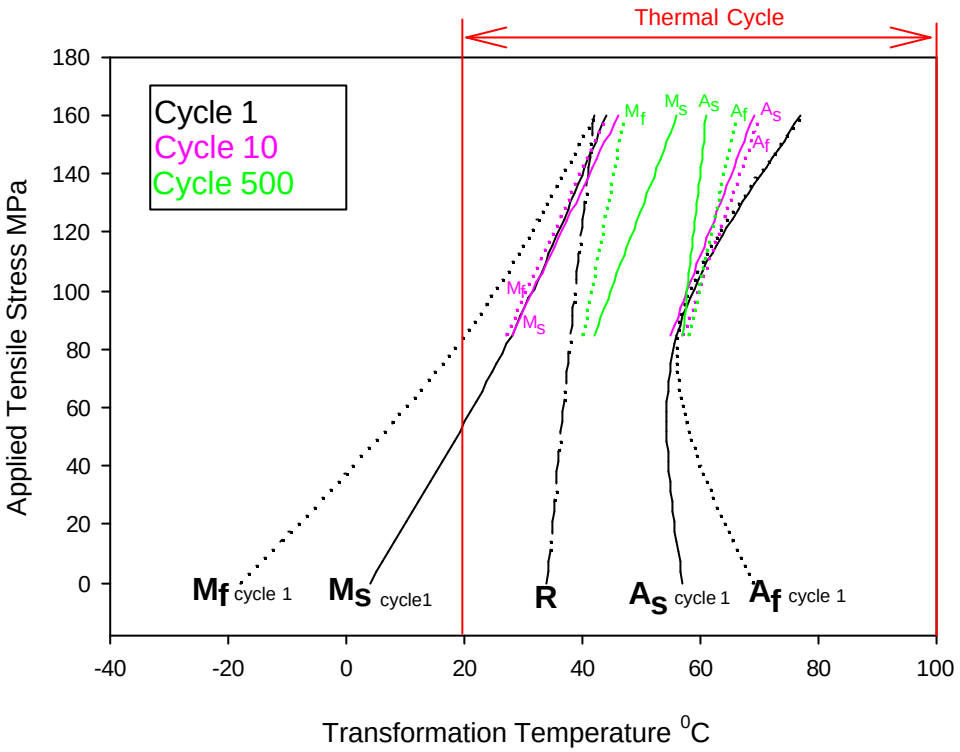

Graph 9-1 The Transformation Temperatures of samples 10 and 14 Before and After Thermal Cycling Against an Applied Stress

Graph 9-1 shows how the martensite transformation temperatures (M_s and M_f) of the alloys under test gradually increased. The M_s temperatures at the two stress levels increased by approximately the same amount over 500 cycles (12°C - 14°C). The M_f temperatures however, increased by varying degrees. At 85MPa the M_f increased by a similar amount to the M_s. At a stress of 165MPa the M_f increased by less than half the amount of the increase in M_s.

The parent phase transformation temperatures at 165MPa shifted in the opposite direction to the martensite temperatures and at 85MPa remained constant. In a similar way to the martensite temperatures, the A_s temperature shift was greater than the A_f shift.

The affect on hysteresis profiles can be also be taken from this graph. At the higher stress level, the hysteresis width, (A_s – M_s), becomes smaller and more sloping (i.e. the temperature interval between the start and finish temperatures of the respective transformations increases) whilst at 85MPa, only the hysteresis width, (A_s – M_s) changes, becoming smaller. The temperature interval between the start and finish of transformation remains virtually constant.

9.2 SMC (50.26at%Ni-Ti), 30% Cold Work, 400°C Heat Treatment

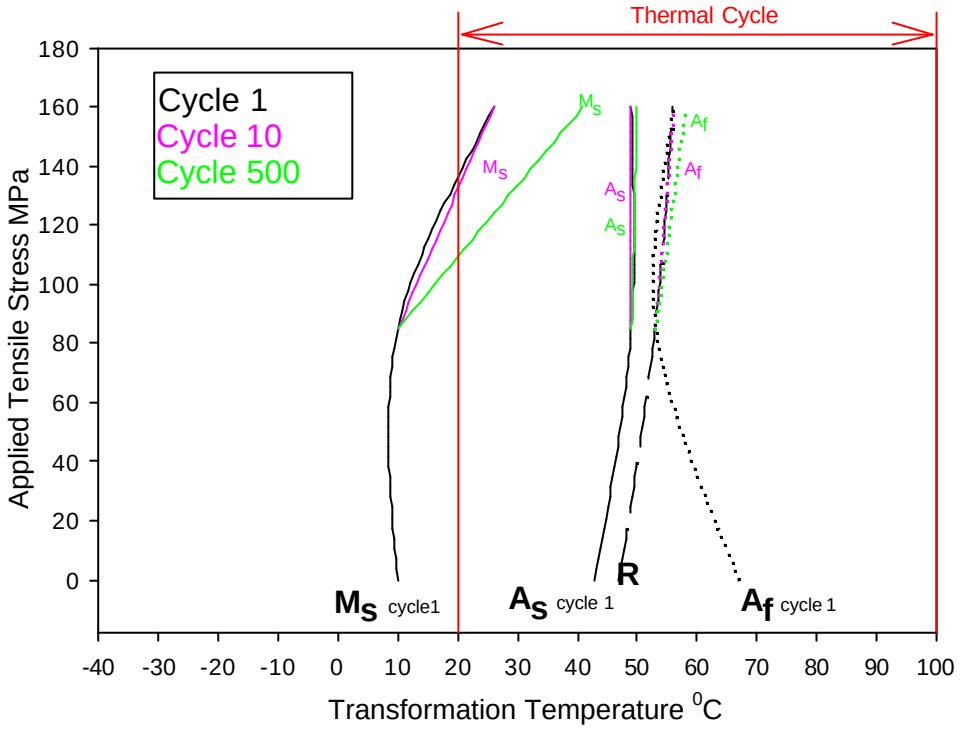

Graph 9-2 The Transformation Temperatures of samples 9 and 13 Before and After Thermal Cycling Against an Applied Stress

In **Graph 9-2** the M_f temperatures are not shown. This is because they could not be measured under stress due to the fact that they were sub ambient. Likewise, the M_s temperature at 85MPa was also below ambient temperature and in the graph above, is estimated so as to complete the curve.

Because the M_s temperature was not reached during cycling at 85MPa, the transformation strain was purely due to the R-phase transformation. The R-phase start temperature is above the reverse A_s temperature.

At 165MPa, the early cycles were also due almost purely to the R-phase transformation. Interestingly though, as the number of cycles increased, the M_s temperature also gradually increased. This resulted in a larger volume fraction of the martensite phase transforming at cycle 500 than at cycle 10 and therefore an increased recovery strain.

9.3 SMC (50.26at%Ni-Ti), 6% Cold Work, 500°C Heat Treatment

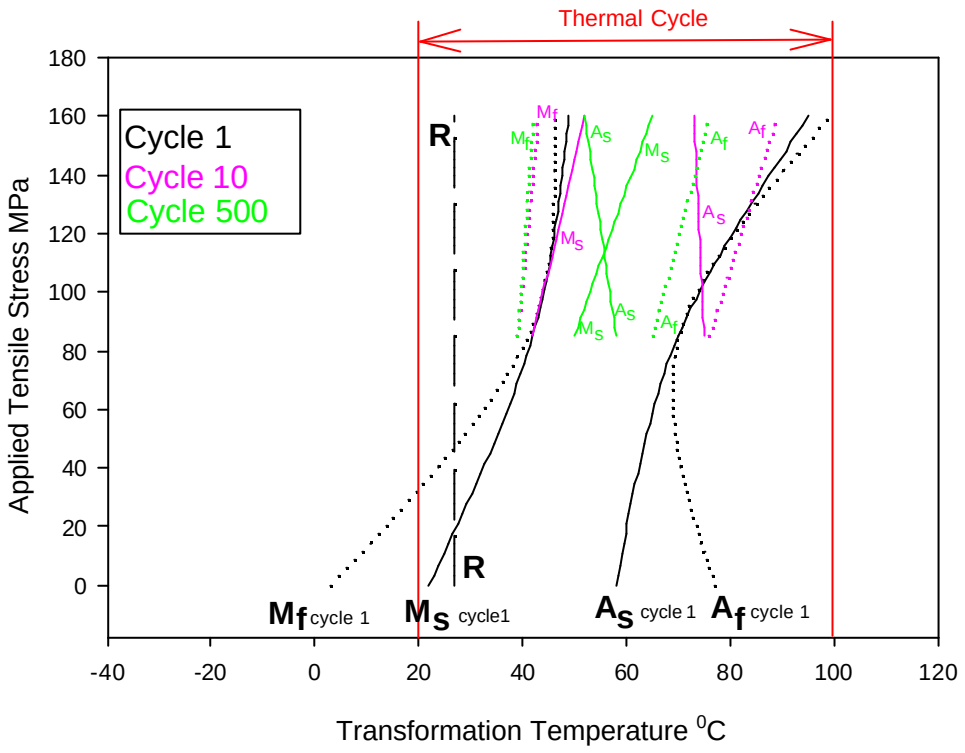

Graph 9-3 The Transformation Temperatures of samples 2 and 6 Before and After Thermal Cycling Against an Applied Stress

In **Graph 9-3,** the R-phase temperatures are plotted for reference. In fact the applied stresses were such that the martensite transformation temperatures

were raised by a sufficient amount to suppress the R-phase completely resulting in pure martensite-parent phase cycles.

The M_s temperatures increased considerably at both stresses whilst the M_f appeared to decrease slightly. The change in shape of the hysteresis profile was such that its width, (A_s – M_s), decreased considerably. The temperature interval between the start and finish of transformations increased as the slope of the hysteresis profile increased. However, the extreme change in hysteresis shape may decrease the accuracy of the temperature measurement.

The A_s and A_f temperatures decreased during cycling, particularly at 165MPa where the measured A_s decreased so much that at cycle 500 it was less than the M_s. At cycle 500 the measured A_s at 165MPa was less than that at 85MPa.

9.4 SMC (50.26at%Ni-Ti), 6% Cold Work, 400°C Heat Treatment

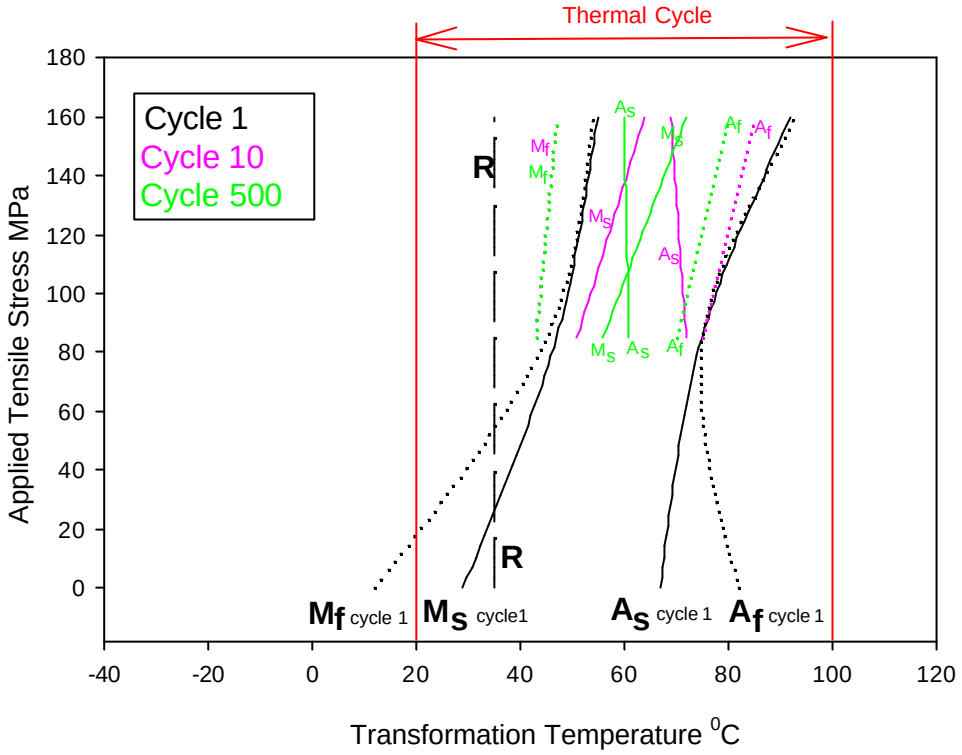

Graph 9-4 The Transformation Temperatures of samples 1 and 5 Before and After Thermal Cycling Against an Applied Stress

The curves shown in **Graph 9-4** follow very similar trends to those shown in **Graph 9-3**, i.e. the M_f temperatures decreased, the M_s temperatures increased, the A_f temperatures decreased and the A_s temperatures decreased. Again, at 165MPa the A_s temperature decreased so much that by cycle 500, it is less than the M_s.

As in **Graph 9-3**, the temperature changes were greatest in the samples cycled at the higher stress, 165MPa.

9.5 SMA (49.88at%Ni-Ti), 30% Cold Work, 500°C Heat Treatment

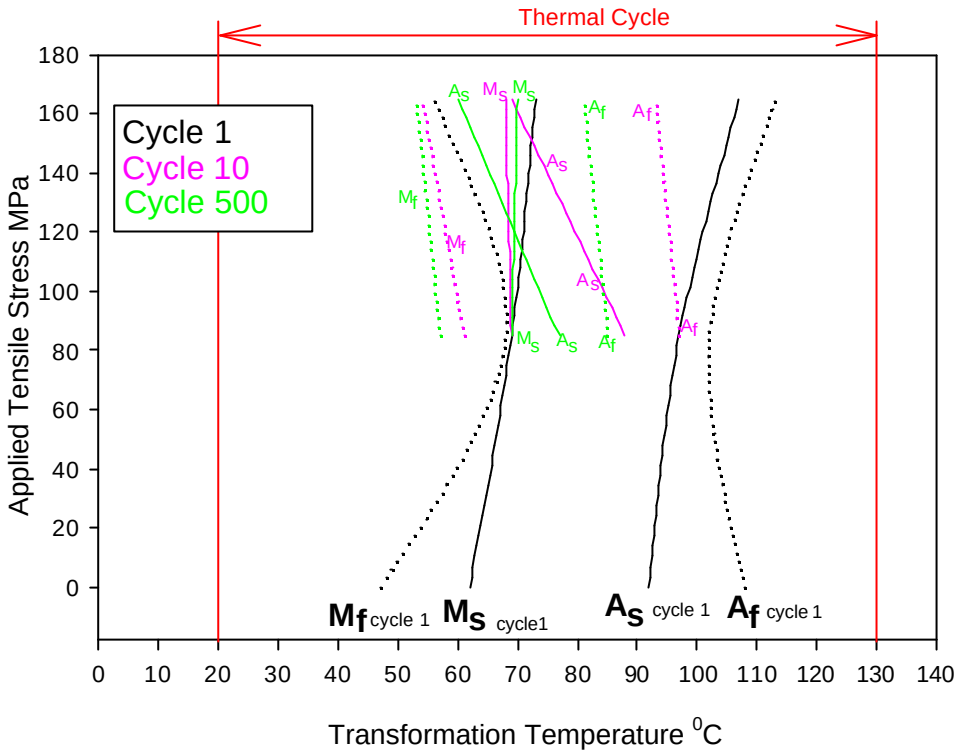

Graph 9-5 The Transformation Temperatures of samples 26 and 30 Before and After Thermal Cycling Against an Applied Stress

Graph 9-5 shows that the martensite transformation temperatures (M_s and M_f) gradually decreased during thermal cycling against applied stress. The decrease in martensite temperatures, however, was small when compared to the decrease in parent phase transformation temperatures. Both the A_s and A_f temperatures decreased considerably with thermal cycling against the applied stress levels. In fact, because the parent phase temperature decrease was greatest at the 165MPa applied stress, the A_s and A_f temperatures were greater at 85MPa than at 165MPa. This is true even after just 10 thermal cycles.

The temperature interval between the start and finish of each transformation direction also increased with thermal cycling, particularly at the higher applied

stress. Hysteresis width (A_s – M_s) decreased with thermal cycling and applied stress level.

9.6 SMA (49.88at%Ni-Ti), 30% Cold Work, 400°C Heat Treatment

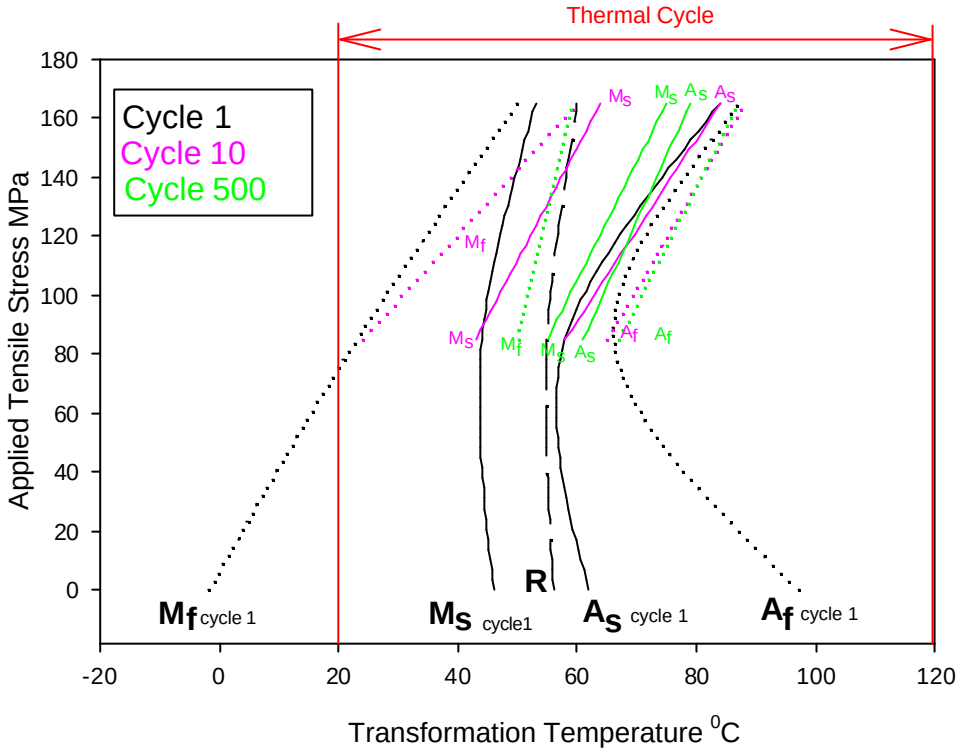

Graph 9-6 The Transformation Temperatures of samples 25 and 29 Before and After Thermal Cycling Against an Applied Stress

Thermal cycling against applied stress in the Ti rich alloy, heat treated at 400°C after 30% cold work, caused all the transformation temperatures to increase. This is shown above in **Graph 9-6**.

During the early cycles, at 85MPa, the phase change during cooling, consisted of both R-phase and partial martensite transformations. Gradually, as the number of thermal cycles increased, so the M_s temperature increased. Eventually, at cycle 500, the M_s was such that the R-phase was suppressed and the transformation was purely martensitic. Suppression of the R-phase at 165MPa occurred much earlier. By cycle 10 the transformation was purely martensitic.

Apart from the martensite phase change at 85MPa, the temperature difference between the start and finish temperatures of the martensite and parent phase transformations increased with cycling. At 85MPa stress, the temperature change between M_s and M_f actually decreased with thermal cycling.

The width of hysteresis (A_s – M_s) at both stress levels decreased considerably during cycling.

9.7 SMA (49.88at%Ni-Ti), 6% Cold Work, 500°C Heat Treatment

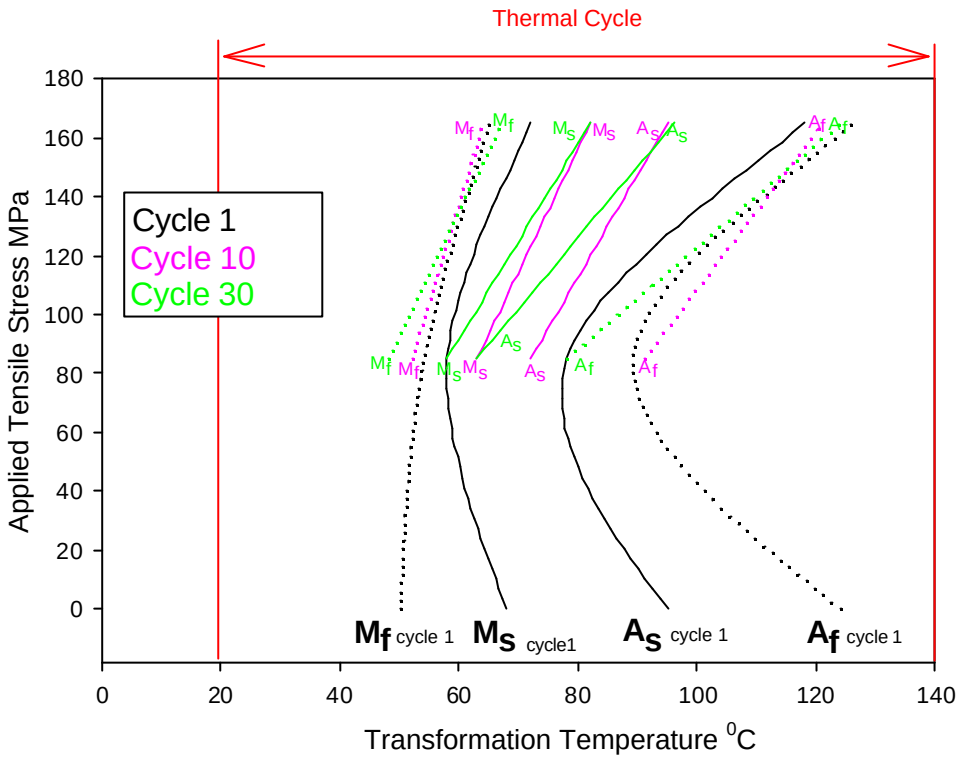

Graph 9-7 The Transformation Temperatures of samples 18 and 22 Before and After Thermal Cycling Against an Applied Stress

Because of the large amount of residual strain during cycling displayed by these alloys, the changes of transformation temperature are only shown up to cycle 30. Beyond this, the transformation strain could not be measured using the X-Y recorder.

It is shown in **Graph 9-7** that the transformation temperatures actually tend to decrease when the stress is applied, i.e. between 0MPa and 85MPa. This observation does not obey the Clausius-Clapeyron relationship, which states the temperatures should increase with applied stress.

The greatest changes of temperature during thermal cycling shown in **Graph 9-7,** occurred in the transformation start temperatures. The M_s temperatures increased and the A_s temperatures decreased. In the alloy cycled at 165MPa,

the changes in transformation temperature appeared to be saturated by cycle 10. It was also observed that at 85MPa, the M_s temperature appeared to increase (cycle 10) and then subsequently decrease (cycle 30).

The temperature interval between the start and finish temperatures of transformation increased with cycling and the hysteresis width (A_s – M_s) decreased at both stresses. The greatest decrease in hysteresis width occurred in the alloy cycled at 85MPa.

The M_f temperatures changed little in either alloy. The A_f temperature decreased in the alloy cycled at 85MPa but did not change significantly in the alloy cycled at 185MPa.

9.8 SMA (49.88at%Ni-Ti), 6% Cold Work, 400°C Heat Treatment

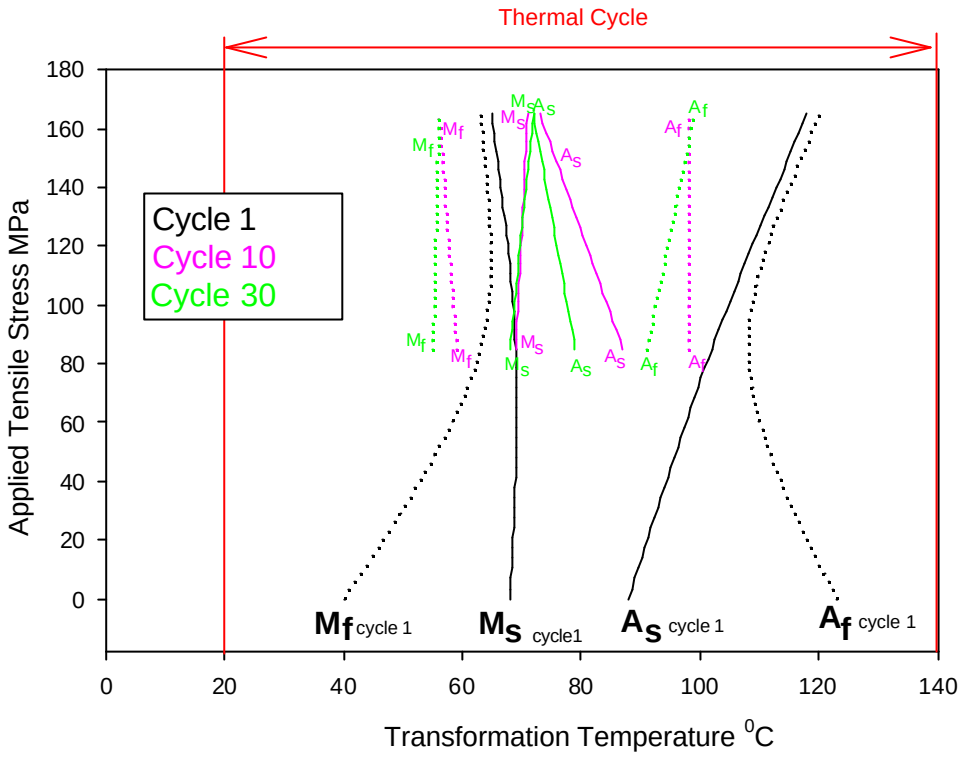

Graph 9-8 The Transformation Temperatures of samples 17 and 21 Before and After Thermal Cycling Against an Applied Stress

Again, the residual deformation of these alloys was so great that **Graph 9-8** is only plotted as far as cycle number 30.

As with the equivalent alloy heat treated at 500°C, the greatest change in temperatures occurred at the start of transformation. The M_s increased and the A_s decreased. However the increase of M_s at 85MPa was slight. At 165MPa, the temperature changes appeared to be almost saturated by cycle 10.

The martensite transformation finish temperatures tended to decrease with thermal cycling. Again, this decrease appeared to be saturated by cycle 10 in the alloy transforming against 165MPa.

At 85MPa, the martensite phase start temperature appeared to increase during early cycles (cycle 10) and then decrease during subsequent cycles (cycle 30).

This effect was also observed in **Graph 9-7**, (the equivalent alloy heat treated at 500°C).

The temperature interval between the start and finish temperatures of transformation increased with cycling at both stress levels. The hysteresis width, ($A_s - M_s$), decreased at both stress levels.

9.9 Summary of Cycling Effects on Transformation Temperatures and Hysteresis

Ni Rich Alloys

In all the Ni rich alloys the M_s temperature increased with cycling and the A_s decreased. In general, the amount of drift in these temperatures increased with increasing applied stress, increasing heat treatment temperature and decreasing cold work. The most stable transformation temperatures were those associated with the pure R-phase cycling shown in **Graph 9-2**.

In all the samples that exhibited at least partial martensitic transformation, the hysteresis width (defined as $A_s - M_s$), decreased with the number of cycles. In addition, the temperature interval between the start and finish temperatures of transformation increased with cycling. Again, these changes tended to be greatest in the samples with: high applied stress, high heat treatment temperature and low cold work.

Ti Rich Alloys

In the 6% cold worked, Ti rich alloys, the A_s temperatures decreased with cycling at both stress levels. The M_s increased at the 165MPa stress level, but remained constant at 85MPa.

In the 30% cold worked, Ti rich alloys, the A_s temperatures only decreased in the samples heat treated at 500°C. The A_s remained virtually constant for the samples heat treated at 400°C.

As in the Ni rich alloys, the hysteresis width (defined as $A_s - M_s$), decreased with the number of cycles as did the temperature interval between the start and finish temperatures of transformation. Again, the samples with: high applied stress,

high heat treatment temperature and low cold work appeared to be most sensitive to these effects.

10 The Effect of Cycling against an Applied Stress on the Tensile Properties of the Factorial Analysis Alloys

Subsequent to the thermal cycling tests, all the samples were tested to destruction in a tensile machine. It was hoped that these tests would yield information on the structural effects of thermal cycling against applied stresses.

10.1 Shape of the Tensile Curves

The tests showed that the reorientation plateau observed in the samples prior to cycling, had disappeared in all alloys apart from those where R-phase transformation was the dominant reaction taking place during cycling. This is because the preferred variant reorientation of the martensite had already occurred during the last martensite cycle. Therefore, the martensite variants had already orientated in the direction of applied stress and when the tensile tests were carried out, the reorientation plateau did not occur.

10.2 Ultimate Tensile Strength

Interesting observations can be made from the ultimate tensile strength and elongation to failure, of the alloys before and after cycling. **Table 10-1** shows the ultimate tensile strength of the alloys with no prior thermal cycles and the ultimate tensile strength of the 32 samples subjected to repeated cycling against an applied stress.

The elongation to failure decreased in all the specimens after thermal cycling, in particular, the specimens that showed excessive permanent strains after cycling (i.e. 18, 21, 22, 24 and 32). In these alloys the elongation to failure reduced from approximately 60% prior to cycling, to less than 10% after cycling.

These same alloys also displayed a large reduction in ultimate tensile strength after repeated cycling, **Table 10-1**. This is interesting as one might expect the UTS to increase as a reduction of elongation to failure implies the alloy has work hardened.

Sample Code	Elongation to Failure With No Prior Thermal Cyling %	Elongation to Failure After Thermal Cyling %	Ultimate Tensile Strength With No Prior Thermal Cycling MPa	Ultimate Tensile Strength After Thermal Cycling MPa
1	60	45	1067	1038
2	60	55	965	1041
3	60	52	1067	1052
4	60	51	965	1040
5	60	44	1067	1072
6	60	45	965	1060
7	60	45	1067	1038
8	60	50	965	1025
9	19	17	1447	1400
10	25	13	1169	1140
11	19	18	1447	1420
12	25	14	1169	1110
13	19	11	1447	1430
14	25	14	1169	1155
15	19	13	1447	1315
16	25	16	1169	1100
17	60	41	1052	980
18	60	9	935	800
19	60	44	1052	980
20	60	41	935	900
21	60	9	1052	427
22	60	9	935	660
23	60	37	1052	1010
24	60	8	935	700
25	25	15	1344	1286
26	40	30	1052	1008
27	25	13	1344	1300
28	40	34	1052	1023
29	25	14	1344	1310
30	40	22	1052	994
31	25	13	1344	1271
32	40	9	1052	1136

Table 10-1 Ultimate Tensile Strength Before and After Thermal Cycling Against an Applied Stress

The elongation to failure with no prior cycling was by far the greatest in the low cold work alloys, i.e. samples 1 to 8 and 17 to 24. This corresponds to a comparatively ductile starting structure prior to cycling.

Interestingly, comparing the elongation to failure of the high cold work alloys before cycling, i.e. samples 9 to 16 and 25 to 32, the Ti rich samples (25 to 32) showed the greater elongation to failure. Therefore, the Ti rich, 30% cold work alloys had a slightly more ductile starting structure than the Ni rich equivalents.

It should be clearly stated again, that the tensile tests after cycling, were carried out after the last, stress assisted martensite transformation had occurred. Therefore the elongation to failure after cycling had no stress assisted variant orientation strain associated with it. The elongations to failure of the alloys prior to cycling, on the other hand, did have a variant orientation plateau strain associated with them.

If the variant orientation components are taken out of the maximum tensile strains, the elongation may easily reduce by 8% strain. If experimental scatter and errors are also considered, a reduction of 10 - 15% elongation is quite possible. Equally an apparent increase of elongation is possible resulting from experimental scatter alone.

It is interesting to consider the strains associated with variant orientation and experimental scatter when analysing the post cycling elongation to failure. Reductions in elongation to failure of less than 15% are not considered significant. Therefore, none of the Ni rich alloys showed a significant reduction in elongation to failure, although the low cold work samples were very close to being significant (samples 1 to 8).

All the Ti rich, low cold work alloys (samples 17 to 24) showed a significant reduction in elongation to failure particularly those where the applied stress was high (samples 21 to 24). Only two of the Ti rich, high cold work alloys showed a significant reduction in elongation to failure after cycling and those are the samples that were cycled against the high applied stress level after heat treatment at the high temperature (i.e. samples 30 and 32).

These results correspond quite well with the permanent strains observed during the factorial analysis. That is, the samples that resulted in significant permanent

strains after cycling against applied stress also result in a significant reduction of elongation to failure when tested after cycling. As stated previously, it is not clear why such a large reduction of elongation to failure should correspond with a reduction in ultimate tensile strength.

11 High Cycle Testing of an Alloy Chosen from Factorial Analysis for its Apparent Cyclic Stability

The factorial analysis has shown that achieving stable actuator elements is a complex trade off between achieving a useful recovery strain and stabilising permanent shape strain. The results imply that for the long term cyclic stability of NiTi actuators operating against constant applied stress, a Ni rich alloy with high prior cold work is likely to be most stable. In addition, to achieve full martensitic transformation a relatively high heat treatment is required.

With this in mind, the alloy chosen to maximise recovery strain whilst maintaining shape stability and operating against an applied stress of 180MPa, was a Ni rich alloy with 30% prior cold work, heat treated at 500°C, this is equivalent to samples 14 and 16 in the factorial analysis.

Graph 11-1 shows the recovery strain of the alloy as a function of the cycle number.

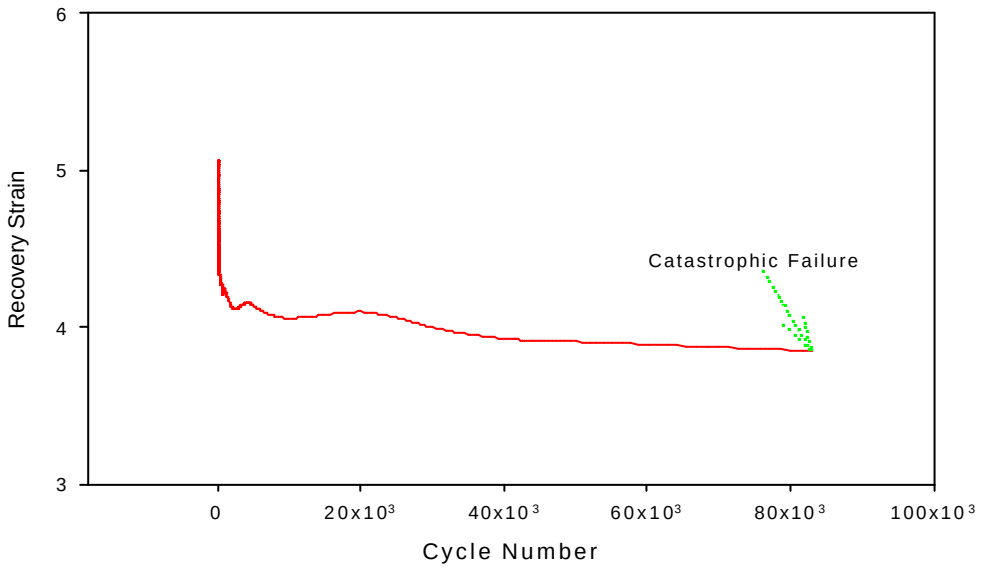

Graph 11-1 Long Term Cyclic Test of Recovery Strain Against Cycle Number

Again, as was found in the factorial tests, considerable degradation of the recovery strain occurred in the early cycles followed by a significant stabilisation. Although the permanent strains are not shown, similar stabilisation effects occurred. Concurrent with the recovery strain and permanent strain stabilisation was a narrowing of the hysteresis width and slight increase of the temperature interval between the start and finish temperatures of transformation.

The cyclic recovery became very stable after approximately 100 thermal cycles. Interestingly, at approximately cycle number N = 83 000, catastrophic failure occurred. There were no obvious changes in recovery strain or permanent shape strain associated with the cycles immediately prior to failure.

The premature failure of the high cycle test emphasises that even if the structure of the NiTi is apparently optimised to resist physical changes such as permanent shape strains from thermal cycling, mechanical failure may still occur. Further analysis of this failure will be made in the discussion section.

12 The Effect of Thermal Cycling and Applied Stress Level on Post Cycling, Stress Free Heats of Transformation

Following the factorial analysis work, it was decided to carry out a series of tests that would establish whether thermal cycling against applied stress results in permanent changes to the transformation temperatures and heats of transformation. It was hoped that differential scanning calorimetry analysis, (DSC), at zero stress after cycling, would establish if permanent changes of internal friction and stored elastic energy occur and what relationship these changes may have to the level of applied stress. It was also hoped that DSC testing would prove a sensitive and direct method of confirming changes of internal stress structure as a result of dislocation generation.

A 50.26at%, 30% cold work alloy, heat treated at 500°C was thermally cycled against five different applied stress levels:-

- 138MPa
- 180MPa
- 245MPa
- 300MPa
- 350MPa

After 100 cycles the alloys were removed from the cycling rig. Small samples were taken from each previously cycled wire for testing by differential scanning calorimetry, (DSC). Post cycling, stress free transformation temperatures and their associated heats of transformation were measured and are shown in the following graphs:

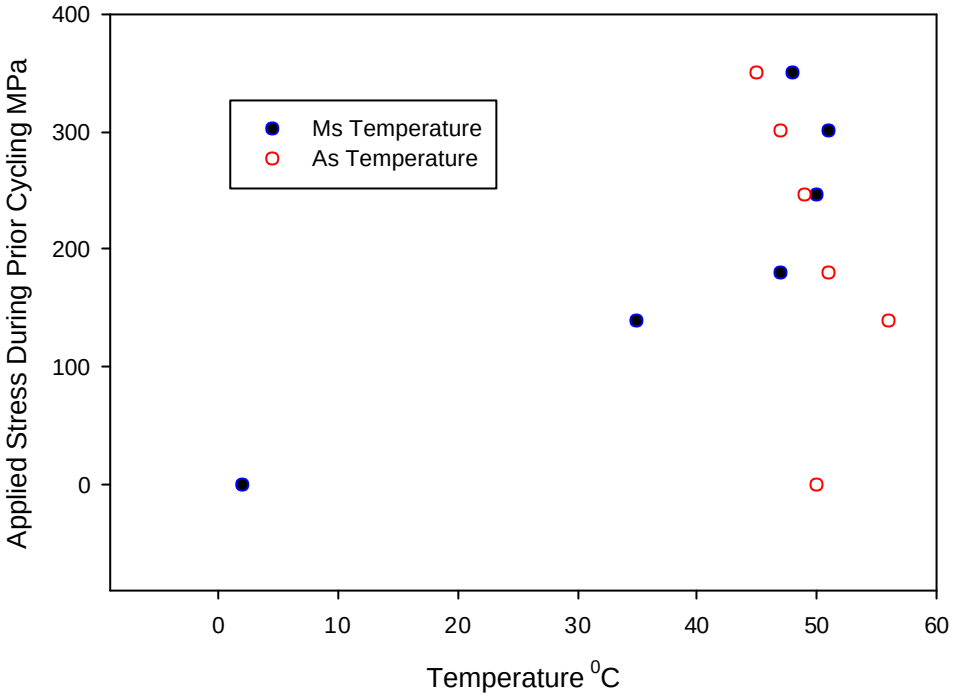

Graph 12-1 The Transformation Start Temperatures Measured by DSC After Cycling at Various Stress Levels

Graph 12-1 shows how, after cycling at five applied stresses, the transformation temperatures changed from the non-cycled value shown at 0MPa. Although similar changes were observed in **Graph 9-1** to **Graph 9-8** in those graphs the temperatures plotted were still under the influence of the applied stress level. **Graph 12-1** indicates the permanent nature of the temperature changes, as here, the applied stress has been removed and the measured temperatures are stress free. The temperatures at 0MPa represent the as heat treated transformation temperatures of the alloy, i.e. the pre-cycling transformation temperatures.

It is shown that a considerable permanent increase of the M_s temperature occurred during applied stress cycling. The increase was large between 0MPa and 138MPa (≈40°C), and then more gradual as the stress increased to

245MPa. Beyond 245MPa, up to 350MPa, the M_s appeared to begin decreasing again.

The A_s temperature of the transformation increased up to 180MPa. Beyond this, the A_s decreased linearly as the stress level of the cycling increased. In fact, because of this decrease, at the higher stresses, the A_s was less than the M_s.

Although specific traces are not shown, the DSC peaks became flatter and more obtuse with the increasing level of cycling stress. Correspondingly the temperature interval between the start and finishing temperatures of transformation increased.

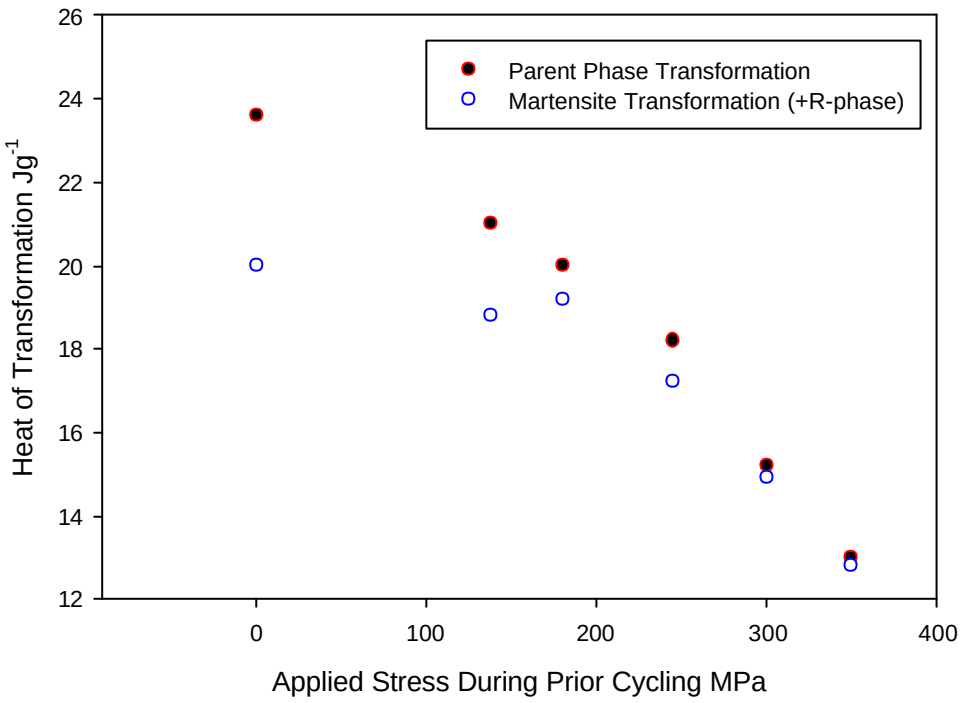

Graph 12-2 Heats of Transformation After 100 thermal Cycles at Five Different Stresses

Graph 12-2 also shows the permanent nature of the changes that take place during cycling at applied stress. Here it is shown that the heats of transformation gradually decreased with the cycling stress level. It is also shown that the

difference in heats of transformation between the forward and reverse reactions decreased with increasing applied stress level. In fact, after cycling against 350MPa the difference in heats of transformation between the martensite formation and parent phase formation cannot be resolved.

Just as the transformation temperatures plotted in **Graph 12-1**, the heats of transformation at 0MPa represent those obtained from the alloy in its pre cycling condition.

13 Discussion

The following discussion considers the effects of the operating and processing variables analysed in the experimental work and develops hypotheses and conclusions based on the cycling data. Comparison of the results with those published in the literature is also carried out to develop and support the final conclusions.

13.1 Dislocation Generation and Internal Stresses

It was found from factorial analysis that cold work had the greatest effect on recovery strain and the second greatest effect on permanent strains. Considerable interaction effects with other variables were also observed. This indicates that the intrinsic dislocation structure of the alloys played an important role in the observed cycling effects.

A gradual decrease of recovery strain with cycle number tended to occur in low cold work alloys when compared to the high cold worked, **Graph 8-11** to **Graph 8-14**. These effects were also observed by Liu and McCormick[146], whilst cycling against increasing applied stress levels. They found that between 21MPa and 60MPa, the recovery strain tended to increase cycle by cycle until a steady recovery strain was attained of approximately 4.5%ε. Above 60MPa a comparatively high starting recovery strain of 6.0%ε tended to decrease with cycling to a steady value of 4.5%ε. The alloy they used was Ti-50.2at%Ni, heat treated at 665°C after 50%cold work. After this heat treatment it is very likely that the alloy had fully recrystallised and had little residual cold work. The permanent strains also increased with stress level and number of cycles.

Liu and McCormick[146] ascribed the gradual decrease of recovery strain at cycling stresses greater than 60MPa, as being due to dislocations and plastic strain. They ascribed the gradual increase of recovery strain at stresses below 60MPa to a developing dislocation structure and internal stress that assists the

formation and growth of stress directed martensite variants. Subsequently they used this hypothesis to optimise a two-way training method.

The reduction of recovery strains they observed were associated with an increase of permanent strain in the parent phase reducing the amount of total strain recovered. Similar results were observed by other authors[131,138,132,91] who also found the permanent strain of the parent phase increased with both stress level and cycle number resulting in a gradual decrease of recovery strain.

All the authors referenced above, carried out their work on wires less than 1mm in diameter and did not carry out any transmission electron microscopy to assess the structural changes taking place. However, they all assigned the changes in recovery strain and the gradual increase of permanent strains to dislocation and defect accumulation during cycling. This is understandable as the very fact that permanent strain increased with stress level does tend to support a dislocation hypothesis. Sandrock et al[171] were the first to directly confirm the generation of high dislocation densities generated by thermal cycling in NiTi alloys with a TEM study.

If dislocation generation is the cause of permanent strain and degradation of recovery strain, then the effect of cold work in the factorial experiments may be easily explained. The low cold work alloys tended to result in the greatest permanent strains and decrease of recovery strain, the only high cold work alloys to show a significant decrease in recovery strain being samples 14 and 16. These both correspond to high heat treatment and high applied stress levels and are therefore two of the most likely to suffer dislocation accumulation. This supports the dislocation generation hypothesis, as the high cold work alloys are likely to be most resistant to dislocation build up.

The first conclusions from the factorial work can now be made:

- *Decreases of recovery strains occurred because of permanent strains in the parent phase*
- *Cold work resists permanent strains and recovery strain degradation*

Lin and Wu[172] support the hypothesis that cold work and dislocations resist permanent strain and degradation of the recovery strain. In their experiments a series of fully annealed (800°C) NiTi alloys was subjected to different amounts of cold work (0% - 40%). As the amount of cold work increased, so the resistance to permanent strain during stress assisted cycling increased. Hardness tests at each cold work level indicated a gradually increasing dislocation structure.

They also found, that when the as annealed, 0% cold work alloy was cycled 100 times, the hardness gradually increased with cycle number. This is shown below in **Figure 13-1**. This very strongly implies that dislocations are generated during cycling and it is this structural hardening that leads to a saturation of the observed cycling effects. They conclude that the process of cold work and thermal cycling strengthens NiTi alloys because of dislocation generation. Concurrent with this is a rise in the critical stress for slip deformation and therefore improved resistance to permanent strain.

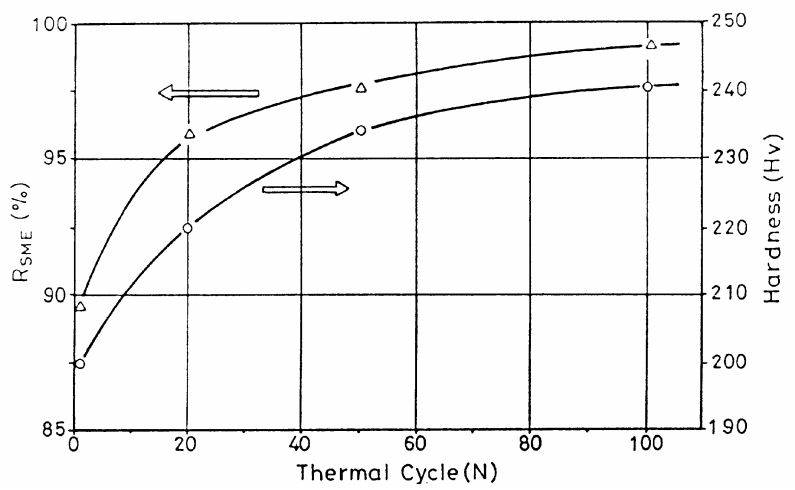

Figure 13-1 Percentage Shape Recovery and Hardness vs. Thermal Cycles for a Repeated Deformation Thermal Cycling Test [172]

In their paper, Lin and Wu[172] miss a very interesting observation. That is, if the hardness accumulated during cycling is correlated with that imparted by prior cold work, it is found that the hardness of the as annealed alloy after 100 cycles is equivalent to approximately 8% cold work. Again, this supports the hypothesis that dislocations are generated during thermal cycling and semi quantifies the degree of strengthening that occurred in their work.

The transformation temperatures of the factorial alloys presented in **Graph 9-1** to **Graph 9-8** also displayed cycling effects and will be discussed in relation to dislocation generation due to transformation cycling[173,174,175] and specifically the findings of Miyazaki et al[133].

Miyazaki et al[133] directly confirmed that dislocations are generated by thermal cycling NiTi alloys, **Figure 13-2**. With thermal cycling the dislocation density increased. Miyazaki used the build up of dislocations to explain the changes of transformation temperatures that occurred during cycling. During pure thermal cycling (i.e. no applied stress) he found that transformation temperatures decreased with cycling. Miyazaki attributed this to a build up of internal stress resulting from dislocation generation. In the same way as cold work suppresses transformation temperatures the dislocations were thought to interfere with the martensite transformation and depress the transformation temperatures. This suppression of the transformation temperatures in alloys that undergo repeated thermal cycles under zero stress is consistent with other authors results[143,144].

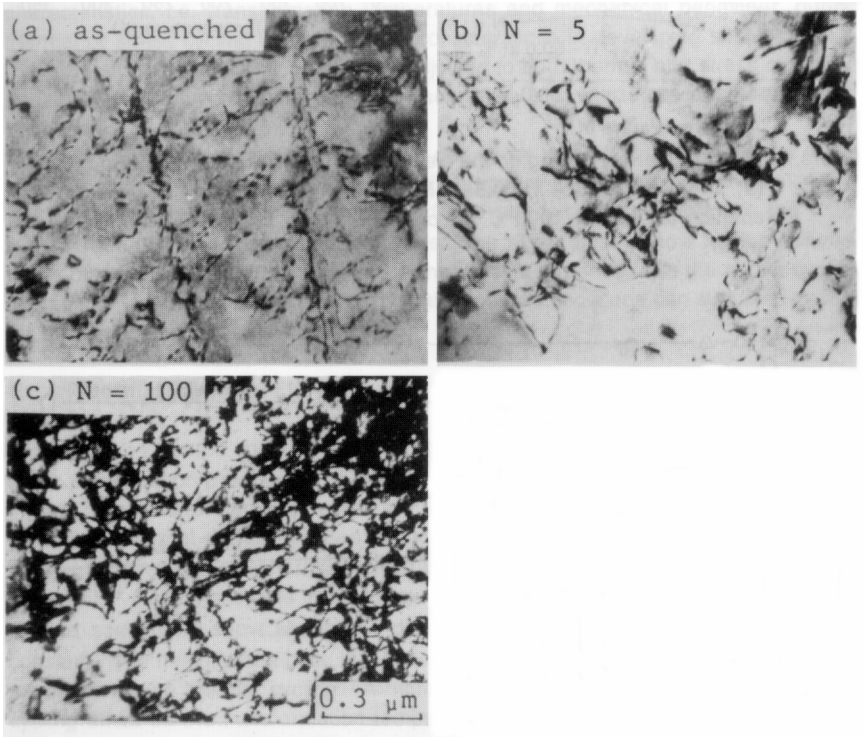

Figure 13-2 Transmission Electron Micrographs of Internal Structure due to Thermal Cycling in a Ti Rich Alloy Heat Treated at 1000°C [133]

Miyazaki also found that if the alloys were imparted with a tensile pre-strain, then the M_s temperature actually increased during thermal cycling, **Figure 5-6**. It was found that higher amounts of pre-strain resulted in a more stable M_s. He ascribed the gradual increase of M_s to new dislocations being induced during cycling and the rearrangement of those already present. He concluded that this would lead to a change of the internal stress state and assist the martensite transformation thereby increasing the M_s temperature.

In Miyazaki's[133] work, the M_s temperature at N=1 was lowered by the tensile pre-strain and this is consistent with cold work suppressing the transformation temperature. However as described in chapter 5, the amount by which the M_s was lowered, actually decreased with increasing pre-strain. This implies that beyond a certain pre-strain level, the transformation is actually assisted by the higher stresses generated by the higher deformations. It has been shown that plastic deformation alone can produce a two-way memory due to anisotropic stress fields assisting the transformation of preferentially orientated martensite variants[87]. It is well documented that normally the M_s temperature will decrease with increasing cold work deformation[176].

The factorial alloys that showed the greatest degree of change in M_s with cycling tended to be those that showed the greatest shape stability, i.e. the Ni rich alloys, **Graph 9-1** to **Graph 9-4** and the 30% cold work, Ti rich alloys, heat treated at 400°C, **Graph 9-6**. This is very interesting as it implies that a relatively dimensionally stable alloy may not necessarily result in stable transformation temperatures. It also implies that structurally, there may have been a different dislocation generation mechanism occurring in those alloys that showed large permanent strains. The hypothesis used by Miyazaki et al[133] to explain changes in M_s, is that dislocations cause internal stresses and that these either act to suppress the martensite transformation and lower M_s or assist the transformation and raise the M_s.

The mechanism proposed by Miyazaki et al[133] and supported by Perkins[177] by which the M_s may actually increase, is that existing dislocations and those introduced by cycling become rearranged during cycling and create a stress that

assists the formation of martensite. If however, the dislocations introduced during cycling hinder the martensite transformation, the M_s will decrease.

Thoma et al[131] state, that in fact, both mechanisms can occur simultaneously. Depending on which mechanism is dominant, the M_s will either increase or decrease. They cycled a series of NiTi wires against an applied stress that had been heat treated at temperatures above and below re-crystallisation. In the wires that were heat treated below re-crystallisation they observed a gradual increase of the M_s temperature with cycle number. However, in wires that were heat treated above the re-crystallisation temperature they observed a decrease of M_s during cycling. In addition, the wires that were heat treated above the re-crystallisation temperature resulted in comparatively high permanent strains.

The results of Miyazaki et al[133] and Thoma et al[131] can be used in conjunction with the stress/temperature diagrams of **Graph 9-1** to **Graph 9-8** to develop a hypothesis on the structural changes that occurred in the factorial analysis samples:

In those samples where permanent strains were comparatively low, existing dislocations and those introduced during cycling became rearranged in such a way that they formed internal stresses assisting the martensite transformation and increasing the M_s temperature.

In samples where high permanent strains occurred during cycling, the dislocations acted to both assist and disrupt the martensite transformation. This resulted in either: a decrease of M_s, no change in M_s or a comparatively small increase of M_s.

If this hypothesis is true, then internal stresses that assist the transformation should result in permanent changes to the transformation temperatures after cycling. Furthermore, if the internal stress assists the forward transformation then it should result in a Clausius-Clapeyron gradient. Although many authors who have carried out thermal cycling experiments, explain increases of transformation temperature with an internal stress hypothesis, none have actually tried to measure it. While plenty of direct and indirect evidence for dislocation

generation has been produced this is not necessarily direct evidence of an internal stress.

The DSC results presented in **Graph 12-1** however, are direct evidence of the existence of internal stresses. If the Clausius-Clapeyron gradient, ($d\sigma/dM_s$), is calculated from **Graph 12-1**, then in the range of 0MPa to 180MPa a remarkable fact arises. That is, the measured ($d\sigma/dM_s$) gradient of 4.1MPaK^{-1} is extremely close to the ($d\sigma/dM_s$) gradient of 4.0MPaK^{-1} measured on a static stress before cycling, ie. the 'cycle 1' curve in **Graph 9-1**. This is remarkable because it not only appears to confirm the existence of an internal stress but also implies that in this applied stress space, the direction and level of residual internal stress imparted due to cycling, is very similar to that applied during cycling. This is shown below in **Graph 13-1** where the M_s temperature curve at cycle 1 from **Graph 9-1** is plotted with the M_s temperature curve after cycling from **Graph 12-1**. Very similar results were found for other factorial analysis alloys measured before and after cycling.

Graph 12-1 also showed that in the alloy tested, the M_s stopped increasing when the applied stress exceeded 180MPa. This implies that at some stress between 180MPa and 245MPa the internal stress assisting the transformation stopped increasing or was balanced by another opposing stress. Up to this point the A_s also increased as the M_s increased. This is logical as internal stresses that favour the forward transformation will oppose the reverse parent phase transformation.

Interestingly, beyond 180MPa at the stress where M_s remained constant and began to decrease despite increasing cycling stress, the A_s temperature also began to decrease. This implies that the internal stresses formed beyond the 180MPa level began to oppose the forward martensite transformation and instead, favour the reverse transformation. Again, the increase of internal stress, that now appeared to favour the parent phase formation, increased linearly with the level of applied stress.

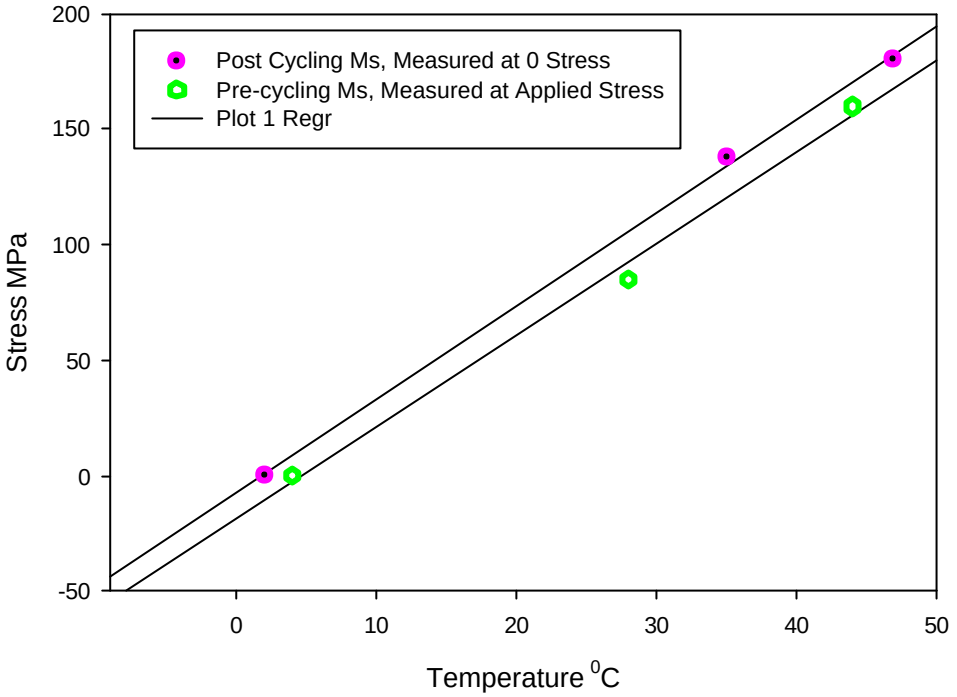

Graph 13-1 Comparison of the d $_S$ /dT gradient in an alloy at applied stress before cycling and for the same alloy at zero stress after cycling against applied stress. The alloy used was 50.26at%Ni with 30% cold work, heat treated at 500° C.

At this point more conclusions can be made:

- *Below a finite applied stress level, a linear increase of internal stress occurred during thermal/stress cycling that favoured the forward martensite transformation and increased M_s.*
- *Beyond a certain cycling stress level, the internal stress generated by cycling began to favour the reverse parent phase transformation resulting in a decrease of M_s and a linear decrease of A_s.*

This agrees with and confirms the hypothesis of Thoma et al[131], that during cycling at applied stress two internal stress mechanisms may occur and depending upon which one dominates, the M_s will increase or decrease.

By studying **Graph 12-2** it is possible to derive a hypothesis explaining the apparently opposing stresses. **Graph 12-2** shows how the heats of transformation vary with increasing cycling stress compared to the starting heats of transformation before cycling plotted at 0MPa.

As shown previously in **Figure 5-2**, and described by Van Humbeeck et al[126], the hysteresis profiles of thermoelastic transformations are greatly influenced by internal frictional energy and stored elastic energy. Salzbrenner and Cohen[39] used equation **(2-10)** to measure the relative contributions of the frictional energy and stored elastic energy on the measured heat of transformation. This is repeated below as equation **(13-1)**.

$$\Delta H_{net} = \Delta H_{ch} + \Delta H_{el} + \Delta H_{I} \qquad \textbf{(13-1)}$$

where ΔH_{net} is the net enthalpy change measured by differential scanning calorimetry (DSC), ΔH_{ch} is the chemical enthalpy, ΔH_{el} is the enthalpy change associated with the strain energy of the transformation and ΔH_{I} arises from the production of internal interfaces during transformation. Liu and McCormick[178] expressed **(13-1)** in terms of a free energy balance between : chemical free energy, elastic energy and frictional energy. At thermal equilibrium this can be expressed as :

$$\Delta G = \Delta G_c + \Delta E_c + \Delta E_f = 0 \qquad \textbf{(13-2)}$$

where the subscripts c, e and f refer to chemical, elastic and friction respectively. The frictional energy term refers to an amount of energy consumed in overcoming the internal resistance to interfacial motion during transformation.

Ortin and Planes[179] state that the internal resistance arises from two sources: barriers to interfacial motion and irreversible plastic accommodation of the transformation strains. As the energy to overcome internal resistance is lost during transformation, a net heat loss should occur[153,180]. In terms of DSC measurement this energy or heat loss will be seen as a difference in the net heat of transformation between the forward and reverse reaction[39]. The closer the net heats of transformation as measured by DSC therefore, the less the energy lost to internal resistance.

Graph 12-2 clearly shows that cycling against applied stress reduced the heat energy lost between the forward and reverse reaction. In fact at stresses of 300MPa and above, the difference in net heats of transformation between the martensite and parent phase transformation can hardly be resolved. This implies therefore, that any dislocation generation above 300MPa applied stress, was not associated with changes of frictional energy, but with stored elastic energy and the increasing permanent strain.

The rate of decrease in internal resistance with applied stress level was greatest below 180MPa. This is interesting as it is within this stress range where the rate of M_s increase was greatest. If the internal resistance energy is due to dislocation generation and plastic accommodation of the martensite variants[179], then the results imply that higher cycling stresses resulted in a saturation of the energy loss due to these barriers. This supports the hypothesis stated earlier in this section and that proposed by Miyazaki et al[133], i.e. an M_s increase during cycling is due to the introduction and rearrangement of existing dislocations that form stress fields and assist the martensite transformation. The introduction of these dislocations and subsequent rearrangement will become saturated and further rearrangement of dislocations that favour the forward transformation will no longer occur.

All the cycling data generated within the factorial analysis tended to show the greatest changes in the early cycles. For instance the rate of changing recovery strain, **Graph 8-11** to **Graph 8-16**, and the rate of change in the transformation temperatures, **Graph 9-1** to **Graph 9-8**, tended to be greatest in the first ten cycles. This implies that dislocation generation and rearrangement also tended

to occur at a greater rate in the first cycles. This is consistent with virtually all published cycling data[107,117,129,131,132,133,135]. It is also logical that dislocation generation should saturate fastest at high stress levels[131].

More conclusions can now be made:

- *During thermal cycling against applied load, existing dislocations and those generated from cycling, become rearranged in such a way that they form anisotropic stress fields that assist the martensite transformation.*
- *The stress field created within the alloy follows the Clausius-Clapeyron relationship resulting in a $d\sigma/dM_s$ stress rate gradient that is the same as that of an un-cycled alloy transforming against an applied stress.*
- *Concurrent with the internal stress assistance is a rise in the M_s temperature.*
- *During cycling the energy loss due to dislocation generation and rearrangement becomes saturated. This saturation occurs at a greater rate in the early cycles and at a higher stress.*

After the internal resistance (or friction) that results in an energy loss (and hysteresis) stops decreasing and the M_s temperature stops increasing, **Graph 12-1**, another internal stress effect appears to dominate the transformation. As described by Liu and McCormick[178] and Salzbrenner and Cohen[39] the resulting free net energy of transformation contains an elastic energy term. The net free energy and associated elastic energy term was defined previously in equation **(13-2)**[178]. The elastic energy term is a reversible energy, whereby energy stored during the forward martensite transformation is released during the reverse, parent phase transformation.

Where as the internal resistance energy tends to be associated with *plastic* accommodation of the martensite plates[39], the stored elastic energy stems from the strain generated by *elastic* accommodation[39]. Perkins[177] states that dislocations formed during cycling, pile-up at martensite/parent boundaries resulting in a back stress on the transforming plates. In the factorial experiments,

It is likely that even during the early cycles, where the decrease of internal resistance energy was shown to be dominant, the elastic energy was still increasing due to the associated increase of dislocation density.

Perkins[177] states that the dislocation pile-ups accommodate the transforming plates elastically and expand the transformation into a temperature interval due to the storage of strain energy during the forward transformation[178]. The stored energy is subsequently released during the reverse transformation thus decreasing the A_s temperature. The effect on the hysteresis profile of elastic energy was described by Van Humbeeck et al[126] and was shown previously in **Figure 5-2**.

The increase of the temperature intervals: ($M_s - M_f$) and ($A_s - A_f$), that occurred during cycling of the factorial alloys was shown in **Graph 9-1** to **Graph 9-8**. This strongly implies that an increase of elastic energy stored during transformation (and therefore dislocation pile-ups) occurred during applied stress cycling.

The fact that elastic energy storage occurs due to dislocation pile-ups[177], implies that it should increase with dislocation saturation and plastic deformation. As the storage of elastic energy is due to dislocations and therefore a permanent change in the microstructure, differences in elastic energy due to cycling should also be shown by the post cycling DSC data of **Graph 12-1** and **Graph 12-2**.

Graph 12-1 shows that above 180MPa applied stress, the post cycling A_s temperature decreased. This is consistent with an increase of stored elastic energy as the increased back stress reduces the extent of the over heating required for parent phase transformation. The decrease of A_s is linear as the applied stress level is increased beyond 180MPa.

Further confirmation of an increase in stored elastic energy during cycling is given by **Graph 12-2**. As the elastic energy is stored during the forward transformation and released during the reverse, the net heat of transformation as measured by DSC will be reduced in both directions[39,178]. This is confirmed by **Graph 12-2** as a linear decrease in the measured heat of transformation occurred in both the forward and reverse reaction above 180MPa.

The back stress created by the elastic energy will oppose the forward transformation and either reduce M_s, or prevent it from increasing any further.

Relating this to the factorial experiments, the specimens that tended to show the least increase in M_s or even a decrease in M_s, tended to be those where the greatest permanent strains resulted. Specifically these were the Ti rich 6% cold work alloys, and the Ti rich, 30% cold work alloys that had undergone heat treatment at the higher temperature.

More conclusions can now be formulated:

- *Concurrent with stress fields that favour the forward reaction, dislocations generated during cycling result in an increase of elastic energy stored during the forward transformation. The back stress generated by these dislocations opposes the martensite transformation but favours the parent phase transformation.*
- *An increase of the stored elastic energy results in a decrease of the A_s temperature during cycling and an increase of the transformation start and finish temperature interval. In addition, the net heat of transformation as measured by DSC is reduced for both the forward and reverse transformation.*
- *The Ti rich alloys were shown by factorial analysis to result in greater permanent strains than the Ni rich equivalents. These strains resulted in considerable plastic deformation and high elastic energy opposing the forward transformation.*

13.2 A Comparison of the Factorial Analysis Results with Superelastic Cycling and Martensite Stabilisation

Permanent internal stresses also have important implications for martensite stabilisation. Miyazaki et al[122] showed, in a study on the cyclic deformation characteristics of NiTi in the superelastic condition, that residual martensite plates form during cycling. **Figure 13-3** shows how, after 100 stress induced cycles, residual martensite plates remain in the parent phase after unloading. Miyazaki[122] found that the number of residual martensite plates left in the parent phase after being unloaded increased with cycle number. He attributed this to increasing internal stress caused by dislocations and considered these stabilised plates to be the cause of residual parent phase strain caused by cyclic deformation. The hysteresis curves where Miyazaki observed these permanent strains were first shown in **Figure 5-1**, and are repeated below in **Figure 13-4**.

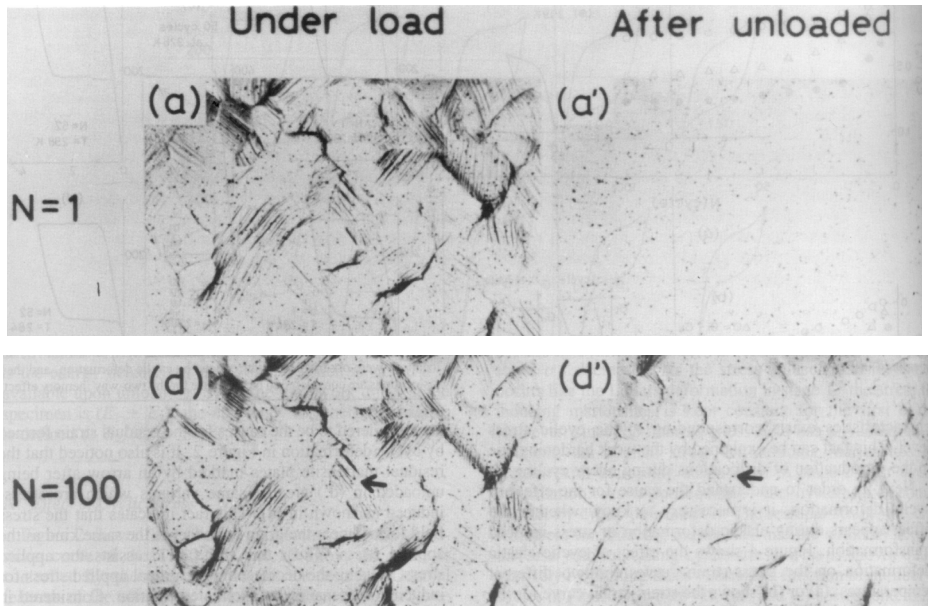

Figure 13-3 Successive optical micrographs of a superelastic alloy under load (a) and after unloading (a'), at cycle N=1 and cycle N=100[122]

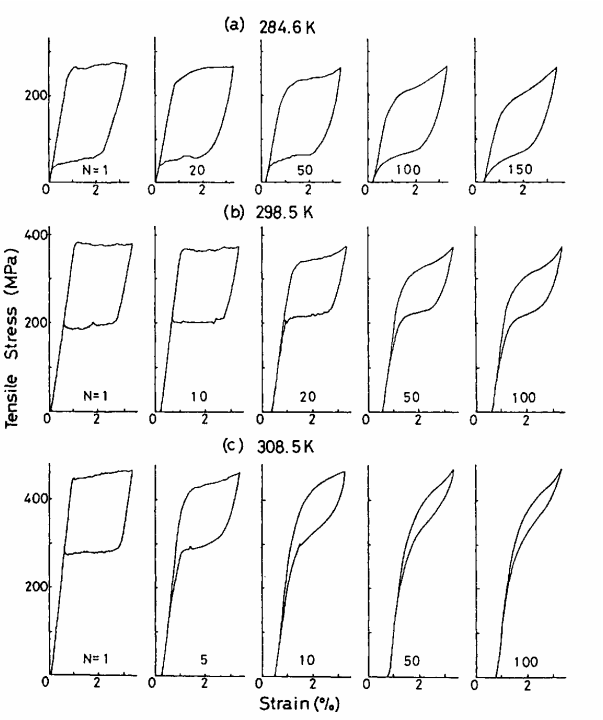

Figure 13-4 The effect of cyclic deformation on stress-strain curves at various temperatures for the Ti-50.5at%Ni alloy which was annealed at 1000°C for 1hr followed by furnace cooling[122].

Miyazaki's[122] curves shown in **Figure 13-4**, are particularly interesting as they show the same effects observed during the factorial cycling experiments. If the stress axes of the curves shown in **Figure 13-4** were replaced by temperature axes, the cycling effects observed by Miyazaki[122] would be the same as those observed during the factorial analysis experiment.

That is, with increasing cycle number, the stress hysteresis decreases (corresponding to decreasing internal resistance energy) and the stress interval between the start and finish of transformation increases (corresponding to increasing stored elastic energy). As the test temperature is raised in **Figure 13-4**, so the stress required for inducing the martensite increases. This increase of applied stress during cycling corresponds with: an increasing stored elastic energy, a decreasing internal resistance, an increasing permanent strain of the parent phase and an increasing amount stabilised martensite plates[122].

The increasing permanent strain in the parent phase then, appears to be due to increasing dislocation densities resulting in an increase of stabilised martensite.

The internal stress caused by the dislocations, stabilises the martensite so that even at 0MPa applied stress, the internal stress fields are great enough to induce martensite. Miyazaki also noted that the stabilised variants are the same as those stress induced by applied stress. He states that therefore the stress field that causes the stabilisation of the variant, operates in the same sense as the applied stress. The factorial experiment, Clausius-Clapeyron gradient measured from the post cycling DSC data, **Graph 13-1**, also appears to confirm this.

The internal stress field therefore, assists the applied stress in Miyazaki's[122] experiments and causes a decrease in the critical applied stress for inducing martensite, **Figure 13-5 (b)**. This is directly analogous to the increasing M_s observed during the factorial experiments and shown in **Graph 9-1** to **Graph 9-8**, and the changes of internal stress and transformation energies discussed earlier in this chapter.

The increasing strain in the parent phase after repeated superelastic cycling is also directly analogous to the permanent strain of the parent phase observed during the factorial experiment. In **Figure 13-5 (a)** and **Figure 13-5 (c)** Miyazaki et al[122] show how the increasing permanent strain of the parent phase, **(a)**, is concurrent with a decreasing strain hysteresis, **Figure 13-5 (c)**. The decreasing strain hysteresis is analogous to the decreasing recovery strain observed in the factorial experiments.

Miyazaki et al[122] carried out these experiments on a Ni rich alloy after cold drawing and heat treatment at 1000°C. This is well above the re-crystallisation temperature and will result in a relatively dislocation free structure prior to superelastic cycling. The starting structure then, is also analogous with the factorial specimens that showed the greatest reductions of recovery strain, i.e. those with low prior cold work.

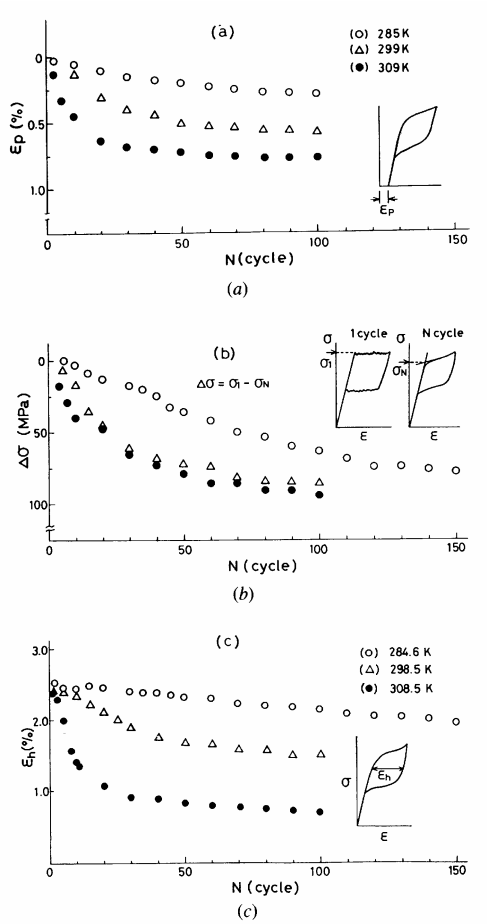

Figure 13-5 The effect of cyclic deformation on (a) residual strain, (b) critical stress for inducing martensite, and (c) the strain hysteresis, as measured from Figure 13-4[122]

The similarity between Miyazaki's[122] superelastic results and those of the factorial experiment, strongly indicates that the effects observed during thermal cycling against an applied stress and the effects of superelastic cycling are the same. In addition, the cause of the cycling effects also appear to be the same, i.e. increasing dislocation density, decreasing internal resistance, increasing stored elastic energy etc. The stress stabilised martensite variants that Miyazaki observed therefore, and which he connected to the permanent strains generated in the parent phase, are also likely to be the cause of the generally decreasing recovery strains observed in the low cold work factorial specimens.

Figure 13-6 shows an electron micrograph of sample 6 after 500 thermal cycles against an applied stress. Prior to imaging in the scanning electron microscope

(SEM), the specimen was polished to a ¼µm finish then taken to a temperature above A_f and subsequently cooled to below M_f under zero stress. This was carried out to prevent external applied stress orientating the martensite variants during cooling. However, despite the absence of an externally applied stress, **Figure 13-6** still shows preferentially orientated martensite. This confirms the presence of an internal stress field and strongly implies that stabilised martensite variants may remain in the parent phase, thus explaining the observed reductions in recovery strain. It is also this type of internal stress orientation that is responsible for the two-way memory effect.

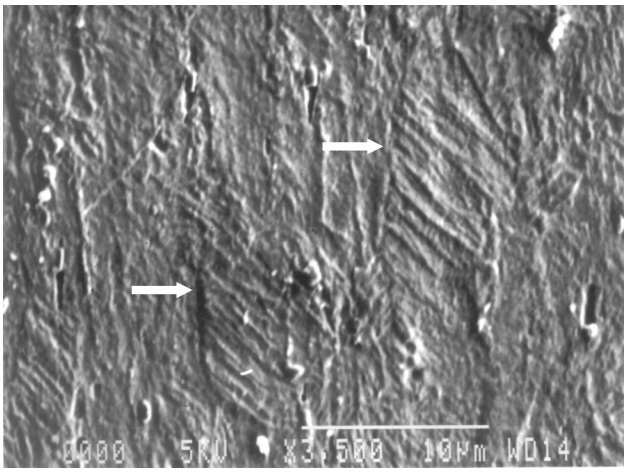

Figure 13-6 An electron micrograph of Factorial Sample 6, after 500 thermal-applied stress cycles, followed by 1 stress free thermal cycle. Martensite variants that are of the same orientation, are marked with arrows.

To further emphasise the connection between superelastic cycling and thermal cycling against applied stress, **Graph 13-2** shows the result of repeated stress induced martensitic transformations carried out on the Ni rich factorial alloy with 30% cold work, heat treated at 500°C.

The alloy was cycled at a temperature approximately 10°C above its 0 stress A_f temperature of 70°C, i.e. 80°C. This ensured superelastic transformation. The alloy wire was cycled in an environmental chamber fitted to an Instron tensile testing machine.

Graph 13-2 shows how after 35 stress transformations the stress required to induce the martensite reduced by approximately 90MPa. Just as a linear increase of the M_s temperature was observed in this alloy during thermal cycling against applied stress, so the stress required for martensitic transformation reduced linearly with superelastic cycling. This confirms similar results from other authors[118,124,122] and further emphasises the connection between superelastic cycling effects and thermal cycling effects when operating against applied stress. Subsequent DSC measurement showed the M_s temperature had increased by 15°.

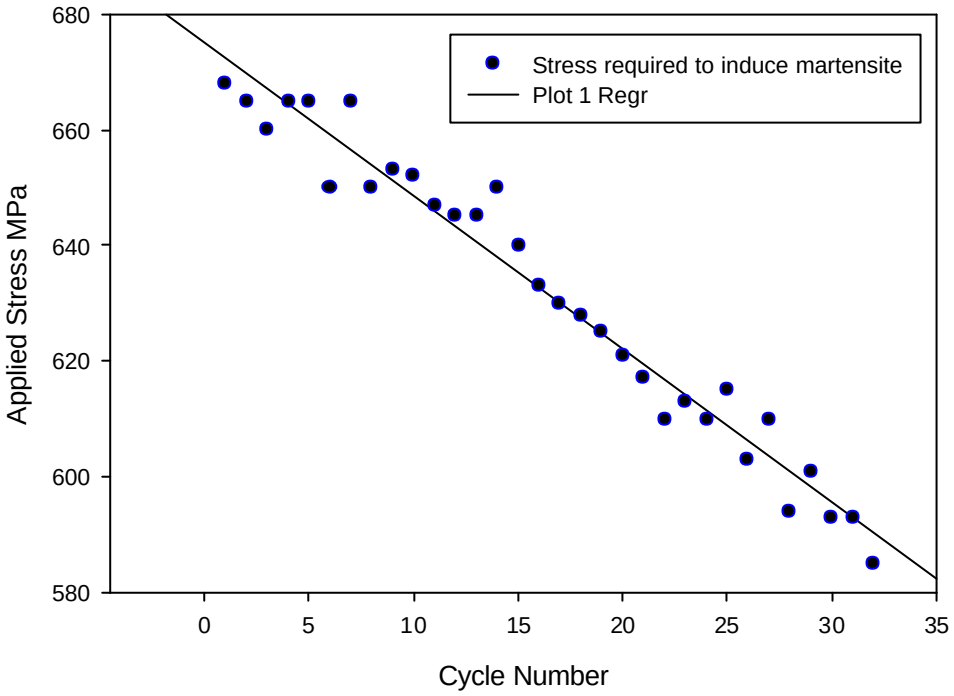

Graph 13-2 The level of applied stress required for stress inducing martensite in the Ni rich factorial alloy, heat treated at 500°C after 30% cold work.

Further conclusions can now be made:-

- *Very similar cycling effects are observed between superelastic transformations and thermal transformations against an applied stress.*
- *It has been shown*[122] *that superelastic transformations result in stabilised martensite variants that do not revert to the parent phase even at zero applied stress. This results in permanent strain of the parent phase and a decrease in the strain hysteresis. Similar parent phase strains and reductions of recovery strain occur in the factorial alloys. Preferentially orientated variants were observed in the post cycling factorial alloys below* M_f*. It is not known whether these variants will remain at temperatures above* A_f *however.*
- *Superelastic cycling of the Ni rich factorial alloy, cold worked by 30% and subsequently heat treated at 500°C resulted in a linear decrease of the stress required to induce the martensite transformation. This may be correlated with an increase of the* M_s *temperature observed during thermal cycling of the same alloy against an applied stress.*
- *The same dislocation and internal stress effects are thought to occur during both superelastic cycling and thermal cycling against applied stress.*

As dislocation generation and the resultant changes of internal stress that these cause appear to be at the heart of the observed cycling effects, it is logical that increasing the resistance to slip will improve cyclic stability. This explains therefore, why cold work, heat treatment and applied stress were all found to be very significant in the factorial analysis of the processing and operating factors. However, it is not only the resistance to slip and dislocations that make these factors so important.

13.3 Transformation Temperatures and Phase Sequence

It was shown in **Graph 8-12** that the 30% cold work, Ni rich alloys resulted in considerable scatter of the recovery strains achieved by these samples. This can

be explained by referring to the corresponding stress/temperature diagrams shown in **Graph 9-1** and **Graph 9-2**.

The comparatively low recovery strains of the 30% cold work, Ni rich, 400°C heat treatment samples (i.e.: 9,11,13 and 15) was due to their respective M_s temperatures and phase transformation sequence. **Graph 9-2** shows how the phase transformation in sample 9 was purely R-phase and correspondingly resulted in a recovery strain of just 0.4%ε. The transformation in Sample 13, shown on the same graph was almost purely R-phase at cycle 1 and had a recovery strain of approximately 1.0%ε, after 500 cycles however, the M_s temperature increased enough to allow some martensite plates to form and the recovery strain increased to approximately 1.4%ε. Samples 13 and 15 are the fast cycling rate equivalents of 9 and 11.

The shape stability of the pure R-phase transformations was extremely stable and no permanent strains occurred in either the parent phase or R-phase. This stability confirms the work of other workers including: Stachowiak et al[135], Todoroki et al[138] and Tobushi et al[121].

Phase sequence and transformation temperature drift also explains why increasing recovery strains are observed in some samples. For instance it was shown in **Graph 8-12** that the recovery strain of sample 10 and its fast rate equivalent, sample 12, increased greatly over 500 cycles. Accordingly, the permanent strain measured in the martensite phase of these samples was much greater than that of the parent phase.

Studying the phase sequence in sample 10 as shown by **Graph 9-1**, it can be seen that as the cycling proceeds, the M_f temperature gradually increases from a value very close to 20°C (the ambient temperature and lowest achieved during cycling) to approximately 40°C at cycle 500. Concurrent with this increase of M_f is a gradual suppression of the R-phase and increase in the volume fraction of martensite formation as the M_f increases further above ambient.

Further conclusions can now be made:-

- *Conditions that suppress the M_s temperature of NiTi alloys will favour the R-phase transformation. These conditions are: High Ni content, low heat treatment temperature, high prior cold work and low operating stresses.*
- *Pure R-phase transformation results in very stable recovery strains and no permanent strains.*
- *If the applied stress or heat treatment temperature is high then an increase of the M_s and M_f temperatures during cycling may occur. Pure R-phase transformation may no longer occur and the associated strain stability will be lost.*

13.4 Mechanical Integrity and Alloy Composition

Table 10-1 showed how the ultimate tensile strength and elongation to failure of the factorial alloys changed after 500 thermal cycles operating against applied stress. The most significant change in tensile behaviour occurred in those specimens where the permanent strains during cycling were large, i.e. samples: 18, 21, 22, 24 and 32. Of these, samples: 18, 21, 22 and 24 were Ti rich alloys with 6% cold work and: 21, 22 and 24 were operating against high applied stress.

Following the hypothesis developed earlier in the discussion, it is logical that low cold work alloys operating against high applied stress will result in the most significant permanent strains as these conditions will favour dislocation generation. However why the permanent strains should be so large in these alloys is less clear, dislocation generation was found to have an effect on internal stresses and therefore martensite stabilisation. Dislocation generation and changes of internal stress does not account for permanent strains of 50% or more as found in these samples.

In addition, as shown in **Table 10-1**, when the samples that resulted in the greatest permanent strains were tested in the tensile machine after cycling, they displayed a substantial reduction in ultimate tensile strength and elongation to failure. A reduction in elongation to failure is consistent with high dislocation

generation as the alloy becomes less ductile. However, the large reduction of UTS displayed by the same samples is not consistent with dislocation generation and associated work hardening effects.

Two effects need to be explained therefore:-

Why the Ti rich alloys result in greater permanent strains, as confirmed by the fact that alloy composition had the greatest factorial main effect on permanent strains?

Why the elongation to failure and ultimate tensile strength should decrease simultaneously in the Ti rich alloys that showed the greatest permanent strains?

It was found during the initial alloy characterisation, that the strength of the martensite phase in the two alloys was very similar, **Graph 8-1** and **Graph 8-2**. The strength of the parent phase however, is quite different. **Graph 13-3** shows tensile data generated from the parent phase of the alloys. Testing was carried out at 180°C, this temperature being high enough to prevent martensite being induced by the tensile stress.

It is very interesting to compare the yield stress of the parent phases to the yield stress of the martensite phases shown previously as stress 2 in **Graph 8-1** and **Graph 8-2**. Whilst the Ni rich alloys show very similar yield values, the Ti rich alloys show a marked reduction in yield strength of the parent phase. In fact the parent phase of the Ti rich, 6% cold work, 500°C alloys is just 270MPa. This indicates that the parent phase is much less resistant to slip than the martensite phase in the Ti rich alloys. It is possible therefore, that the residual permanent strains observed during cycling of the 6% cold work, Ti rich alloys, occurred through real plastic deformation of the parent phase. This also explains why the permanent strains of the Ni rich alloys are slight compared to those of the Ti rich alloys.

In addition, the time spent in the parent phase at applied stress may also affect the amount of permanent strain that occurs and may help to explain the observed cycling effects. **Table 8-19** showed how, consistent with this hypothesis, the high Ti alloys, with low cold work and cycled at the slow rate, yield by far the greatest permanent strains.

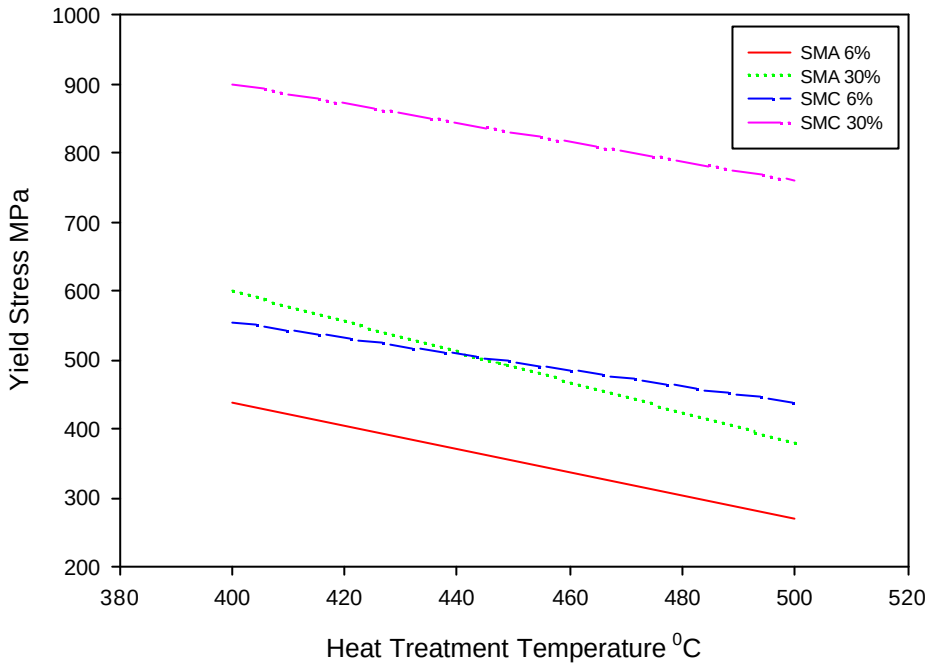

Graph 13-3 Parent phase yield stress of the factorial alloys

The hypothesis of permanent slip occurring in the parent phase, leading to large permanent strain is not consistent with a decrease of UTS however.

A polished cross section of sample 21 shown in **Figure 13-7** provides an explanation of why these apparently opposing effects occur. **Figure 13-7** shows bands of gross internal cracking. The internal cracking was not observed in the same alloy before cycling and therefore the cracks are a real effect resulting from thermal cycling against applied stress.

Cracks of this type will reduce the strength and ductility of the alloy and explains why in the specimens where large permanent strains were observed these

effects also occurred. Some discrete cracks were also found after cycling in Ti rich alloys where very large permanent strains were not observed. No cracks were found in the Ni rich alloys.

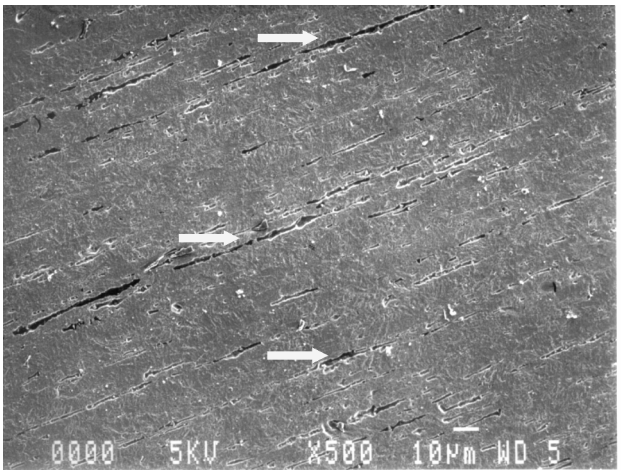

Figure 13-7 Gross internal cracking observed in factorial sample 21, i.e. the 50.12at%Ti-Ni alloy with 6% cold work, heat treated at 400°C and cycled against 185MPa at 170s/cycle

Internal cracking was also observed by Miyazaki[181], **Figure 13-8**.

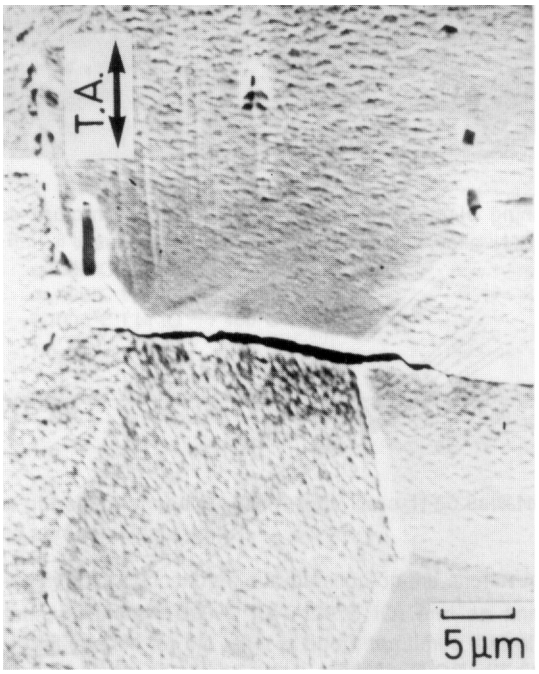

Figure 13-8 Fatigue crack nucleation along a grain boundary in a NiTi alloy[181]

The internal cracking observed by Miyazaki was due to superelastic cycling. Miyazaki states that internal fatigue cracks may occur during superelastic cycling and are initiated at areas of high stress concentration such as second phase particles and grain boundaries.

Further conclusions can now be made:-

- *The yield stress of the parent phase in the Ni rich alloys is approximately the same as the martensite phase.*
- *The yield stress of the parent phase in the Ti rich alloys is considerably lower than the martensite phase and the Ni rich parent phase.*
- *The very large permanent strains displayed by the Ti rich, low cold work specimens are associated with a comparatively low parent phase yield stress.*
- *Gross internal cracking was observed in the specimens with high permanent strains. This is concurrent with a decrease of ductility and ultimate tensile strength.*

13.5 High Cycle Failure

As described in **chapter 11**, even an apparently stable, Ni rich alloy with high prior cold work may not provide high cycle life. At cycle N=83 000, catastrophic failure occurred. Subsequent fractography in the scanning electron microscope, **Figure 13-9**, revealed extensive fatigue striations across the fracture surface.

This thesis has concentrated on how thermal cycling and stress cycling degrades memory parameters and how these degradation effects may be effectively suppressed by optimising the thermo-mechanical treatments. However, the classical type of fatigue failure observed in **Figure 13-9**, implies that mechanical damage resulting in eventual fast fracture may still accumulate even in those alloys optimised to resist memory effect degradation.

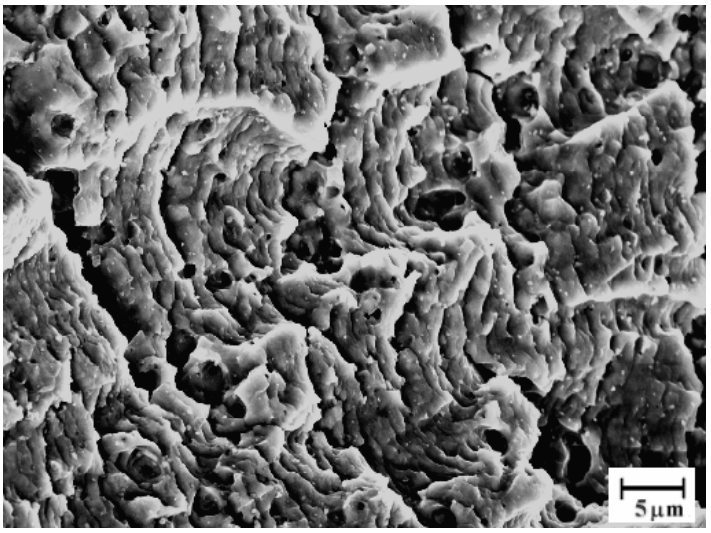

Figure 13-9 Fatigue striations on the fracture surface of the high cycle failure

Fatigue testing of conventional structural materials consists of tension and/or compression cycling to simulate the loading modes experienced during service. During this type of fatigue testing it is usual to keep either the strain or stress levels constant. During thermal-phase transformation cycling of NiTi against constant stress, the strain in the wire is cycled freely between the shorter parent phase length and the longer martensite phase length. An analogy may therefore be drawn with conventional fatigue tests where in order to maintain cyclic stress levels the strain amplitude is allowed to drift with crack growth.

It is well understood that during conventional fatigue, as mean stress level, stress amplitude and strain amplitude increase so the number of cycles to failure decrease. During transformation cycling of the NiTi alloys within this thesis, the stress level is kept constant at a positive value and depending upon the processing procedure the strain amplitude of transformation varies from 0.5%ε - 4.5%ε. Within conventional fatigue testing even strain amplitudes of 0.1% are considered relatively high and result in a much reduced fatigue life. It is possible therefore that the high strain amplitudes associated with the memory effect will result in low cycle lives.

Conventional fatigue cracks are almost always initiated at a free surface. In the few cases where fatigue cracks are initiated internally, it is always associated with some form of internal interface. When discussing the high cycle fatigue failure described in **Chapter 11** it is important to consider how and where the nucleation of the fatigue crack occurs.

Fatigue cracks in conventional materials are often initiated at a free surface. This may be due to surface defects or slip-band intrusions and slip-band extrusions[182]. Surface defects may result in stress concentrations leading to greatly reduced fatigue life as the crack grows from the defect and propagates through the material. Equally surface intrusions and extrusions formed by fine slip bands may also result in stress concentrations due to the build up of notches or ridges at the surface. Crack growth as a result of either process is dependant upon cyclic loading opening and closing the crack during each progressive cycle. In this way crack growth may be thought of as a mechanical process resulting from elastic and plastic deformation strains.

When fatigue cracks are initiated internally, they are a result of internal interfaces that produce stress concentrations due to defects and/or interfacial breakdown. Again the fatigue mechanism may be thought of as a mechanical process resulting from deformation strain.

When considering how conventional fatigue type failure may occur in the alloy cycled in **Chapter 11** it is important to realise that the strain amplitude of each cycle, although comparatively high, is due to *phase transformation strains* not *deformation strains*. That is, strain amplitudes of 4.0ε% are not due to deformation strain in the classical sense. They are due to the martensite/parent phase transformation and the preferred stress orientation of martensite variants. Therefore the actual strain amplitudes of shape memory cycling against applied stress is likely to be a complicated function of transformation strain and real deformation strain of individual phases.

Where permanent strains of individual phases are kept to a minimum, as is the case with the alloy described in **Chapter 11**, it is possible to assume that cycling strain amplitude is almost entirely due to the memory transformation. If this is the case then fatigue crack initiation and propagation is most likely to occur at areas

of high stress concentration such as interfaces between areas that fully transform and those that do not, thereby creating a strain differential across the interface.

The internal cracking observed in some of the Ti rich alloys and shown in **Figure 13-7**, is also likely to be due to differential strains created across second phase particle/matrix interfaces. Comparatively large transformation strains within the matrix material will result in high stress concentrations at the second phase particle/matrix interface which may lead to crack initiation and growth. In **Section 13.4** it was shown how these internal cracks lead to reductions of ultimate tensile strength within the Ti rich alloys.

Although such internal cracking was not observed within the Ni rich alloys, it is possible that after higher numbers of thermal cycles such cracking may even occur in Ni rich alloys. In fact internal cracking has been confirmed as a failure mechanism in Ni rich superelastic alloys by Miyakaki[175] who observed fatigue cracks nucleating at TiC particles and grain boundaries, **Figure 13-8**. In a similar way to classical fatigue via crack growth and plastic blunting, cracks initiated around second phase particles or at grain boundaries may subsequently grow with each transformation cycle resulting in eventual failure. A mechanism such as that described will yield a fracture surface consisting of fatigue striations as observed in **Figure 13-9**. It is also possible that internally stabilised variants, **Section 13.2**, and the internal stresses that cause them, **Section 13.1**, will lead to high localised stress concentrations, crack nucleation and growth.

If internal cracking is not responsible for the fatigue failure observed in **Figure 13-9** then it is possible the crack may have been initiated at the wire surface. Imperfections at free surfaces are the most common cause of conventional fatigue failure. During shape memory cycles it is possible that the very high strains associated with the transformation will cause stress concentrations at sites of surface defects or slip-band intrusions and extrusions. In addition, a further cause of surface imperfection may be hypothesised. It was shown in **Section 13.2** how martensite variants become stabilised due to thermal cycling and the associated generation of internal stress fields. The surface relief where the stabilised plates intersect the free surface and the stress concentrations

created between transforming plates and stabilised plates may also serve as crack nucleation sites.

The striation pattern shown in **Figure 13-9** appeared to start at the wire surface. Therefore in this case, it is likely that during cycling, surface defects concentrated the stress, leading to crack growth and eventual catastrophic failure. The premature failure of the high cycle test however, emphasises that even if the operating and processing conditions are optimised to resist physical changes from thermal cycling, conventional fatigue failure may still occur. This of course has very important implications for commercial applications where high cycle lives are required. These are given in the following conclusions:-

- *It is possible that even alloys that have been optimised to resist memory effect degradation may fail via conventional fatigue type failure. This has very important implications for high cycle superelastic and shape memory applications.*
- *The Nucleation and growth of fatigue cracks may occur internally due to stress concentrations around impurities, second phase particles and grain boundaries.*
- *Surface finish must also be added to the list of important processing factors for high cycle life. Poor surface finish may result in fatigue failure of NiTi actuators via conventional crack growth mechanisms.*
- *Stabilised martensite variants and the associated internal stress fields may also result in stress concentrations both internally and at free surfaces.*

14 Conclusions

15 On The Commercial Future of NiTi Shape Memory Alloys

1. The differentiating benefits of high strains and high work outputs achieved through the use of NiTi shape memory alloy actuators offer real opportunities for innovative design.

2. Certain market segments are beginning to exert a genuine pull on the shape memory industry. The medical market in particular is looking for ever more functional materials, and the unique mechanical properties of NiTi and its associated bio-compatibility offer real opportunities in this market.

3. The potential of using shape memory alloy actuators for unique applications is very attractive to engineers aware of the effect. However, because of the complicated design codes and lack of consistent reliability data, applications using the full martensitic transformation are few.

4. Increasing interdisciplinary alliances between: shape memory alloy manufacturers, materials scientists and end market users, may help to achieve accurate property evaluation and focus on market relevant research.

5. The experimental work contained in this thesis has highlighted the reliability problems associated with NiTi shape memory alloys when operating as a high cycle, thermal actuator. Although parameters that may improve this reliability have been identified, it has also served to further emphasise the complications of using shape memory alloy actuators in real commercial applications.

6. It has been shown that even when the processing and operating conditions are optimised to resist memory effect degradation, mechanical damage can

still occur, resulting in catastrophic failure. This implies that even if stable memory properties can be obtained, commercial applications where comparatively high numbers of transformation cycles are required may not be possible.

16 On the Strain Stability of the Shape Memory Effect When Operating against Constant Stress

1. Factorial experimental design was successfully employed to systematically analyse the main effects of operating and processing variables on the stability of the shape memory effect in NiTi when operating against constant stress.

2. A high percentage of prior cold work, in conjunction with comparatively low heat treatment temperatures was shown to increase the resistance of NiTi actuators to recovery strain degradation and permanent shape strains.

3. The Ni rich alloys employed in the factorial analysis were shown to be considerably more resistant to permanent strains than the Ti rich equivalents. Correspondingly, the parent phase of the Ti rich alloys was found to be considerably less resistant than the martensite phase and considerably less resistant than the parent phase and martensite phase of the Ni rich alloys.

4. Cycling rate was found to have an effect on cyclic stability. Slower cycling rates resulted in greater permanent strain and generally, increased recovery strains. Slow cycling rates were found to be particularly significant for the stability of the low cold work, high heat treatment, Ti rich alloys, and was therefore considered to be associated with the longer time spent in the lower strength parent phase.

5. The factors that were most important were those associated with maximising the resistance of the actuators to dislocation generation and permanent slip.

17 On Dislocation Generation and Changes of Internal States when Actuating against Constant Applied Stress

1. During thermal cycling against applied stress, differential scanning calorimetery (DSC) confirmed the hypotheses of other authors[133,177] that existing dislocations and those generated from cycling become rearranged in such a way that they form stress fields and assist the martensite transformation.

2. The stress fields created within the alloy were found to obey the Clausius-Clapeyron relationship. This resulted in a $d\sigma/dM_s$ stress rate gradient that was the same as that of the non-cycled alloy transforming against an applied stress. This confirmed the superelastic hypothesis of Miyazaki[122], i.e. internally generated stress fields act in the same sense as the stress that formed them.

3. Concurrent with an increase of internal stress assisted martensite, was a rise in the M_s temperature.

4. During cycling, the energy loss due to dislocation generation and rearrangement became saturated. This saturation occurred at a greater rate in the early cycles and at higher stresses.

5. Concurrent with stress fields that favoured the forward reaction, dislocations generated during cycling resulted in an increase of elastic energy stored during the forward transformation. The back stress generated by these dislocations opposed the martensite transformation but favoured the parent phase transformation.

6. An increase of the stored elastic energy resulted in a decrease of the A_s temperature during cycling and an increase of the transformation start and

finish temperature interval. In addition, the net heat of transformation as measured by DSC reduced for both the forward and reverse transformation, confirming the hypothesis of Liu and McCormick[178].

18 On the Relationship between Superelastic Stress Induced Cycling and Thermal Cycling against Constant Stress

1. Very similar cycling effects were observed between superelastic transformations carried out by others[122] and the effects observed during the thermal cycling against applied stress carried out during the factorial analysis.

2. It has been shown[122] that superelastic transformations result in stabilised martensite variants that do not revert to the parent phase even at zero applied stress. This results in permanent strain of the parent phase and a decrease in the strain hysteresis. Similar parent phase strains and reductions of recovery strain occurred in the factorial alloys. Preferentially orientated variants were observed in the post cycling factorial alloys below M_f. It is not known whether these variants remained in the parent phase, i.e. at temperatures above A_f.

3. Superelastic cycling of the Ni rich factorial alloy, cold worked by 30% and subsequently heat treated at 500°C, resulted in a linear decrease of the stress required to induce the martensite transformation. This may be correlated with an increase of the M_s temperature observed during thermal cycling of the same alloy against an applied stress.

4. The same dislocation and internal stress effects were thought to occur during both the superelastic cycling and the thermal cycling against applied stress.

19 On the Transformation Phase Sequence

1. Conditions that suppressed the M_s temperature of NiTi alloys favoured the R-phase transformation. These conditions were: high Ni content, low heat treatment temperature, high prior cold work and low operating stress.

2. Pure R-phase transformation resulted in very stable recovery strains and no permanent strains.

3. If an increase of the M_s temperature occurred during R-phase cycling such that the martensitic transformation began to occur, then the associated strain stability of the R-phase was lost.

20 On the Mechanical Integrity When Operating against Applied Stress

1. The very large permanent strains displayed by the Ti rich, low cold work specimens were associated with the comparatively low parent phase yield stress.

2. Gross internal cracking was observed in the specimens with high permanent strains. This was concurrent with a post cycling, decrease of ductility and ultimate tensile strength.

3. After 83 000 thermal cycles against an applied stress in an actuator optimised to resist permanent strain, conventional fatigue failure via crack growth was found to occur.

4. Fatigue crack initiation may occur at internal cracks associated with differential strains across second phase particles and/or grain boundaries.

21 Future Work

1. Within this thesis the memory effect degradation and stabilisation has been strongly linked to dislocation generation via differential scanning calorimetry and mechanical testing, no observational evidence has been obtained. A study of alloy microstructures and how they relate to the observed changes in heats and temperatures of transformation would provide a more direct method of studying dislocation generation. Future work is therefore required to link transmission electron microscopy of dislocation densities and distributions with internal stress field generation.

2. The alloys tested within this thesis that demonstrated R-phase only transformations were shown to demonstrate particularly stable memory strains. Further research and testing to characterise the R-phase and how stable it is after very high numbers of transformation cycles would be of particular interest.

3. Whilst this thesis has indicated how stable memory properties may be achieved in NiTi actuators, it has also shown that other degradation effects can also occur. Future work should aim to characterise internal cracking in relation to differential strains around impurities, second phase particles and grain boundaries. In particular the relationship between internal cracking, transformation strain amplitudes and microstructural homogeneity is essential for high cycle number applications.

References

[1] Duerig, T.W., Engineering Aspects of Shape Memory Alloys, Butterworth-Heinemann Ltd., 1990, intro.
[2] Ölander, A., Z. Krystall, 1932, **83A**, p 145.
[3] Greninger, A.B. and Mooradian, V.G., Trans AIME, 1938, **128**, p 337.
[4] Chang, L.C. and Read, T.A., Trans. AIME, 1951, **189**, p 47.
[5] Melton, K.N. and Harrison, J.D., Proc. 1st Int. Conf. On Shape Memory and Superelastic Technologies, Pacific Grove, California, 1994, p 187.
[6] Wever, D.J., Veldhuizen, A.G., Sanders, M.M., Schakenraad, J.M. and Van Horn, J.R., Biomaterials, 1997, **18**, p 1115.
[7] Dutta, R.S., Madangopal, K., Gadiyar, H.S., Banerjee S., Brit. Corr. J., 1993, **28**, p 217.
[8] Ryhanen, J., Ph.D. Thesis, Department of Surgery, Oulu University, Finland, 1999.
[9] Fernald, R., Fritz, D., Sievert, C. and Stice, J., Proc. 1st Int. Conf. On Shape Memory and Superelastic Technologies, Pacific Grove, California, 1994, p 341.
[10] Finander, B.V. and Liu, Y., Proc. 1st Int. Conf. On Shape Memory and Superelastic Technologies, Pacific Grove, California, 1994, p 151.
[11] Andraesen, G.F., Am J. Orthod, 1980, **78**, p 528.
[12] Shape Memory Applications Inc., U.S.A., Shape Your Future With…, Company Product Brochure, 1996.
[13] Duerig, T., Int. Conf. on Martensitic Transformations, Bariloche, Argentina, 1998, in print.
[14] Cwikiel, W., Stridbeck, H. and Trandberg, K.G., Radiology, 1993, **187**, pp 661.
[15] Furukawa Electric Co. Ltd., Japan, Product Brochure.
[16] Molloy, K., The Mail on Sunday, May 28, 1995 p 42.
[17] Thomas Bolton Ltd., England, S.M.A. The Metal With a Mind, Product Brochure,
[18] Kapgan, M. and Melton, K.N., Engineering Aspects of Shape Memory Alloys, Butterworth-Heinemann Ltd., 1990, p 137.
[19] Raychem, U.S.A., Unilok™ Rings, Product Brochure, 1993.
[20] Harrison, J.D. and Hodgson, D.E., Shape Memory Effects in Alloys, Plenum Press for the AIME, Ed. J. Perkins, 1975, p 517.
[21] Michael, A.D., Proc. 1st Int. Conf. On Shape Memory and Superelastic Technologies, Pacific Grove, California, 1994, p 283.
[22] Van Moorlegham, W. and Otte., Engineering Aspects of Shape Memory Alloys, Butterworth-Heinemann Ltd., 1990, p 295.
[23] Kao, M., Schmitz, D., Thoma, P., Klaus, M. and Angst, D., Proc. Actuator 96, Bremen, Germany, 1996, p 124.
[24] Hashimoto, M., Takeda, M., Sagawa, H., Chiba, I. and Sato, K., J. of Robotic Systems, 1985, **2**, p 3.
[25] Internet Search on www.yahoo.com
[26] Guénin, G. and Gaudez, Ph., Proc. 3rd ICIM/ECSSM, Lyon, France, 1996, p 493.
[27] Benzaoui, H., Lexcellent, C., Chaillet, N., Lang, B. and Bourjault, A., J. of Intell. Mat. Syst. And Struct., 1997, **8**, p 619.
[28] Tamura, H., Suzuki, Y. and Todoroki, T., *Proc. Int. Conf. On Martensitic Transformations, Nara*, Japan, 1986, p 736.
[29] Cohen, M., Machlin, E.S. and Paranjpe, V.G., Thermodynamics in Physical Metallurgy, American Society for Metals, 1949, p 242.
[30] Wayman, C.M., *Proc. 6 th Int. Conf. On Martensitic Transformations, Sydney,* 1989, p 1.
[31] Reed-Hill, R.E., Physical Metallurgy Principles, 2nd Ed, PWS Publishers division of Wadsworth, Inc., 1973, p 611.
[32] Petty, E.R., Martensite, Longman Group Ltd., 1970.
[33] Greninger, A.B. and Troiano, A.R., Trans. AIME, 1940, 140, p 307.
[34] Greninger, A.B. and Troiano, A.R., Trans. AIME, 1949, 185, p 590.
[35] Bain, E.C., Trans AIME, **70**, 1924, p 25.
[36] Bilby, B.A. and Christian, J.W., 1955, Inst. Met. Monograph No.18, p 121.
[37] Wechsler, M.S., Lieberman, D.S. and Read, T.A., Trans. AIME, 1953, **197**, p 1503
[38] Bowles, J.S. and Mackenzie, J.K., Acta Met., 1954, **2**, p 129.

[39] Salzbrenner, R.J. and Cohen, M., Acta. Met, 1979, **27**, p 748.
[40] Airoldi, G., Riva, G. and Rivolta, B., *Proc. 6 th Int. Conf. On Martensitic Transformations, Sydney,* 1989, p151.
[41] Tong, H.C. and Wayman, C.M., Acta. Metall., 1974, **27**, p 739.
[42] Morii , K., Miyazaki, S. and Nakanishi, N., *Proc. Int. Conf. On Martensitic Transformations, Monterey* 1992, p 1125.
[43] Tamuri, I. and Wayman, C.M., Martensite, ASM International, USA, 1992, p 227.
[44] Patel, J.R. and Cohen, M., Acta. Metall., 1953, **1**, p 531.
[45] Otsuka, K. and Shimizu, K., Int. Mat. Rev., 1986, **31**, 3, p 93.
[46] Wollants, P., Roos, J.R. and Delaey, L., Prog. In Mat. Sci., 1993, **37**, p 227.
[47] Krishnan, R.V., Delaey, L. and Tas, H., J. Mat. Sci., 1974, **9**, p 1536.
[48] Otsuka, K., Wayman, C.M., Nakai, K., Sakamoto, H. and Shimizu, K., Acta. Metall., 1976, **24**, p 207.
[49] Burkart, M.W. and Read, T.A., J. Met. 1953, **5**, p 1516.
[50] Perkins, J., J. of Mat. Sci. and Eng., 1974, **51**, p 182.
[51] Schroeder, T.A. and Wayman, C.M., Scr. Metall., 1977, **11**, p 225.
[52] Saburi, T. and Nenno, S., Scr. Metall., 1974, **8**, p 1363.
[53] Oshima, R. and Naya, E., J. Jpn. Inst. Met., 1975, **39**, p 175.
[54] Takezawa, T. and Sato, S., Proc. 1st JIM Int. Symp. On New aspects of martensitic transformations, Suppl. Trans. JIM, 1976, **17**, p 233.
[55] Zhu and Yang, Scripta. Metall., 1988, **22**, p 5.
[56] Haritos, G.K., Smart Structures and Materials, American Soc. of Mech. Eng., 1991
[57] Chang, L.C. and Read, T.A., Trans. AIME, 1951, **189**, p 47.
[58] Beuhler, W.J., Gilfrich, J.W. and Wiley, R.C., J. Appl. Phys., 1963, **34**, p 1475.
[59] Reyhani, M.M. and McCormick. P.G., Scripta. Metall. Et Mat., 1994, **31**, No 8, p 875.
[60] Maki, T., Shape Memory Materials, Cambridge University Press, 1998, p 117.
[61] Maki, T., *Proc. 6 th Int. Conf. On Martensitic Transformations, Sydney,* 1989, p 157.
[62] Buehler, W.J., Wiley, R.C., United States Patent Office, 1965, No – 3 174 851
[63] Buehler, W.J., Gilfrich, J.W. and Wiley, R.C., J. Appl. Phys., 1963, **34**, p 1475.
[64] Jackson, C.M., Wagner, H.J. and Wasilewski, R.J., NASA Report SP 5110, 1972.
[65] Margolin, H., Ence, E. and Nielson, J.P., Trans. AIME, 1953, **197**, p 243.
[66] Murray, J.L., Binary Alloy Phase Diagrams, American Society for Metals,1986, p 1763.
[67] Duwez, P. and Taylor, J.L., Trans. of AIME, 1950, **188**, p 1173.
[68] Poole, D.M. and Hume Rothery, W., J. Inst. Metals, 1954-55, **83**, p 473.
[69] Chattopadhyay, G. and Kleykamp H., Z Metallkd, 1983, **74**, p 182.
[70] Melton, K.N. Enginering Aspects of Shape Memory Alloys, Butterworth and Heinemann, 1990, p 21.
[71] Wasilewski, R.J., Butler, S.R., Hanlon, J.E. and Worden, D., J. Metals, 1969, **21**, No 3, p 41A .
[72] Wasilewski, R.J., Butler, S.R., and Hanlon, J.E., Met. Sci. J., 1967, **1**, p 104.
[73] Wasilewski, R.J., Butler, S.R., Hanlon, J.E. and Worden, D., Metall. Trans., 1971, **2**, p 229.
[74] Purdy, G.R. and Parr, J.G., Trans. of AIME, 1961, **221**, p 636.
[75] Bastin, G.F. and Rieck, G.D., Metall. Trans., 1974, **5**, p 1817.
[76] Saburi,T., Shape Memory Materials, Cambridge University Press, 1998, p 49.
[77] Michal, G.M. and Sinclair, R., Acta. Cryst., 1981, B**37**, p 1803.
[78] Kudoh, Y., Tokonami, M., Miyazaki, S. and Otsuka, K., 1985, *Acta. Metall.*, 1985, **33**, p 2049.
[79] Golestaneh, A.A. and Carpenter, A.M., *Acta. Metall. Mater.*, 1990, **38**, 7, p 1291.
[80] Otsuka, K., Sawamura, T. and Shimizu, K., *phys. Stat. Sol. (a)*, 1971, **5**, p 457.
[81] Miyazaki, S. and Otsuka, K., *Metall. Trans.*, 1986, **17A**, p 53.
[82] Miyazaki, S., Ohmi, Y., Otsuka, K. and Suzuki, Y., *ICOMAT 82*. *J. DE Phys.,*1982, **43**, C4 p 255.
[83] Otsuka, K., Enginering Aspects of Shape Memory Alloys, Butterworth and Heinemann, 1990, p 36.
[84] Saburi, T., Tatsumi, T. and Nenno, S., *ICOMAT 82*. *J. de Phys.,*1982, **43**, C4 p 261.
[85] Salamon, M.B., Meichle, M.E. and Wayman, C.M., *Phys. Rev. B*, 1985, **31**, p 7306.

[86] Hwang, C.M. and Wayman, C.M., *Scr. Metall.*, 1983, **17**, p 381.
[87] Liu, Y., Liu, Y. and Van Humbeeck, J., *Acta Mater.*, 1999, **47**, 1, p199.
[88] Delaey, L., Krishnan, R.V. and Tas, H., *J. Mat Sci.*, 1974, **9**, p 1521.
[89] Perkins, J., *Scripta Met.,* 1974, **8**, p 1469.
[90] Melton, K.N. and Mercier, O., *Metall. Trans.*, 1978, **9A**, p 1487.
[91] Stachowiak, G. and McCormick, P., *Scripta. Metall.*, 1987, **21**, p 403.
[92] Miyazaki, S., Otsuka, K. and Suzuki, Y., *Scripta. Metall.*, 1981, **15**, p 287.
[93] Liu, Y. and McCormick, P.G., *ISIJ Int.*, 1989, **29**, 5, p 417.
[94] Duerig, T.W., Melton, K.N., Stöckel, D. and Wayman, C.M., Enginering Aspects of Shape Memory Alloys, Butterworth and Heinemann, 1990.
[95] http://www.sma-inc.com/NiTiProperties.html
[96] http://www.amtbe.com/techinfo/techinfo.html
[97] http://www.memory-metalle.de/properties.html
[98] Melton, K.N., Shape Memory Materials,Cambridge University Press, 1998, p 220.
[99] Myers, S. and Marquis, D.G., Successful Industrial Innovation, National Science Foundation, Washington D.C., 1969. P221.
[100] Beta Metals Company Brochure.
[101] Yaeger, J.R., Mech. Eng., 1984, **54**,
[102] Stoeckel D., Advanced Materials and Processes. (Oct 1990) p 33.
[103] Porter M., Competitive advantage: creating and sustaining superior performance (Free Press, New York, 1985)
[104] Humbeeck, J.Van., Proc. European Symposium on Martensitic Transformations and Shape Memory Properties,1991, p 189.
[105] Loveridge R., Pitt M., The strategic management of technological innovation (John Wiley and Sons, Chichester, 1990) p 39.
[106] Shape Memory Applications, Inc. News, a publication of SMA Inc., 1997, **7**, (1).
[107] Todoroki, T. and Tamura, H., Trans. Japan Inst. Metals,1928, **28**, (2), p 83.
[108] Furukawa Company brochure (1)
[109] Furukawa Company brochure (2)
[110] Shape Memory Applications, Inc. News, a publication of SMA Inc., 1998, **8**, (1).
[111] Thompson, B.S. and Gandhi, M.V., Smart Materials and Structures Technologies, The Impending Revolution, Technomic Publishing Company Inc., 1990, p 77.
[112] Chamberlain, G., Design News, 1995, **50**, p 70.
[113] Sheehan, T., The Architects Journal, 1995, **202**, 2, p 37.
[114] Rogers, C.A., Scientific American, 1995, September, p 122.
[115] Kaounides L., Advanced materials, corporate strategies for competitive advantage (FT management reports, Pearson Professional Ltd, London, 1995)
[116] Morgan, N.B. and Friend, C.M., 4th European Symposium on Martensitic Transformations, Enschede, The Netherlands, 1997, p 615.
[117] Van Humbeeck, J., 2nd European Symposium on Martensitic Transformations, Enschede, The Netherlands, 199, p C4-189.
[118] Tobushi, H., Iwanaga, H., Tanaka, K., Hori, T., and Sawada, T., *JSME Int. J.*, 1992, **35**, 3, p 271.
[119] Miyazaki, S., Imai, T., Otsuka, K. and Suzuki, Y., *Scripta Met.* ,1981, **15**, p 853.
[120] Picornell, C., Sade, M. and Cesari, E., *Metall. And Mater. Trans A*, 1994, **25A**, p 687.
[121] Tobushi, H., Yamada, S., Hachisuka, T., Ikai, A. and Tanaka, K., *J. Smart. Mater. Struct.*,1996, **5**, p 788.
[122] Miyazaki, S., Imai, T., Igo, Y. and Otsuka, K., *Met. Trans. A.*, 1986, **17A**, p 115.
[123] Tautzenberger, P., Kehre,H.P., Nußkern,H. and Kocher,H.H., *Pro. Int. Conf. On Martensitic Transformations 1992*, 1993, p 1295.
[124] Kawaguchi, M. and Ohashi, Y., *JSME Int. J.*, 1991, **34**, 1, p 76.
[125] Miyazaki, S., Imai, T., Otsuka, K. and Suzuki, Y. *Scripta. Met.*, 1981, **15**, p 853.
[126] Van Humbeeck, J., Stalmans, R., Chandrasekaran, M. and Delaey L., *Engineering Aspects of Shape Memory Alloys*, Butterworth-Heinemann, 1990, p 96.
[127] Gall, K., Sehitoglu,H., Chumlyakov, Y.I. and Kireva, I.V., *Scripta. Materialia*, **40**, 1, p 7.

[128] Melton, K.N. and Mercier, O., *Acta Metall.*, 1979, **27**, p 137.
[129] Tobushi, H., Iwanaga, H., Ohashi, Y., Inaba, A., Kawaguchi, M. and Saida, H., *JSME Int. J.*, 1990, **33**, p 256.
[130] Suzuki, Y. and Tamura, H., *Engineering Aspects of Shape Memory Alloys*, Butterworth-Heinemann, 1990, p 36.
[131] Thoma, P.E., Blok, A.M. and Kao, M-Y., *Mat. Res. Soc. Symp. Proc.*, 1992, **246**, p 321.
[132] Tobushi, H., Tanaka, K., Kimura, K., Hori, T. and Sawada, T., *JSME Int. J.*, 1992, **35**, 3, p 84.
[133] Miyazaki, S., Igo, Y. and Otsuka, K., *Acta. Metall.,*1986, **34**, 10, p 2045.
[134] Thoma, P.E., Zhang,C., Boeham, J.J. and Zee, R.H., *ESOMAT 97, J. de Physique iv, colloque C5*, 1997, **7**, p C5 483.
[135] Stachowiak, G.B. and McCormick, P.G., *Acta. Metall.*, 1988, **36**, 2, p 291.
[136] de Araújo, C.J., Morin, M. and Guénin, G., *ESOMAT 97, J. de Physique iv, colloque C5*, 1997, **7**, p C5 501.
[137] Tamura, H., Suzuki, Y. and Todoroki, T., *Proc. Int. Conf. On Martensitic Transformations*, 1986, p 736.
[138] Todoroki,T., Tamura,H. and Suzuki,Y., *Proc. Int. Conf. On Martensitic Transformations*, 1986, p 748.
[139] Tamura, H., *Furukawa Rev.*, 1988, **6**, p123.
[140] Friend, C.M., *Proc. 1st European Conf. On Smart Structures and Materials*, Glasgow, EOS/SPIE and IOP Publishing Ltd,1992, p181.
[141] Honma, T., Matsumoto, M., Shugo, Y., Nishida, M. and Yamazaki, I., *4th Int. Cof. On Ti*, 1980, p 1454.
[142] Miyazaki, S., Imai, T., Igo, Y. and Otsuka, K., *Met. Trans. A.*, 1986, **17A**, p 53.
[143] Guangming, L., Gang,F. and Jinxiu, Z., *Mat. Sci. Forum*, 1990, **56-58**, p 591.
[144] Matsumoto, H., *J. Mat. Sci. Lett.*, 1989, **8**, p 232.
[145] Matsumoto, H., *J. Mat. Sci. Lett.*, 1991, **10**, p 408.
[146] Liu. Y. and McCormick P.G., *Acta. Metall. Mater.*, 1990, **7**, 38, p 1321.
[147] McNichols, J.L., Brooks, P.C. and Cory, J.S., *J. Appl. Phys.*, 1981, **52**, 12, p 7442.
[148] Tobushi, H. Ohashi, Y., Hori, T. and Yamamoto, H., *J. Exp. Mechanics*, 1992, p 304.
[149] Filip, P. and Mazanec, K., *Scripta. Met. Et Mat.*, 1994, **30**, p 67.
[150] Edo, S., *J. Mat. Sci. Lett.*, 1989, **24**, p 3991.
[151] Bigeon, M.J. and Morin, M., *3rd ICIM/ECSSM, Lyon, France*, 1996, p 481.
[152] Guangming,L., Gang,F. and Jinxiu,Z., *Mat. Sci. Forum.*, 1990, **56-58**, p591.
[153] Airoldi,G., Rivolta,B. and Turco,C., *Proc. Int. Conf. On Martensitic Transformations*, 1986, p 691.
[154] Friend, C.M., *Scripta. Metall.*, 1986, **20**, p 995.
[155] Stalmans, R., Van Humbeeck, J. and Delaey, L. *Scripta.. Met.and Mater.*, 1994, **31**, 11, p 1573.
[156] Perkins, J. and Muesing, W.E., *Met. Trans. A*, 1983, **14A**, p 33.
[157] Friend, C.M., *Scripta. Met.*, 1987, **21**, p 581.
[158] Guilemany,J.M. and Fernández,J., *Scripta Met. et Mater.*, 1994, **30**, 1, p 59.
[159] Reyhani,M.M. and McCormick,P.G., *Scripta Met. et Mater.*, 1994, **31**, 7, p 875
[160] Kajiwara,S. and Owen, W.S., *Metall. Trans.*, 1974, **5**, p 2074.
[161] Tadaki,T., Katsuki, K. and Shimizu, K., *New Aspects of Martensitic Transformation*, Japan Inst. Metals, 1976, p 187.
[162] Unemento,M. and Wayman, C.M., *Metall. Trans. A,* 1978, **9**, p 891.
[163] Perkins, J., *Metall. Trans.*, 1973, **4**, p 2709.
[164] Kajiwara, S., *New Aspects of Martensitic Transformation*, Japan Inst. Metals, 1976, p 81.
[165] Nakamura, F., Kusui, J., Shimizu, Y. and Takamura, *J. Japan Inst. Metals*, 1980, **44**, p 1302.
[166] Kennon, N.F., Dunne, D.P. and Middleton, L., *Metall. Trans. A*, 1982, **13**, p 551.
[167] Todoroki, T., PhD Thesis, Tohoku University, Sendai, (1986) p 199.
[168] Friend, C.M. and Morgan N.B., J. de Physique, (1995), **5**, p C2-415.

[169] Friend, C.M. and Morgan N.B., Proc. Smart Structures and Materials, SPIE, (1994), **2361**, p 94.
[170] www.sma-inc.com/SMAPaper.html
[171] Sandrock, G.D. and Perkins, A.J. and Hehemann, R.F. Met. Trans., 1971, **2**, p 2769.
[172] Lin, H.C. and Wu S.K., *Scripta Met. et Mater.,* 1992, **26**, 1, p 59-62
[173] Ritter, A., Yang, N.Y.C., Pope, D.P. and Laird, C., *Metall. Trans. A.,* **10A**, p 667.
[174] Pons, J., Lovey, F.C. and Cesari, E., *Acta. Metall. Mater.*, 1990, **38**, 12, p 2733.
[175] Zhu, M. and Yang, D.Z., *Scripta. Metall.* , 1988, **22**, p 5.
[176] Abujudom, D.N., Thoma, P.E. and Fariabi, S., *Mat. Sci. Forum*., 1990, **56 – 58**, p 565.
[177] Perkins, J., Met. Trans., 1973, **4**, p 2709.
[178] Liu, Y. and McCormick, P.G., *Proc. Int. Conf. On Martensitic Transformations, Monterey 1992,* p 923.
[179] Ortin, J and Planes, A., *Acta. Metall.*, 1988, **36**, p 1873.
[180] Delaey, L. and Aernoudt, E., *Proc. Int. Conf. On Martensitic Transformations, Nara*, Japan, 1986, p 926.
[181] Miyazaki, S., Engineering Aspects of Shape Memory Alloys, Butterworth-Heinemann Ltd., 1990, p 394.
[182] Dieter, G.E., Mechanical Metallurgy, McGraw Hill, 1976, p 415.